

## CONTENTS

Performance Comparison of Machine Learning Classifiers on Aircraft Databases <i>Nur Diyana Kamarudin, Syarifah Bahiyah Rahayu, Zuraini Zainol, Mohd Shahrizal Rusli &amp; Kamaruddin Abdul Ghani</i>	154 - 169
Evaluation of Scheme Selection and Parameter Effects in the Reconfigurable Transmitting Power in Wireless Network-on-Chip <i>Mohd Shahrizal Rusli, Nur Diyana Kamarudin, Ab. Al-Hadi Ab. Rahman &amp; M. Nadzir Marsono</i>	170 - 180
Calibration of Lightweight Thermal Sensor for Fully Autonomous UAV <i>Yaakob Mansor, Shattri Mansor, Helmi Zulhaidi Abdul Rahman Ramli &amp; Ajibola I. Isola</i>	181 - 191
Evaluation of Global Navigation Satellite System (GNSS) Space Service Volume (SSV) Performance via Trimble Planning <i>Dinesh Sathyamoorthy, Zainal Fitry M Amin &amp; Shahrudin Abu Hassan</i>	192 - 201
A Novel Architecture for the Realisation of IOT-Enabled ECG Signal Quality Assessment Using Wavelet Decomposition for Baseline Wander Removal <i>Ramesh Babu Chukka &amp; Chennupati Sumanth Kumar</i>	202 - 208
Mechanical Properties of Hybrid Kenaf / Kevlar Fibre Reinforced Thermoplastic Composites <i>Sivakumar Dhar Malingam, Ng Lin Feng, Ng Cher Sean, Kathiravan Subramaniam, Nadlene Razali &amp; Zaleha Mustafa</i>	209 - 224
Characterisation of Hybrid Oil Palm Empty Fruit Bunch and Kenaf Fibre Reinforced Thermoplastic Composites <i>Muhd Ridzuan Mansor, Muhammad Taufiq Jumadi, Mohd Azli Salim, Mohd Zaid Akop, Musthafah Mohd Tahir, Muhamad Fahmi Mohd Noor, Mohd Shukor Salleh &amp; Zaleha Mustafa</i>	225 - 236
Indentation Behaviour of Eco-Friendly Fibre Metal Laminates in Different Stacking Configurations <i>Fadzila Hussain, Sivakumar Dhar Malingam, Mohd Ahadlin Mohd Daud, Siva Irulappasamy &amp; Maciej Klószak</i>	237 - 247
Study of Delamination Factors on the Abrasive Water-Jet Drilling of Fibre Metal Laminates for Military Cargo Aircraft <i>Thirukumar Manoharan, Winowlin Jappes Jebbas Thangaiah, Siva Irulappasamy, Sivakumar Dhar Malingam &amp; Sandro Campos Amico</i>	248 - 258
Identification of High Level Vibration on Rotor Bearing System Using Experimental Data Analysis <i>Yogeswaran Sinnasamy, Noor Aishah Sa'at, Hasril Nain, Ibrahim Tahir, Ahmad Subardi Mohd Wazir, Hanizah Kasmoni, Elizabeth Louisnaden &amp; Khairul Anuar Ahmad</i>	259 - 264
Magnetic Assessment of Newly Installed on Board Degaussing System <i>Abdul Rauf Abdul Manap, Mohd Hambali Anuar, Mahdi Che Isa, Mohd Hazri Rahmat, Roslan Slamatt, Mohd Yusri Othman, Hasril Nain, Zuraini Abdul Manaf &amp; Muhammad Syauqat Abd Khalid</i>	265 - 276
Effect of Low Frequency Excitation for Crack Detection Using Nonlinear Vibro-Acoustic Modulation Method <i>Tino Hermanto, Ruziamreen Jenal, Abd. Rahman Dullah, Azma Putra &amp; Nor Salim Muhammad</i>	277 - 286
Enhancement of Defect Signature for Acoustic Wave Source Location from Two Wave Modes in Pipe <i>Nor Salim Muhammad, Ahmad Fuad Ab Ghani, Rokhmadi, Abd Rahman Dullah &amp; Azma Putra</i>	287 - 298
Food Security and Proper Nutrition: A Public Health and Humanitarian Priority in Pre- and Post-CBRN Events <i>Stefania Moramarco</i>	299 - 309
First Responder CBRN 9-Liner Pocket Response Card <i>Patrick Wengler, Orlando Cenciarelli, Gian Marco Ludovici, Andrea Duggento, Maria Guerrisi, Andrea Malizia &amp; Pasquale Gaudio</i>	310 - 316
Identification of Spiking Chemicals Related to the Chemical Weapons Convention in Water Sample During an Interlaboratory Competency Test <i>Faris Rudi, Hidayah Aziz, Norliza Hussein, Norhayaty Zahari, Shalwa Abu Bakar &amp; Shamsul Ismail</i>	317 - 330
Defence Spending in an Era of Uncertainty and Budgetary Constraints <i>Ananthan Subramaniam*, Amirudin Sulaiman &amp; Wong Wai Loong</i>	331 - 337
Demystifying Ship Operational Availability: An Innovative Approach for Management of In-Service Support Contracts <i>Al-Shafiq Abdul Wahid, Mohd Zamani Ahmad, Khairol Amali Ahmad, Joshua P. Taylor, Aisha Abdullah, Al-Athirah Al-Shafiq, Arifah Ali &amp; Keizo Kitagawa</i>	338 - 360



## **EDITORIAL BOARD**

### **Chief Editor**

Gs. Dr. Dinesh Sathyamoorthy

### **Deputy Chief Editor**

Dr. Mahdi bin Che Isa

### **Associate Editors**

Dr. Ridwan bin Yahaya

Dr. Norliza bt Hussein

Dr. Rafidah bt Abd Malik

Ir. Dr. Shamsul Akmar bin Ab Aziz

Nor Hafizah bt Mohamed

Masliza bt Mustafar

Kathryn Tham Bee Lin

Siti Rozanna bt Yusuf



## AIMS AND SCOPE

The Defence S&T Technical Bulletin is the official technical bulletin of the Science & Technology Research Institute for Defence (STRIDE). The bulletin, which is indexed in, among others, Scopus, Index Corpenicus, ProQuest and EBSCO, contains manuscripts on research findings in various fields of defence science & technology. The primary purpose of this bulletin is to act as a channel for the publication of defence-based research work undertaken by researchers both within and outside the country.

## WRITING FOR THE DEFENCE S&T TECHNICAL BULLETIN

Contributions to the bulletin should be based on original research in areas related to defence science & technology. All contributions should be in English.

## PUBLICATION

The editors' decision with regard to publication of any item is final. A manuscript is accepted on the understanding that it is an original piece of work that has not been accepted for publication elsewhere.

## PRESENTATION OF MANUSCRIPTS

The format of the manuscript is as follows:

- a) Page size A4
- b) MS Word format
- c) Single space
- d) Justified
- e) In Times New Roman ,11-point font
- f) Should not exceed 20 pages, including references
- g) Texts in charts and tables should be in 10-point font.

Please e-mail the manuscript to:

- 1) Gs. Dr. Dinesh Sathyamoorthy (dinesh.sathyamoorthy@stride.gov.my)
- 2) Dr. Mahdi bin Che Isa (mahdi.cheisa@stride.gov.my)

The next edition of the bulletin (Vol. 12, Num. 1) is expected to be published in April 2019. The due date for submissions is 30 January 2019. **It is strongly iterated that authors are solely responsible for taking the necessary steps to ensure that the submitted manuscripts do not contain confidential or sensitive material.**

The template of the manuscript is as follows:

# TITLE OF MANUSCRIPT

Name(s) of author(s)

Affiliation(s)

Email:

## ABSTRACT

*Contents of abstract.*

**Keywords:** *Keyword 1; keyword 2; keyword 3; keyword 4; keyword 5.*

### 1. TOPIC 1

Paragraph 1.

Paragraph 2.

#### 1.1 Sub Topic 1

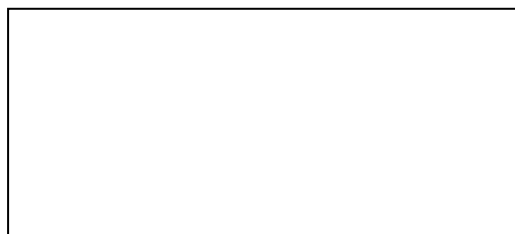
Paragraph 1.

Paragraph 2.

### 2. TOPIC 2

Paragraph 1.

Paragraph 2.



**Figure 1: Title of figure.**

**Table 1: Title of table.**

Content	Content	Content
Content	Content	Content
Content	Content	Content
Content	Content	Content

Equation 1 (1)  
Equation 2 (2)

## REFERENCES

Long lists of notes of bibliographical references are generally not required. The method of citing references in the text is 'name date' style, e.g. 'Hanis (1993) claimed that...', or '...including the lack of interoperability (Bohara *et al.*, 2003)'. End references should be in alphabetical order. The following reference style is to be adhered to:

### Books

Serra, J. (1982). *Image Analysis and Mathematical Morphology*. Academic Press, London.

### Book Chapters

Goodchild, M.F. & Quattrochi, D.A. (1997). Scale, multiscaling, remote sensing and GIS. In Quattrochi, D.A. & Goodchild, M.F. (Eds.), *Scale in Remote Sensing and GIS*. Lewis Publishers, Boca Raton, Florida, pp. 1-11.

### Journals / Serials

Jang, B.K. & Chin, R.T. (1990). Analysis of thinning algorithms using mathematical morphology. *IEEE T. Pattern Anal.*, **12**: 541-550.

### Online Sources

GTOPO30 (1996). *GTOPO30: Global 30 Arc Second Elevation Data Set*. Available online at: <http://edcwww.cr.usgs.gov/landdaac/gtopo30/gtopo30.html> (Last access date: 1 June 2009).

### Unpublished Materials (e.g. theses, reports and documents)

Wood, J. (1996). *The Geomorphological Characterization of Digital Elevation Models*. PhD Thesis, Department of Geography, University of Leicester, Leicester.

# PERFORMANCE COMPARISON OF MACHINE LEARNING CLASSIFIERS ON AIRCRAFT DATABASES

Nur Diyana Kamarudin<sup>1\*</sup>, Syarifah Bahiyah Rahayu<sup>1</sup>, Zuraini Zainol<sup>2</sup>, Mohd Shahrizal Rusli<sup>3</sup> & Kamaruddin Abdul Ghani<sup>1</sup>

<sup>1</sup>Cyber Security Centre, National Defence University of Malaysia (UPNM), Malaysia

<sup>2</sup>Department of Computer Science, Faculty of Science and Defence Technology, National Defence University of Malaysia (UPNM), Malaysia

<sup>3</sup>Electronic and Computer Engineering Department, Faculty of Electrical Engineering, Universiti Teknologi Malaysia (UTM), Malaysia

\*Email: nurdiyana@upnm.edu.my

## ABSTRACT

*The aim of this research is to analyse the performance of six different classifiers, which are k-Nearest Neighbours (kNN), Naive Bayes, Random Tree, J48 Decision Tree, Random Forest Tree and Sequential Minimal Optimisation (SMO), using aircraft databases and optimize their cost parameter for better accuracy. The six algorithms are implemented to classify aircraft type and its country of origin using a Waikato Environment for Knowledge Analysis (WEKA) workbench. Additionally, we report our parameter optimisation results for SMO by varying the cost parameters to obtain the optimum result. It is observed that in both classifications, SMO with linear kernel obtained the best performance as compared to the other classifiers in terms of classification accuracy, which is 100%.*

**Keywords:** *Data mining; comparative analysis; machine learning classifiers; aircraft classification; parameter optimisation.*

## 1. INTRODUCTION

With the continuous growth of the aviation industry, air traffic poses a huge challenge towards air traffic management. Inefficient itinerary, harsh weather and airspace restriction are some of the common problems faced in managing air traffic flow. Delays jeopardise airlines marketing strategies, since carriers rely on customers' loyalty to support their frequent-flyer programmes (Manley & Sherry, 2008; Pai, 2010; Cheng *et al.*, 2016). Such big traffic can create significant challenge in air traffic management, and having the right human capital and technology (Campanelli *et al.*, 2014; Mellat-Parast *et al.*, 2015) enables the sustainability of air traffic management procedures, processes and capabilities.

Statistical analysis methods would have been sufficient to handle smaller amount of aircraft activity data, but with aviation data collected at every moment and archived in databases, the data volume grows in an exponential rate. Thus, the need for machine learning and data management is increasingly significant in this area. For Malaysian air traffic, the Civil Aviation Authority of Malaysia (CAAM), formerly known as the Department of Civil Aviation Malaysia (DCA) is currently launching several initiatives to increase the efficiency of the air traffic, such as Air Traffic Flow Management and Collaborative Decision Making (ATFM/CDM) (Weber, 2012). There have been many works that use machine learning to solve air traffic management (Nazeri & Zhang, 2002; Schumann *et al.*, 2011; Busquets *et al.*, 2016; Janakiraman & Nielsen, 2016; Mack *et al.*, 2017; Sternberg *et al.*, 2017). However, prior work on Malaysian air traffic flow (Nusyirwan & Rohani, 2017) only consists of data collection and analysis to predict the delay. There are various data mining

techniques to handle big data. Depending on the distribution of data, different classifiers may have better performance. In this work, we focus on analysing six different types of machine learning algorithms, which are  $k$ -Nearest Neighbours (kNN), Naive Bayes, Random Tree, J48 Decision Tree, Random Forest Tree and Sequential Minimal Optimisation (SMO), for analysing Malaysian aircraft activity data. The analysis was done using prominent Waikato Environment for Knowledge Analysis (WEKA) machine learning workbench, which includes illustrative  $R$  environment codes and working implementation of various machine learning methods. Besides being an easier tool to use, WEKA has grown enormously in its data mining capacities, where it offers automated experiments with numerous machine learning algorithms and significance test on the results (Witten *et al.*, 2016). For our analysis, we used six machine learning classifiers to classify aircraft type and its country of origin.

The remainder of the paper is organised as follows: Section 2 discusses related work and discusses the data mining background in this work. Section 3 presents the methodology to setup the experiment and data collection planning. Section 4 presents the implementation of kNN, Naive Bayes, Random Tree, J48, Random Forest and SMO techniques to analyse their performance and cost parameter optimisation. Finally, the conclusion of the study is made in Section 5.

## 2. BACKGROUND AND RELATED WORKS

### 2.1 Background

Data mining (DM) is referred to a process of discovering interesting structures (knowledge) from a large collection of data (Roiger, 2017). This structure can be found in the form of a set of rules, a graph, a tree, equations, etc. DM is one of the five important steps within the Knowledge Discovery of Databases (KDD) process model, as can be seen in Figure 1. The KDD process model consists of a methodology for entire knowledge extraction process, comprising how data is stored, how to apply efficient algorithms for analysing data, how to understand and visualize the results, and how to model and support the interaction between human and machine (Cios *et al.*, 2007).

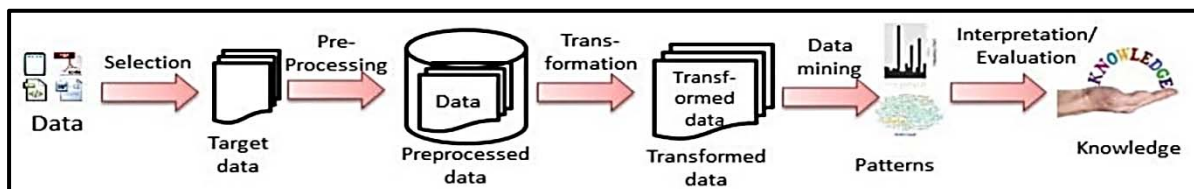


Figure 1: The KDD process model (Fayyad *et al.*, 1996).

According to Dunham (2006), DM is applied to extract interesting information and patterns using data mining tasks and techniques. These information and patterns may assist the top management levels in making decisions. Nohuddin *et al.* (2018) summarised some common data mining tasks and techniques.

Classification is referred to a process of finding a model for that defines and differentiates data classes (Han *et al.*, 2011). The model is basically built from input attributes (independent variables) to predict a class label (dependent variables) for a given unlabelled point. Classification tasks consist of three common features: (i) supervised learning, (ii) dependent variable is categorical and (iii) building models (Roiger, 2017). Classification has been widely applied in many real world applications, for example, predicting student performance (Xing *et al.*, 2015; Asif *et al.*, 2017; Patil *et al.*, 2017), healthcare (Chaurasia & Pal, 2017; Rahim *et al.*, 2017; Phakhounthong *et al.*, 2018), credit card fraudulent detection (Rushin *et al.*, 2017; Save *et al.*, 2017; Yee *et al.*, 2018), and classifying bank loans (Kim *et al.*, 2016; Sudhakar & Reddy, 2016).

In this study, six types of supervised classification techniques are implemented. *k*-Nearest Neighbours (kNN) classifier is a lazy learner algorithm (Aha *et al.*, 1991). This classifier builds a model after a query of the data is placed. kNN estimates the location of data points based on its nearest points. Generally, kNN selects appropriate value of *k* based on cross validation. On the other hand, Naïve Bayes (John & Langley, 1995) uses Bayes' theorem to classify data. This classifier assumes that all attributes of a data point are independent of each other. Analysis of training data will yield a numeric estimator precision values. Moreover, the accuracy level of Naïve Bayes is dependable on the quantity of datasets.

The decision tree technique that is extensively used in WEKA is known as J48 (Quinlan, 1993). Decision tree is a graphical representation of trees with nodes on numbers of branches. This structured decision process is represented by nodes, actions and specific choices. A series of paths from root to last node until an action is reached is known as a rule. A set of rules will be applied into a database to retrieve data for classification purposes. Another type of decision tree is a random tree. Random tree is building trees randomly, but WEKA defines a random tree as a decision tree constructed based on a random subset of columns (Breiman, 2001). Like random tree, a random forest tree also constructs trees randomly, but in a large number (forest). This classifier constructs a forest of random decision trees by analysing sets of variables without performing pruning.

Sequential Minimal Optimisation (SMO) is an algorithm to train support vector machines (Platt, 1999). By default, all attributes are normalised. SMO also replaces all the missing values and transform nominal attributes into binary one. In Quadratic Programming, SMO is a statistical learning algorithm that is much faster and has better scaling properties for difficult Quadratic Programming problems. It is widely known for sparse data classification (Ancona *et al.*, 2004).

## 2.2 Related Work

A comprehensive study was carried out to study air traffic in the Kuala Lumpur Flight Information Region (KLFIR) by Nusyirwan & Rohani (2017). They reported the details of air traffic performance based on general air traffic movement parameters. The parameters adopted were level allocation, number of movements, sector load and analysis. The data was stored in a database which was then used to analyse cases such as aircraft delays in the Kuala Lumpur International Airport (KLIA). However, this paper did not discuss in detail about its data analysis. In 2009, a study conducted by Pan *et al.* (2009) using several classification methods to identify definitions in aviation domain. They observed that Support Vector Machine (SVM) yields the highest precision rate compared to Naïve Bayes. SVM separates the classes with an optimal hyperplane that maximises the margin between classes where the training accuracy is not dependent on the number of datasets used in the training procedure (James *et al.*, 2013).

Mining aviation data was proposed by Busquets *et al.* (2016) to improve the quality of airspace and prediction of air traffic growth. The data was applied in various researches, such as airspace system performance monitoring (Nazeri & Zhang, 2002), diagnostic and monitoring (Schumann *et al.*, 2011; Mack *et al.*, 2017), and anomaly detection (Bay & Schwabacher, 2003; Das *et al.*, 2010; Janakiraman & Nielsen, 2016).

In Nazeri & Zhang (2002), the aviation data was used to analyse the impact of ground weather on flight system performance. The study employed a decision tree learning algorithm with 100-fold cross validation. Two rules were applied, where the first rule (two-class data) achieved 81% accuracy and second rule (covers all the instances except first rule's instances) achieved 69.5%. Hence, it was proved that flight performance is dependable on several factors such as air traffic, airport conditions, ground weather, and policies and decision by authorities.

In an earlier work by Bay & Schwabacher (2003), where a modified kNN algorithm was implemented to mine the distance-based outliers on a continuous and discrete features. By using large databases,



they demonstrated a simple nested loop algorithm that achieved near linear time performance. The data was adopted in random order and a simple pruning rule is implemented to reduce the execution time. Additional work by Das *et al.* (2010) used Multiple Kernel Anomaly Detection (MKAD) technique with one-class SVM model to prove that MKAD required a large memory for building and storing multiple kernels. Belcastro *et al.* (2016) designed a prediction system for flight delay due to poor weather conditions. The study used various classification methods, namely C4.5, SVM, Random Forest, Stochastic Gradient Descent, Naive Bayes and Logistic Regression. The results showed that Random Forest gives the best performance in terms of highest accuracy and recall. In Janakiraman & Nielsen (2016), aviation data was used to discover and study safety events in the US National Airspace System. This study used different types of auto-encoder model of the Extreme Learning Machine (ELM) algorithm to detect anomalies on real aviation problems and focused on techniques to reduce the execution time.

More recent work by Mack *et al.* (2017) employed the Tree Augmented Naïve Bayesian learning algorithm (Friedman *et al.*, 1997), which is also called the Bayesian TAN classifier (TAN) algorithm, from WEKA toolkit to augment aircraft diagnostic reference models. WEKA is a well-known data mining system with various machine learning algorithms for data pre-processing, classification, regression, clustering, association rules, and visualisation (Hall *et al.*, 2009). This research used 10-fold cross validation and achieved around 99.5% of its average classification accuracy. We have summarized these related works in Table 1.

Overall, there have been several researches that implemented data mining and classification techniques for prediction in various fields using aviation data. However, to the best of our knowledge, there is no comparison on classifier's performance and parameter optimisation based on aviation data to date. Hence, this research attempts to compare and analyse classifier performance while discussing on parameter optimisation for better classification by using six classification algorithms, which are kNN, Naive Bayes, Random Tree, J48, Random Forest and SMO.

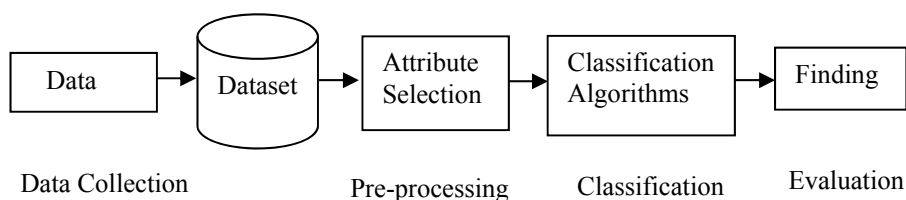
**Table 1: Summary of related works.**

<i>Previous Works</i>	<i>Methods Applied</i>	<i>Strengths</i>	<i>Drawbacks</i>
Air traffic study in the Kuala Lumpur Flight Information Region (KLFIR) by Nusyirwan & Rohani (2017)	Not mentioned	Report the details of air traffic performance based on general air traffic movement parameters	No detail discussion on its data analysis
A study to identify definitions in aviation domain by Pan <i>et al.</i> (2009)	Support Vector Machine (SVM), Naïve Bayes	SVM yields the highest precision rate	Naïve Bayes performance is unsatisfactory.
Analyse the impact of ground weather on flight system performance by Nazeri & Zhang (2002)	Decision tree learning algorithm with 100-fold cross validation	Flight performance is dependable on several factors such as air traffic, airport conditions, ground weather, and policies and decision by authorities	The performance of the second rule which covers all the instances except first rule's instances achieved only 69.5%
Mining the distance-based outliers using continuous and discrete features by	<i>k</i> -Nearest Neighbours (kNN) algorithm	Execution time is reduced	Using a random order and a simple pruning rule

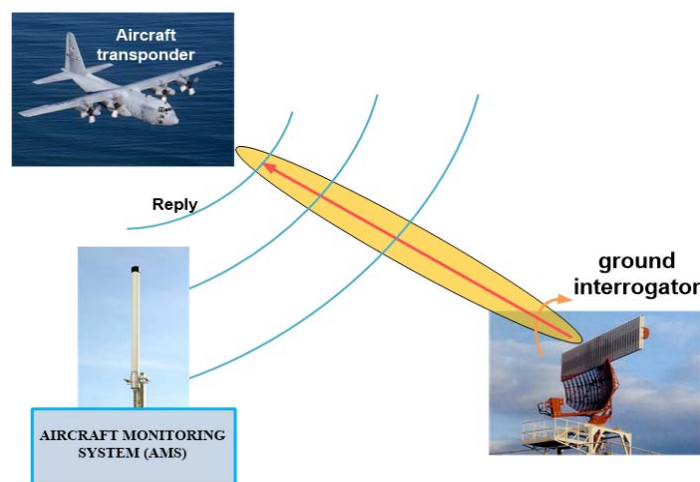
Bay & Schwabacher (2003)			
A prediction system for flight delay due to poor weather conditions by Belcastro <i>et al.</i> (2016)	C4.5, SVM, Random Forest, Stochastic Gradient Descent, Naive Bayes and Logistic Regression	Random Forest gives the best performance in terms of highest accuracy and recall	Other algorithms' performance tested are satisfactory
Discover and study safety events in the US National Airspace System by Janakiraman & Nielsen (2016)	Auto-encoder model of the Extreme Learning Machine (ELM) algorithm	Detect anomalies on real aviation problems and focused on techniques to reduce the execution time	Only use the random kernel (the random feature mapping of the input data)
Augment aircraft diagnostic reference models by Mack <i>et al.</i> (2017)	Bayesian TAN classifier (TAN)	Average classification accuracy is 99.5%	Lack of sufficient data to make the generality of the classifiers hard to test.

### 3. DATA COLLECTION AND METHODOLOGY

Figure 2 illustrates the proposed framework for classifying the air traffic growth of general, military and unknown aircrafts using WEKA. The Aircraft Monitoring System (AMS) is employed to monitor and record aircraft activities in the radius of of 450 km of the AMS's located on top of the tallest building in the National Defence University of Malaysia (UPNM), Kuala Lumpur, Malaysia. The fundamental operation of AMS is shown in Figure 3, where the data transmitted from transponder is also picked up by the AMS.



**Figure 2: Proposed framework of classification model.**



**Figure 3: AMS operational structure (Mindmatics Sdn. Bhd., 2017).**

Real time data collection is done using a real-time monitoring system and raw data is collected in one-hour duration. This software consists of flight mapping airways and real-time databases of flying aircraft as shown in Figure 4. For data mining purposes, International Civil Aviation Organization (ICAO) number, date of flight, time of flight, aircraft type, aircraft registration country or country of origin were pre-processed, trained and classified using WEKA.

The data attributes used in aircraft classification are shown in Table 2. The data set is divided into 10 equally sized folds using the 10-fold cross validation procedure provided by WEKA to assess the predictive performance of the classifiers. In 10-fold cross-validation, the original sample is randomly partitioned into 10 equal sized subsamples. Of the 10 subsamples, a single subsample is reserved as the validation data for testing, and the remaining nine subsamples are used as training. There are in total of 957 instances or features and six classification algorithms used in this study. The selected classification algorithms are kNN, J48 Decision Tree, Naïve Bayes, Random Tree, Random Forest and SMO. The first five algorithms (kNN, J48 Decision Tree, Naïve Bayes, Random Tree and Random Forest) are tested using default setting parameters in WEKA. SMO Classifier was experimented using different tuning parameters and kernels, which will be discussed further in the next section.

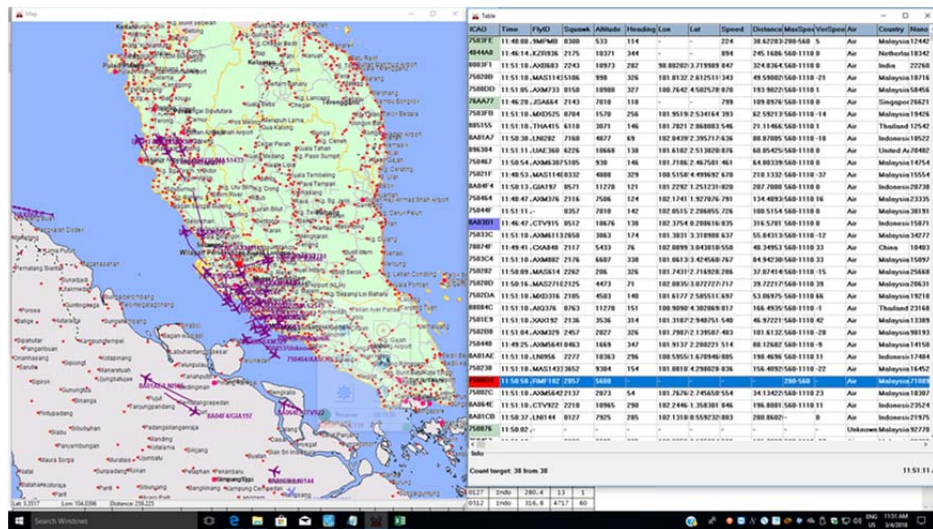


Figure 4: Aircraft mapping airways and databases on AMS.

Table 2: Classification attributes.

Attributes	Type
ICAO Number	String
Date of Flight	String
Time of Flight	String
Country of Origin	Nominal
Type of Aircraft	Nominal

#### 4. RESULTS AND DISCUSSION

The objective of this paper is mainly to analyse the performance of six classifiers (kNN, Naïve Bayes, Random Tree, Random Forest, J48 and SMO) using aircraft databases on WEKA Platform. There are in total of 957 instances of aircraft databases in this study. The attributes are segregated as ICAO number, date of flight, time of flight, country of origin and aircraft type. Only two attributes (aircraft type and country of origin) are implemented to predict the classifier's performance. We used several validation measurements to compare the performance of the classifiers between the observed and

predicted binary classifications. They are the True Positive (TP) rate, False Positive (FP) rate, Precision, Recall, F-measure, Mathews Correlation Coefficient (MCC), Receiver Operating Characteristic (ROC) area and Precision-Recall Curve (PRC) area. These analytical measurements are widely used in machine learning analysis and are associated based on mathematical relationships between TP rate, FP rate, Precision and Recall in their designated formulas.

#### 4.1 Results of Aircraft Type Classification

Based on the weighted averages in Tables 3-8 respectively, it is observed that kNN has correctly classified 957 instances with 99% of True Positive (TP) rate by using the 10-fold cross-validation technique to classify the aircraft type. The precision value is recorded at 99% for kNN. However, Naïve Bayes correctly classified 957 instances with 98% of TP rate by using the 10-fold cross-validation technique to classify the aircraft type. The precision value recorded is lower than kNN at 97%.

On the other hand, Random Tree correctly classified the 957 instances with 90% with precision value recorded at also 90% as shown in Table 5. In Table 6, it is observed that J48 correctly classified 957 instances with 100% of TP and precision rate. By looking at the classes classification for kNN, Naïve Bayes, Random Tree and J48, general aircraft type has the highest classification rate as compared to military and unknown aircraft.

Moreover, by adopting the 10-fold cross-validation technique, Random Forest correctly classified 957 instances with 100% TP rate. The precision value is also recorded at 100%. Finally, in Table 8, it is been observed that the SMO with linear kernel correctly classified 957 instances with 100% of TP rate. For Random Forest and SMO, all the types of aircrafts have shown highest classification of TP rate and precision at 100%.

**Table 3: Classification results for kNN for aircraft type.**

<i>Class</i>	<i>TP Rate</i>	<i>FP Rate</i>	<i>Precision</i>	<i>Recall</i>	<i>F-Measure</i>	<i>MCC</i>	<i>ROC Area</i>	<i>PRC Area</i>
General	1.00	0.05	0.98	1.00	0.99	0.97	1.00	1.00
Unknown	0.96	0.00	1.00	0.96	0.98	0.97	0.99	0.99
Military	0.50	0.00	1.00	0.5	0.67	0.71	1.00	1.00
<b>Weighted Avg.</b>	<b>0.99</b>	<b>0.03</b>	<b>0.99</b>	<b>0.99</b>	<b>0.99</b>	<b>0.97</b>	<b>0.99</b>	<b>0.99</b>

**Table 4: Classification results of Naive Bayes for aircraft type.**

<b>Class</b>	<b>TP Rate</b>	<b>FP Rate</b>	<b>Precision</b>	<b>Recall</b>	<b>F-Measure</b>	<b>MCC</b>	<b>ROC Area</b>	<b>PRC Area</b>
General	0.99	0.59	0.98	0.99	0.98	0.95	0.99	0.99
Unknown	0.95	0.008	0.98	0.95	0.97	0.95	0.99	0.99
Military	0.00	0.003	0.00	0.00	0.00	-0.004	0.95	0.21
<b>Weighted Avg.</b>	<b>0.98</b>	<b>0.04</b>	<b>0.97</b>	<b>0.98</b>	<b>0.97</b>	<b>0.94</b>	<b>0.99</b>	<b>0.99</b>

**Table 5: Classification results of Random Tree for aircraft type.**

<i>Class</i>	<i>TP Rate</i>	<i>FP Rate</i>	<i>Precision</i>	<i>Recall</i>	<i>F-Measure</i>	<i>MCC</i>	<i>ROC Area</i>	<i>PRC Area</i>
General	0.99	0.32	0.88	0.99	0.93	0.75	0.93	0.96
Unknown	0.68	0.001	0.96	0.68	0.80	0.75	0.93	0.87
Military	0.75	0.000	1.00	0.75	0.86	0.87	0.98	0.76
<b>Weighted Avg.</b>	<b>0.90</b>	<b>0.23</b>	<b>0.90</b>	<b>0.90</b>	<b>0.89</b>	<b>0.75</b>	<b>0.93</b>	<b>0.93</b>

**Table 6: Classification results of J48 classifier for aircraft type.**

<i>Class</i>	<i>TP Rate</i>	<i>FP Rate</i>	<i>Precision</i>	<i>Recall</i>	<i>F-Measure</i>	<i>MCC</i>	<i>ROC Area</i>	<i>PRC Area</i>
General	1.00	1.00	1.00	1.00	1.00	1.00	1.00	1.00
Unknown	1.00	1.00	1.00	1.00	1.00	1.00	1.00	1.00
Military	1.00	1.00	1.00	1.00	1.00	1.00	1.00	1.00
<b>Weighted Avg.</b>	<b>1.00</b>	<b>1.00</b>	<b>1.00</b>	<b>1.00</b>	<b>1.00</b>	<b>1.00</b>	<b>1.00</b>	<b>1.00</b>

**Table 7: Classification results of Random Forest for aircraft type.**

<i>Class</i>	<i>TP Rate</i>	<i>FP Rate</i>	<i>Precision</i>	<i>Recall</i>	<i>F-Measure</i>	<i>MCC</i>	<i>ROC Area</i>	<i>PRC Area</i>
General	1.00	1.00	1.00	1.00	1.00	1.00	1.00	1.00
Unknown	1.00	1.00	1.00	1.00	1.00	1.00	1.00	1.00
Military	1.00	1.00	1.00	1.00	1.00	1.00	1.00	1.00
<b>Weighted Avg.</b>	<b>1.00</b>	<b>1.00</b>	<b>1.00</b>	<b>1.00</b>	<b>1.00</b>	<b>1.00</b>	<b>1.00</b>	<b>1.00</b>

**Table 8: Classification results of SMO classifier using linear kernel for aircraft type.**

<i>Class</i>	<i>TP Rate</i>	<i>FP Rate</i>	<i>Precision</i>	<i>Recall</i>	<i>F-Measure</i>	<i>MCC</i>	<i>ROC Area</i>	<i>PRC Area</i>
General	1.00	1.00	1.00	1.00	1.00	1.00	1.00	1.00
Unknown	1.00	1.00	1.00	1.00	1.00	1.00	1.00	1.00
Military	1.00	1.00	1.00	1.00	1.00	1.00	1.00	1.00
<b>Weighted Avg.</b>	<b>1.00</b>	<b>1.00</b>	<b>1.00</b>	<b>1.00</b>	<b>1.00</b>	<b>1.00</b>	<b>1.00</b>	<b>1.00</b>

## 4.2 Results of Country of Origin Classification

By looking at the country of origin classification results in Tables 9-14, the best TP rate is 100%, which is gained by SMO with linear kernel. The accuracy rate is recorded at 99% for J48, 97% for kNN, and 87% for Naïve Bayes and Random Tree. Brunei, Qatar, Netherlands, Philippines and China's aircrafts are observed as the highest correctly classified rate as compared to other countries of origin based on ICAO number for kNN classification, while Malaysian aircraft has the highest correctly classification rate as compared to other countries of origin based on its ICAO number for Naïve Bayes classifier. For kNN classifier, low variance (features are tightly clustered together)

datasets might boost the accuracy for these four countries (Brunei, Qatar, Netherlands, Philippines and China) when looking at their data distribution graphically. Naïve Bayes is somehow superior in sparsely distributed data classification where it has widely known in text classification or string categorisation for large number of datasets from Malaysian aircraft. For Random Tree, it is observed that Brunei and China are correctly classified at the highest rate as compared to any other countries. In J48 and Random Forest, most of the countries of origin data are correctly classified at 100% based on their ICAO number. In SMO, Qatar, Netherlands and Philippines are among the highest TP rate. In conclusion, the performance of machine learning classifier is very dependable on the number of samples or features and the distribution of datasets. Small datasets can be compromised by using simple classifiers like kNN or decision tree while SMO can usually tolerates with any number of datasets since it provides multi choice of kernels to deal with different types of datasets.

**Table 9: Classification results of kNN for aircraft country of origin.**

<i>Class</i>	<i>TP Rate</i>	<i>FP Rate</i>	<i>Precision</i>	<i>Recall</i>	<i>F-Measure</i>	<i>MCC</i>	<i>ROC Area</i>	<i>PRC Area</i>
Malaysia	0.99	0.05	0.95	0.99	0.98	0.95	0.99	0.99
India	0.97	0.00	1.00	0.97	0.98	0.98	1.00	0.99
Indonesia	0.94	0.00	0.98	0.94	0.96	0.95	0.99	0.98
United States	0.98	0.00	1.00	0.98	0.99	0.99	1.00	1.00
Singapore	0.91	0.00	1.00	0.91	0.95	0.95	1.00	0.99
Brunei	1.00	0.00	1.00	1.00	1.00	1.00	1.00	1.00
Thailand	0.88	0.00	1.00	0.88	1.00	0.94	1.00	0.99
Qatar	1.00	0.00	1.00	1.00	1.00	1.00	1.00	1.00
Netherlands	1.00	0.00	1.00	1.00	1.00	1.00	1.00	1.00
Philippines	1.00	0.00	1.00	1.00	1.00	1.00	1.00	1.00
China	1.00	0.00	1.00	1.00	1.00	1.00	1.00	1.00
<b>Weighted Avg.</b>	<b>0.97</b>	<b>0.03</b>	<b>0.97</b>	<b>0.97</b>	<b>0.97</b>	<b>0.96</b>	<b>0.99</b>	<b>0.99</b>

**Table 10: Classification results of Naive Bayes for aircraft country of origin.**

<i>Class</i>	<i>TP Rate</i>	<i>FP Rate</i>	<i>Precision</i>	<i>Recall</i>	<i>F-Measure</i>	<i>MCC</i>	<i>ROC Area</i>	<i>PRC Area</i>
Malaysia	1.00	0.05	0.98	1.00	0.99	0.97	1.00	1.00
India	0.96	0.00	1.00	0.96	0.98	0.97	0.99	0.99
Indonesia	0.50	0.00	1.00	0.5	0.67	0.71	1.00	1.00
United States	0.63	0.01	0.96	0.63	0.76	0.77	0.99	0.99
Singapore	0.86	0.00	0.96	0.86	0.90	0.89	1.00	0.99
Brunei	0.89	0.00	1.00	0.89	0.94	0.94	1.00	1.00
Thailand	0.36	0.00	1.00	0.36	0.53	0.59	0.99	0.98
Qatar	0.27	0.00	1.00	0.27	0.43	0.52	1.00	1.00
Netherlands	0.17	0.00	1.00	0.17	0.29	0.41	1.00	1.00
Philippines	0.90	0.00	1.00	0.90	0.95	0.95	1.00	1.00
China	0.00	0.00	-	0.00	-	-	0.99	0.27
<b>Weighted Avg.</b>	<b>0.87</b>	<b>0.12</b>	<b>-</b>	<b>0.99</b>	<b>-</b>	<b>-</b>	<b>0.98</b>	<b>0.98</b>

**Table 11: Classification results of Random Tree for aircraft country of origin.**

<i>Class</i>	<i>TP Rate</i>	<i>FP Rate</i>	<i>Precision</i>	<i>Recall</i>	<i>F-Measure</i>	<i>MCC</i>	<i>ROC Area</i>	<i>PRC Area</i>
Malaysia	0.97	0.22	0.83	0.97	0.90	0.77	0.96	0.96
India	0.77	0.00	0.96	0.77	0.85	0.85	0.91	0.80
Indonesia	0.73	0.02	0.92	0.73	0.81	0.78	0.94	0.85
United States	0.77	0.00	0.97	0.77	0.86	0.86	0.92	0.80
Singapore	0.78	0.00	0.97	0.78	0.86	0.85	0.95	0.87
Brunei	1.00	0.00	0.90	1.00	0.95	0.95	0.99	0.90
Thailand	0.76	0.00	0.95	0.76	0.84	0.85	0.94	0.78
Qatar	0.82	0.00	1.00	0.82	0.90	0.90	0.95	0.83
Netherlands	0.58	0.00	1.00	0.58	0.74	0.76	0.76	0.59
Philippines	0.80	0.00	0.73	0.80	0.76	0.76	0.99	0.61
China	1.00	0.00	1.00	1.00	1.00	1.00	1.00	1.00
<b>Weighted Avg.</b>	<b>0.87</b>	<b>0.12</b>	<b>0.88</b>	<b>0.87</b>	<b>0.87</b>	<b>0.80</b>	<b>0.80</b>	<b>0.90</b>

**Table 12: Classification results of Naive Bayes for aircraft country of origin.**

<i>Class</i>	<i>TP Rate</i>	<i>FP Rate</i>	<i>Precision</i>	<i>Recall</i>	<i>F-Measure</i>	<i>MCC</i>	<i>ROC Area</i>	<i>PRC Area</i>
Malaysia	1.00	0.00	0.99	1.00	0.99	0.99	1.00	1.00
India	1.00	0.00	1.00	1.00	1.00	1.00	1.00	1.00
Indonesia	0.99	0.00	1.00	0.99	1.00	0.99	1.00	1.00
United States	1.00	0.01	1.00	1.00	1.00	1.00	1.00	1.00
Singapore	1.00	0.00	1.00	1.00	1.00	1.00	1.00	1.00
Brunei	1.00	0.00	1.00	1.00	1.00	1.00	1.00	1.00
Thailand	1.00	0.00	1.00	1.00	1.00	1.00	1.00	1.00
Qatar	1.00	0.00	1.00	1.00	1.00	1.00	1.00	1.00
Netherlands	1.00	0.00	1.00	1.00	1.00	1.00	1.00	1.00
Philippines	1.00	0.00	1.00	1.00	1.00	1.00	1.00	1.00
China	1.00	0.00	1.00	1.00	1.00	1.00	1.00	1.00
<b>Weighted Avg.</b>	<b>0.99</b>	<b>0.00</b>	<b>0.99</b>	<b>0.99</b>	<b>0.99</b>	<b>0.99</b>	<b>1.00</b>	<b>1.00</b>

**Table 13: Classification results of Random Forest for aircraft country of origin.**

<i>Class</i>	<i>TP Rate</i>	<i>FP Rate</i>	<i>Precision</i>	<i>Recall</i>	<i>F-Measure</i>	<i>MCC</i>	<i>ROC Area</i>	<i>PRC Area</i>
Malaysia	1.00	0.01	0.99	1.00	0.99	0.99	1.00	1.00
India	1.00	0.00	1.00	1.00	1.00	1.00	1.00	1.00
Indonesia	0.99	0.00	1.00	0.99	0.99	0.99	1.00	1.00
United States	1.00	0.00	1.00	1.00	1.00	1.00	1.00	1.00
Singapore	1.00	0.00	1.00	1.00	1.00	1.00	1.00	1.00
Brunei	1.00	0.00	1.00	1.00	1.00	1.00	1.00	1.00
Thailand	1.00	0.00	1.00	1.00	1.00	1.00	1.00	1.00
Qatar	1.00	0.00	1.00	1.00	1.00	1.00	1.00	1.00
Netherlands	1.00	0.00	1.00	1.00	1.00	1.00	1.00	1.00
Philippines	1.00	0.00	1.00	1.00	1.00	1.00	1.00	1.00
China	1.00	0.00	1.00	1.00	1.00	1.00	1.00	1.00
<b>Weighted Avg.</b>	<b>0.99</b>	<b>0.003</b>	<b>0.99</b>	<b>0.99</b>	<b>0.99</b>	<b>0.99</b>	<b>1.00</b>	<b>1.00</b>

By looking at the country of origin with different kernels classifications for SMO (Table 14), the weighted TP rate is 96% for Radial Basis Function (RBF kernel) and 100% for linear kernel. Hence, in this study, it is clearly understood that linear kernel outperformed RBF kernel in all eight measurements (TP rate, FP rate, Precision, Recall, F-measure, MCC, ROC area and PRC area). This is because, in decision tree leaves, we can see that the highest rank of attributes used for classification is mainly based on ICAO number, where the data distribution is straightforward and linear. In contrast, RBF kernel in SVM is well suited for noisy and high variance data.

### 4.3 Parameter Optimisation in kNN and SMO Classifier

In kNN, we have varied the number of neighbours  $k$  to observe the performance accuracy. For  $k > 1$ , the TP rate measured is gradually reduced to 11.42% when  $k = 6$ . Furthermore, we have extended our research to foresee the performance of SMO, where we have varied  $C$  (a parameter that trades off margin maximisation and error toleration) and gamma  $\gamma$  values of RBF kernel. In SMO,  $C$  is the parameter that trades off misclassification of training examples against simplicity of the decision surface. It can be defined as the spread of the kernel and the decision boundary of the model. A low  $C$  makes the decision surface smooth, while a high  $C$  aims at classifying all training examples correctly by giving the model freedom to select more samples as support vectors. The  $\gamma$  value is the inverse of the standard deviation of the RBF kernel (Gaussian) which is used as a similarity measure between two points. Intuitively, a small  $\gamma$  value defines a Gaussian function with large variance. In Table 15, it is observed that,  $\gamma = 0.5$  with  $C = 1.0$  is the best tuned parameter for RBF kernel to achieve 96% true classification rate as compared to smaller  $\gamma$  value. Nevertheless, the accuracy seems to decrease when  $\gamma$  is set bigger than 0.5 due to overfitting and poor regularisation problems.

In Table 16, it is observed that higher values of  $C$  gives the classification model freedom to choose more samples as support vectors. In this case, the classification model is getting more complex with larger memory needed to accommodate large number of support vectors. Hence, the execution time in the WEKA platform is higher as compared to lower  $C$  values. In this study, the best  $C$  parameter in this case is recorded at 3.0 and  $\gamma = 0.5$  with larger number of support vectors recorded at 170 as compared to lower  $C$  values, which are 162 and 132. Hence, the resulting classifier will have low bias but high variance model. Finally, for intermediate  $\gamma$  value, we observed an equally performing model when  $C$  becomes too large. This shows that the model is starting to regularised by limiting the number of support vectors for faster prediction (Kamarudin *et al.*, 2017).

### 4.4 Overall Comparison of Results of Aircraft Databases using Different Classifiers

By implementing high feature space of 957 features, SMO with linear kernel outperformed the other classifiers in terms of classification accuracy, where both classification results (aircraft type and country of origin) in Tables 17 and 18 have obtained 100% TP rate as compared with other five classifiers. It is known that SMO is a powerful classifier to handle high dimensional data sets and is computationally efficient when handling non-separable data with multi attributes.



**Table 14: Classification results of SMO classifier using different kernels for aircraft country of origin.**

<i>Performance</i>	<i>TP Rate</i>		<i>FP Rate</i>		<i>Precision</i>		<i>Recall</i>		<i>F-Measure</i>		<i>MCC</i>		<i>ROC Area</i>		<i>PRC Area</i>	
	Class/Kernel	RBF	Linear	RBF	Linear	RBF	Linear	RBF	Linear	RBF	Linear	RBF	Linear	RBF	Linear	RBF
Malaysia	0.99	1.00	0.09	0.00	0.93	1.00	0.99	1.00	0.96	1.00	0.91	1.00	0.95	1.00	0.92	1.00
India	0.93	1.00	0.00	0.00	1.00	1.00	0.93	1.00	0.97	1.00	0.97	1.00	1.00	1.00	1.00	1.00
Indonesia	0.93	1.00	0.00	0.00	0.99	1.00	0.93	1.00	0.96	1.00	0.95	1.00	0.98	1.00	0.94	1.00
United States	0.95	1.00	0.00	0.00	1.00	1.00	0.95	1.00	0.98	1.00	0.98	1.00	1.00	1.00	1.00	1.00
Singapore	0.86	1.00	0.00	0.00	1.00	1.00	0.86	1.00	0.92	1.00	0.92	1.00	0.96	1.00	0.89	1.00
Brunei	0.89	1.00	0.00	0.00	1.00	1.00	0.89	1.00	0.94	1.00	0.94	1.00	1.00	1.00	1.00	1.00
Thailand	0.84	1.00	0.00	0.00	1.00	1.00	0.84	1.00	0.91	1.00	0.91	1.00	1.00	1.00	1.00	1.00
Qatar	1.00	1.00	0.00	0.00	1.00	1.00	1.00	1.00	1.00	1.00	1.00	1.00	1.00	1.00	1.00	1.00
Netherlands	1.00	1.00	0.00	0.00	1.00	1.00	1.00	1.00	1.00	1.00	1.00	1.00	1.00	1.00	1.00	1.00
Philippines	1.00	1.00	0.00	0.00	1.00	1.00	1.00	1.00	1.00	1.00	1.00	1.00	1.00	1.00	1.00	1.00
China	0.00	1.00	0.00	0.00	-	1.00	0.00	1.00	-	1.00	-	1.00	0.44	1.00	0.00	1.00
<b>Weighted Avg.</b>	<b>0.96</b>	<b>1.00</b>	<b>0.05</b>	<b>0.00</b>	<b>-</b>	<b>1.00</b>	<b>0.96</b>	<b>1.00</b>	<b>-</b>	<b>1.00</b>	<b>-</b>	<b>1.00</b>	<b>0.97</b>	<b>1.00</b>	<b>0.94</b>	<b>1.00</b>

**Table 15: Classification results of SMO classifier using RBF kernel with different gamma  $\gamma$  values for aircraft country of origin.**

<i>Performance</i>	<i>TP Rate (True Positive Rate)</i>						
<b>Class/Kernel</b>	<b>RBF C = 1.0 <math>\gamma = 0.01</math></b>	<b>RBF C = 1.0 <math>\gamma = 0.06</math></b>	<b>RBF C = 1.0 <math>\gamma = 0.1</math></b>	<b>RBF C = 1.0 <math>\gamma = 0.2</math></b>	<b>RBF C = 1.0 <math>\gamma = 0.5</math></b>	<b>RBF C = 1.0 <math>\gamma = 1.5</math></b>	<b>RBF C = 1.0 <math>\gamma = 2.0</math></b>
Malaysia	1.00	1.00	1.00	1.00	0.99	0.99	1.00
India	0.00	0.83	0.83	0.87	0.93	0.23	0.23
Indonesia	0.00	0.60	0.81	0.89	0.93	0.53	0.32
United States	0.00	0.51	0.95	0.95	0.95	0.40	0.35
Singapore	0.00	0.43	0.79	0.83	0.86	0.36	0.30
Brunei	0.00	0.78	1.00	1.00	0.89	0.78	0.78
Thailand	0.00	0.48	0.84	0.84	0.84	0.44	0.40
Qatar	0.00	0.82	1.00	1.00	1.00	0.64	0.55
Netherlands	0.00	1.00	1.00	1.00	1.00	0.08	0.08
Philippines	0.00	0.80	1.00	1.00	1.00	0.80	0.80
China	0.00	0.00	0.00	0.00	0.00	0.00	0.00
<b>Weighted Avg.</b>	<b>0.52</b>	<b>0.81</b>	<b>0.93</b>	<b>0.95</b>	<b>0.96</b>	<b>0.73</b>	<b>0.69</b>

**Table 16: Classification results of SMO classifier using RBF kernel with different C values for aircraft country of origin.**

<i>Performance</i>	<i>TP Rate (True Positive Rate)</i>							
<b>Class/Kernel</b>	<b>RBF C = 0.1, <math>\gamma = 0.5</math></b>	<b>No. of support vectors</b>	<b>RBF C = 1.0, <math>\gamma = 0.5</math></b>	<b>No. of support vectors</b>	<b>RBF C = 3.0, <math>\gamma = 0.5</math></b>	<b>No. of support vectors</b>	<b>RBF C = 5.0, <math>\gamma = 0.5</math></b>	<b>No. of support vectors</b>
General	1.00		1.00		1.00		1.00	
Military	0.00		0.89		0.97		0.97	
Unknown	0.00	132	0.25	162	1.00	170	1.00	170
<b>Weighted Average</b>	<b>0.70</b>		<b>0.96</b>		<b>0.99</b>		<b>0.99</b>	

**Table 17: Comparative analysis of different classifiers for aircraft type (the best results are in bold).**

<i>Classifier/Performance</i>	<i>True Rate</i>	<i>False Rate</i>	<i>Precision</i>
kNN	0.99	0.03	0.99
Naïve Bayes	0.98	0.04	0.97
Random Tree	0.90	0.23	0.90
<b>J48</b>	<b>1</b>	<b>0.00</b>	<b>1</b>
<b>Random Forest</b>	<b>1</b>	<b>0.00</b>	<b>1</b>
<b>SMO (linear kernel)</b>	<b>1</b>	<b>0.00</b>	<b>1</b>

**Table 18: Comparative analysis of different classifiers for aircraft country of origin (the best results are in bold).**

<i>Classifier/Performance</i>	<i>True Rate</i>	<i>False Rate</i>	<i>Precision</i>
kNN	0.97	0.03	0.97
Naïve Bayes	0.87	0.12	-
Random Tree	0.87	0.12	0.88
J48	0.99	0.003	0.99
Random Forest	0.99	0.003	0.99
<b>SMO (linear kernel)</b>	<b>1.00</b>	<b>0.00</b>	<b>1.00</b>

## 5. CONCLUSION

This research implemented six classification algorithms, which are kNN, Naive Bayes, Random Tree, J48, Random Forest Tree and SMO, on AMS databases to classify aircraft type and country of origin using WEKA workbench. We applied real time data of aircrafts consisting of ICAO number, flight date, flight time, country of origin and aircraft type, which were collected from AMS in one-hour duration. In comparison with other classifiers, SMO with linear kernel was identified as the best classifier in terms of classification accuracy which is 100% of TP rate in both experiments. Future works will be focusing on adding more attributes of aviation data to predict aircraft flight pattern to measure air traffic growth and promote flight safety.

## ACKNOWLEDGMENT

The authors wish to thank the Spectrum Security & Monitoring Lab, Cyber Security Centre, National Defence University of Malaysia (UPNM) for the use of Aircraft Monitoring System (AMS) facility. This study was supported using academic budget from UPNM.

## REFERENCES

- Aha, D.W., Kibler, D. & Albert, M.K. (1991). Instance-based learning algorithms. *Mach. Learn.*, **6**:37-66.
- Ancona, N., Maglietta, R. & Stella, E. (2004). Sparse representations and performances in support vector machines. *Proc. Int. Conf. Mach. Learn. Appl. (ICMLA)*, Louisville, Kentucky, USA, pp. 29-38.
- Asif, R., Merceron, A., Ali, S.A. & Haider, N.G. (2017). Analysing undergraduate students' performance using educational data mining. *Comput. & Educ.*, **113**:177-194.
- Bay, S.D. & Schwabacher, M. (2003). Mining distance-based outliers in near linear time with randomization and a simple pruning rule. *Proc. 9<sup>th</sup> ACM SIGKDD Int. Conf. Know. Discovery Data Mining*, Washington, pp. 29-38.
- Belcastro, L., Marozzo, F., Talia, D. & Trunfio, P. (2016). Using scalable data mining for predicting flight delays. *ACM T. Intel. Syst. Tec. (TIST)*, **8**:5.
- Breiman, L. (2001). Random forests. *Mach. Learn.*, **45**:5-32.
- Busquets, J.G., Alonso, E. & Evans, A. (2016). Application of data mining to forecast air traffic: a 3-stage model using discrete choice modelling, *Proc. 16<sup>th</sup> AIAA Aviation Tech., Integration Operations Conf.*, Washington D.C., USA, pp. 1-9.
- Campanelli, B., Fleurquin, P., Eguíluz, V., Ramasco, J., Arranz, A., Extebarria, I. & Ciruelos, C. (2014). Modeling reactionary delays in the European air transport network. *Proc SESAR Innovation Days 2014*, 25-27 November 2014.

- Chaurasia, V. & Pal, S. (2014). A novel approach for breast cancer detection using data mining techniques. *Int. J. Inn. Res. Comput. Commun. Eng.*, **2**:2456-2465.
- Cheng, J., Rong, C., Ye, H. & Zheng, X. (2015). Risk management using big real-time data. *IEEE Proc. 7<sup>th</sup> Int. Conf. Cloud Comput. Tech. Sci.*, Vancouver, Canada, pp. 542–547.
- Cios, K.J., Pedrycz, W., Swiniarski, R.W. & Kurgan, L.A. (2007). *Data Mining: A Knowledge Discovery Approach*. Springer Science & Business Media, Spring Street, New York.
- Das, S., Matthews, B.L., Srivastava, A.N, & Oza, N.C. (2010). Multiple kernel learning for heterogeneous anomaly detection: algorithm and aviation safety case study. *Proc. 16<sup>th</sup> ACM SIGKDD Int. Conf. Know. Discovery Data Mining*, Washington DC, DC, USA, pp. 47-56.
- Dunham, M.H. (2006). *Data Mining: Introductory and Advanced Topics*. Pearson Education, India.
- Fayyad, U., Piatetsky-Shapiro, G. & Smyth, P. (1996). The KDD process for extracting useful knowledge from volumes of data. *Commun. ACM*, **39**:27-34.
- Friedman, N., Geiger, D. & Goldszmidt, M. (1997). Bayesian network classifiers. *Mach. Learn.*, **29**: 131-163.
- Hall, M., Frank, E., Holmes, G., Pfahringer, B., Reutemann, P. & Witten, I. H. (2009). The WEKA data mining software: an update. *ACM SIGKDD Explorations Newsl.*, **11**:10-18.
- Han, J., Pei, J. & Kamber, M. (2011). *Data mining: concepts and techniques*. Elsevier, Waltham, MA 02451, USA.
- James, G., Witten, D., Hastie, T., & Tibshirani, R. (2013). *An Introduction to Statistical Learning*. Springer, New York.
- Janakiraman, V.M. & Nielsen, D. (2016). Anomaly detection in aviation data using extreme learning machines. *Proc. IEEE IJCNN*, Vancouver, BC, Canada, pp. 1993-2000.
- John, G.H., & Langley, P. (1995). Estimating continuous distributions in Bayesian classifiers. *Proc. 11<sup>th</sup> Conf. Uncertainty Artif. Int.*, Montreal, Canada, pp. 338-345
- Kamarudin, N.D., Ooi, C.Y., Kawanabe, T., Odaguchi, H. & Kobayashi, F. (2017). A fast SVM-based tongue's colour classification aided by k-means clustering identifiers and colour attributes as computer-assisted tool for tongue diagnosis. *J. Healthc. Eng.*, **13**: 1-13.
- Kim, B., Tunas, N. & Green, A. (2016). Analysing risks for home loans during financial crisis of 2008 using data mining. *Issues Inf. Syst.*, **17**:206-211.
- Mack, D.L., Biswas, G., Koutsoukos, X.D. & Mylaraswamy, D. (2017). Learning bayesian network structures to augment aircraft diagnostic reference models. *IEEE T. Autom. Sci. Eng.*, **14**:358-369.
- Manley, B. & Sherry, L. (2008). Impact of ground delay program rationing rules on passenger and airline equity. *Proc. Int. Multi-Conf. on Engineering Tech. Innovation (IMET 2008)*, Bethesda, MD, USA, pp. 325–330.
- Mellat-Parast, M., Golmohammadi, D., McFadden, K. & Miller, J. (2015). Linking business strategy to service failures and financial performance: Empirical evidence from the U.S. domestic airline industry. *J. Operat. Manage.*, **38**: 14–24.
- Mindmatics Sdn Bhd. (2017). *AMS Operating Procedure Manual*. Mindmatics Sdn Bhd, Kuala Lumpur.
- Nazeri, Z. & Zhang, J. (2002). Mining aviation data to understand impacts of severe weather on airspace system performance. *Proc. Int. Conf. Inf. Tech.: Coding Computing*, Las Vegas, USA, pp.518-523.
- Nohuddin, P.N.E., Zainol, Z., Lee, A.S.H., Nordin, A.I. & Yusoff, Z. (2018). A Case study in knowledge acquisition for logistic cargo distribution data mining framework. *Int. J. Adv. Appl. Sci.*, **5**: 8-14.
- Nusyirwan, I. & Rohani, J. M. (2017). Study of air traffic over KLFIR. *IOP Conf. Ser.: Mater. Sci. Eng.* **270**: 012033.
- Pai, V. (2010). On the factors that affect airline flight frequency and aircraft size. *J. of Air Transport Manage.*, **16**: 169–177.
- Pan, X., Gu, H., & Sun, C. (2009). A classification approach to identify definitions in aviation domain. *Proc. Chinese Conf. Pattern Recogn.*, Nanjing, China, pp.1-7.

- Patil, M. M., Hanni, A., Tejeshwar, C., & Patil, P. (2017). A qualitative analysis of the performance of MongoDB vs MySQL database based on insertion and retrieval operations using a web/android application to explore load balancing—Sharding in MongoDB and its advantages. *Proc. Int. Conf. IoT Soc., Mob., Analytics Cloud*, Palladam, India, pp. 325-330.
- Phakhounthong, K., Chaovalit, P., Jittamala, P., Blacksell, S. D., Carter, M. J., Turner, P., Chheng, K., Sona, S., Kumar, V., Day, N. P. J., White, L.J., Pan-ngum, W., (2018). Predicting the severity of dengue fever in children on admission based on clinical features and laboratory indicators: application of classification tree analysis. *BMC Pediatr.*, **18**: 109.
- Platt, J. C. (1999). 12 fast training of support vector machines using sequential minimal optimization. *Advances in Kernel Methods*. The MIT Press, London, United Kingdom.
- Quinlan, J. R. (1993). *C4. 5: Programming for Machine Learning*. Morgan Kauffmann Publishers, San Mateo, CA94403, United States.
- Rahim, N., Taib, S., & Abidin, A. (2017). Dengue fatality prediction using data mining. *J. Fund. Appl. Sci.*, **9**: 671-683.
- Roiger, R. J. (2017). *Data Mining: A Tutorial-Based Primer*. CRC Press, Boca Raton, Florida.
- Rushin, G., Stancil, C., Sun, M., Adams, S. & Beling, P. (2017). Horse race analysis in credit card fraud—deep learning, logistic regression, and Gradient Boosted Tree. *Syst. Inf. Eng. Des. Symp. (SIEDS)*, Charlottesville, VA, USA, pp.117-121.
- Save, P., Tiwarekar, P., Jain, K.N. & Mahyavanshi, N. (2017). A novel idea for credit card fraud detection using decision tree. *Int. J. Comput. Appl.*, **161**:6-9.
- Schumann, J.M., Mbaya, T. & Mengshoel, O. J. (2011). Bayesian software health management for aircraft guidance, navigation, and control. *Proc. Annual Conf. Prognostics Health Manage. Soc.*, Montreal, Quebec, Canada, pp.1-10.
- Sternberg, A., Soares, J., Carvalho, D. & Ogasawara, E. (2017). *A Review on Flight Delay Prediction*. Cornell University Library, New York, United States.
- Sudhakar, M. & Reddy, C. (2016). Two step credit risk assessment models for retail bank loan applications using decision tree data mining technique. *Int. J. Advanced Res. Comput. Eng. & Tech.*, **5**:705-718.
- Weber, L. (2012). *International Civil Aviation Organization (ICAO)*: Kluwer Law International.
- Witten, I.H., Frank, E., Hall, M.A. & Pal, C.J. (2016). *Data Mining: Practical Machine Learning Tools and Techniques*. Morgan Kaufmann, Cambridge, MA, United States.
- Xing, W., Guo, R., Petakovic, E. & Goggins, S. (2015). Participation-based student final performance prediction model through interpretable genetic programming: integrating learning analytics, educational data mining and theory. *Comput. Hum. Behav.*, **47**:168-181.
- Yee, O.S., Sagadevan, S. & Malim, N.H.A.H. (2018). Credit card fraud detection using machine learning as data mining technique. *J. Telecomm., Electron. Comput. Eng.*, **10**: 23-27.

# EVALUATION OF SCHEME SELECTION AND PARAMETER EFFECTS IN THE RECONFIGURABLE TRANSMITTING POWER IN WIRELESS NETWORK-ON-CHIP

Mohd Shahrizal Rusli<sup>1\*</sup>, Nur Diyana Kamarudin<sup>2</sup>, Ab. Al-Hadi Ab. Rahman<sup>1</sup> & M. Nadzir Marsono<sup>1</sup>

<sup>1</sup>Electronic and Computer Engineering Department, Faculty of Electrical Engineering, Universiti Teknologi Malaysia (UTM), Malaysia

<sup>2</sup>Cyber Security Centre, National Defense University Malaysia (UPNM), Malaysia

\*Email: shahrizal@fke.utm.my

## ABSTRACT

*Wireless Network-on-Chip (WiNoC) introduces long-range and high bandwidth radio frequency (RF) interconnects that can possibly reduce the multi-hop communication of the planar metal interconnects in conventional NoC platforms. In WiNoC, RF transceivers account for a significant power consumption, particularly its transmitter, out of its total communication energy. Current WiNoC architectures employ constant maximum transmitting power for communicating radio hubs regardless of physical location of the receiver. Recently, two closed loop reconfigurable power schemes that dynamically calibrate the transmitting power level needed for communication between the hubs based on bit error rate (BER) have been proposed. In this paper, these schemes are compared in terms of latency, power and area overheads. Both schemes achieve significant energy savings with limited performance degradation and insignificant impact on throughput. Only a small fraction of both area and power overheads are introduced (about 0.1%). The schemes are general and can be applied on any WiNoC architecture.*

**Keywords:** *Wireless network-on-chip (WiNoC); power reconfiguration; distributed management; centralised management; bit error rate (BER).*

## 1. INTRODUCTION

Chip Multiprocessors (CMP) is gaining significant attention recently in biomedical, multimedia, aviation and several other applications. This involves quintillion operations per second to meet the target applications. The existing Network-on-Chip (NoC) does not scale to very large-scale core counts due to several challenges. In addition to that, the International Technology Roadmap for Semiconductors (ITRS) predicts that the industry will need to explore new on-chip communication perspectives because the wire-based interconnects will no longer improve performance metric in future many-core architectures. Hence, several improved NoC architectures have been proposed such as 3D NoC (Pavlidis & Friedman, 2007; Feero & Pande, 2009), photonic NoC (Shacham *et al.*, 2008) and WiNoC (Ganguly *et al.*, 2010; DiTomaso *et al.*, 2011; Deb *et al.*, 2012; Rezaei *et al.*, 2016). WiNoC provides improvement to design low-power and high-bandwidth massive multicore chips. WiNoC introduces long-range and high bandwidth radio frequency (RF) interconnects that can possibly reduce the multi-hop communication of the planar metal interconnects in conventional NoC platforms. The WiNoC communication infrastructure is constituted by a wireless backbone that is augmented on the conventional NoC architectures. This new structure requires new hardware resources such as transceivers and antennas. Unfortunately, area overhead is significantly introduced by the new structures, encouraging several architectures proposed to compromise between the communication capability and the area overhead (Deb *et al.*, 2012).

On average, implementing WiNoC architecture improves performance and energy savings of about 20 and 30% respectively, over the fully wired NoC links (Deb *et al.*, 2012; DiTomaso *et al.*, 2013).

Power and energy management continue to play an important role in the on-chip communication issue, even for WiNoC. Adding wireless link structures increase total power consumption. Recently, several energy-efficient transceiver designs have been proposed to overcome the energy consumption overhead introduced in WiNoC (Catania *et al.*, 2016; Hemanta *et al.*, 2017). Hence, there is a need to manage the power consumption at both wired and wireless links. It has been shown that RF transmitter front-end dissipates power by about 50% in Daly & Chandrakasan (2007) and about 74% in Yu *et al.* (2014) for network sizes of 128, 256 and 512 cores in terms of WiNoC transceiver consumption. Current WiNoC efforts employ the maximum transmitting power for each transmitter regardless of the physical location of the receiver antenna. Low power techniques such as voltage-frequency island (Ryan *et al.*, 2016) and dynamic voltage scaling as well as static power (Hemanta *et al.*, 2016) in WiNoC components have been proposed.

Considering the above factors, implementing a dynamic power reconfiguration on fixed location offers improvement in energy dissipation while satisfying system performance constraint as opposed to one-off power reconfiguration scheme as proposed by Mineo *et al.* (2014). This is due to the fact that attenuation characterisation has to be made practical during design time with a very accurate model that takes into account all the material effects on on-chip wireless transmission. The dynamic approach however allows for dynamic transmission power calibration after a certain period. In this paper, two schemes that dynamically reconfigure transmitting power at transmitter module are compared and presented. These approaches apply a closed loop self-reconfigure scheme at run-time for transmitting power at each transmitter based on packet granularity.

The rest of the paper is organised as follow. In Section 2, the theoretical concept of centralised and distributed power schemes are introduced. The centralised scheme (Rusli *et al.*, 2014) allows transmitting power configurability to be done by a centralised power manager based on bit error rate (BER) information of WiNoC transceivers and the scheme is described whereby the distributed self-reconfigure transmission power scheme (Mineo *et al.*, 2015) is performed by respective radio hub. Finally, the experimental results for various specific cases are shown in Section 3.

## 2. RECONFIGURABLE TRANSMISSION SCHEMES

### 2.1 Reconfigurable Transmission Scheme

In this section, a comparison between centralised and distributed power management scheme is detailed out. In addition, the basic requirement of transmission power to guarantee a certain BER is introduced followed by the design implementation of WiNoC architecture using distributed and centralised power management scheme.

### 2.2 Signal Strength Requirement

Equations 1 and 2 are used to estimate signal attenuation due to the wireless medium. Since the reliability of the Amplitude Shift Keying – On/Off Key (ASK-OOK) modulation is related to the energy per bit,  $E_b$ , spent to reach the receiver's antenna, the power required by the transmitter for each value of the attenuation  $G_a$  can be determined as follows:

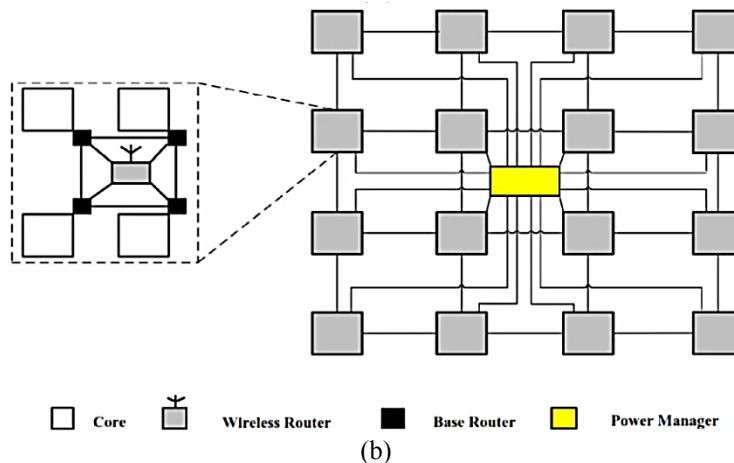
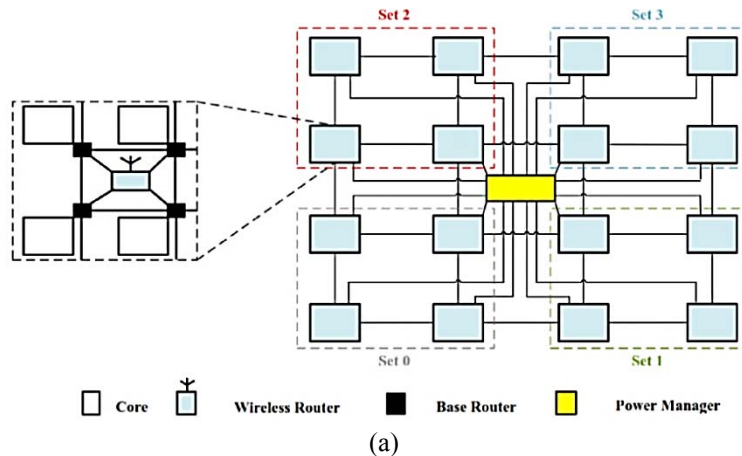
$$BER = Q \sqrt{\frac{E_b}{N_o}} \quad (1)$$

where  $N_o$  is the transceiver noise spectral density and the  $Q$  function is the tail probability of the standard normal distribution. Since  $E_b = P_r/R_b$ , where  $R_b$  is the data rate, the minimum transmitting power to reach a certain receiver guaranteeing a maximum BER can be computed as:

$$P_t(dB) = P_r(dB) - G_a(dB) \quad (2)$$

where  $P_r(dB)$  is power received at the receiver while  $G_a(dB)$  is computed using a field solver with the Friis Transmission Equation (Kim *et al.*, 2005) when power is expressed in  $dB$  and converted to  $dBm$ . The main idea in the proposed architecture is to introduce power configurability to the transceiver based on BER information. Based on the Friis formula, the source and destination transceivers' power profiles are characterised by different attenuation gain,  $G_a$ . Equipped with a good error detection module at the receiver module, the architecture is assumed to be able to provide accurate statistical bit error information to the power management scheme. To the best of our knowledge, there has been no proposed work on detecting or measuring the BER in WiNoC. However, the error detection can be designed based on incomplete arriving packets or erroneous packets detected by the receiver module.

In the distributed scheme (Mineo *et al.*, 2015), WiNoC operates in two periods, namely Reconfiguration Period (RP) and Reconfiguration State (RS). Receiver radio hub module collects BER information from each radio hub during RP that adopts the power requirement of both source and destination radio hubs, which guarantee reliability and finally distributes the decision for self-calibration transmission power at the radio hub level. Each radio hub consists of reconfigurable variable gain controller (R-VGA) that drives the reconfigurable power system by selecting the transmitting power level in the form of lookup table updated by the distributed algorithm. As soon as the destination radio hub detects a string of packet errors in incoming packets from source radio hub, R-VGA of the source radio hub is informed to increase its transmitting power for the next communication cycle.



**Figure 1: Proposed power manager module implemented on two WiNoC architectures: (a) iWise (b) WCube.**



The power management is activated as soon as an error is detected in a packet with source radio hub. There is a control network circuit for sending a simple reconfiguration command to the VGA of source radio hub for increasing or decreasing the transmitting power when communicating with receiver.

In comparison, Figure 1 shows the centralised power management architecture, applied on the two most commonly used WiNoC architectures, namely WCube and iWise. Similar to the previous scheme, two periods are employed: RP and RS. During RP, the power manager remains in its idle state for a number of clock cycles. It then switches to RS, whereby it collects the BER statistics from the radio hubs and based on the power management strategy, updates the look-up table of the VGA controller in each radio hub. During RS, WiNoC is stalled and it does not allow any data communication. The algorithm is formulated by the work in Rusli *et al.* (2014).

### 2.3 Centralised and Distributed Reconfigurable Transmitting Power Schemes

Table 1 shows the comparison between the centralised and distributed power management scheme. The significant difference between both schemes is in the error control, error detection frequency and stall condition of the WiNoC during power management. Error control acknowledgement in the centralised scheme is not opted assuming that there is no closed loop centralised acknowledgement.

The similar features of both schemes are: 1) Both proposed works utilise BER detection to reconfigure transmitting power. However, the work can be proposed based on the number of erroneous packets. 2) Both modules are equipped with an error detection module respectively, which reports BER values for decision-making. The rest of the features are differences of both schemes.

**Table 1: Comparison between centralised and distributed transmitting power scheme.**

<b>Criteria/Scheme</b>	<b>Centralised</b>	<b>Distributed</b>
<b>Signal Strength Requirement</b>	Packet error detection (BER)	Packet error detection (BER)
<b>Error Detection</b>	Triggered by error detection module in WiNoC	Triggered by error detection module in WiNoC
<b>Error Control Acknowledgment</b>	No mechanism for knowing whether the reconfigurable scheme is adopted by the respective core or not	Yes. Done via control packet transmitted by transmitting radio hub
<b>Frequency of Error Detection</b>	Based on interval. WiNoC is stalled, power management takes place	Throughout platform runtime. Frequency depends on network size. Larger network size, the lesser the frequency
<b>Mechanism</b>	WiNoC stalled, power manager calibrates power level of all cores	On runtime, token ring flow control mechanism adopted in control network without interfering actual data transmission. Acknowledgment sent by transmitter hub.

## 2.4 Implementation on WiNoC Platforms

The first design considered for implementation is the centralised power management on the iWise and WCube platforms. A centralised power manager is located on the wireless subnet layer and is connected to each radio hub via dedicated control link. It regulates the transmission power based on online closed-loop control mechanism. Overall, given a certain reliability requirement expressed by means of a maximum allowable error rate for the platform, the manager allows dynamic tuning of transmitting power for each transmitter and receiver communication pair with minimum energy consumption. Figure 1 visualises the proposed designs on both the aforementioned WiNoC architectures.

In the distributed scheme, the power management scheme is regulated by the control switch employing token ring flow control for on-line power self-calibration. Each receiver periodically informs its dedicated power management module inside the control switch about the error rate detected in packets received from transmitters. Based on the certain allowable reliability requirement expressed by the error rate quantity, the transmitter and receiver pair dynamically tunes the transmitting power to meet the requirement with minimum energy consumption. The control information is sent through the wired links circulating the entire platform in the ring protocol manner.

Figure 2 visualises the proposed designs on both WiNoC architectures. The proposed distributed power management only allows a one-way power management regulation that is performed by the control switches in the control network. At the beginning of the power management, the control switch with identification number 0 (located at the right top most layer in the figure) activates the token as soon as the network operates. In the best case scenario, the token hops on the entire network and returns back to the control switch 0 after 16 cycles due to only one clock cycle being needed to pass on each switch. In the worst case scenario, when all radio hubs generate control packets to regulate the power management, the token return time may take approximately 32 cycles, considering two clock cycles are spent to generate and passing the token to the next radio hubs.

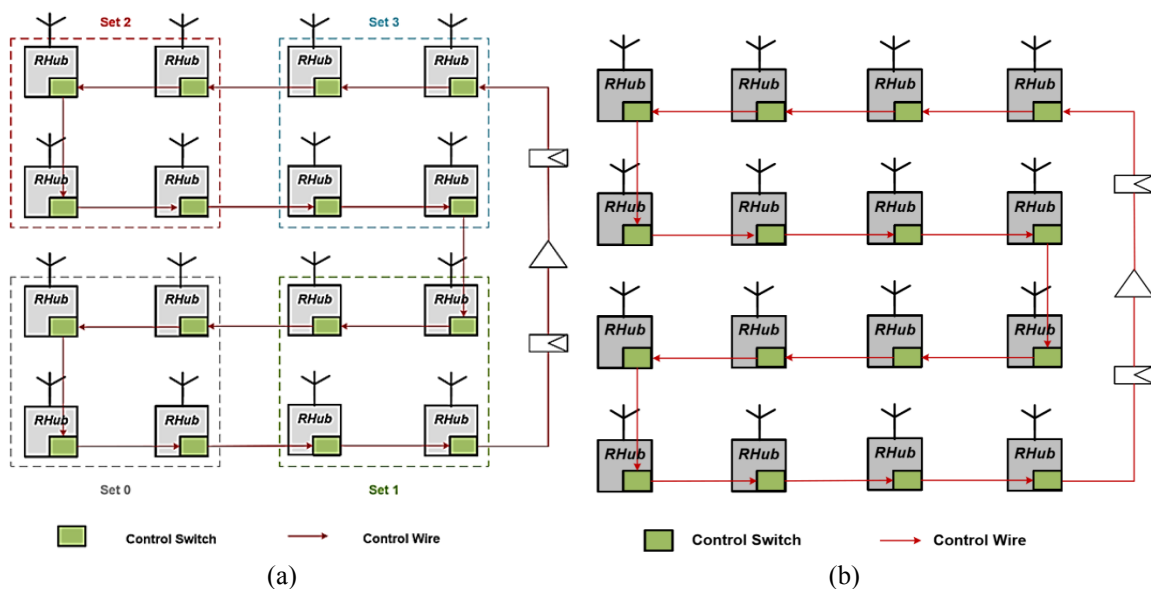


Figure 2: Proposed distributed scheme on two WiNoC architectures: (a) iWise (b) WCube.

## 3. RESULTS & DISCUSSION

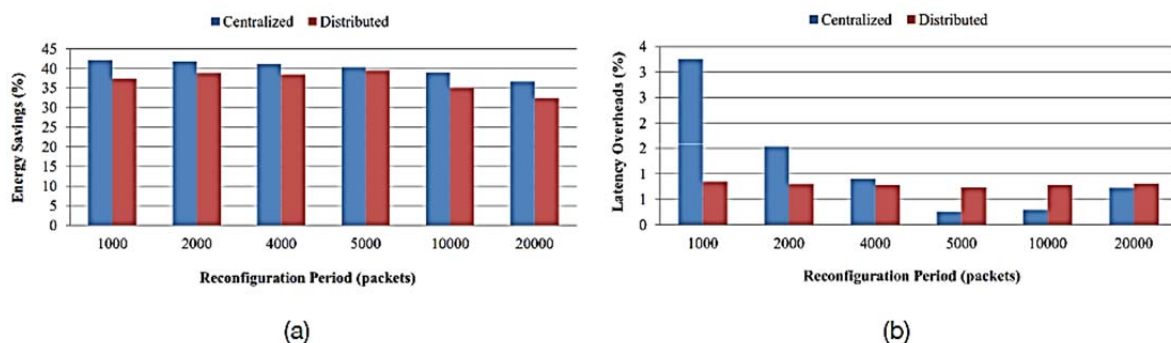
In this section, we consider the experimental results for a generic mesh-based architecture over a 20 mm x 20 mm die on iWise and WCube WiNoC architectures. We implement the proposed technique

in an extended version of Noxim10 supporting wireless communications. It is applied on the two common WiNoC architectures: iWise and WCube. A VGA controller with eight power steps is applied and the number of radio hubs is fixed to 16. Hence, the number of look-up table entries in the VGA controller changes proportionally with the network size. The proposed design is modelled in VHDL, synthesised using Synopsys Design Compiler, and mapped on 28nm CMOS standard cell-library from Taiwan Semiconductor Manufacturing Company Limited (TSMC) operating at 1 GHz. The network size is limited to 64 cores for both schemes. This is done so to suit Stanford Parallel Applications for Shared-Memory-2 (SPLASH-2) and Princeton Application Repository for Shared-Memory Computers (PARSEC) benchmark suites applications that have been designed for 64 multiprocessor systems. For verification purposes, application-based SPLASH-2 and PARSEC benchmark suites are used in this experiment. The suites cover applications in the area of high performance computing, such as finance, cloud computing and gaming, to evaluate multiprocessors designs. The experimental results sections (Section 3.1. to 3.4) discuss the effects of selection of the schemes, benchmark suites applications performance, packet length effect on power, and the area and power overheads of the proposed architectures.

### 3.1 Effects of Selection of the Reconfigurable Transmitting Power Scheme (Centralised versus Distributed)

In this experiment, two reconfigurable transmitting power schemes (as described in the previous section) are compared to see their effects of implementation on energy savings and latency. Applying the proposed design on WCube architecture, the centralised power management scheme is compared with the distributed scheme in terms of RP to observe the energy and latency impacts. The RP inputs for both schemes range between 1,000 and 20,000 clock cycles, packet injection rate (PIR) is set to low and RS for centralised power management is set to 16 clock cycles to represent minimum percentage delay.

Energy savings graph in Figure 3(a) shows better performance of applying the centralised reconfigurable transmitting power technique over the distributed approach. However, larger network sizes such as 256 or 512 cores can be investigated to see the energy saving pattern. Overall, the centralised self-reconfigure scheme has an energy saving of above 35% for all RPs, slightly better than its corresponding scheme. Hence, it is valid to mention that the technique performs better in terms of energy reduction for 64 cores network size.



**Figure 3: Performance analysis in terms of (a) energy savings and (b) latency impacts on WiNoC architectures between the centralised and distributed reconfigurable transmitted power schemes.**

Referring to Figure 3(b), percentage of increased latency in the proposed centralised mechanism is higher than the distributed technique for RP 1,000 until RP 4,000, well under 4%. However, from RP 5,000 until RP 20,000, the performance of the centralised scheme is better than the distributed technique. Minimum latency for the centralised scheme occurs at RP 5,000, which is less than 1%

overhead from the baseline architecture. Even though the latency pattern is quadratic, it is unpredictable due to various individual application domains of the benchmark suites. However, between RP 1,000 and RP 20,000, the latency overhead is below 4%. Overall, both schemes introduce less than 4% latency overhead with most RPs having latency of below 2% overhead. The centralised scheme introduces a reconfiguration power management scheme after each completed RP, causing the percentage of increased latency fluctuation as seen in the figure. The distributed scheme, however, has a consistent latency of about 1.5% due to the introduction of an extra area and power overheads of the control switches. These control switches that are attached to dedicated radio hub regulate the transmission power via control packet protocol and token ring control scheme.

There are some considerations that must be taken into account when applying the distributed reconfiguration transmission power scheme. In the case of an error notification being sent to a transmitter while the network is in data transmission mode, generation of error control packet and notification to the source radio hub will consume time. This causes a waste of power caused by erroneous power reconfiguration action generated as well as frequent packet retransmissions. Another important consideration in this scheme is that when a number of corrupted packets are received in sequential, there is possibility of multiple power increment commands to be sent. This causes oversupplied transmitting power, leading to a waste of energy. However, this is not the case in the centralised strategy during the time the power management is regulated, the entire platform will be stalled. Hence, the observed performance is still in a controllable manner. The error rate is first accumulated prior to power regulation action by the power manager to take place.

### **3.2 Performance of SPLASH-2 and PARSEC Benchmark Suites**

The experiment and result from Section 3.1. are obtained by utilising the SPLASH-2 and PARSEC benchmarks suites. The figures presented are the average energy savings and latency of application files in the benchmark suites. In this section, the individual application files energy savings and latency are analysed in detail. The energy savings performances of the application files when RP values are varied are shown in Figures 4(a) and 4(b). Based on the figures, both WiNoC architectures have unique energy savings trends in each application as compared to each other. The energy savings decrease as RP is increased.

Further analysis on the latency metric is detailed out as shown in Figures 4(c) and 4(d). It is observed that the WCube architecture with the proposed scheme results in reducing latency overheads as RP is increased. The slight increase in latency overheads in RP 2,000 as compared to the other RPs (RP 1,000 and RP 4,000) is interesting to study in future. Due to the core communication patterns, the performance of individual applications is clearly different from one to another. By verifying the proposed work on the seven selected application files, the variations of energy savings as well as latency values may open up possibilities of research in many core communication energy optimisation researches.

Varying the period for reconfiguration phase affects system performance for the centralised scheme. The latency of the proposed work with varied RS values differ from the baseline by a magnitude of one clock cycle unit. Presented in Figure 5, the graph shows the performance effect in terms of percentage. As the reconfiguration phase is greater than 16 clock cycles, system latency increases about double the previous latency value. Communication latency varies from about 4% to more than 8% when reconfiguration phase is manipulated to 24 and 32 clock cycles respectively. The iWise architecture works well under 3% performance degradation for the reconfiguration phase of 16 clock cycles and below.

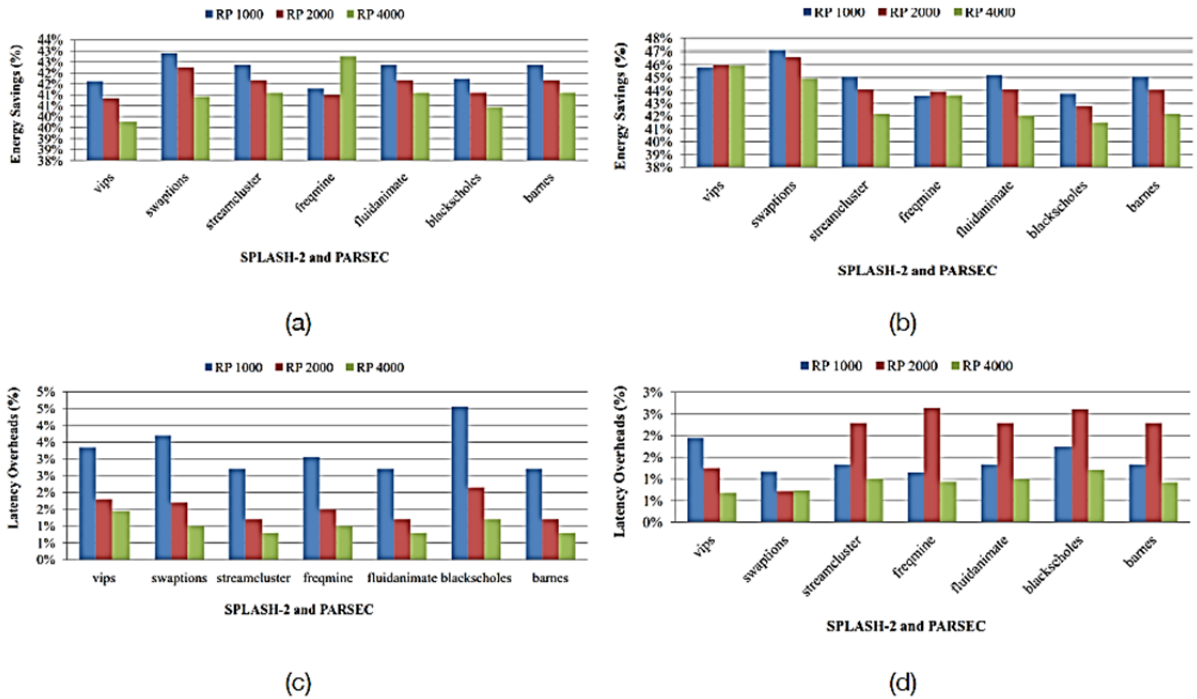


Figure 4: Performance analysis in terms of energy savings for (a) WCube and (b) iWise, as well as latency impacts for (c) WCube and (d) iWise using seven application files in the SPLASH-2 and PARSEC benchmark suites.

The latency maintains at 2% for RS value of 16 cycles and lower. This means that to achieve optimised delay metric below the percentage, a power manager is assigned to a maximum of 16 radio hubs, considering 1 RS cycle represents a transmitting power management command to a radio hub. However, as RS increases from 24 to 32 cycles, the platform becomes less efficient due to increased power management burden that can be handled by the manager. Similar trend applies to the WCube architecture, in which the communication latency rises sharply as the reconfiguration stage goes beyond 16 clock cycle thresholds.

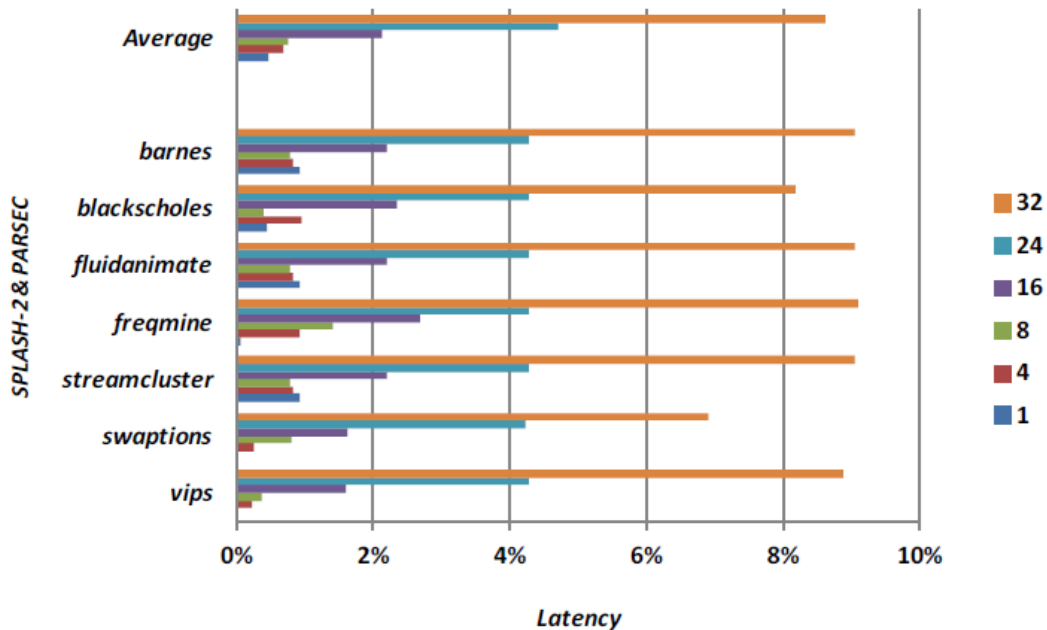


Figure 5: Percentage latency impact on iWise-64 architecture with SPLASH-2 and PARSEC benchmark suites for different penalties with RP 2,000.

### 3.3 Effects of Packet Lengths on VGA Power Consumption

In this section, the toggle rate that shows the frequency of VGA controller changing the transmitting power steps based on the header flit's destination radio hub is investigated. The VGA controller is located at the front-end transmitter that triggers the power amplifier for actual transmission power to the receiver radio hub. The toggle rate factor of the power manager module is consistently about 50% from the control packet inputs. Changing the size of network has limited impact on this parameter because the power manager only communicates with the radio hubs through the three-tuple control message protocol. The toggle rate of the VGA controller is inversely proportional to the packet size. This is due to the fact that the controller selects a suitable transmitting power step based on the destination address field at the header packet information, and the bigger the packet size, the lower the toggle rate is. Power dissipation of such controller is investigated using the CMOS standard cell library from TSMC operating at 1 GHz. Medium packet injection rate is considered in the experiment. For a 10-flit 32 bits long message, it is estimated that the power dissipation is about 30  $\mu\text{W}$ , as shown in Figure 6. If a bigger packet length (in term of flits per packet) is introduced, the power dissipation is as low as about 30  $\mu\text{W}$ , which is negligible as compared to the power dissipated by the other elements of the transceiver and the router, both in the order of mW.

### 3.4 Effects of Area and Power Overheads

The area and power overheads are synthesised and mapped on a 28 nm CMOS standard cell library from TSMC operating at 1 GHz. Referring to Table 2, the proposed VGA controller, which is the only overhead in the proposed centralised reconfigurable transmitting power design as compared to an extant work, accounts for less than 0.1% both in terms of area and power. The power manager occupies a small fraction of time to operate during the RS period as compared to the time taken by the WiNoC platform during the RP period, when the power manager is idle. In the distributed reconfigurable transmitting power scheme, the power and area overheads due to the introduction of the control network, R-VGA, and the encoding/decoding logic for the error detection are investigated. Based on the Synopsys Design Compiler and Mentor Graphics tool, the control switch implementing the token ring access control strategy consumes power about 0.7 mW, giving about 3% overhead from the common ASK-OOK transceiver power consumption which is about 21 mW (Wanas *et al.*, 2013).

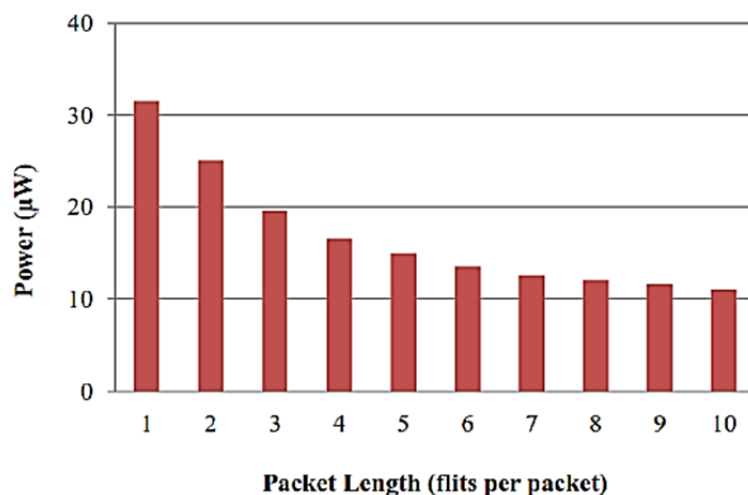


Figure 6: Power consumption per packet in VGA controller for different packet lengths of 10 flits.

**Table 2: Area and power overheads of the proposed centralised reconfigurable transmitting power design.**

	<b>Area</b>	<b>Power</b>
<b>Transceivers</b>	80.1	90.7
<b>Router</b>	19.8	9.2
<b>VGA Controller</b>	0.1	0.1

Some modules depend on the number of radio hubs in the networks due to the fact that the number of bits used for encoding the address of the radio hub and number counters in the R-VGA depend on the total number of radio hubs in the network. Best, medium and worst case scenarios are considered corresponding to the network sizes of 4, 8, and 16 radio hubs. In the worst case scenario, the total power and area overheads introduced by the proposed scheme do not exceed 2.6 and 5%, respectively.

#### 4. CONCLUSION

A reconfigurable transmitting power scheme has been studied and 30% energy saving with considerably low performance degradation (about 3%) has been offered. WiNoC transmitting power can be reconfigured based on the Friis Transmission Equation to guarantee reliability of the WiNoC system. The energy savings as well as performance degradation achieved by both the centralised and distributed power management schemes do not vary significantly from each other. The techniques are general and can be applied on most WiNoC platforms with small area and power overheads in terms of silicon area. Allowing the self-calibration feature on WiNoC, the network is self-adaptive to organise optimal power consumption to achieve reliability. The suitability of the centralised and distributed scheme implementation on larger network sizes such as 256, 512 and 1,024 cores can be investigated to evaluate their performance and limitation. Besides that, run-time error detection, control network and other parameters that affect performance may also be included in the future work.

#### REFERENCES

- Catania, V., Mineo, A., Monteleone, S., Palesi, M. & Patti, D. (2016). Improving the Energy Efficiency of Wireless Network on Chip Architectures Through Online Selective Buffers and Receivers Shutdown. *Proc. 13th IEEE Annual Conf. Consumer Comm. & Netw.* (CCNC), Las Vegas, NV, USA, pp. 668-673.
- Daly, D.C. & Chandrakasan, A. P. (2007). An energy-efficient OOK transceiver for wireless sensor networks. *IEEE J. Solid-State Cir.*, **42**: 1003-1011.
- Deb, S., Chang, K., Ganguly, A., Yu, X., Teuscher, C., Pande, P., Heo, D. & Belzer, B., (2012). Design of an efficient NoC architecture using millimeter-wave wireless links. *13<sup>th</sup> Int. Symp. Quality Electron. Des. (ISQED)*, Santa Clara, CA, USA, pp. 165-172.
- Deb, S., Ganguly, A., Pande, P. P., Belzer, B. & Heo, D. (2012). Wireless NoC as interconnection backbone for multicore chips: Promises and challenges. *IEEE J. Emerg. Selected Topics Cir. Sys.*, **2**: 228-239.
- DiTomaso, D., Kodi, A., Kaya, S. & Matolak, D. (2011). iWISE: Inter-router wireless scalable express channels for network-on-chips (NoCs) architecture. *IEEE 19th Annual Symp. High Perform. Interconnects (HOTI)*, Santa Clara, CA, USA, pp. 11-18.
- DiTomaso, D., Kodi, A., Matolak, D., Kaya, S., Laha, S. & Rayess, W. (2013). Energy-efficient adaptive wireless NoCs architecture. *IEEE/ACM 7<sup>th</sup> Int. Symp. Netw. Chip (NoCS)*, Tempe, AZ, USA, pp. 1-8.

- Feero, B.S. & Pande, P.P. (2009). Networks-on-chip in a three-dimensional environment: A performance evaluation. *IEEE Trans. Comput.*, **58**: 32-45.
- Ganguly, A., Chang, K., Deb, S., Pande, P. P., Belzer, B. & Teuscher, C. (2010). Scalable hybrid wireless network-on-chip architectures for multicore systems. *IEEE Trans. Comput.*, **10**: 1485-1502.
- Kim, K., Floyd, B.A., Mehta, J.L., Yoon, H., Hung, C.M., Bravo, D., Dickson, T.O., Guo, X., Li, R., Trichy, N. and Caserta, J. (2005). On-chip antennas in silicon ICs and their application. *IEEE Trans. on Electron Devices*, **52**: 1312–1323.
- Kim, R. G., Choi, W., Liu, G., Mohandesi, E., Pande, P. P., Marculescu, D. & Marculescu, R. (2016). Wireless NoC for VFI-enabled multicore chip design: Performance evaluation and design trade-offs. *IEEE Trans. Comput.*, **65**: 1323-1336.
- Mineo, A., Palesi, M., Ascia, G. & Catania, V. (2014). An adaptive transmitting power technique for energy efficient mm-wave wireless NoCs. *Proc. Conf. Des., Automat. & Test*, Dresden, Germany, pp. 1-6.
- Mineo, A., Rusli, M.S., Palesi, M., Ascia, G., Catania, V. & Marsono, M.N. (2015). A closed loop transmitting power self-calibration scheme for energy efficient winoc architectures. *2015 Proc. Conf. & Exhibition Des., Automat. & Test*, San Jose, CA, USA, pp. 513-518.
- Mondal, H.K., Gade, S.H., Kishore, R. & Deb, S. (2016). Adaptive multi-voltage scaling in wireless NoC for high performance low power applications. *2016 Proc. Conf. Exhib. Des., Automat. & Test*, Dresden, Germany, pp. 1315-1320.
- Mondal, H. K., Kaushik, S., Gade, S. H., & Deb, S. (2017). Energy-efficient Transceiver for Wireless NoC. *30<sup>th</sup> Int. Conf. on VLSI Des. & 16<sup>th</sup> Int. Conf. Embedded Sys.*, Hyderabad, India, pp. 87- 92.
- Pavlidis, V.F. & Friedman, E.G. (2007). 3-D topologies for networks-on-chip. *IEEE Trans. Very Large Scale Integ. (VLSI) Sys.*, **15**: 1081-1090.
- Rezaei, A., Daneshtalab, M., Safaei, F. & Zhao, D. (2016). Hierarchical approach for hybrid wireless network-on-chip in many-core era. *Comput. & Electr. Eng.*, **51**: 225-234.
- Rusli, M. S., Mineo, A., Palesi, M., Ascia, G., Catania, V. & Marsono, M.N. (2014). A Closed Loop Control based Power Manager for WiNoC Architectures. *Proc. Int. Worksh. Manycore Embedded Sys.* New York, NY, USA, pp. 60-64.
- Shacham, A., Bergman, K., & Carloni, L.P. (2008). Photonic networks-on-chip for future generations of chip multiprocessors. *IEEE Trans. Comput.*, **57**: 1246-1260.
- Wanas, M.A., El Ghany, M.A.A. & Hofmann, K. (2013). Hybrid mesh-ring wireless noc for multi-core system. *IEEE 16<sup>th</sup> Int. Symp. Des. Diagnostics Electron. Cir. & Sys. (DDECS)*, Karlovy Vary, Czech Republic, pp. 295-296.
- Yu, X., Baylon, J., Wettin, P., Heo, D., Pande, P.P. & Mirabbasi, S. (2014). Architecture and design of multichannel millimeter-wave wireless NoC. *IEEE Des. Test*, **31**: 19-28.



# CALIBRATION OF LIGHTWEIGHT THERMAL SENSOR FOR FULLY AUTONOMOUS UAV

Yaakob Mansor<sup>1,2\*</sup>, Shattri Mansor<sup>2,3</sup>, Helmi Zulhaidi<sup>2,3</sup>, Abdul Rahman Ramli<sup>4</sup> & Ajibola I. Isola<sup>2</sup>

<sup>1</sup>Centre of Foundation Studies for Agricultural Science

<sup>2</sup>Geospatial Information Science Research Centre (GISRC)

<sup>3</sup>Department of Civil, Faculty of Engineering

<sup>4</sup>Department of Computer and Communication System, Faculty of Engineering  
Universiti Putra Malaysia (UPM), Malaysia

\*Email: yaakobms@upm.edu.my

## ABSTRACT

*This research successfully developed a low-cost technique for calibration of lightweight uncooled thermal sensor for fully autonomous unmanned aerial vehicle (UAV). A MobIR M8 uncooled thermal infrared sensor (TIRS), with weight of 350 g and long-wave infrared (8-14  $\mu\text{m}$ ) temperature range from  $-20$  to  $250$   $^{\circ}\text{C}$  was used. The calibration was based on upwelling water (with and without using thermo-sensor) commercial blackbody radiators and lens distortion correction model. From the experiments, the coefficient of determination ( $R^2$ ) values were found to be 0.9455 for upwelling water radiation without thermo-sensor, and 1 for both upwelling water radiations with thermo-sensor and blackbody radiator. From this analysis, upwelling water radiation with thermo-sensor was found to be accurate and comparable with a blackbody radiator. The Brown-Conrady distortion algorithm successfully corrected lens distortions introduced by the thermal sensor's wide-angle camera due to misalignment between the lens and detector plane.*

**Keywords:** Unmanned aerial vehicle (UAV); blackbody; thermal sensor; radiance; upwelling.

## 1. INTRODUCTION

Using suitable gimbal sensors, low-cost thermal sensors are increasingly being placed on lightweight rotary-wing unmanned aerial vehicles (UAVs) to perform aerial acquisitions at very low altitude (Berni, 2011; Pérez, 2011; Joshua, 2012; Matase, 2018; Mesas, 2018). Reliability data analysis is generated from the correction of undesirable and defects of sensor characteristics. Here, sensor correction and calibration methods are employed, such as geometric, radiometric, vignetting, resolution and directional effects. For multi-temporal or multi-sensor image analysis, relative digital number (DN)-to-radiance radiometric calibration is performed (Bendig, 2012; Hecker, 2013; Sebastian, 2015).

In order to achieve the flexibility necessities of thermal infrared sensors (TIRS), a fundamental experimental, which concentrates on the examination of upwelling water, for the arrangement of TIRS is conducted in this paper. Several research activities have been conducted based on blackbody calibration of thermal infrared (IR) sensors and radiometric devices (Bower, 2009; Hu Sheng, 2010; Gomez, 2016) and blackbody radiator (Berni, 2011; Xiong, 2012; Jeseck, 2013; Smigaj, 2015; Santesteban, 2017).

The general objectives of this research are to develop a low-cost TIRS calibration method that is comparable to commercial blackbody calibration. Cooled and uncooled are the two types of TIRS. Cooled TIRS, which is normally expensive, is specialised to improve sensitivity and resolution. A low cost, low power consumption and smaller size uncooled TIRS would be more suitable for lightweight UAVs. The objective of the calibrated thermal sensor is to relate the relationship between the blackbody camera response and temperature. By mounting the thermal sensor directly above the centre of water surface, the intensities of those pixels imaging the region temperature measurement are determined.

## 2. METHODOLOGY

The radiometric calibration methodology has two levels. The first level requires sensor calibration information to be converted from sensor DN at sensor radiances to the Earth's surface radiance. The second radiometric level is difficult to calibrate because it requires the location of the image and real-time atmospheric conditions. This research used a MobIR M8 uncooled TIRS with weight of 350 g and long-wave infrared (8 – 14  $\mu\text{m}$ ) temperature ranging between  $-20$  to  $250$   $^{\circ}\text{C}$ . The detector has a resolution of  $160 \times 120$  pixels,  $25$   $\mu\text{m}$  uncooled focal plane array (FPA) microbolometer, and  $60$  Hz frequency with thermal sensor sensitivity ranges of  $\leq 0.1$   $^{\circ}\text{C}$  at  $30$   $^{\circ}\text{C}$ . The infra-fusion includes visual and IR blending and spectral response as shown in Figure 1.

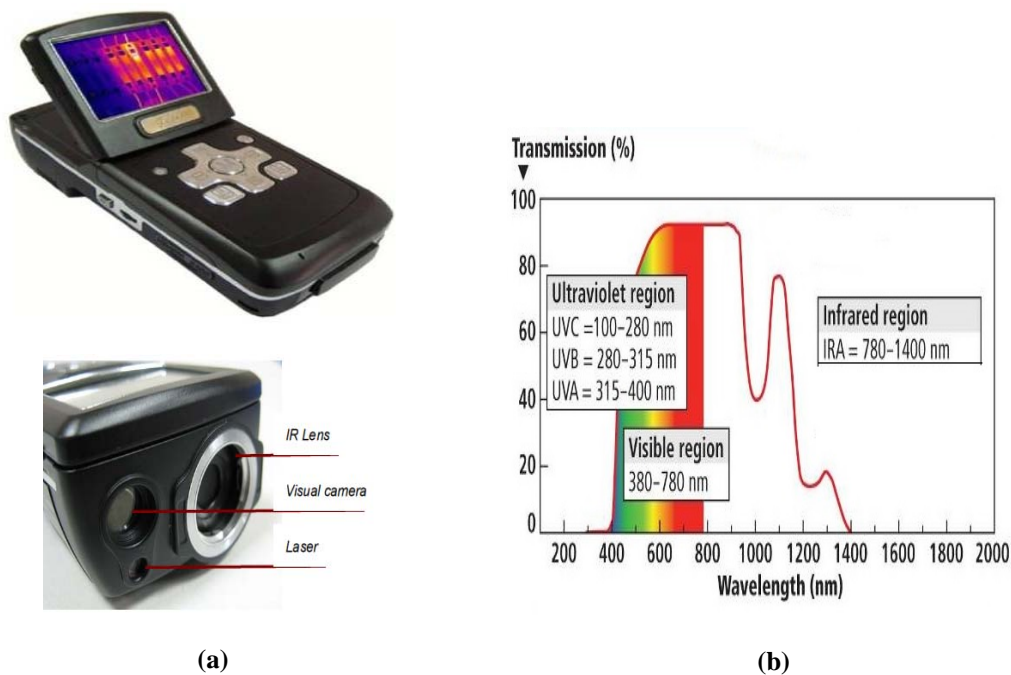


Figure 1: (a) MobIR M8 TIRS. (b) Spectral response.

### 2.1 Upwelling Water

For a thermal sensor of low-cost calibration, the temperature range is typically between  $0$  and  $100$   $^{\circ}\text{C}$ . Based on the temperature measured by a thermal sensor of an upwelling flow of water, level intensity of the temperature image colour is achieved. Given the relatively expensive commercial blackbody procedure, a new method was used without sacrificing the

quality of the calibration, i.e., using water as the source of radiation (emissivity,  $\varepsilon = 0.98$ ). These experiments used colour instead of grey level. The overall output colour level of the thermal sensor is given as:

$$r(T_{ss}, T_a) = r(T_{ss}) + r(T_a) \quad (1)$$

where  $r(T_{ss})$  refers to the colour level when viewing the selected surface at certain temperature  $T_{ss}$  and parameter  $r(T_a)$  refers to the colour output from the ambient materials. The calibration experiment process is shown in Figure 2.

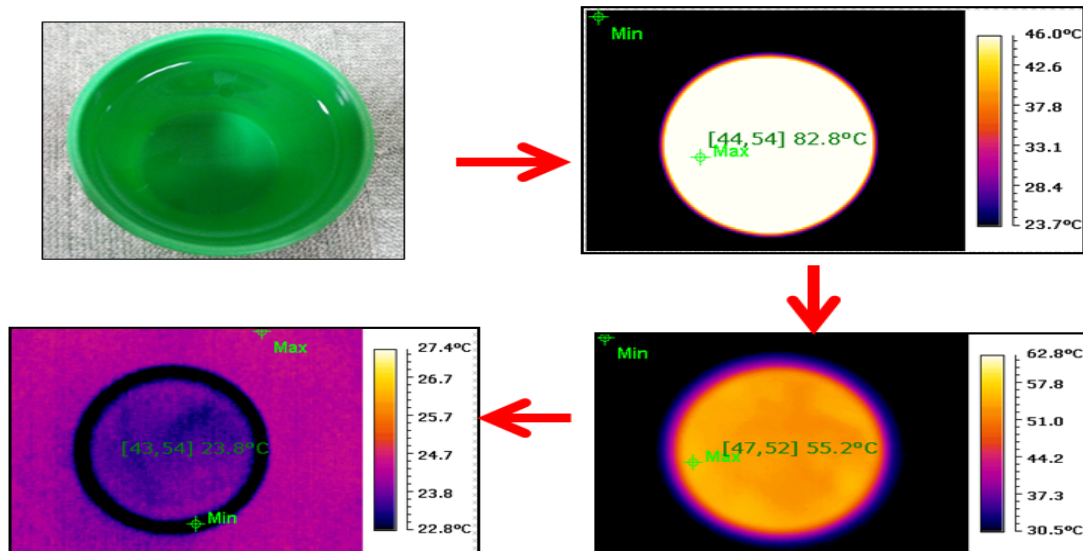


Figure 2: Upwelling water ( $\varepsilon = 0.98$ ) calibration with different temperatures.

## 2.2 Upwelling Water with Thermo-Sensor

A thermo-sensor Pasco Xplorer GLX with scaling of 0.1 °C provides accurate readings. This experiment takes approximately 90 min, in which the sensor data calibration is recorded every 3 min as the sensor display keeps changing over time. According to Stabentheiner *et al.* (2012), if the reference radiator of Pyrex glass remains visible in the infrared display, the results will be better.

A simple precision blackbody reference radiator of high accuracy was prepared by pouring hot water into a Pyrex glass, in which the inner surface is covered with insulating materials. In this experiment, the insulating fabric materials increased the emissivity to a value of more than 0.995, where theoretically this achieved the ideal blackbody ( $\varepsilon = 1$ ). In this case, the emissivity result (0.98) taken directly from the thermal sensor was used. The accuracy of blackbody depends basically on the accuracy of the upwelling temperature calibration.

Figure 3 shows the experimental method for a simple blackbody radiator. Similar to the previous upwelling experiment, the thermal sensor was placed directly on the water surface, whereby the water surface was aligned with the centre of the TIRS image. Recording intensities were obtained from the region of the temperature measurement.

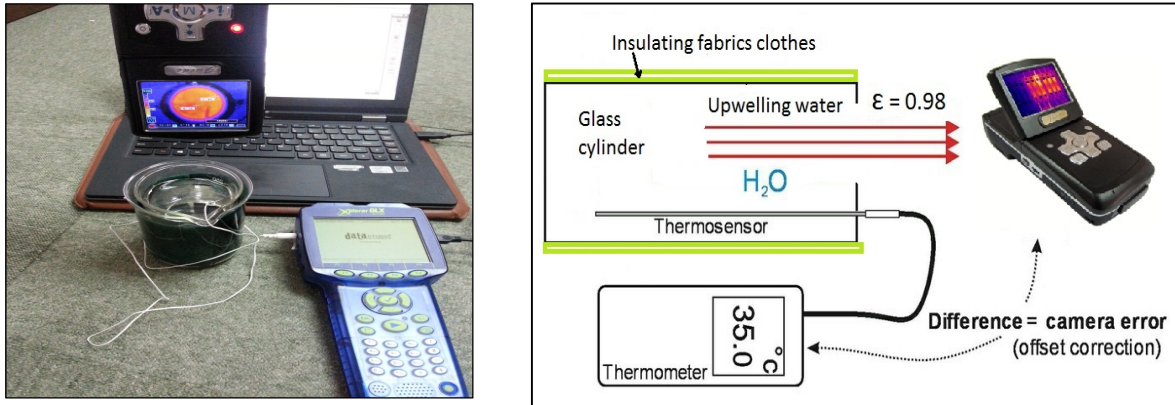


Figure 3: Image on the left upwelling calibration using MobIR sensor and thermosensor above the water surface and right the schematic diagram.

### 2.3 Commercial Blackbody Radiator Methodology

This experiment used a portable R1200P Landcal blackbody ( $\epsilon = 0.98$ ), with working temperature of 1,200 °C. The recommended temperature range was between 350 and 1,150 °C, and it is designed for use on any flat surface as shown in Figure 4. It is also designed for heat resisting steel with a cylindrical target diameter of 55 mm. A thermocouple with a display resolution of  $\pm 1$  °C inside the blackbody radiator measures the temperatures.



Figure Error! No text of specified style in document : R1200P blackbody radiation temperature accuracy measurements.

### 2.4 Lens Distortion Correction Methodology

Lens distortion occurs as a result of non-uniform magnification and misalignment between the lens and detector plane, characterised by a radial shifting of measurements. This is known as a barrel or pincushion distortion, which shifts either away or towards the image centre (Jin, 2014; Arfaoui, 2015; Qiu, 2015; Shortis, 2015; Drap, 2016; Abeles, 2018).

This photogrammetric method used the Agisoft Lens software (Agisoft, 2018), which uses the Brown-Conrady distortion pinhole camera algorithm for lens calibration. This Brown-Conrady algorithm corrects both for radial and tangential distortions caused by physical elements in a lens not being perfectly aligned. The chessboard calibration pattern was used for the experiment (Figure 5) in room light where the intrinsic and extrinsic values were generated.



Figure 5: Image of an (a) incorrect and (b) correct calibration target.

### 3. RESULTS & DISCUSSION

#### 3.1 Upwelling Water

The objective of this thermal sensor calibration was to determine the connection between temperature and blackbody sensor response. Figure 6 shows an example of calibration for temperature of 54.1 °C with colour means of 33.6. Figure 7 shows a graph of colour level analysis, where the coefficient of determination ( $R^2$ ) was found to be 0.9455.

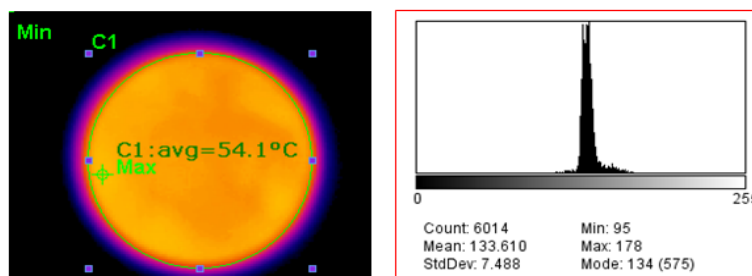


Figure 6: Calibration for the temperature of 54.1 °C with colour mean 33.6.

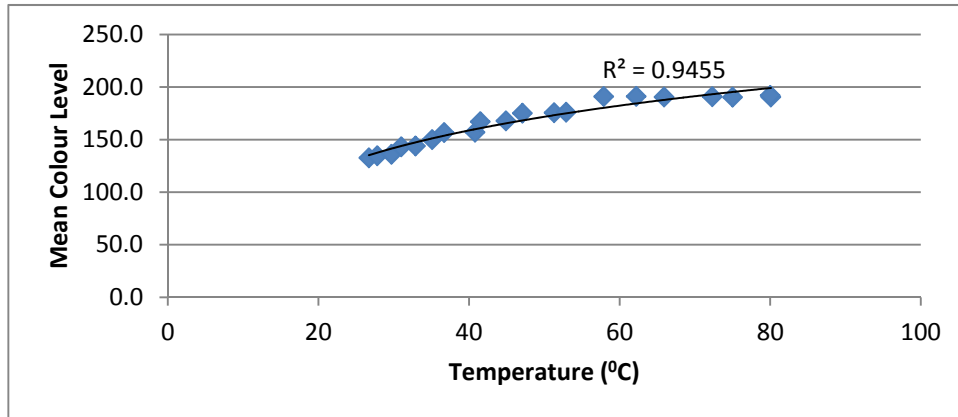


Figure 7: Mean colour level analysis.

### 3.2 Upwelling Water With Thermosensor

The results of Picture in Picture (PIP) or overlay of a thermal image with a visible image are shown in Figure 8. Figure 9 shows the results of offset correction between the thermal sensor and thermosensor for the 90 min experiment. From the experiments,  $R^2$  was found to be 1.



Figure 8: Overlay of a visible image with a thermal image.

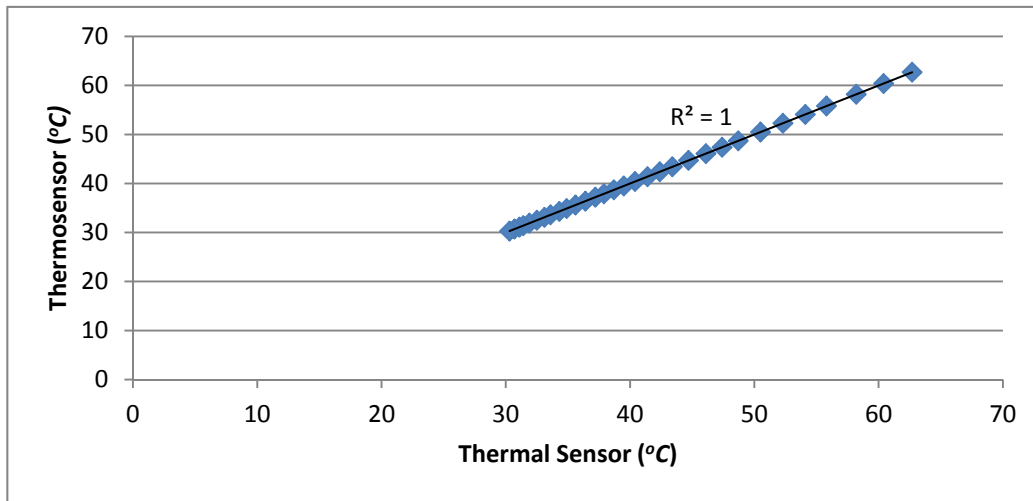


Figure 9: Results of offset correction between the thermal sensor and thermosensor

### 3.3 Commercial Blackbody Radiator

This experiment was run for 90 min. The changes in radiometric temperature were measured using the thermal sensor after power-on over the course of the experiment (Table 1). The average room temperature for this experiment was  $23 \pm 1$  °C. The average relative humidity was  $52 \pm 2\%$ , while the emissivity of the blackbody was 0.98.

With a sensitivity of less than 0.1 °C, the thermal sensor can detect temperature differences between areas from which the image was generated. Environmental data such as humidity, ambient temperature and the gap between the measured object are the most important for accurate reading of a thermal calibration. As shown in Table 1, since the resulting errors are only -2 °C (less than the -5 °C tolerance), the thermal sensor needs no further adjustments. The results of blackbody calibration are shown in Figures 10, where  $R^2$  was found to be 1.

Table 1: R1200P and MobIR Blackbody calibration.

R1200P Blackbody Calibrator (°C)	MobIR M8 Blackbody Calibrator (°C)	Error (°C)
50	48	-2
100	98	-2
150	148	-2
200	198	-2
250	248	-2

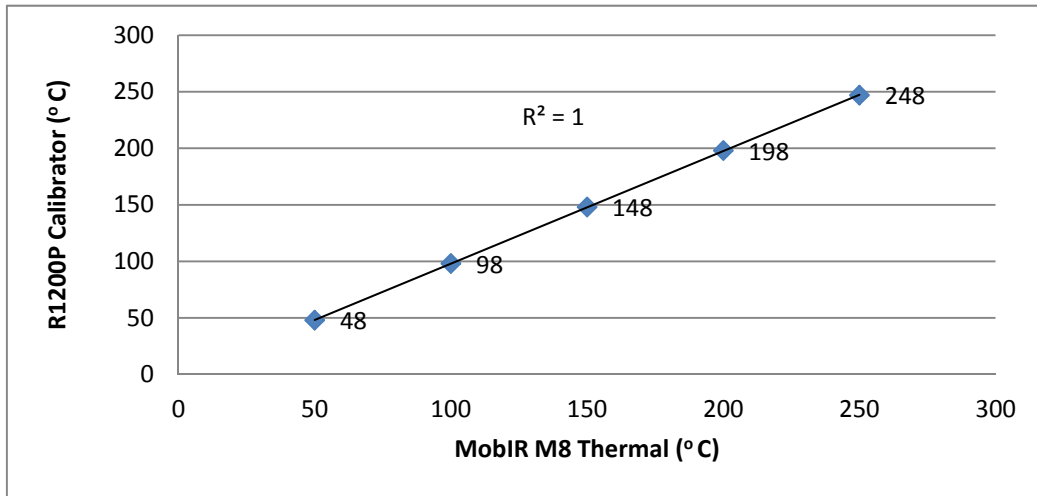


Figure 10: Blackbody calibration between R1200P and MobIR M8.

### 3.4 Lens Distortion Correction

The Brown-Conrady model requires specific intrinsic and extrinsic coefficients of the sensor. These coefficients are calculated between the known geometric properties of the calibration panel and the distorted geometric images (Table 2). Figure 11 shows the calibration technique at different angles, while Figure 12 displays the results from the eight sample visible images from the thermal sensor. The radial and tangential distortion plots of the thermal are shown in Figure 13. The correction model specifies the transformation of the point into the  $x$ ,  $y$ ,  $z$  coordinates, which represent right, down and towards viewing. In addition, the Brown-Conrady distortion algorithm successfully corrected the radial and tangential distortions introduced by the thermal sensor's wide-angle camera.

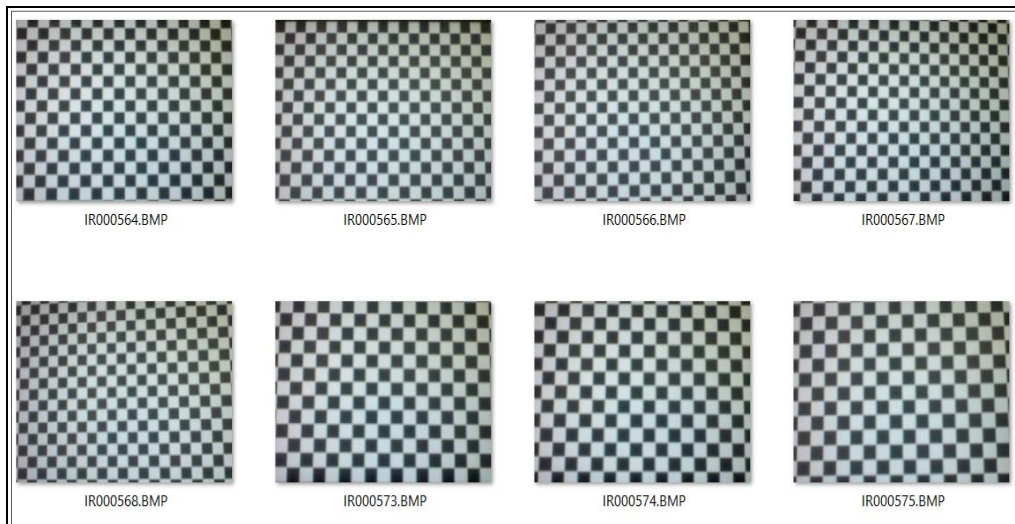
Table 2: Calibration results of the thermal sensor.

Parameter	Value	Std Error
Image width (pixel)	320	
Image height (pixel)	240	
Focal length ( $x$ ) (mm)	1083.41	755.91
Focal length ( $y$ ) (mm)	1051.96	689.65
Principal point ( $x$ )	213.492	87.6118
Principal point ( $y$ )	-217.596	378.908
Skew	9.30341	23.6066
Radial $K_1$	0.0243985	0.122343
Radial $K_2$	-0.177076	1.21281
Radial $K_3$	0.764478	5.5001
Tangential $P_1$	-0.00178613	0.0167498
Tangential $P_2$	0.00354569	0.00956188

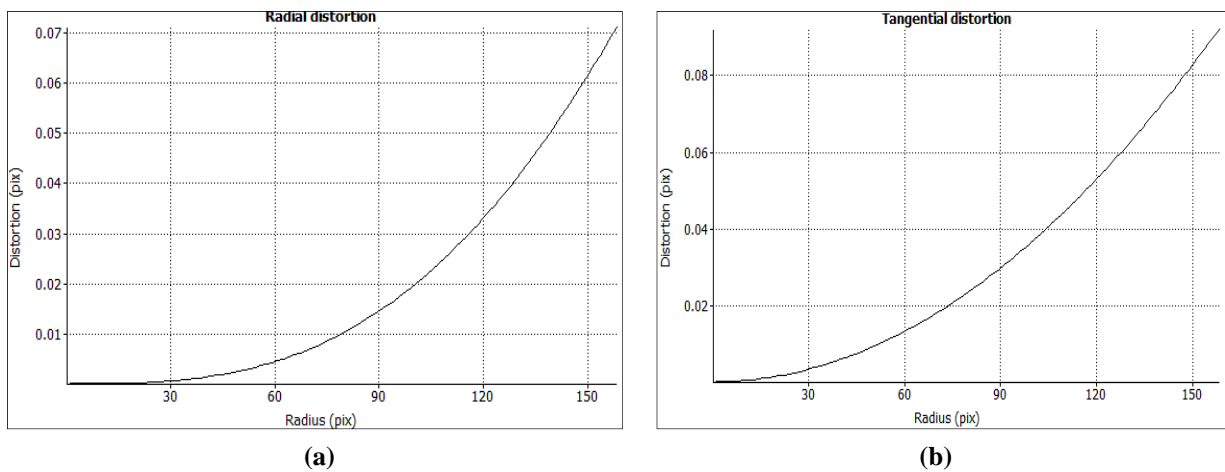




**Figure 11: Calibration with different angles for the thermal sensor.**



**Figure 12: Thermal sensor calibration images using different angles.**



**Figure 13: (a) Radial and (b) tangential distortion plots of the thermal sensor.**

#### 4. CONCLUSION

For the experiments, the  $R^2$  values were found to be 0.9455 for upwelling water radiation without thermo-sensor, and 1 for both upwelling water radiations with thermo-sensor and blackbody radiator. From this analysis, upwelling water radiation with the thermal sensor was found to be accurate and comparable with the blackbody radiator. The emitted heat provides information for corrections to the measured probe temperatures. Hence, the upwelling water method is cost-effective and practical for thermal calibration.

#### REFERENCES

- Abeles, P. (2018). Inverse radial distortion formula. Less than optimal. Available online: <http://peterabeles.com/blog/?p=73> (Last access date: 29 May 2018).
- Agisoft Software (2018). *Lens Corrections*. Available online at: <https://downloads.agisoft.ru/lens/doc/en/lens.pdf> (Last access date: 20 January 2018).
- Arfaoui A. (2015). Geometric image rectification: A review of most commonly used calibration patterns. *Int. J. Signal Image Process.*, **1**:1–8.
- Bendig, J., Bolten, A. & Bareth, G. (2012). Introducing a low-cost mini UAV for thermal and multispectral imaging. *Int. Arch. Photogramm. Remote Sens. Spat. Inf. Sci.*, **39**: 345–349.
- Berni, J.A.J., Zarco-Tejada, P.J., Suárez, L., González-Dugo, V. & Fereres, E. (2011). Remote sensing of vegetation from UAV platforms using lightweight multispectral and thermal imaging sensors. *Int. Arch. Photogramm. Remote Sens. Spatial Inform.*, **38**:6-11.
- Bower, S.M., Kou, J. & Saylor, R. (2009). A method for the temperature calibration of an infrared camera using water as a radiative source. *Review of Scientific Inst.*, **80**: 095107.
- Drap, P. & Lefèvre, J. (2016). An exact formula for calculating inverse radial lens distortions. *Sensors*, **16**: 807.
- Gomez-Candon, D., Virlet, N., Labbe, S., Jolivot, A. & Regnard, J.L. (2016). Field phenotyping of water stress at tree scale by UAV-sensed imagery: New insights for thermal acquisition and calibration. *Precis. Agric*, **17**: 786–800.
- Hecker, C.A., Smith, T.E.L., Luz, B.R. & Wooster, M.J. (2013). Thermal infrared spectroscopy in the laboratory and field in support of land surface remote sensing. In Kuenzer, C. & Dech, S. (Eds.), *Thermal Infrared Remote Sensing: Sensors, Methods, Applications*, Springer, Dordrecht, pp. 43-67.
- Jeseck, Y., Camy-Peyret, C., Payan, S., Briauudeau, M. & Fanjeaux, M. (2013). High emissivity blackbody for radiometric calibration near ambient temperature. *Metrologia*, **40**: 24.
- Joshua, K. & Arko, L. (2012). Sensor correction and radiometric calibration of a 6-band multispectral imaging sensor for UAV remote sensing. *Int. Arch. Photogramm. Remote Sens. Spatial Inform.*, **B1**: 393-398.
- Matese, A. & Di Gennaro, S.F. (2018). Practical applications of a multisensor UAV platform based on multispectral, thermal and RGB high-resolution images in precision viticulture. *Agriculture*, **8**:116.
- Mesas-Carrascosa, F.-J., Pérez-Porras, F., Meroño de Larriva, J.E., Mena Frau, C., Agüera-Vega, F., Carvajal-Ramírez, F., Martínez-Carricondo, P. & García-Ferrer, A. (2018). Drift correction of lightweight microbolometer thermal sensors on-board unmanned aerial vehicles. *Rem. Sens.* **10**: 615.
- Pérez, M., Agüera, F. & Carvajal, F. (2011). Digital camera calibration using images taken from an unmanned aerial vehicle. *Int. Arch. Photogramm. Remote Sens. Spat. Inf. Sci.*, **C22**: 14-16.
- Jin H. (2014). Method and apparatus for removing general lens distortion from images. *US Patent*, US8265422B1.
- Santesteban, L.G., Di Gennaro, S.F., Herrero-Langreo, A., Miranda, C., Royo, J.B. & Matese, A. (2017). High-resolution UAV-based thermal imaging to estimate the instantaneous and

- seasonal variability of plant water status within a vineyard. *Agric. Water Manag.*, **183**, 49–59.
- Sebastian, C., Fabio, R., Michaela D.G, Marco, D. & Mario, G. (2015). Evaluating multispectral images and vegetation indices for precision farming applications from UAV images. *Remote Sens.* **7**: 4026-4047.
- Sheng, H. & Jinlu C.H. (2010). Low-cost UAV-based thermal infrared remote sensing: Platform, calibration, and applications. *Mechatronics and Embedded Syst and Apps, IEEE/ASME Inte.* pp. 38 – 43.
- Shortis, M. (2015). Calibration techniques for accurate measurements by underwater camera systems. *Sensors*, **15**: 30810–30826.
- Smigaj, M., Gaulton, R., Barr, S.L., Suárez, J.C. (2015). UAV-borne thermal imaging for forest health monitoring: Detection of disease-induced canopy temperature increase. *Int. Arch. Photogramm. Remote Sens. Spatial Inf. Sci.*, **XL-3/W3**: 349–354.
- Stabentheiner, A., Kovac, H., Hetz, S.K., Kafer, H. & Stabentheiner, G. (2012). Assessing honey bee and wasp thermoregulation and energetics - New insights by a combination of flow-through respirometry with infrared thermography. *Thermochimica Acta*, **53**: 77–86.
- Qiu, L.S. (2015). A simple method of radial distortion correction with centre of distortion estimation. *Journal of Math. Imag. and Vision*, **35**: 165-172
- Xiong, X., Butler, J., Wu, A., Chiang, V., Efremova, B., Madhavan, S., Mcintire, J. & Oudrari, H. (2012). Comparison of MODIS and VIIRS onboard blackbody performance. *SPIE Proc.*, 853318.
- Yaakob, M., Shattri, M., Helmi, Z., Abdul, R.R. & Ajibola, I.I. (2017). Development of lightweight and low-cost fully autonomous hexacopter UAV. *Defense S&T Tech. Bull.*, **10**: 187-198.

# A NOVEL ARCHITECTURE FOR THE REALISATION OF IOT-ENABLED ECG SIGNAL QUALITY ASSESSMENT USING WAVELET DECOMPOSITION FOR BASELINE WANDER REMOVAL

Ramesh Babu Chukka<sup>1\*</sup> & Chennupati Sumanth Kumar<sup>2</sup>

<sup>1</sup>Department of Electronics & Communication Engineering, Vignan's Institute of Engineering for Women, India

<sup>2</sup>Department of Electronics & Communication Engineering, GITAM Institute of Technology, India

\*Email: rameshbabuchukka@gmail.com

## ABSTRACT

*In this paper, a technique to remove baseline wander (BW) from electrocardiogram (ECG) signals based on wavelet decomposition and also a novel signal quality assessment-aware Internet of Things (IoT)-enabled ECG telemetry system for continuous cardiac health monitoring applications are proposed. The main objectives of this paper are to design and develop a ECG signal quality assessment (SQA) method for automatically classifying the acquired ECG signal into GOOD or BAD, and real-time implementation of the proposed IoT-enabled ECG framework using ECG signals taken from the Massachusetts Institute of Technology-Beth Israel Hospital Arrhythmia (MITBIHA) database. The ECG signals are pre-processed using notch filter at 50Hz, with wavelet decomposition used to remove BW noise that is present in the ECG signal. The processed ECG signal performance is mathematically calculated in terms of sensitivity, correlation criterion and signal-to-noise ratio. The experimental results demonstrated that the proposed ECG SQA performs well in terms of sensitivity, correlation and signal-to-noise ratio.*

**Keywords:** *Electrocardiogram (ECG); baseline wander (BW); signal quality assessment (SQA); tele monitoring; Internet of Things (IoT).*

## 1. INTRODUCTION

Internet of Things (IoT)-event driven paradigms enable continuous monitoring of individuals (Kolios, 2016) with applications in chronic conditions, such as obesity, hypertension, diabetes, hypertriglyceridemia, heart failure, asthma, depression, elderly care support, preventive care, and wellness (Catarinucci *et al.*, 2015). The IoT paradigms can play a significant role in improving the health and wellness monitoring system, such as cardiovascular disease diagnosis, arrhythmias recognition, physiological feedback, sleep apnea detection, chronic patient surveillance, sudden cardiac arrest prediction, biometric, and emotional and physical activity recognition system (Satija *et al.*, 2017).

Challenges faced in the field of long term healthcare monitoring systems design includes portability in size, weight and low cost by increasing the availability and quality of care, and dramatically lowering the treatment cost and frequent travel (Ramesh Babu, 2018). Most electrocardiogram (ECG) analysis systems require relatively noise-free ECG signals for obtaining the ECG measurements more accurately and reliably (Satija *et al.*, 2018).

In practice, the interpretation of ECG signals in real time recordings are often corrupted by various kinds of artifacts and noise, including flat line (FL) due to electrode disconnection, baseline wander (BW) due

to the respiration, abrupt change (AC) due to the physical activities, muscle artifacts due to the muscle contraction, power line interference (PLI), and recording instrument noise (Satija *et al.*, 2018). Therefore, automatic assessment of ECG signal is highly demanded in reducing the false alarms due to presence of unacceptable level of noises. Signal quality assessment (SQA) is an essential step for the intelligent ECG analysis. The corrupted ECG data could lead to medical misdiagnosis via cardiac monitors (Clifford *et al.*, 2012).

In this paper, we aimed to present an IoT enabled architecture and also we propose a light ECG SQA method for automatically classifying the acquired ECG signals into GOOD or BAD signals with classification. The output of the algorithm is given in a binary format; GOOD (i.e., a reliable heart rate (HR) can be derived) and BAD (i.e., a reliable HR cannot be derived) to simplify interpretation and facilitate applicability, and also results in low battery power consumption by transmitting only the GOOD signals.

## 2. PROPOSED IoT - ENABLED ECG TELEMETRY FRAMEWORK

The main module of our SQA aware-IoT framework is as shown in Figure 1. It consists of three modules: 1) ECG data acquisition module; 2) automated SQA module; and 3) SQA aware ECG analysis and transmission module. In this paper, we mainly focus on the design and real time implementation assessment of the suitability of ECG signals for deriving reliable HR. In this paper, ECG SQA is implemented based on wavelet decomposition based filtering for BW removal and decision rules.

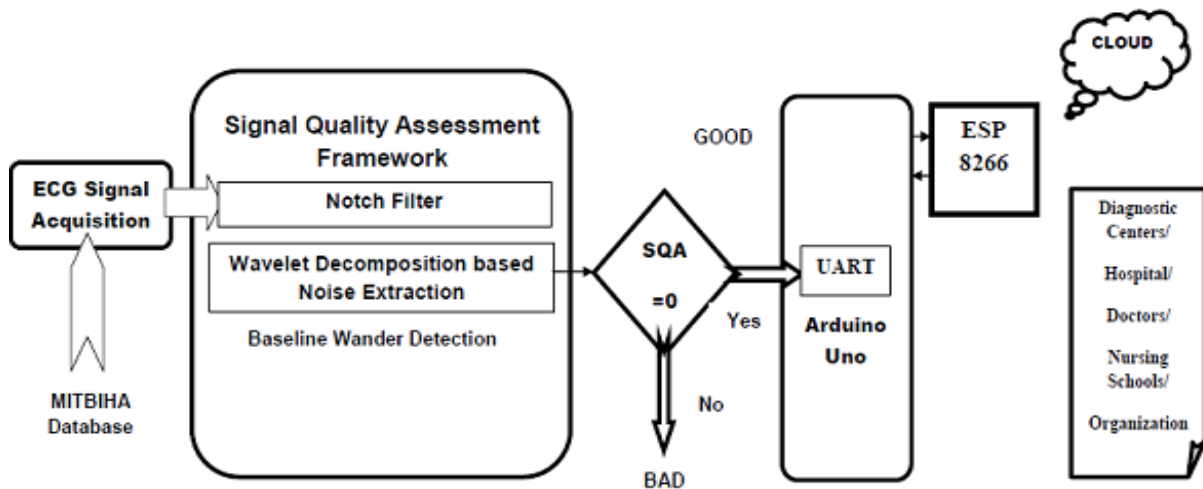
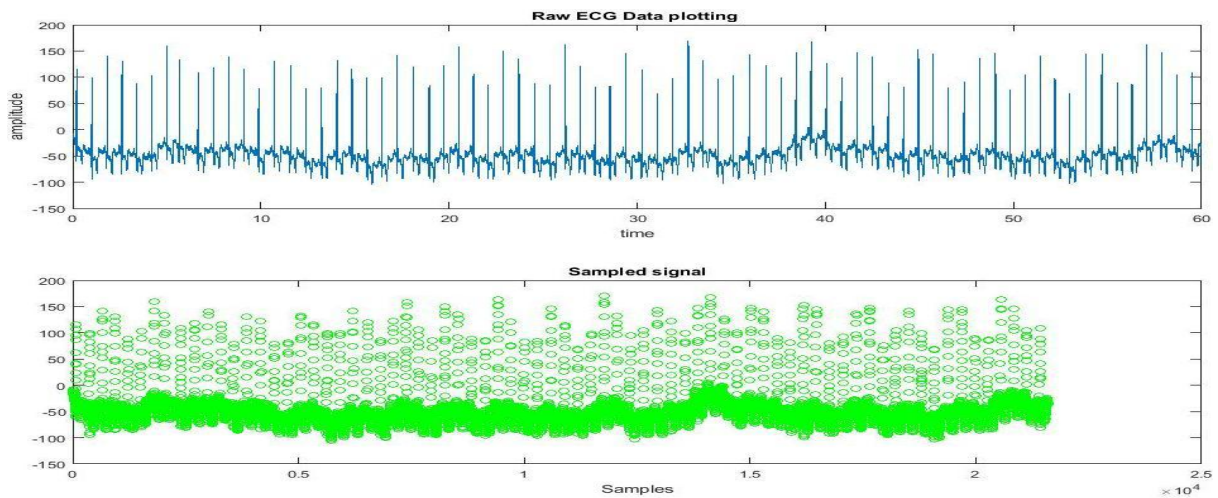


Figure 1: Proposed IoT-enabled framework for energy and resource-efficient ECG telemetry system.

### 2.1 Databases

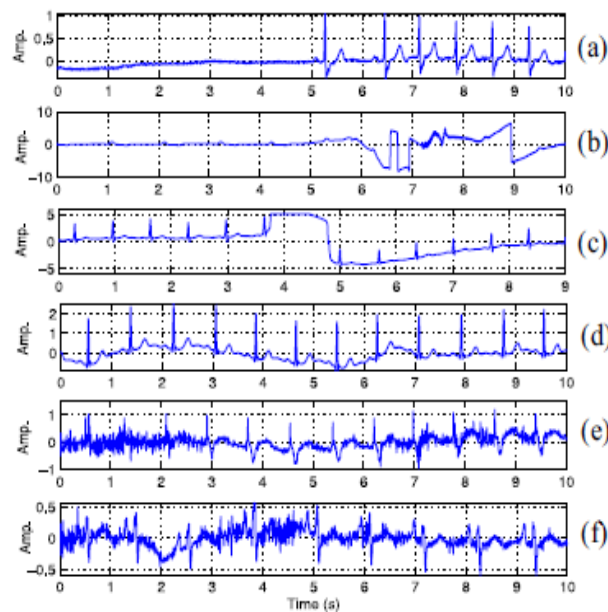
For the implementation and analysis, ECG records are taken from standard ECG databases, including the Massachusetts Institute of Technology - Beth Israel Hospital Arrhythmia (MITBIHA) database. The specifications of ECG recordings are no. of records: 48, duration: 30mins, sampling frequency: 360 Hz, no. of leads: 2, and mostly the records are noise free (Mark, 2001). For this study, the ECG signal is taken from the database sampled at 360 Hz, as shown in Figure 2.



**Figure 2: Raw ECG data plot and sampled signal.**

## 2.2 Baseline Wander (BW) Removal Using Discrete Wavelet Transform Decomposition

A major challenge in healthcare monitoring systems is de-noising. For visual inspection, the noisy ECG signals taken from the standard ECG databases are shown in Figure 3.



**Figure 3: ECG signals corrupted with different kinds of artifacts and noise. The ECG signals are taken from the ECG databases. (a)–(c) Records with pause and abrupt BW. (d) ECG signal corrupted with BW. (e) and (f) ECG signals corrupted with severe muscle artifacts.**

BW in ECG signals is mainly caused by the movement and respiration process of the patient and it mainly appears as low-frequency artifacts in the ECG signals. Removal of BW is necessary for better visual interpretation and detection of certain patterns in the ECG signal for subsequent automatic processing. The use of high pass filtering for BW removal is not recommended as it can distort the ECG waveform because of variations in the frequency spectrum of the ECG signal. Furthermore, transmission of poor quality ECG signals to the cloud server can reduce the lifetime of on-device batteries in body area

networks as well as increase false alarm rates in unsupervised health monitoring applications. To overcome this key challenge, an optimised technique to remove BW from ECG signals based on the wavelet decomposition technique with notch filter is implemented.

### 2.2.1 Notch Filter

In practical ECG measurements, the primary signal is often contaminated by strong disturbances, which must be removed before the signal is registered for further analysis. The varying ECG contact potentials and breathing artifacts (below 0.5 Hz) cause unwanted baseline drift. For stress ECG recordings, this drift may sometimes make the recording impossible. Such unwanted signals are effectively removed by using appropriate linear phase notch filters. Notch filters are also used to suppress the secondary artifacts that arise due to electrical interference, as well as cross coupling from frontal ECG while analysing ECG signal. Figure 4 shows the filtered ECG signal using notch filter at 50 Hz.

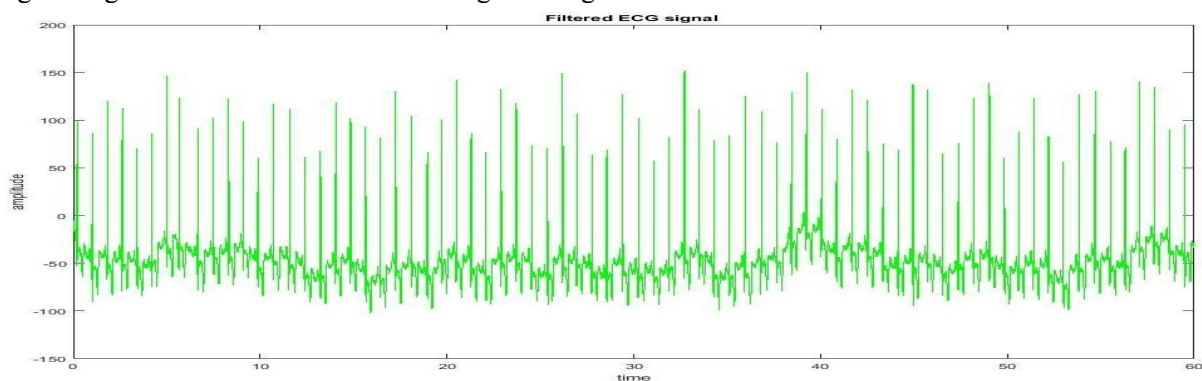


Figure 4: Filtered signal using notch filter at 50 Hz.

### 2.2.2 Wavelet Decomposition

Unlike Fourier transform, wavelet transform (WT) provides more information on its domain, which includes both frequency and time representation. A very efficient and reliable algorithm is used to compute the discrete WT (DWT) decompositions using consecutive filters and decimators as shown in the Figure 5. The high pass filter (HPF) and low pass filter (LPF) determine the corresponding details and approximations coefficients of the applied signal. The downsamplers ( $\downarrow 2$ ) are used to remove redundant samples from the output of the filters and keep the same total number of samples. According to the characteristics of the applied signal and required degree of processing we can reapply the approximation to the most recent decomposition segment several times (Cvetkovic *et al.*, 2008).

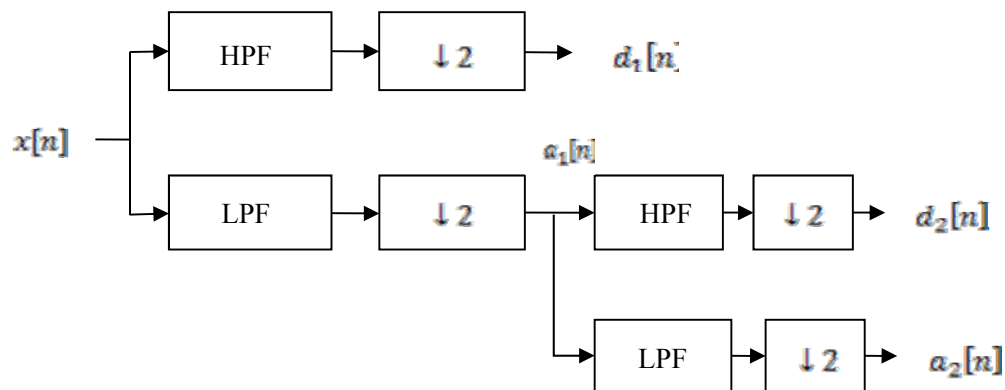
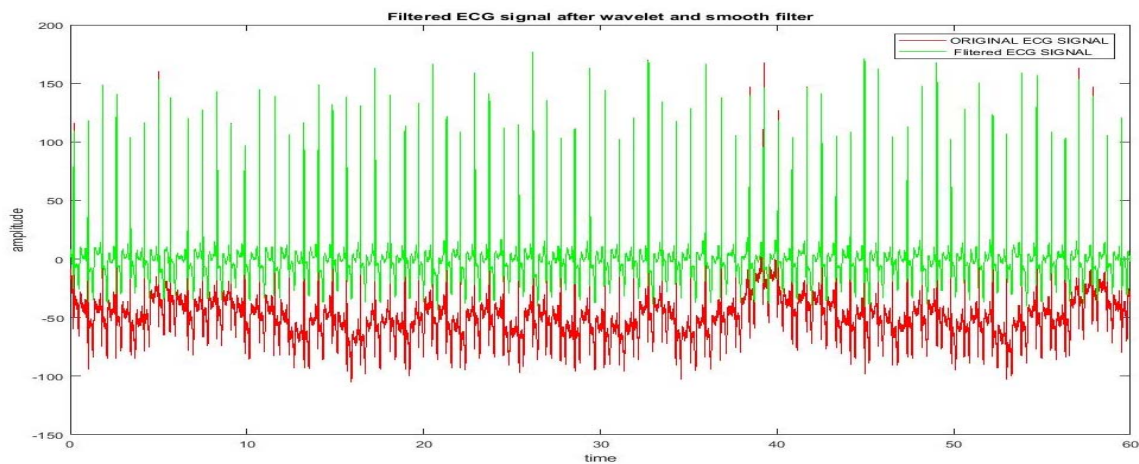


Figure 5: Two levels of wavelet decomposition (Cvetkovic *et al.*, 2008).

The decomposition of signal at every level consists of two digital filters, the first filter is high pass in nature, is known as discrete mother wavelet, and the second one is low pass in nature, is the mirror version of first filter. Two downsamplers downsample the resulting signals by 2. The downsampled output of the high pass filter yields the detail coefficient ( $d_1$ ) and the downsampled output of the low pass filter provides the approximation coefficient ( $a_1$ ). The first approximation is further decomposed and this process is continued. The approximation coefficients are related to the low frequency part of the signal, which contains the main features and information. The detail coefficients are used to preserve the perfect shape when reconstruction is invoked. It is noticeable that detail coefficients at higher levels of noiseless signals are sparse. Therefore, in these high levels, larger coefficients can be assumed to be actual coefficients plus noise, while the remaining coefficients are considered as pure noise (Cvetkovic *et al.*, 2008). Figure 6 shows the BW removal using wavelet decomposition.



**Figure 6: BW removal using wavelet decomposition.**

### 2.3 Development of SQA

For ECG QRS peak detection, we used the widely accepted Pan-Tompkins algorithm, where QRS (represents the depolarisation (activation) of the ventricles) detection is divided into two sections. The pre-processor section performs linear and nonlinear filtering of the ECG signal and produces a set of periodic vectors that describe events. The decision rule section operates on the output of the preprocessor, classifies each event as either a QRS complex or noise, and saves the temporal location of each of the identified QRS complexes. The decision rules for a QRS detector are generally built from a number of components each having experimentally determined parameters. The most important task of the decision rule section is the determination of detection thresholds. Other common components of QRS decision rules are blanking, where events immediately following a QRS detection are ignored for a set time, search back, where previously rejected events are re-evaluated when a significant time has passed without a detection, and use of slope to distinguish between T-waves (due to ventricular repolarisation) and early occurring ectopic beats (Hamilton & Tompkins, 1986).

In order to develop the ECG SQA Algorithm, we used relevant rules to classify the signal as shown in Figure 7, using a custom annotation graphical user interface (GUI) written in MATLAB.



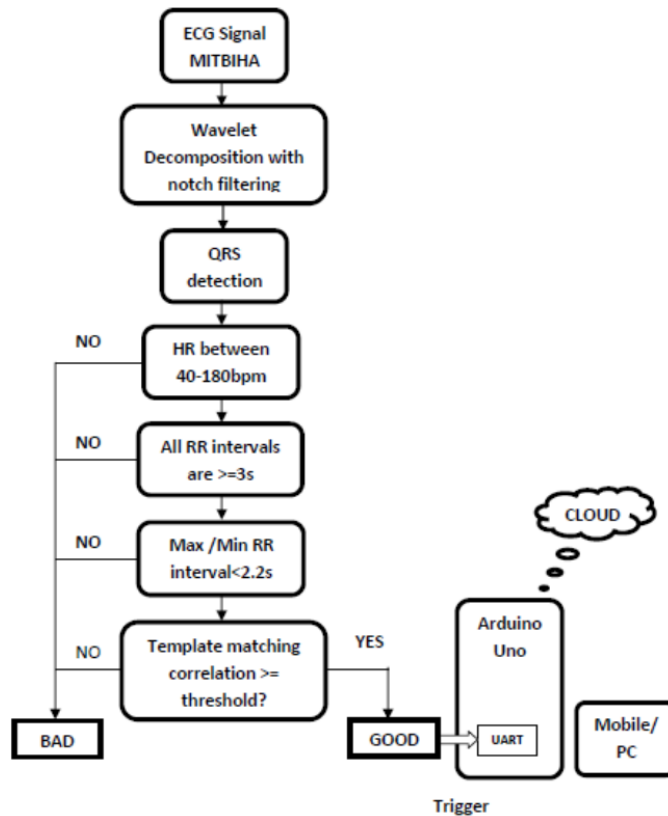


Figure 7: IoT – enabled SQA with feasibility rules.

### 2.3.2 Feasibility Rules

The first step of the SQA algorithm is to perform peak detection on an ECG sample, which is passed through the notch filter and wavelet transformation to get a better HR value by removing BW. Then, the output of the detector is compared with a set of the following three relevant rules, which are applied sequentially. If any one rule is not satisfied, then the sample is classified as BAD. Otherwise it is classified as GOOD (Christina, 2015). The feasibility rules are as follows:

- **Rule 1:** The range of HR value extrapolated from the 10s sample should be between 40-180 beats per min (bpm). There is theoretically a chance of getting values outside this range, but this is the physiologically probable range of HR for the adult population.
- **Rule 2:** The maximum acceptable gap between successive peaks should be less than or equal to 3s to ensure that not more than one beat is missed.
- **Rule 3:** The ratio of the maximum to minimum beat-to-beat interval within the sample should be less than 2.2. We use a limit of 2.2 to allow a single missed beat, because we would not expect the HR to change by more than 10% in a 10s sample.

If all the three rules are satisfied, an adaptive template matching approach is used, as explained next.

### 2.3.3 Adaptive Template Matching

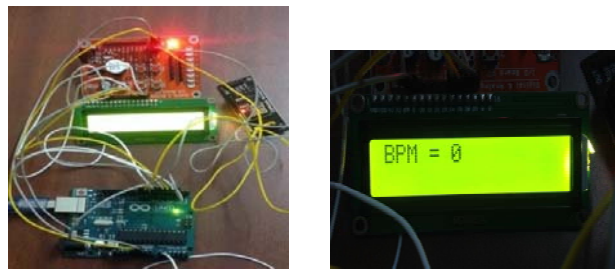
This template searches for regularity in the morphology of the QRS complexes in a given ECG sample. The QRS complex is a name for the combination of three of the graphical deflections seen in a typical

electrocardiogram. It corresponds to the depolarisation of the right and left ventricles of the human heart and contraction of the large ventricular muscles. In adults, the QRS complex normally lasts 0.06-0.10 s, while in children and during physical activity, it may be shorter. Our approach for template matching is as follows:

- Using all the detected R-peaks of each ECG sample, the median beat-to-beat interval is calculated.
- Individual QRS complex waves are then extracted by taking a window, the width of which is the median beat-to-beat interval, centred on each detected R-peak.
- The average QRS template is then obtained by taking the mean of all QRS complexes in the sample. The correlation coefficient of each individual QRS complex with the average QRS template is then calculated.
- The average correlation coefficient is finally obtained by averaging all correlation coefficients over the whole ECG sample.

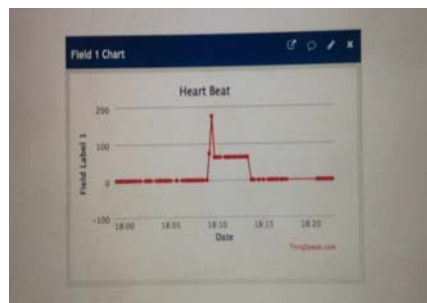
### 2.3 Validation of SQA IoT Enabled ECG Telemetry System

Once the sample is classified as GOOD, it is then given as a trigger to an ARDUINO-UNO board (Kolioset *al.*, 2016), where the HR value is calculated for the given ECG signal using a simple embedded C program. The output HR value can be observed on a LCD display as shown in Figure 8.



**Figure 8: Continuous recording of heart rates (HRs).**

By using an ESP8266Wi-Fi module, the data can be transmitted to the doctor or family members through longer distances through a cloud server. Therefore, the doctor can monitor the condition of the patient depending on the obtained output values that can be seen in the mobile phone using the Things Speak app, as shown in Figure 9.



**Figure 9: IoT enabled ECG telemetry system.**

### 3. EXPERIMENTAL RESULTS & DISCUSSION

In order to test the performance of the proposed ECG SQA method, a wide variety of ECG signals are taken from the MITBIHA database, which contains 48two-channel records of noise-free and noisy ECG signals with varying ECG waveforms morphologies. A total of 17 ECG records, available at sampling rate of 360Hz, are used to test the performance of the proposed algorithm. Statistical parameters are also used to evaluate the algorithms.

The performance of the proposed SQA method is evaluated using sensitivity ( $Se$ ) and detection error rate ( $DER$ ), which is computed as:

$$Se (\%) = TP/(TP + FN) \times 100 \quad (1)$$

$$DER = (FP+FN/\text{Total no. of beats}) \times 100 \quad (2)$$

where  $TP$  is true positive,  $FP$  is false positive,  $FN$  is false negative and  $DER$  is detection error rate.

The performance of the proposed method is assessed by the correlation criterion ( $\gamma$ ), which is defined as:

$$\gamma = \frac{\langle x, x' \rangle}{\|x\| \|x'\|} \quad (3)$$

where  $x$  and  $x'$  are the ECG recordings with artificial BW and baseline corrected ECG respectively.

By using above equation, we can evaluate the similarities between two signals. If the value of  $\gamma$  is 1, then two signals are identical. If the value of  $\gamma$  is -1, then two signals are the inverse of each other.

The performance of the proposed method can also be evaluated by the signal-to-noise ratio ( $SNR$ ), which is defined as

$$SNR = 10 \log_{10} \frac{x'_{\sigma}}{N_{\sigma}} \quad (4)$$

where  $x'$  and  $N$  denote the clean ECG signal (baseline corrected ECG) and BW signal, respectively.

The proposed automated SQA IoT framework is implemented on the DWT decomposition based BW noise filtering. The proposed was tested on some of the samples of ECG signals taken from MITBIHA database and the results are summarised in Table 1. From the results, it is found that the proposed SQA method can achieve high SNR, which shows that we can acquire better results in denoising the ECG signal by removing the BW noise.

We implemented the SQA method using the well-known Pan-Tomkins R-peak detector, which is widely used in SQA methods, for validating the performances using the pathological and non-pathological ECG signals taken from standard databases. The R-peaks are first identified by using the conventional Pan-Tomkins algorithm. Then, the ECG beats are extracted by using the location of detected R-peaks. The SNR calibration and correlation are performed between the individual beats and averaged PQRST (one complete heart beat in ECG signal-Atrial and ventricular depolarization and repolarization are represented on the ECG as a series of waves: the P wave followed by the QRS complex and the T wavebeat). From the results, it is noted that the ensemble heartbeat and all the extracted heartbeats exhibits a high correlation for the ECG signals with regular heartbeat patterns. The correlation between the ensemble heartbeats and other heartbeats is poor in case of ECG signals with different type of PQRST complexes.

By using this technique, the R-peaks have been detected with high sensitivity of 99.84%, which results in the calculation of heart rate value accurately with low detection error rate of around 0.01%, which helps in saving of lives of the patients in time because of monitoring the patient's condition correctly.

**Table 1: Experimental results.**

ECG records	Actual no.of beats	TP	FP	FN	FP+FN	Detection error rate	Sensitivity	Correlation	SNR
200	2601	2585	0	1	1	0.04	99.9	0.9863787	27.1229
201	1963	1955	2	12	14	0.71	99.3	0.9421236	24.4681
202	2136	2130	8	0	8	0.37	100	0.9973932	28.2829
203	2982	2956	2	30	32	1.07	98.9	0.9911091	31.9607
205	2656	2644	0	1	1	0.05	99.9	0.9853247	18.8084
208	2956	1857	0	5	5	0.16	100	0.9856602	27.1252
209	3004	2527	0	0	0	0	99.8	0.9528809	21.8086
210	2647	2644	0	4	4	0.15	99.8	0.9574652	21.6429
212	2748	2174	0	4	4	0.16	99.9	0.9822321	28.4056
213	3251	3247	0	2	2	0.06	99.9	0.8756344	26.8662
215	3363	2569	6	0	6	0.18	100	0.9569218	24.966
217	2208	2128	0	0	0	0	100	0.9912986	25.379
219	2154	2273	0	0	0	0	100	0.6777032	18.1411
220	2048	2048	0	0	0	0	100	0.994475	22.515
221	2427	1863	0	4	4	0.16	99.8	0.9306548	20.88
222	2484	2174	0	20	20	0.81	99.2	0.9425236	24.5281
223	2605	2083	0	0	0	0	100	0.9972986	25.37
<b>Average</b>	2448	2345	1	4.8	5.94	0.01	<b>99.84</b>	<b>0.949828</b>	<b>24.064</b>

Similarly in the case of record contamination, performance assessment is by means of the correlation coefficient and signal to noise ratio calculation. This approach also provides us with a better performance by obtaining the output correlation value as 0.94 and SNR as 24.064. Therefore, the performance estimation is relatively good, with the results after extraction showing satisfactory BW elimination by using this technique. Therefore, the proposed method can provide good SQA performance for the dissimilar heartbeats within a quality decision-making interval.

#### 4. CONCLUSION

In this paper, we presented a novel SQA IoT-enabled ECG telemetry system for cardiac health monitoring applications. This paper proposes an ECG SQA method for automatically assessing the quality of ECG signals. The experimental results demonstrated that the proposed ECG SQA performs well in terms of detection error rate and sensitivity. Based on these findings, we believe that the proposed quality-aware IoT-enabled framework has significant potential in improving resource utilisation efficiency and reliability of ECG signals analysis for reducing false alarm rates under severe noisy ECG recordings. The proposed method can be effectively used in defence applications for the energy consumption of targets and assessing the quality in tracking. In future an ECG classifier using statistical method can be proposed, for categorisation of various kinds of abnormalities.

#### REFERENCES

- Cvetkovic, D., Ubeyli, E. & Irena, C. (2008). Wavelet transform feature extraction from human PPG, ECG, and EEG signal responses to ELF PEMF exposures: A pilot study. *J. Digital Signal Proc...*, **18**: 861–874.
- Clifford, G.D., Behar, J., Li, Q. & Rezek, I. (2012). Signal quality indices and data fusion for determining clinical acceptability of electrocardiograms. *J. Physiol Meas.*, **33**: 1419–1433.
- Christina, O., Timothy, B., Peter, C., David, C., David, V. & Lionel, T. (2015). Signal-quality indices for the electrocardiogram and photoplethysmogram: Derivation and applications to wireless monitoring. *IEEE T. Biomed. Health Inform.*, **3**: 832-838.
- Catarinucci, L., Donno, D., Mainetti, L., Palano, L., Patrono, L., Stefanizzi, M.L. & Tarricone, L. (2015). An IoT-aware architecture for smart healthcare systems. *IEEE T. Internet Things*, **2**: 515–526.
- Hamilton, P S. & Tompkins, W.J. (1986). Quantitative investigation of QRS detection rules using MIT/BIH arrhythmia database. *IEEE T. Biomed. Eng*, **33**: 1157-1165.
- Kolios, P., Panayiotou, C., Ellinas, G. & Polycarpou, M. (2016). Data-driven event triggering for IoT applications. *IEEE T. Internet Things.*, **3**: 1146–1158.
- Moody, G.B. & Mark, R.G. (2001). The impact of the MIT-BIH arrhythmia database. *IEEE M. Eng. Med. Biol.*, **20**: 45–50.
- Ramesh Babu, Ch. (2018). & Sumanth Kumar, Ch. A novel architecture for IoT enabled ECG signal quality assessment using HVD based on PSoC system: A survey. *J. Adv. Res. Dynamical Control Sys.*, **10**: 333–339.
- Satija, U., Ramkumar, B. & Manikandan, M.S. (2017). Real-time signal quality-aware ECG telemetry system for IoT-based health care monitoring. *IEEE T. Internet Things*, **4**: 815-823.
- Satija, U., Ramkumar, B. & Manikandan, M.S. (2018). Automated ECG noise detection and classification system for unsupervised healthcare monitoring. *IEEE J. Biomed. Health Inform.*, **2**: 722-732.

# EVALUATION OF GLOBAL NAVIGATION SATELLITE SYSTEM (GNSS) SPACE SERVICE VOLUME (SSV) PERFORMANCE VIA TRIMBLE PLANNING

Dinesh Sathyamoorthy\*, Zainal Fitry M Amin & Shahrudin Abu Hassan

Science & Technology Research Institute for Defence (STRIDE), Ministry of Defence, Malaysia

\*Email: dinesh.sathyamoorthy@stride.gov.my

## ABSTRACT

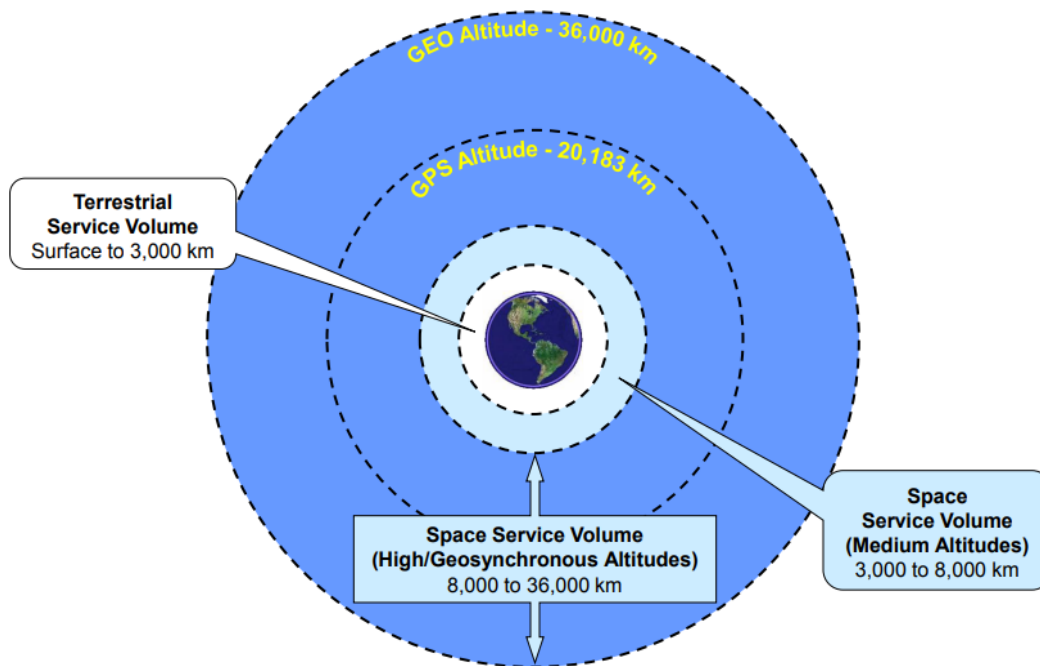
*This study is aimed at evaluating Global Navigation Satellite System (GNSS) Space Service Volume (SSV) performance in terms of number of visible GNSS satellites. This study focuses on the two GNSS systems that currently have full operating capability (FOC), namely Global Positioning System (GPS) and Globalnaya Navigatsionnaya Sputnikovaya Sistema (GLONASS). The study is conducted using Trimble Planning, which is a mission planning tool used to predict GNSS coverage at a given location and time. It is observed that GPS and GLONASS can each provide continuous coverage for up to altitude of 8,000 km. Combined use of GPS and GLONASS allows for increased GNSS satellite availability at altitude of 8,000 km, and continuous coverage at altitude of 12,000 km. The availability then degrades with increasing altitude, due to increasingly poor GNSS satellite geometry. It is proposed that further studies be conducted via GNSS simulation, whereby the accuracy of GNSS readings at various altitudes can be measured.*

**Keywords:** *Global Navigation Satellite System (GNSS); Space Service Volume (SSV); Trimble Planning; number of visible GNSS satellites; GNSS satellite geometry.*

## 1. INTRODUCTION

Continuous availability of Global Navigation Satellite System (GNSS) coverage has become a standard expectation for GNSS users for altitude of up to 3,000 km, which is a region of space known as the GNSS Terrestrial Service Volume (TSV). However, as users move above altitudes beyond 3,000 km, GNSS coverage decreases due to poor GNSS satellite geometry. This more challenging GNSS signal processing environment has been designated as the GNSS Space Service Volume (SSV), which is the region of space between altitude of 3,000 km and the geosynchronous orbit (GEO) altitude of 36,000 km (Figure 1). Use of GNSS in the SSV would support increased satellite autonomy for missions, lowering mission operations costs; significantly improve space vehicle navigation performance in these orbits; and enable new / enhanced capabilities and better performance for future missions, such as improved weather prediction using advanced weather satellites, space weather observations, astrophysics observations, space vehicle formation flying and constellation missions, and space situational awareness and proximity operations. To this end, there has been concerted effort by various space industries to support space missions at these high altitudes (Bauer, 2015; Miller *et al.*, 2016; Majithiya *et al.*, 2017).

This study is aimed evaluating GNSS SSV performance in terms of number of visible GNSS satellites. This study focuses on the two GNSS systems that currently have full operating capability (FOC), namely Global Positioning System (GPS) and *Globalnaya Navigatsionnaya Sputnikovaya Sistema* (GLONASS). The study is conducted using Trimble Planning, which is a mission planning tool used to predict GNSS coverage at a given location and time (Trimble, 2018a)



**Figure 1: GNSS Terrestrial Service Volume (TSV) and Space Service Volume (SSV) coverage (Source: Bauer, 2015).**

## 2. METHODOLOGY

GNSS consists of a core volume of satellites in the Medium Earth Orbit (MEO) transmitting one-way radio signals that are used to calculate 3D position and time. In order to achieve this, at least four GNSS satellites are needed to be within line-of-sight at any given time for the formation of a navigation solution (USACE, 2011; Kaplan & Hegarty, 2017).

In this study, Trimble Planning is used to predict the number of visible satellites at various altitudes, from 0 to 36,000 km. The location is set as Kajang, Selangor (N 2° 58', E 101° 48'), while the almanac for the date of the study (27 July 2018) is downloaded from the Trimble Planning Resources website (Trimble, 2018b). The almanac for this date provides a total number of 55 available GNSS satellites, consisting of 31 GPS and 24 GLONASS satellites.

## 3. RESULTS & DISCUSSION

The number of visible GNSS satellites at the various altitudes for GPS only, GLONASS only, and GPS and GLONASS are shown in Figures 2-4 respectively. It is observed that GPS is able to provide continuous coverage for up to altitude of 8,000 km. GLONASS is also able to provide continuous coverage at this altitude, albeit with some instances of discontinuities, where the number of visible GLONASS satellites falls below four. As the altitude is increased, the coverages for both GNSS systems become poorer, with GPS having somewhat better performance due to its larger number of satellites.

Combined use of GPS and GLONASS allows for increased GNSS satellite availability at altitude of 8,000 km, and continuous coverage at altitude of 12,000 km. The availability then degrades with increasing altitude, due to increasingly poor GNSS satellite geometry. The expansion of the number of GNSS constellations, such as Galileo and BeiDou can improve navigation performance at higher altitudes through improved signal geometry.

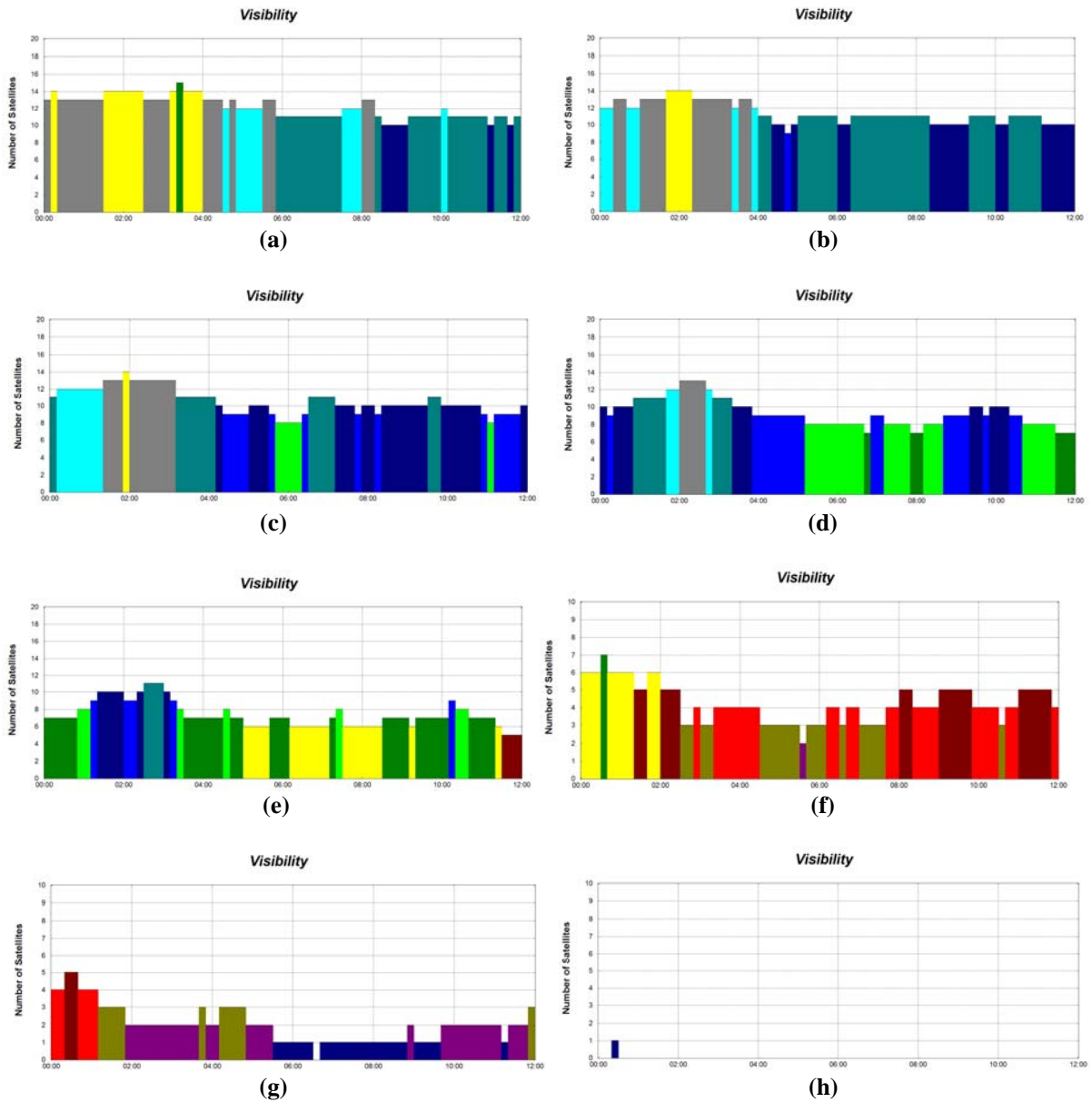


Figure 2: Number of visible GPS satellites at altitudes of: (a) 0 km (b) 1,000 km (c) 3,000 km (d) 5,000 km (e) 8,000 m (f) 12,000 km (g) 16,000 km (h) 20,000 km.



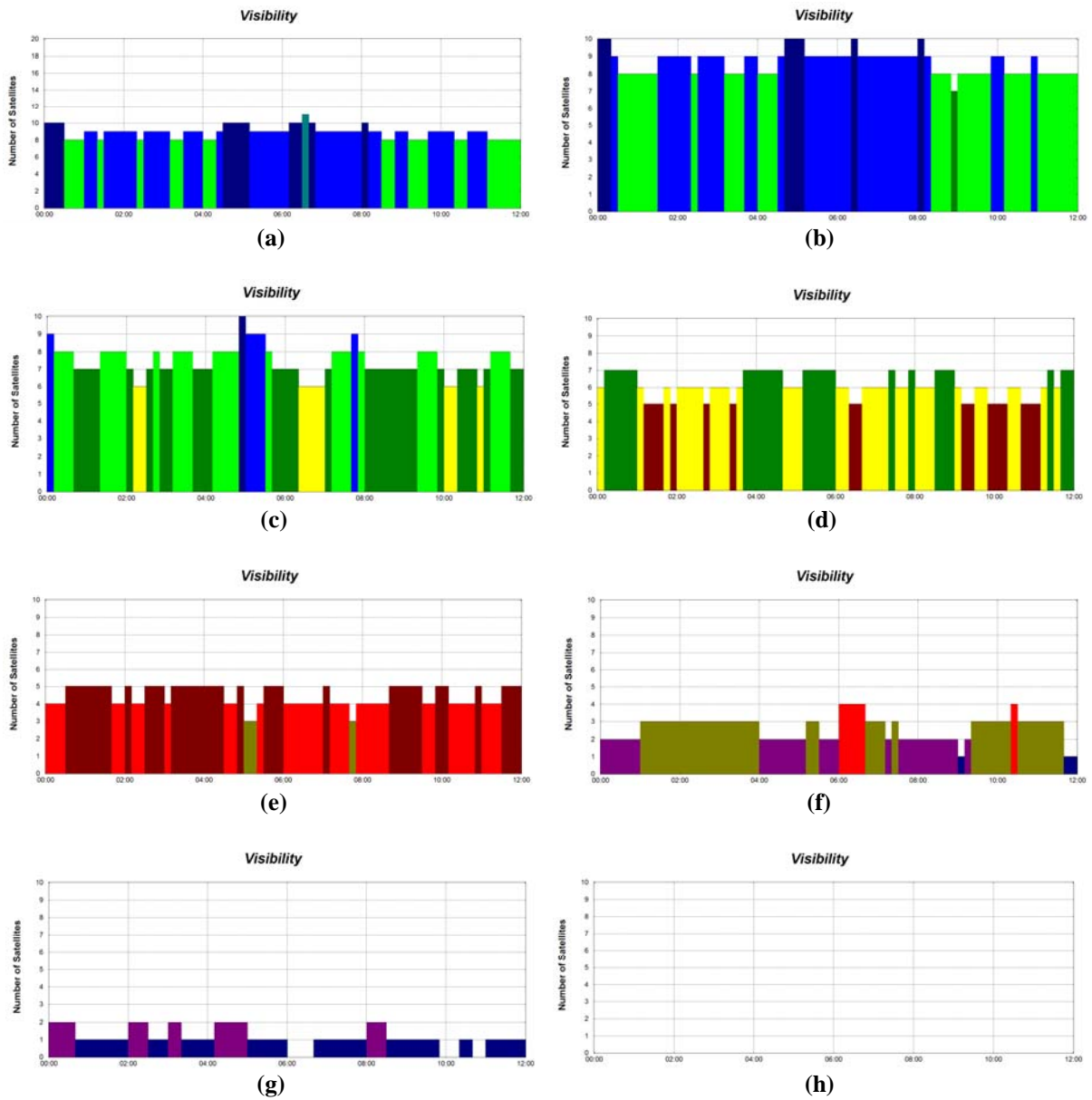


Figure 3: Number of visible GLONASS satellites at altitudes of: (a) 0 km (b) 1,000 km (c) 3,000 km (d) 5,000 km (e) 8,000 m (f) 12,000 km (g) 16,000 km (h) 20,000 km.

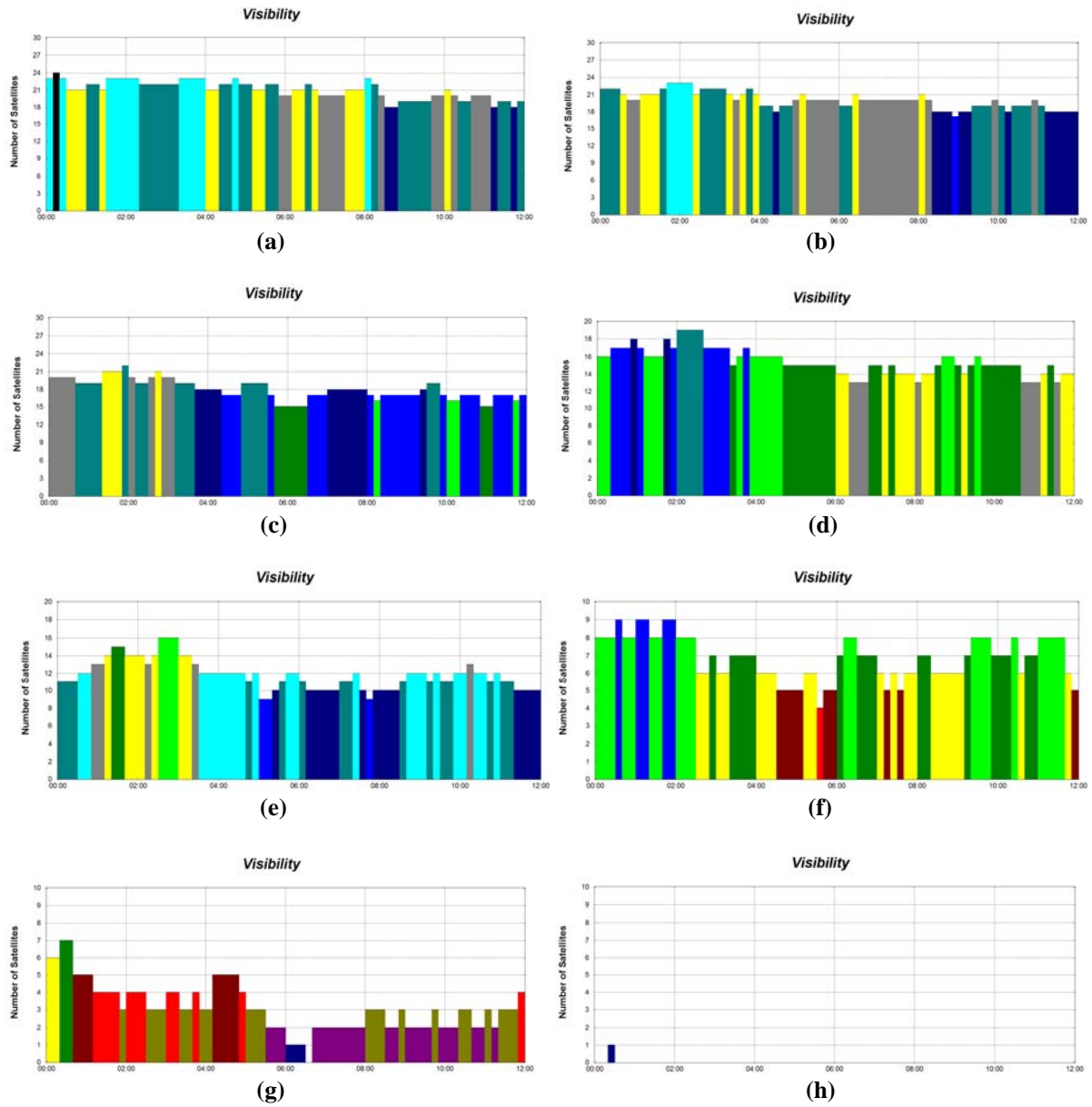


Figure 4: Number of visible GPS and GLONASS satellites at altitudes of: (a) 0 km (b) 1,000 km (c) 3,000 km (d) 5,000 km (e) 8,000 m (f) 12,000 km (g) 16,000 km (h) 20,000 km.

This study only considers number of visible GNSS satellites predicted at various altitudes using Trimble Planning. A more effective way method of performing such an evaluation would be using GNSS simulation, whereby the accuracy of GNSS readings can be measured. In previous studies conducted by STRIDE, GPS simulation was used to evaluate the vulnerabilities of GPS to radio frequency interference (RFI) (Dinesh *et al.*, 2012, 2014a, 2017a), GPS satellite clock error (Dinesh *et al.*, 2015a), varying speeds (Dinesh *et al.*, 2015b), power consumption (Dinesh *et al.*, 2016) and GPS antenna orientation (Dinesh *et al.*, 2017b). However, the present GPS simulator in STRIDE only supports altitude of up to 20 km, and thus, is not able to be used for the evaluation of GPS SSV performance. Furthermore, the simulator only supports the GPS constellation, and thus, cannot be used to study the performance of the other GNSS systems (GLONASS, Galileo and BeiDou).

Another limitation of this study is that it only takes into consideration the narrow, main Earth GNSS coverage signal that is typically used for TSV applications. Recent space flight experiments have demonstrated the viability of using GNSS in high SSV orbits by using the residual side-lobe GNSS signals that radiate over the limb of the Earth. On-orbit mission measurements have demonstrated that using residual signals broadcasted by GNSS satellites on the other side of the Earth, geosynchronous satellites at altitude of approximately 36,000 m are able to continuously track the required minimum number of four GNSS signals (Bauer, 2015; Miller *et al.*, 2016; Majithiya *et al.*, 2017).

#### 4. CONCLUSION

This study was aimed evaluating GNSS SSV performance in terms of number of visible GNSS satellites using Trimble Planning. It was observed that GPS and GLONASS can each provide continuous coverage for up to altitude of 8,000 km. Combined use of GPS and GLONASS allows for increased GNSS satellite availability at altitude of 8,000 km, and continuous coverage at altitude of 12,000 km. The GNSS satellite availability then degrades with increasing altitude, due to decreasing number of available GNSS satellites. It is proposed that further studies be conducted via GNSS simulation, whereby the accuracy of GNSS readings at various altitudes can be measured.

#### REFERENCES

- Bauer, F.H. (2015). GPS Space Service Volume (SSV): Ensuring consistent utility across GPS design builds for space users. *15<sup>th</sup> PNT Advisory Board Meeting*, 11 June 2015.
- Dinesh, S, Mohd Faudzi, M. & Zainal Fitry, M.A. (2012). Evaluation of the effect of radio frequency interference (RFI) on Global Positioning System (GPS) accuracy via GPS simulation. *Defence. Sci. J.*, **62**: 338-347.
- Dinesh, S., Shalini, S., Zainal Fitry, M.A. & Siti Zainun, A. (2013). Evaluation of the repeatability of Global Positioning System (GPS) performance with respect to GPS satellite orbital passes. *Defence S&T Tech. Bull.*, **6**: 130-140.
- Dinesh, S., Mohd Faudzi, M., Rafidah, M., Nor Irza Shakhira, B., Siti Robiah, A., Shalini, S., Aliah, I., Lim, B.T., Zainal Fitry, M.A., Mohd Rizal, A.K. & Mohd Hasrol Hisam, M.Y. (2014a). Evaluation of the effect of radio frequency interference (RFI) on Global Positioning System (GPS) receivers via GPS simulation. *ASM Sci. J.*, **8**: 11-20.
- Dinesh, S., Shalini, S., Zainal Fitry, M.A., Siti Zainun, A., Siti Robiah, A., Mohd Idris, I. & Mohd Hasrol Hisam, M.Y. (2014b). Evaluation of the effect of commonly used materials on multipath propagation of Global Positioning System (GPS) signals via GPS simulation. *Adv. Mil. Tech.*, **9**: 81-95.
- Dinesh, S., Shalini, S., Zainal Fitry, M.A., Asmariah, J. & Siti Zainun, A. (2015a). Evaluation of the effect of Global Positioning System (GPS) satellite clock error via GPS simulation. *Defence S&T Tech. Bull.*, **8**: 51-62.
- Dinesh, S., Shalini, S., Zainal Fitry, M.A., Asmariah, J. & Siti Zainun, A. (2015b). Evaluation of the accuracy of Global Positioning System (GPS) speed measurement via GPS simulation. *Defence S&T Tech. Bull.*, **8**: 121-128.

- Dinesh, S., Shalini, S., Zainal Fitry, M.A., Asmariah, J. & Siti Zainun, A. (2016). Evaluation of trade-off between Global Positioning System (GPS) accuracy and power saving from reduction of number of GPS receiver channels. *Appl. Geomatics*, **8**: 67-75.
- Dinesh, S., Zainal Fitry, M.A. & Shahrudin, A.H. (2017a). Evaluation of Global Positioning System (GPS) adjacent band compatibility via GPS simulation. *Defence S&T Tech. Bull.*, **10**: 229 – 235.
- Dinesh, S., Shalini, S., Zainal Fitry, M.A., Mohamad Firdaus, A., Asmariah, J. & Siti Zainun, A. (2017b). Evaluation of the effect of Global Positioning System (GPS) antenna orientation on GPS performance. *Defence S&T Tech. Bull.*, **10**: 33-39.
- Kaplan, E.D. & Hegarty, C.J. (2017). *Understanding GPS / GNSS: Principles and Applications*, 3<sup>rd</sup> Ed. Artech House, Norwood, Massachusetts.
- Majithiya, P., Khatri, K., Bera, S., Sarkar, S. & Parikh, K.S. (2017). Future space service of NavIC (IRNSS) constellation. *GPS World*, **2017 (4)**: 40-45.
- Miller, J.J., Bauer, F.H., Donaldson, J.E., Oria, A.J., Page, S., Parker, J.J.K & Welch, B.(2016). Navigating in space: Taking GNSS to new heights. *GPS World*, **2017(6)**: 44-49.
- Trimble (2018a). *Trimble GNSS Planning*. Trimble Inc., Sunnyvale, California.
- Trimble (2018b). *GPS Data Resources*. Available online at: [https://www.trimble.com/Support/GPD\\_Data\\_Resources.aspx](https://www.trimble.com/Support/GPD_Data_Resources.aspx) (Last access date: 27 July 2018).
- USACE (US Army Corps of Engineers) (2011). *Engineer Manual EM 1110-1-1003: NAVSTAR Global Positioning System Surveying*. US Army Corps of Engineers (USACE), Washington D.C.

# MECHANICAL PROPERTIES OF HYBRID KENAF / KEVLAR FIBRE REINFORCED THERMOPLASTIC COMPOSITES

Sivakumar Dhar Malingam<sup>1\*</sup>, Ng Lin Feng<sup>1</sup>, Ng Cher Sean<sup>1</sup>, Kathiravan Subramaniam<sup>1</sup>, Nadlene Razali<sup>1</sup> & Zaleha Mustafa<sup>2</sup>

<sup>1</sup>Centre for Advanced Research on Energy, Fakulti Kejuruteraan Mekanikal

<sup>2</sup>Advanced Manufacturing Centre, Fakulti Kejuruteraan Pembuatan  
Universiti Teknikal Malaysia Melaka (UTeM), Malaysia

\*Email: sivakumard@utem.edu.my

## ABSTRACT

*Hybrid composites consist of two or more different fibres in a single matrix has become an interesting topic in the field of fibre reinforced polymers. In this study, woven kenaf and Kevlar fibre along with polypropylene were used to fabricate hybrid composites. Different fibre configurations of composite laminate materials were introduced to study its effects on the tensile, quasi-static indentation and low-velocity impact characteristics of hybrid and non-hybrid composite materials. The composites were fabricated through a hot press compression moulding process. From the results, it was noticed that the hybrid kenaf / Kevlar fibre reinforced polypropylene composites showed a positive hybrid effect in which they demonstrated higher tensile and penetration resistance, compared to the non-hybrid kenaf fibre reinforced composites. Furthermore, partial incorporation of Kevlar fibre in the non-hybrid kenaf reinforced polypropylene composites also improved the low-velocity impact resistance of such materials. The findings revealed that a balance between the mechanical strength and the environmental friendliness could be achieved through hybridisation.*

**Keyword:** *Hybrid composites; kenaf fibre; tensile properties; quasi-static indentation; low-velocity impact*

## 1. INTRODUCTION

The present materials such as metallic alloys have been widely employed in a wide variety of engineering applications. Nevertheless, such materials could not warrant the requirements of high specific properties in transportation sectors. The substitution of metallic alloys with composite materials provides the flexibility to tailor the material properties for certain applications. Composite materials have been a well-known material in industries since past decades (Sivakumar *et al.*, 2016). Composite is a material made from two or more constituents with different physical or chemical properties, which are classified as matrix and reinforcement. Composite materials possess high specific strength and modulus which make them becoming attractive among industries (Nunna *et al.*, 2012). Furthermore, they are relatively fatigue insensitive towards fatigue loading in comparison with metallic alloys (Sadighi *et al.*, 2012). Nowadays, engineering fields such as automotive and aerospace use fibre reinforced polymers (FRPs) in the applications of the interior door panel of vehicle and fuselage of aerospace.

The demand for synthetic fibres has been increasing magnificently since the 1960s, causing natural fibres to lose its market share. This phenomenon lasts for a few decades until December 2006 when United Nations General Assembly declared, the International Year of Natural Fibres in 2009. This is to enhance the awareness of consumer about natural fibres and increase the need for natural fibre based products (Jawaid *et al.*, 2011). Natural fibres have gained the attraction of researchers, and scientists as an alternative reinforcement for fibre reinforced polymer composites due to their

outstanding properties such as high specific properties, low density, non-abrasive, eco-friendly and bio-degradable characteristics (Ng *et al.*, 2017; Asgarinia *et al.*, 2015). Harish *et al.* (2009) stated that natural fibres are not only strong and lightweight but also relatively very cheap. Although natural fibres possess numerous attractive advantages in comparison with synthetic fibres, their hydrophilic nature and relatively poor mechanical strength retard their utilisation in structural applications. The hydrophilic nature of natural fibres attracts the moisture which weakens the fibre-matrix bonding, leading to the deterioration in the mechanical strength of composite materials (Sivakumar *et al.*, 2018). One of the efficient methods to rectify these shortcomings in natural fibre reinforced composite is through hybridisation. Hybridisation with synthetic fibre in natural fibre reinforced composites could reduce the moisture sensitivity and improve the mechanical strength. Kenaf fibre is well-known for its high economic value and has a high potential for future applications (Sulaiman *et al.*, 2017; Cieh *et al.*, 2017). According to Yahaya *et al.* (2014), kenaf fibre was the most suitable natural fibre for hybridisation with Kevlar using the analytical hierarchy process (AHP). Moreover, literature studies have evidenced the potential of employing hybrid composite materials over non-hybrid composite materials (Sivakumar *et al.*, 2018; Ng *et al.*, 2017). Kevlar fibre is known to have high toughness, high stiffness and excellent impact resistance.

Quasi-static indentation (QSI) resistance of composite structures characterises the energy dissipating capacity of the structures under transverse loading without dynamic and rate effects. Salman *et al.* (2018) studied the QSI behaviour of kenaf and aramid fibre reinforced polyvinyl butyral hybrid composite laminates. The results showed that the hybrid composite laminates attested higher energy absorption capacity compared to non-hybrid kenaf reinforced composites. Erkendirici & Haque (2012) carried out experiments to investigate the QSI behaviour of glass fibre reinforced composite with different polymer and types of glass fibre. They revealed that S-2 glass and E-glass fibre reinforced high density polyethylene showed lower stiffness, lower peak force, higher deflection, lower damage area and lower energy dissipation compared to S-2 glass fibre reinforced epoxy composites. Bulut *et al.* (2016) investigated the effect of hybridisation on the penetration resistance of composites. They concluded the Kevlar fibre had the highest energy dissipation capability compared to carbon and glass fibres. Furthermore, the highest positive hybrid effect was observed in carbon / Kevlar composites where the carbon fibres were located in the outermost of the composites. Subramaniam *et al.* (2017) carried out an experimental investigation on the quasi-static indentation of kenaf/glass hybrid composite metal laminates. Similar results were obtained where the placement of high strength glass fibre at the surface of hybrid composites possessed the highest penetration resistance.

Low-velocity impact (LVI) causes excessive stress across the interface between layers with different angles, resulting in delamination after the failure of interface material. Numerous studies have been conducted to characterise the impact behaviour of composite materials. Ying *et al.* (2017) studied low-velocity impact properties of carbon/Kevlar fibre reinforced hybrid composites with different fibre configurations. The findings demonstrated that the placement of high strength carbon fibres in the outermost layers of composite enhanced the impact resistance. Sevkati *et al.* (2013) conducted drop-weight impact test on the glass / graphite fibre reinforced epoxy composites to determine their low-velocity impact response. They revealed that the composites with glass fibres in the outer skin layers exhibited better resistance towards impact loading. Thus, it was concluded that the fibre stacking sequence of composites has a significant effect on the impact properties. Sayer *et al.* (2010) conducted an experimental investigation to study the impact behaviour of hybrid composite laminates based on carbon and glass fibres. The hybrid carbon and glass fibre reinforced composites showed the highest impact resistance when carbon fibres were placed at tension side and glass fibres at impacted side.

To date, the quasi-static indentation and low-velocity impact responses of kenaf / Kevlar fibre reinforced polypropylene hybrid composites remain unexplored. In this study, the tensile, quasi-static indentation and low-velocity impact properties of kenaf / Kevlar fibre reinforced hybrid composites with different fibre configurations are investigated to explore the potential of using hybrid composites in engineering applications.

## 2. METHODOLOGY

### 2.1 Materials

Two types of plain weave fabric which are kenaf and Kevlar were used in this study. Figure 1 shows the plain weave kenaf and Kevlar fabrics. The woven kenaf fabric (K), with a density of  $1.40 \text{ g/cm}^3$  was obtained from National Kenaf and Tobacco Board, Malaysia. Meanwhile, Kevlar fabric (KV) with a density of  $1.44 \text{ g/cm}^3$  was supplied by DuPont Knowledge Center, India. Polypropylene granules (PP) with a density of  $0.90 \text{ g/cm}^3$  were purchased from Al Waha Petrochemical Company, Saudi Arabia. The properties of kenaf and Kevlar fibres are summarised in Table 1.

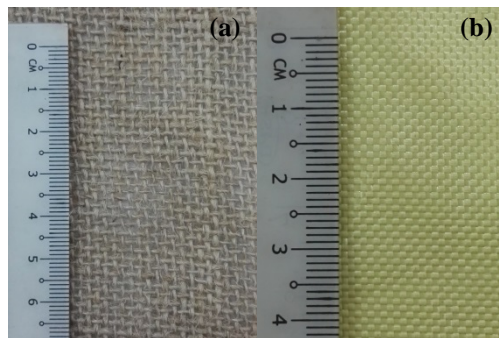


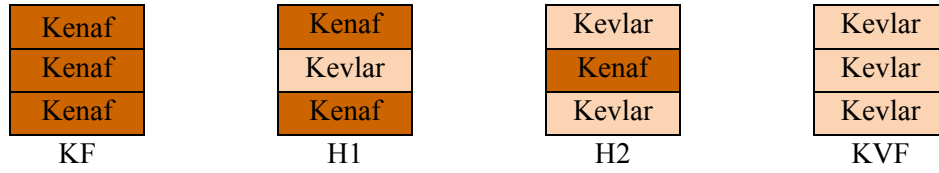
Figure 1: Plain weave woven: (a) Kenaf (b) Kevlar.

Table 1: Properties of kenaf and Kevlar fibres (Dittenber *et al.*, 2012; Bilisik, 2011).

Properties	Kenaf fibres	Kevlar fibres
Tensile strength (MPa)	223 – 930	3,400
Tensile modulus (GPa)	14.5 – 53	99
Elongation (%)	1.5 – 2.7	3.3
Density ( $\text{g/cm}^3$ )	1.4	1.45

### 2.2 Composite Preparation

In this study, there are four different types of fibre configurations in composite laminates. The fibre configurations are referred to KF, H1, H2 and KVF as shown in Figure 2. KF and KVF refer to those of non-hybrid kenaf and Kevlar fibre reinforced polypropylene composites. H1 denotes those hybrid composites with kenaf fabrics at the outermost layers whereas H2 represents those hybrid composites where the Kevlar fabrics are located at the outermost layers. A total number of three fibre layers were fixed in the composite laminates.



**Figure 2: Layup configurations of composites.**

The composites laminates were prepared by stacking PP sheets in between the fibre layers to allow optimum fibre impregnation. The prepared layups were stacked in a picture frame mould with a dimension of 200 x 200 x 3 mm (length x width x thickness). The composite laminates together with picture frame mould were then placed in a hot press machine and preheated for 4 min followed by hot compression at a temperature of 175 °C and pressure of 3.5 MPa for 8 min. The composite panel was cooled to room temperature before taken out from the hot press machine.

Table 2 shows the fibre and matrix volume fraction of the composites. Equation 1 was used to calculate the fibre volume fractions.

$$V_{fibre} = \frac{\frac{w_{kenaf}}{\rho_{kenaf}} + \frac{w_{Kevlar}}{\rho_{Kevlar}}}{\frac{w_{kenaf}}{\rho_{kenaf}} + \frac{w_{Kevlar}}{\rho_{Kevlar}} + \frac{w_{pp}}{\rho_{pp}}} \quad (1)$$

Where  $w_{kenaf}$  is the weight of kenaf fibre,  $w_{kevlar}$  is the weight of Kevlar fibre,  $w_{pp}$  is the weight of polypropylene,  $\rho_{kenaf}$  is the density of kenaf fibre,  $\rho_{kevlar}$  is the density of Kevlar fibre, and  $\rho_{pp}$  is the density of polypropylene.

**Table 2: Fibre and matrix volume fraction in composite laminates.**

Volume Fraction (%)	KF	H1	H2	KVF
Kenaf fibre	21.07	14.05	8.4	0
Kevlar fibre	0	4.2	7.16	13.21
Total fibre	21.07	18.25	15.56	13.21
Polypropylene	78.93	81.75	84.44	86.79

### 2.3 Experimental Works

The tensile test was conducted according to ASTM D3039 on the composite laminates with different fibre configurations to determine the tensile properties at cross-head displacement rate of 2 mm/min and room temperature. The tensile test was carried out using a Universal Testing Machine (UTM) Instron 8872 with 25 kN load cell capacity. Average results were recorded for further analysis and evaluation.

The QSI test was conducted at a cross-head displacement rate of 1.25 mm/min according to ASTM D6264 to study the damage evolution and penetration resistance behaviour of the hybrid composites using UTM Instron 5585 with 150 kN load cell capacity. A series of quasi-static indentation tests in edge supported configuration was carried out using a hemispherical shaped steel indenter with 12.7 mm diameter. The penetration resistance force-displacement curves were recorded and further evaluated.



The Drop weight impact tests were carried out according to ASTM D7136 using Instron drop tower impact Ceast 9340 machine. The impactor nose has a hemispherical shape with the diameter of 12.7mm and the mass of 6.5 kg. The coupon edge was clamped to the fixture and the impact point was located at the sample centre. Impact energies were fixed at 10, 20 and 30J by changing the height of the impactor. The impact properties include peak load, energy absorption and displacement were recorded and compared. The damages on the front and rear fracture surfaces were investigated.

### 3. RESULTS AND DISCUSSION

#### 3.1 Tensile Properties

Figure 3 depicts the tensile strength and tensile modulus of composites with different fibre configurations. Overall, non-hybrid Kevlar fibre reinforced composites showed the highest tensile strength in comparison with hybrid composites and non-hybrid kenaf fibre reinforced composites. In contrast, non-hybrid kenaf reinforced composites attested the lowest tensile strength at 28.759 MPa. It was observed that the increase of Kevlar fibre layer in the composite laminates improved the tensile strength. The improvement in the tensile strength is due to the intrinsic higher mechanical strength of Kevlar fibre. When Kevlar fibre replaced middle layer of non-hybrid kenaf fibre, improvement of 123.62 % in the tensile strength was observed. Hybrid composites with H2 fibre configuration showed a tensile strength of 109.85 MPa which is 281.95 % higher than non-hybrid KF composites. However, it is interesting to note that H2 composite laminates exhibited comparable tensile strength to the non-hybrid KVF composites. Since the outer layers govern the tensile strength in the composite laminates, thus H2 composites possesses the comparable tensile strength to the non-hybrid KVF composites. The results are in agreement with the study conducted by Feng *et al.* (2017) where the hybrid glass/kenaf reinforced composite laminates with the incorporation of glass fibre at the outer layers have a comparable tensile strength to the non-hybrid glass fibre reinforced composite composite laminates.

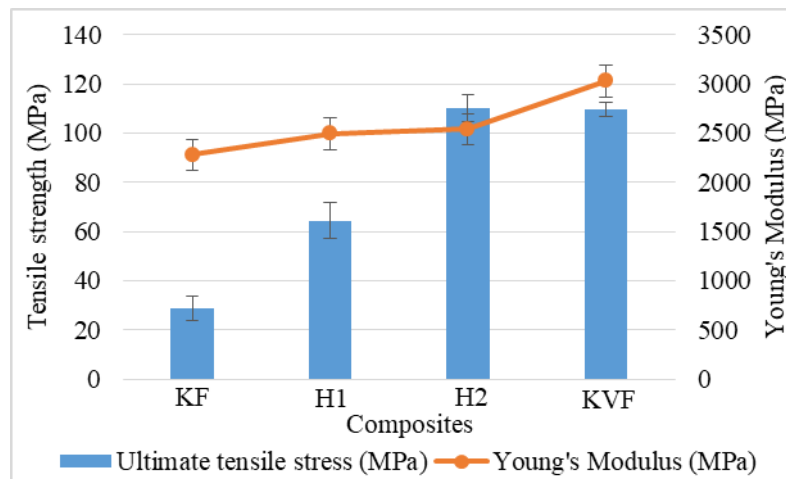


Figure 3: Tensile strength and tensile modulus of composite laminates.

#### 3.2 Quasi-Static Indentation Properties

Quasi-static indentation tests were carried out to understand the penetration resistance of composite laminates with different stacking sequences. Figure 4 shows the load-displacement curves of composite laminates with different fibre configurations. The curve can be separated into three regions: penetration (region A), perforation (region B) and friction (region C). A similar observation was also obtained for glass fibre reinforced polyester composites (Sabet *et al.*, 2009). The penetration happened after the initial linear part where the initial failure occurred. At region B, the perforations

begin, penetration force decreases as matrix failure start to occur, followed by fibre breakage. Finally, region C is associated with the residual frictional force of indenter and fibres. It was clear that non-hybrid Kevlar fibre reinforced composites exhibited the highest peak load of 4302.87 N, followed by H2 with 3194.46 N, H1 with 2198.72 N and non-hybrid KF with 845.88N. Figure 5 shows the peak load and energy absorption of the composite laminates for quasi-static indentation test. The trend demonstrates the positive hybrid effect in which the energy absorption of composites containing Kevlar fibres is better than non-hybrid kenaf fibre reinforced composites. In fact, the perforation resistance is governed by the bending stiffness of the materials. Therefore, the incorporation of high stiffness Kevlar fibres in the composite laminates improves the perforation resistance. Moreover, it was noticed that the incorporation of Kevlar fibres in the outermost layer of composites had greater energy absorption and load resistance. In comparison with kenaf fibres, Kevlar fibres require higher penetration force and elongation to fracture. Thus, the placement of high strength Kevlar fibres in the outermost layers of the composites improves the peak load and energy absorption.

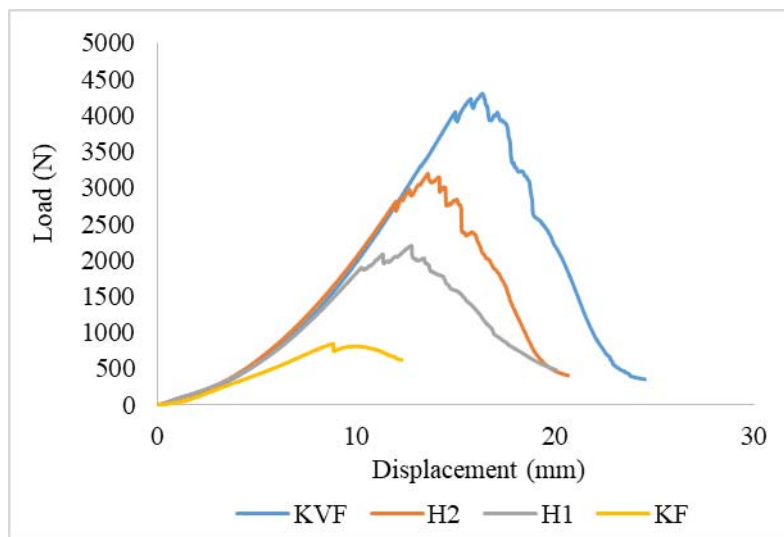


Figure 4: Load-displacement curves of composite laminates with different fibre configurations.

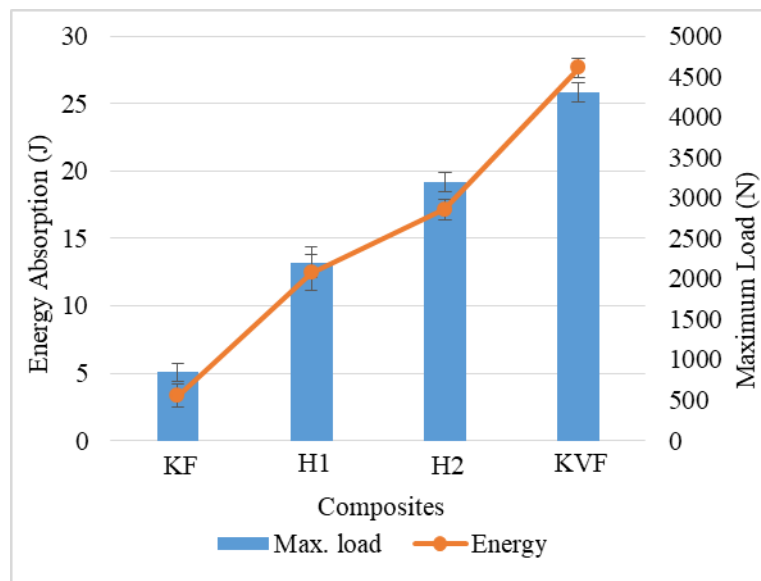
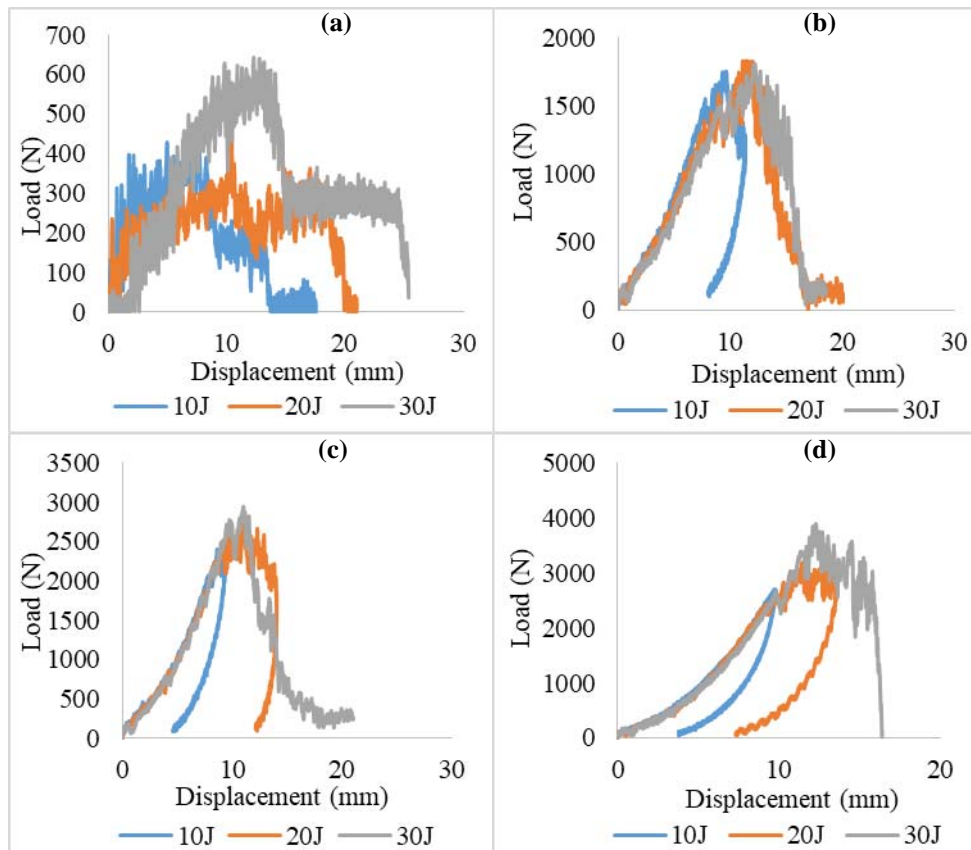


Figure 5: Maximum load and energy absorption of composite laminates under quasi-static indentation.

### 3.3 Low-velocity Impact Properties

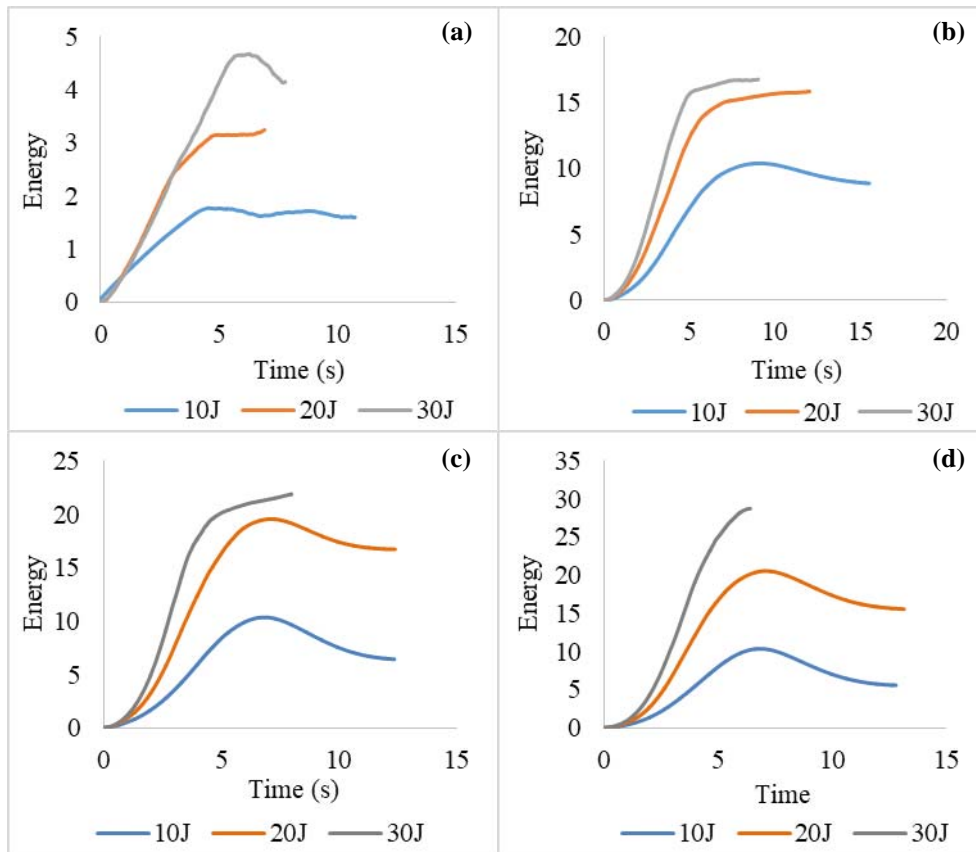
Figure 6 shows the contact load-displacement curves of composites with different fibre configurations and energy levels. The curves express the impact behaviour of each specimen. According to Ahmed *et al.* (2016), there are two kinds of curve which are closed and open. The closed curve indicates the occurrence of rebounding during impact. In this stage, the curve shows the elastic response of composite to impact and minimum or no damage happens during this stage. Nevertheless, as the impact energy increased, the curves change from closed to open type. Open curve indicates the occurrence of almost complete failure in the composite structure. Figure 6(a) shows the load-displacement curve of KF composites for 10, 20 and 30J impact energies. Penetration was observed to happen in KF composites irrespective of energy levels. This explained that non-hybrid kenaf fibre reinforced composites have the lowest resistance to the impact loading. When hybridising the kenaf/polypropylene composite with one layer of Kevlar fibre at the centre, the result was significantly improved. Rebounding occurred at 10J for H1 composites as shown in Figure 6(b). However, the curves changed from closed to open type when the impact energy was increased to 20 and 30 J, implying that penetration has occurred. Both non-hybrid KVF composites and H2 composites as depicted in Figure 6(c) and Figure 6(d) showed a similar trend where rebounding occurred up to 20 J and then penetration occurred at 30 J.



**Figure 6: Load-displacement curves of composite laminates with different fibre configurations: (a) KF (b) H1 (c) H2 (d) KVF.**

Figure 7 represents the energy-time curves of composite laminates with different fibre configurations. According to Shishevan *et al.* (2017), impact energy is defined as the total potential energy that the impactor received from the test instrument during the test and transformed it to the kinetic energy that is eventually received by the specimens. It was noticed in Figure 7(a) that the penetration was observed in non-hybrid kenaf fibre reinforced composites during the impact loading regardless of energy levels. The improvement was observed in H1 hybrid composite laminates where the rebounding occurred at 10J as shown in Figure 7(b). However, the impact energy as can be seen in

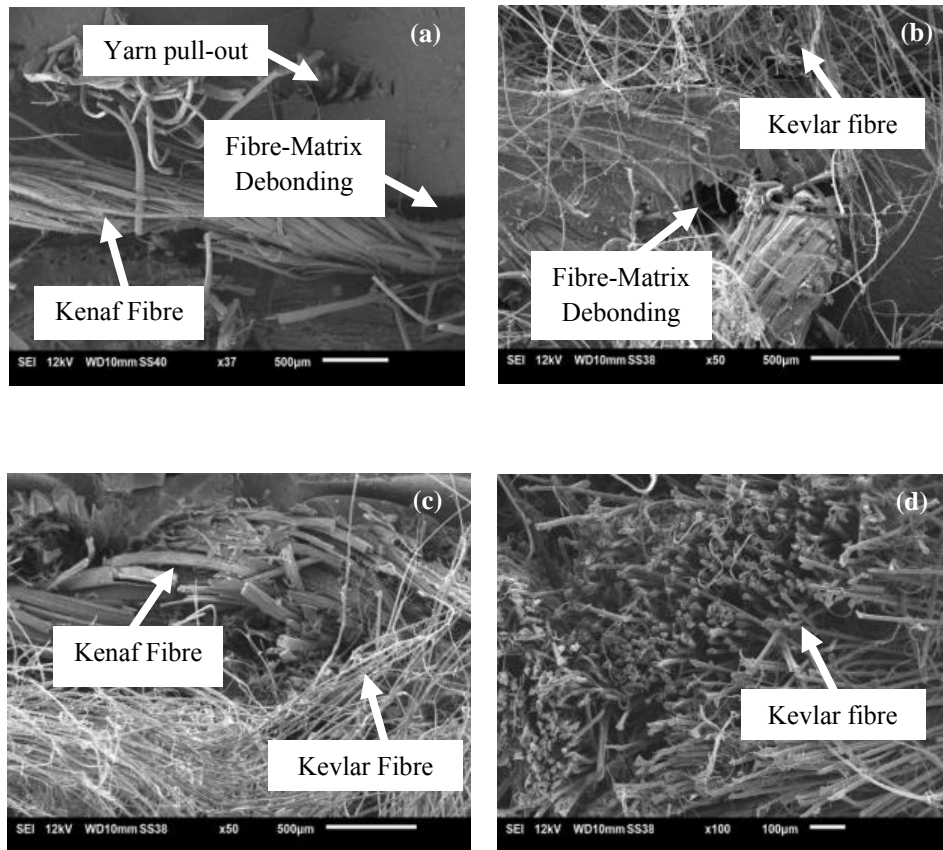
Figure 7(c) and Figure 7(d) was not enough for the penetration of the non-hybrid Kevlar fibres reinforced composites and H2 hybrid composites during the impact loading at 10 and 20 J where rebounding occurred. Conversely, at energy 30J, the penetration occurred. Overall, the total energy absorbed for non-hybrid KF configuration was the lowest compared to others.



**Figure 7: Energy-time curves of composite laminates with different fibre configurations: (a) KF (b) H1 (c) H2 (d) KVF.**

### 3.4 Damage Assessment

The morphological analysis of the fractured surface of specimens was examined by using the scanning electron microscopy (SEM). Figure 8 illustrates the SEM images of failure surface of woven kenaf/Kevlar hybrid composites due to tensile loading. The failure modes observed from SEM images showed that both the reinforcement and matrix were the load carriers. This statement can be proved by the occurrence of fibre failure (breakage) and matrix failure (cracks) in the hybrid composites. Furthermore, fibre pull-out and fibre/matrix debonding were also noticed in the hybrid composites, particularly in the Kevlar dominated composite laminates, indicating that Kevlar fibres are less compatible with the polymer matrix.








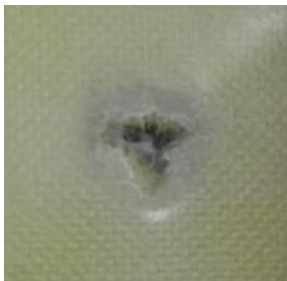


**Figure 8: SEM micrograph of tensile fracture specimens: (a) KF (b) H1 (c) H2 (d) KVF.**







The failure mechanism of specimens for the indented and rear surface after quasi-static indentation test was also determined. Table 3 shows the damaged surface after the quasi-static indentation tests for all composites. It was evident that all the penetrated composites exhibited an out-of-plane plastic deformation. Kenaf fibres were wholly fractured due to its brittle nature whereas the Kevlar fibres showed fibre pull-out. Matrix failure and delamination were noticed in the composite laminates. For H1 configuration, kenaf fibres at the front surface were compressed due to plunger punch and an exact plunger shaped cavity was created. At the rear surface, delamination of kenaf fibres happened in a spall-form when the full penetration was achieved.

Many types of failure modes can occur during low-velocity impact test such as microcracks, debonding, delamination and fibres breakage, which are similar to the indentation tests. Generally, the damage pattern depends on the mechanical properties of composites. Tables 4-7 show the drop weight impact damage of composite laminates with different fibre configurations. At an energy of 10 J, KF composites exhibited catastrophic failure at the front and rear surfaces. The partial replacement of middle kenaf fabric to Kevlar fabric drastically reduced the damage propagation. A small dent was observed in the H1 composite laminates on the front surface. The rear surface of H1 composite laminates exhibited crack propagation.







**Table 3: Failure surface of composite laminates under quasi-static indentation test.**

<b>Composites</b>	<b>Front</b>	<b>Rear</b>
<b>KF</b>		
<b>H1</b>		
<b>H2</b>		
<b>KVF</b>		

**Table 4: Failure surface of KF composite under low-velocity impact test.**







Energy levels	KF composite laminates	
	Front	Rear
10 J		
20 J		
30 J		

**Table 5: Failure surface of H1 composite under low-velocity impact test.**







Energy levels	H1 composite laminates	
	Front	Rear
10 J		
20 J		
30 J		



**Table 6: Failure surface of H2 composite under low-velocity impact test.**

Energy levels	H2 composite laminates	
	Front	Rear
10 J		
20 J		
30 J		

**Table 7: Failure surface of KVF composite under low-velocity impact test.**

Energy levels	KVF composite laminates	
	Front	Rear
10 J		
20 J		
30 J		

H2 and KVF exhibited similar failure mechanism where no visible damage was observed on the front surface. Only limited cracks were noticed on the rear surface of H2 and KVF composite laminates. As the impact energy levels were increased, the damage initiates in all the composite laminates regardless of types of fibres. Dent was observed on the front surface of the H2 and KVF composite laminates at 20 J. A significant matrix failure, fibre-matrix debonding and splitting were noticed in the Kevlar dominated composite laminates when the energy was further increased to 30 J. Characteristics of damage in the LVI test indicated the brittle nature of kenaf fibres and high impact resistance of Kevlar fibres.

#### **4. CONCLUSION**

In this study, the effects of fibre configurations on the tensile, quasi-static penetration and low-velocity impact properties of kenaf/Kevlar fibre reinforced polypropylene composites were investigated. FRP composites with different fibre configurations which include KF, H1, H2 and KVF were fabricated. Based on the results, the following conclusions were made.

1. The tensile result showed that hybridisation could improve the tensile strength of the composite laminates. The findings demonstrated that non-hybrid Kevlar fibre reinforced composites showed the highest tensile strength in comparison to hybrid composites and non-hybrid kenaf fibre reinforced composites. A positive hybrid effect was observed when the Kevlar fabrics were partially incorporated in the hybrid composite laminates. In overall, the tensile properties of hybrid composite laminates are in between those of non-hybrid Kevlar and kenaf fibre reinforced composite laminates. However, it should be emphasized that the H2 hybrid composite laminates attested comparable tensile strength to the non-hybrid Kevlar fibre reinforced composites because the skin layers in composite laminates are the main load carrier compared to the middle layer.
2. The quasi-static indentation test shows, KVF composite laminates has the highest penetration load, which was followed by H2, H1 and lastly KF composite laminates. Besides that, it was found that H2 with kenaf fibre at the middle layer had greater energy absorption and load resistance compared to H1 due to the high penetration resistance of Kevlar fibres at the surface layers. The penetration resistance of composite laminates is governed by the bending stiffness of each fibre ply. Thus, the placement of Kevlar fibre in the surface layers improved the penetration resistance of the laminates.
3. The results obtained from low-velocity impact shows that the non-hybrid kenaf fibre reinforced composites had poor resistance to impact loading. However, by placing one layer of Kevlar fibre in the middle layer, the impact properties were significantly improved. In overall, the hybrid FRP composites can absorb more energy compared to non-hybrid kenaf fibre reinforced composites. However, non-hybrid Kevlar fibre reinforced composite laminates still displayed the highest impact resistance and energy absorption capacity. In overall, hybrid composites improved the overall impact properties of composite laminates compared to non-hybrid kenaf reinforced composites. H2 hybrid laminates attested a similar impact failure mechanism to non-hybrid Kevlar reinforced composites. These findings aroused the further exploration on hybrid composites for military helmet and armour applications.

## ACKNOWLEDGEMENT

The authors would like to thank Universiti Teknikal Malaysia Melaka (UTeM) for the continuous support of this research project. The authors would also wish to express their gratitude towards Skim Zamalah UTeM provided by Universiti Teknikal Malaysia Melaka and grant FRGS/1/2017/STG07/FKM-CARE/F00339 from the Ministry of Education Malaysia.

## REFERENCES

- Ahmed, A., Mohmmed, R., Bingjie, Z. & Wei, L. (2016). Noncontact inspection of impact damage properties of woven fabric-reinforced composites after low-velocity impact by using air-coupled ultrasonic technique. *J. Ind. Text.*, **46**: 809–832.
- Asgarinia, S., Viriyasuthee, C., Phillips, S., Dube, M., Baets, J., Van Vuure, A., Verpoest, I. & Lessard, L. (2015). Tension-tension fatigue behaviour of woven flax/epoxy composites. *J. Reinf. Plast. Compos.*, **34**: 857–867.
- Bilisik, K. (2011). Experimental determination of yarn pull-out properties of para-aramid (Kevlar) woven fabric. *J. Ind. Text.*, **41**: 201–221.
- Bulut, M., Erkliğ A. & Yeter, E. (2016). Hybridization effects on quasi-static penetration resistance in fiber reinforced hybrid composite laminates. *Compos. Part B Eng.*, **98**: 9–22.
- Cieh, N.L., Sulaiman, S., Mokhtar, M.N. & Naim, M.N. (2017). Bleached kenaf microfiber as a support matrix for cyclodextrin glucanotransferase immobilization via covalent binding by different coupling agents. *Process Biochem.*, **56**: 81–89.

- Dittenber, D.B. & GangaRao, H.B.S. (2012). Critical review of recent publications on use of natural composites in infrastructure. *Compos. Part A Appl. Sci. Manuf.*, **43**: 1419–1429.
- Erkendirci, O.F. & Haque, B.Z.G. (2012). Quasi-static penetration resistance behaviour of glass fibre reinforced thermoplastic composites. *Compos. Part B Eng.*, **43**: 3391–3405.
- Feng, N.L., DharMalingam, S., Zakaria, K.A. & Selamat, M.Z. (2017). Investigation on the fatigue life characteristic of kenaf/glass woven-ply reinforced metal sandwich materials. *J. Sandw. Struct. Mater.* doi:10.1177/1099636217729910
- Harish, S., Peter Michael, D., Bensely, A., Mohan Lal, D. & Rajadurai, A. (2009). Mechanical property evaluation of natural fiber coir composite. *Mater. Charact.*, **60**: 44–49.
- Jawaid, M., Abdul Khalil, H.P.S., Abu Bakar, A. & Noorunnisa Khanam, P. (2011). Chemical resistance, void content and tensile properties of oil palm/jute fibre reinforced polymer hybrid composites. *Mater. Des.*, **32**: 1014–1019.
- Ng, L.F., Sivakumar, D., Zakaria, K.A., Bapokutty, O. & Sivaraos. (2017). Influence of kenaf fibre orientation effect on the mechanical properties of hybrid structure of fibre metal laminate. *Pertanika J. Sci. & Technol.*, **25**: 1–8.
- Ng, L.F., Sivakumar, D., Zakaria, K.A. & Selamat, M.Z. (2017). Fatigue performance of hybrid fibre metal laminate structure. *Int. Rev. Mech. Eng.*, **11**: 61–68.
- Nunna, S., Chandra, P.R., Shrivastava, S. & Jalan A.K. (2012). A review on mechanical behavior of natural fiber based hybrid composites. *J. Reinf. Plast. Compos.*, **31**: 759–769.
- Sabet, A.R., Beheshty, M.H. & Rahimi, H. (2009). Experimental study of sharp-tipped projectile perforation of GFRP plates containing sand filler under high-velocity impact and quasi-static loadings. *Polym. Compos.*, **30**: 1497–1509.
- Sadighi, M., Alderliesten, R.C. & Benedictus, R. (2012). Impact resistance of fiber-metal laminates: a review. *Int. J. Impact. Eng.*, **49**: 77–90.
- Salman, S.D., Leman, Z., Ishak, M., Sultan, M. & Cardona, F. (2018). Quasi-static penetration behavior of plain woven kenaf/aramid reinforced polyvinyl butyral hybrid laminates. *J. Ind. Text.*, **47**: 1427–1446.
- Sayer, M., Bektas, N.B. & Sayman, O. (2010). An experimental investigation on the impact behavior of hybrid composite plates. *Compos. Struct.*, **92**: 1256–1262.
- Sevkat, E., Liaw, B. & Delale, F. (2013). Drop-weight impact response of hybrid composites impacted by impactor of various geometries, *Mater. Des.*, **52**: 67–77.
- Shishevan, F.A., Akbulut, H. & Mohtadi-Bonab, M.A. (2017). Low velocity impact behavior of basalt fiber-reinforced polymer composites. *J. Mater. Eng. Perform.*, **26**: 2890–2900.
- Sivakumar, D., Kathiravan, S., Ng, L. F., Ali, M. B., Selamat, M. Z., Sivaraos, S. & Bapokutty, O. (2018). Experimental investigation on charpy impact response of kenaf bast fibre reinforced metal laminate system. *ARPJ. Eng. Appl. Sci.*, **13**: 822–827.
- Sivakumar, D., Ng, L.F., Lau, S.M. & Lim, K.T. (2018). Fatigue life behaviour of glass/kenaf woven-ply polymer hybrid biocomposites. *J. Polym. Environ.*, **26**: 499–507.
- Sivakumar, D., Ng, L.F. & Salmi, N.S. (2016). Eco-hybrid composite failure behavior of two serial bolted joint holes. *J. Eng. Technol.*, **7**: 114–124.
- Subramaniam, K., Dhar Malingam, S., Feng, N.L. & Bapokutty, O. (2017). The effects of stacking configuration on the response of tensile and quasi-static penetration to woven kenaf/glass hybrid composite metal laminate. *Polym. Compos.* doi:10.1002/pc.24691.
- Sulaiman, S., Cieh, N.L., Mokhtar, M.N., Naim, M.N., Kamal, S.M.M. (2017). Covalent immobilization of cyclodextrin glucanotransferase on kenaf cellulose nanofiber and its application in ultrafiltration membrane system. *Process Biochem.*, **55**: 85–95
- Yahaya, R., Sapuan S.M. & Jawaid, M. (2014). Quasi-static penetration and ballistic properties of kenaf-aramid hybrid composites. *Mater. Des.*, **63**: 775–782.
- Yahaya, R., Sapuan, S. & Leman, Z. (2014). Selection of natural fibre for hybrid laminated composites vehicle spall liners using analytical hierarchy process (AHP). *Appl. Mech. Mater.*, **564**: 400–405.
- Ying, S., Mengyun, T., Zhijun, R., Baohui, S. & Li C. (2017). An experimental investigation on the low-velocity impact response of carbon-aramid/epoxy hybrid composite laminates. *J. Reinf. Plast. Compos.*, **36**: 422–434.

# CHARACTERISATION OF HYBRID OIL PALM EMPTY FRUIT BUNCH AND KENAF FIBRE REINFORCED THERMOPLASTIC COMPOSITES

Muhd Ridzuan Mansor<sup>\*1</sup>, Muhammad Taufiq Jumadi<sup>1</sup>, Mohd Azli Salim<sup>1</sup>, Mohd Zaid Akop<sup>1</sup>,  
Musthafah Mohd Tahir<sup>1</sup>, Muhamad Fahmi Mohd Noor<sup>1</sup>, Mohd Shukor Salleh<sup>2</sup>, & Zaleha Mustafa<sup>2</sup>

<sup>1</sup>Faculty of Mechanical Engineering

<sup>2</sup>Faculty of Manufacturing Engineering

Universiti Teknikal Malaysia Melaka (UTeM), Malaysia

\*Email: muhd.ridzuan@utem.edu.my

## ABSTRACT

*Agricultural waste abundance such oil palm empty fruit bunch (OPEFB) can be used for hybrid natural fibre composite production (HNFC). The hybridisation of OPEFB with other natural fibres such as kenaf fibre offer the advantage of producing new class of materials with balance between physical, mechanical and cost performance compared with single fibre composites. In this paper, hybrid OPEFB/kenaf reinforced high density polyethylene (HDPE) composites was developed with OPEFB/kenaf fibre ratio of 100:0, 75:25, 50:50, 25:75, and 0:100. The HFNC was later characterized in terms of their physical and mechanical properties. Characterization results showed that the optimum specific density was at 25:75 OPEFB / kenaf fibre ratio, while the lowest water absorption was found at 50:50 OPEFB / kenaf fibre ratio. For the case of mechanical properties, it was observed that the 25:75 OPEFB / kenaf fibre ratio has satisfied the optimum result for flexural, Shore D hardness, and impact strength properties. Further optical morphological analysis conducted showed that failures of impact fractured samples were due to fibre tearing, fibre pull out and matrix cracking. As a conclusion, the formulation of 25:75 OPEFB / kenaf fibre ratio showed the optimum physical and mechanical properties, and these results are useful to support NFC production by using abundance agricultural wastes from oil palm plantation.*

**Keywords:** *Hybrid natural fibre composites (HNFC); oil palm empty fruit bunch (OPEFB) fibre; kenaf fibre; high density polyethylene (HDPE); physical and mechanical properties.*

## 1. INTRODUCTION

Hybridisation is one of the solution technique to achieve balance between cost and mechanical performance in natural fibre composite (NFC) properties (Radzi *et al.*, 2018). In general, hybrid natural fibre composite (HNFC) can be prepared through the amalgamation of two or more fibres in a polymer matrix (Gururaja & Rao, 2012). The combination of a lesser strength fibre but having lower density and cost with another candidate fibre with higher strength but having higher density and cost will formulate new NHFC material in which its final properties lie between the two single fibres (Mansor *et al.*, 2013). Previous studies found that HNFC has better mechanical properties compared with single fibre especially in terms of strength and modulus (Jawaid *et al.*, 2010a, b, 2011). Some researchers also reported that hybridising natural fibre with synthetic fibre enabled improvements in thermal stability, water absorptivity, stiffness, strength, impact properties as well as acoustic and vibration damping properties (Sanjay & Yogesha, 2017; Yahaya *et al.*, 2018; Kureemun *et al.*, 2018). However, the use of synthetic fibre such as glass fibre may reduce the eco-friendly characteristic of NFC by adding potential health hazards such as respiratory problem and skin irritation (Holbery & Houston, 2006; Singh *et al.*, 2017). In addition, the use of synthetic fibre also contributed to disposable difficulties and declining on the finite petroleum resources (Satyanarayana *et al.*, 2009).

The hybridisation of natural fibres is more favourable towards achieving eco-friendly green composite materials. Furthermore, it is also beneficial to produce HNFC from agricultural wastes as it can reduce the waste abundance in landfill as well as adding market value on agricultural waste. In Malaysia, the potential agricultural waste to be apply as HNFC component is oil palm empty fruit bunch (OPEFB). The OPEFB is a by-product, produced from the extraction process of oil palm fruit bunches. Based on the data from Malaysian Ministry of Plantation Industries and Commodities, the oil palm cultivation was the most dominant commodity crop which covered almost 50% of overall Malaysian farmland in 2015 (MPIC, 2015). In 2016, the oil palm cultivation area recorded was 5,737,985 hectares, whereby the cultivation areas of Peninsular Malaysia and East Malaysia were 2,679,502 and 3,058,483 hectares, respectively (MPOB, 2016). The large cultivation area has boost-up the production of oil palm products. However, it also increased concurrently the by-product produced as much as 15.8 million tons (Sumathi *et al.*, 2008). Thus, hybridising OPEFB fibre with other natural fibre have the potential to reduce the waste abundance by becoming an alternative material for product developments.

Kenaf cultivation has been initiated in Malaysia since year 2000. Under the National Economic Action Council (NEAC), Malaysian government has decided to substitute tobacco cultivation with kenaf cultivation (Hadi *et al.*, 2014). Kenaf is known as fast growing crop, whereby it can achieve an average height up to 3 m with a base diameter between 3 to 5 cm within 3 months of cultivation (Akil *et al.*, 2011). Hence, kenaf products such as kenaf bast and kenaf core fibres have become commercially viable and economically competitive compared with other commodity fibres especially in Malaysia (Saba *et al.*, 2016).

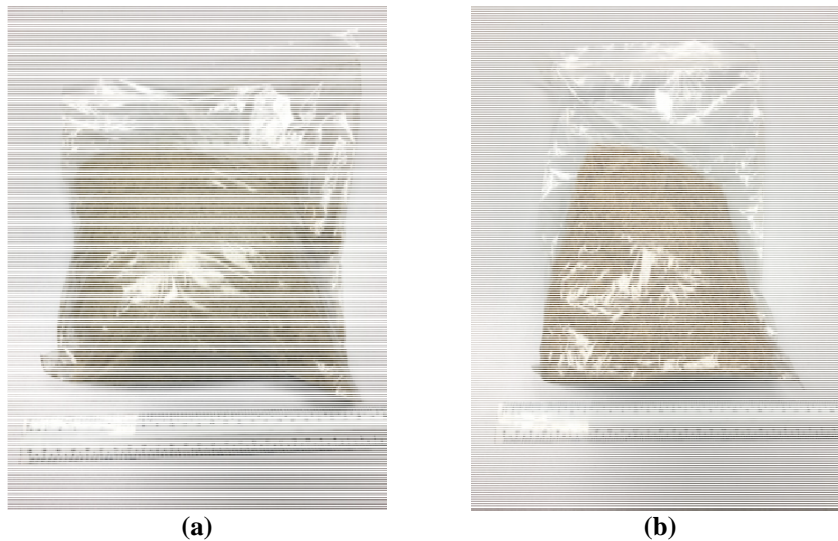
There are many potential applications for HNFC, especially using hybrid OPEFB / kenaf such as for automotive structural and semi-structural components (Hanan *et al.*, 2018), building and construction materials (Khoshnava *et al.*, 2017) and tribology (Shuhimi *et al.*, 2016). Up to date, there are several reported studies on the hybrid OPEFB / kenaf reinforced thermoset composites. Saba *et al.* (2016a) studied the dynamic mechanical properties of hybrid OPEFB / kenaf reinforced epoxy composites. In their study, the addition of OPEFB nano filler into the kenaf / epoxy composites successfully enhanced the storage modulus and loss modulus values of kenaf / epoxy composites. This is due to the fact that addition of OPEFB nano filler effectively alleviated the modulus mismatch between stiff kenaf fibres and epoxy matrix, and thus improved the interfacial bonding between fibres and matrix. In another study, Saba *et al.* (2016b) reported the effect of OPEFB nano filler addition to the mechanical properties of kenaf fibre reinforced epoxy composite. Results obtained showed that the addition of OPEFB nano filler improved the final composites tensile strength, tensile modulus and impact strength by 21, 12, and 24% respectively. The improvement of mechanical properties can be explained through considering the OPEFB nano filler has larger surfaces which act as a connection link between the kenaf fibres and matrix, resulting to better bonding between them. Thus, better stress transfer from matrix to fibre was achieved which delayed fracture or crack initiation mechanisms when load is applied. Furthermore, the addition of OPEFB nano filler also restricted the chain mobility of matrix responsible for elongation, which induced improvement on the toughness and stiffness properties of the composite.

There are many available literatures on hybrid OPEFB / kenaf composites, nevertheless research on hybrid OPEFB / kenaf reinforced thermoplastic composites are still limited, especially using high density polyethylene (HDPE) matrix. Research on HNFC reinforced thermoplastic matrix can highly contribute to the development of fully recyclable green composites, as compared with thermoset based composites. This study presents the development of hybrid OPEFB / kenaf reinforced HDPE thermoplastic composites at varying fibre ratio. The composites were fabricated through melt mixing and compression moulding methods. The HNFC physical and mechanical properties were characterized based on standard testing methods. Further optical morphological study was also conducted on the fractured tensile and impact test samples to identify the mode of failure occurred.

## 2. METHODOLOGY

### 2.1 Material

The OPEFB fibre with density of  $1.55 \text{ g/cm}^3$  was received from Kilang Kelapa Sawit Kempas, Melaka, Malaysia, while the kenaf fibre with density of  $1.45 \text{ g/cm}^3$  was obtained from Lembaga Kenaf dan Tembakau Melaka, Malaysia. The OPEFB fibre was dried to remove moisture using laboratory oven for 6 hours at temperature of  $60 \text{ }^\circ\text{C}$ . The OPEFB and kenaf fibres in long fibre form were later crushed into short fibre form with average length between 2 to 5 mm. Figure 1 shows the short fibres obtained after the crushing process. The HDPE matrix was supplied by the Lotte Chemical Titan, Malaysia. The physical state of HDPE is in solid granule with melting point of  $120 \text{ }^\circ\text{C}$  and specific density in the range between  $0.940\text{-}0.965 \text{ g/cm}^3$ .



**Figure 1: Short natural fibres used for this study; (a) kenaf fibre; (b) OPEFB fibre.**

### 2.2 Sample Preparation

Table 1 shows the formulations used during compounding using twin rotor internal mixer machine at fixed HDPE content of 60 wt.%, while Table 2 shows the parameters used for compounding and moulding processes. The total fibre loadings were also fixed at 40 wt.%. The compounded materials were moulded in a window-framed stainless-steel mould with the dimension of 200 mm width x 200 mm length x 3 mm thickness.

**Table 1: Hybrid composites OPEFB:kenaf fibre ratio.**

Composites fibre ratio	
OPEFB	Kenaf
100	0
75	25
50	50
25	75
0	100

**Table 2: Parameters used for compounding and moulding procedure.**

Process	Test parameter	Value	Unit
<b>Compounding</b>	Compounding temperature	180	°C
	Compounding duration	10	minute
	Rotor speed	50	RPM
<b>Moulding</b>	Moulding temperature	180	°C
	Preheating duration	15	Minute
	Compacting duration	15	Minute
	Cooling duration	5	Minute
	Compacting pressure	20	Tons

### 2.3 Physical Tests

The specific density and water absorption of OPEFB / kenaf composites were measured as the physical properties. The specific density was determined by water immersion method according to ASTM D4052 (2016b) standard. The samples were immersed in distilled water at room temperature  $24 \pm 1$  °C and 50% relative humidity. Meanwhile, the water absorptivity tests were conducted by using water immersion method in accordance to ASTM D570 (2010b) standard. The samples for each formulation were immersed inside a beaker containing distilled water and kept for 24, 48, 72, 144, 168, 192, 216 and 240 h. The water percentage in the composites was calculated based on weight difference between the samples immersed in water and the dry samples using the following equation:

$$\Delta M(t) = \left( \frac{m_t - m_o}{m_o} \right) \times 100\% \quad (1)$$

where  $\Delta M(t)$  is the different of mass which represent water absorptivity,  $m_o$  and  $m_t$  are the mass of the sample before and during immersion, respectively.

### 2.4 Mechanical Tests

Flexural samples were prepared in rectangular shape using compress-moulding process with dimension of 13 mm x 127 mm. The three-point bending tests were conducted on a universal testing machine with crosshead speed of 2 mm/min according to ASTM D790 (2017) standard. For each formulation, five specimens were tested followed by calculated average values.

The Shore D hardness characterisation was conducted on five different points for each sample formulation with 15 mm of width and 60 mm of length, in accordance to ASTM D2240 (2016a) standard. The un-notched impact strength was measured using an impact tester with accordance to ASTM D256 (2010a) standard. The impact samples were prepared with dimensions of 64 mm of length x 13 mm of width with ten replications.

### 2.5 Morphological Analysis

The morphological analysis was conducted using optical microscope to discover the failure mode of fractured samples at 50x magnification.



### 3. RESULTS AND DISCUSSION

#### 3.1 Physical properties

##### 3.1.1 Specific Density

The average specific density of composites from various formulations is presented in Figure 2. After 240 hours of immersion time, it is clearly shown that the 0:100 OPEFB / kenaf ratio has the highest specific density ( $1.08 \text{ g/cm}^3$ ) compared with other formulation. The lowest specific density can be observed on 100:0 OPEFB / kenaf ratio ( $1.05 \text{ g/cm}^3$ ). Both OPEFB / kenaf ratio of 50:50 and 75:25 have similar specific density ( $1.06 \text{ g/cm}^3$ ), while at 25:75 OPEFB / kenaf ratio, the specific density was slightly lower. As can be seen, the addition of the OPEFB into the composite has reduced the density. This trend was similar to the result obtained by Jawaid *et al.* (2011) in the study of hybrid OPEFB/jute fibres composite. They claimed that the reduction on the density was due to presence of voids inside the OPEFB fibre which later reduced the bulk density.

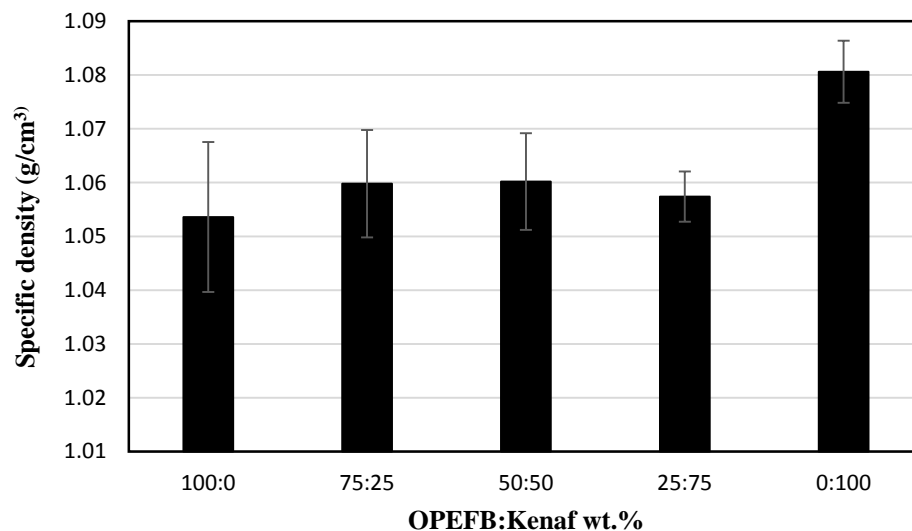


Figure 2: Specific density property of OPEFB / kenaf composites at varying fibre ratio.

##### 3.1.2 Water Absorption

Figure 3 shows the results of water absorptivity based on five immersion durations. The composite with formulation of 100:0 OPEFB / kenaf ratio has the highest water absorptivity, while the 0:100 OPEFB / kenaf ratio has the lowest water absorptivity value. For hybrid composites, the 25:75 and 75:25 OPEFB / kenaf ratio have similar water absorptivity trend, whereas the 50:50 OPEFB / kenaf ratio has the modest water absorptivity.

Furthermore, the hybrid composites at 100:0 OPEFB / kenaf ratio showed the earliest saturation time compared with other formulation, indicating the easiness of water penetration. The addition of OPEFB fibre has significantly increased the saturation time of the final hybrid composites as the OPEFB has the larger cellulose diameter that tends to absorb more water compared with kenaf fibre. As mentioned by several researchers, the water molecules diffused from the surroundings into the composite through microgaps between polymer chains, gaps and flaws at matrix to fibre interfaces, and micro-cracks in the matrix caused by swollen fibres (Dhakal *et al.*, 2014; Espert *et al.*, 2004; Dhakal *et al.*, 2007). Since the OPEFB fibre has higher cellulose content (60 wt.%) compared with kenaf fibre (31 wt.%), it explained the high water absorptivity for composite with rich OPEFB content (>50 wt.%) (Ramesh, 2016). This was supported by Dhakal *et al.* (2007) when they discovered higher cellulose content fibre in composite contributed to more water penetrating into the interface through the micro cracks induced by swelling of fibres.

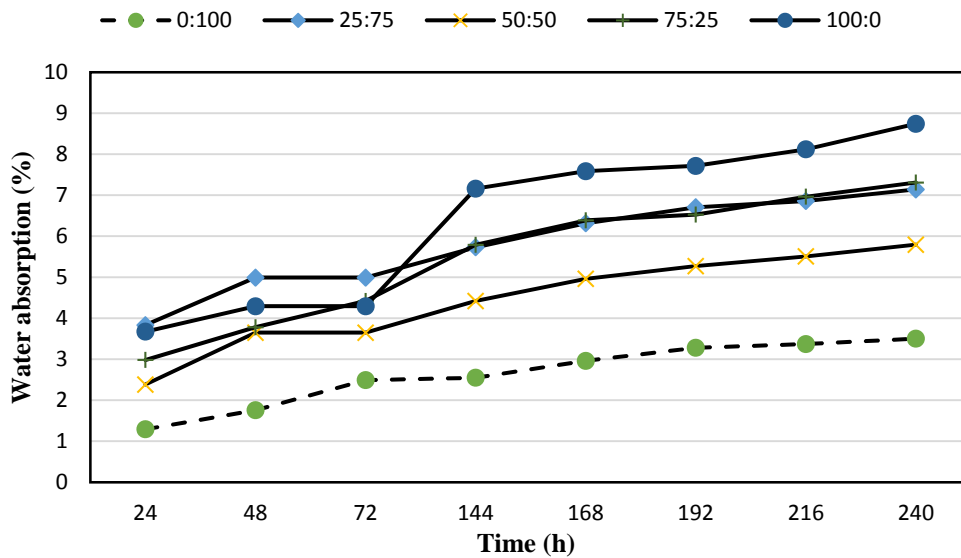


Figure 3: The water absorption property hybrid composites at varying OPEFB:kenaf fibre ratio.

## 3.2 Mechanical Properties

### 3.2.1 Flexural Properties

Flexural properties result from the tests are shown in Figure 4. The highest flexural strength among HNFC was found at 25:75 OPEFB / kenaf ratio, meanwhile the 75:25 OPEFB/kenaf ratio has the highest values flexural modulus. Although the formulation of 25:75 OPEFB/kenaf ratio has 24% lower flexural strength than neat kenaf/HDPE composites, however it showed 6% improvement compared with neat OPEFB/HDPE composites. Similarly, the formulation of 75:25 OPEFB / kenaf ratio showed 23% lower flexural modulus than neat kenaf/HDPE composites, but it still indicates the highest compared with other hybridising formulation.

Alavudeen *et al.* (2015) mentioned that the flexural properties of HFNC depend on the interfacial bonding and the reinforcement strength at the extreme layers. Weak interfacial bonding between matrix and fibre also contributed to poor flexural properties, as mentioned by Abdul Khalil *et al.*,(2007). Another findings on using OPEFB as NFC component, their results indicated that flexural modulus is at 1100-1700 MPa, higher than those obtained in this study (Razak & Kalam, 2012). This difference may be caused by several factors such as the fibre size used in their research (between 180-355  $\mu\text{m}$ ) which is smaller than fibre used in this study (the OPEFB fibres used for this study was 1-5 mm).

For the case of kenaf, based on Wambua *et al.* (2001) and Abdul Aziz *et al.* (2016), the reported flexural modulus for their research on kenaf and HDPE was between 2,000 – 2,500 MPa, whereas the flexural modulus obtained was 1184 MPa. Two factors contributed to this difference which are the fibre size and compatibiliser assistance. Abdul Aziz *et al.* produced NFC with smaller fibre size compared with this study, while Wambua *et al.* (2001) used polypropylene (PP) as the matrix which it has better mechanical properties than HDPE.

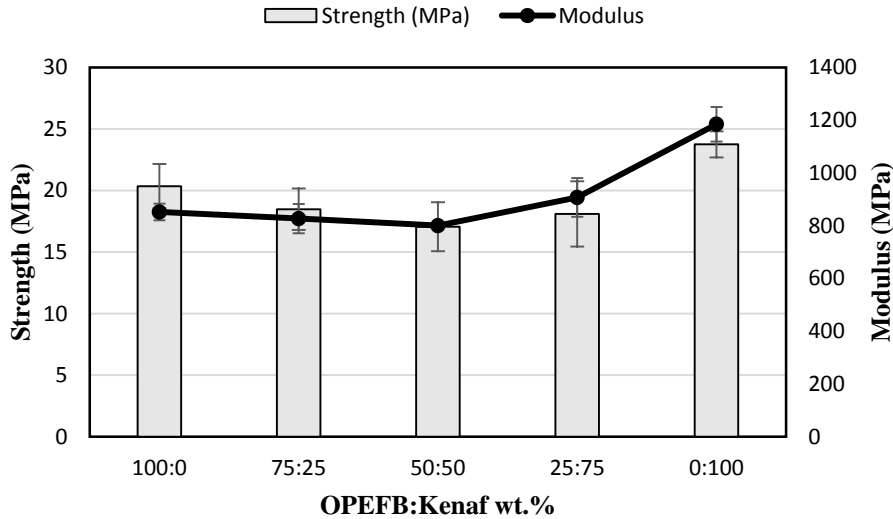


Figure 4: Flexural properties of OPEFB / kenaf composites at varying fibre ratio.

### 3.2.2 Shore D Hardness

Figure 5 shows the Shore D hardness (SH) results, whereby it can be observed that the increase of OPEFB ratio caused reduction in the final HFNC hardness values. The maximum hardness was obtained for neat OPEFB/HDPE (SH = 76) while the minimum hardness value (SH = 61) was obtained for neat kenaf/HDPE. The HFNC samples of 50:50 and 25:75 OPEFB / kenaf ratio both showed comparable hardness performance (SH values of 74 and 73, respectively).

Similar trends obtained in this study was also reported by Hamma *et al.* (2014) using starch-grafted-polypropylene/kenaf hybrid composites. They found that increasing kenaf fibre contents increased the HFNC hardness. Elsewhere, Sreekala *et al.* (2002) mentioned that when the volume of OPEFB fibre increased, the HFNC hardness value reduced. This is probably due to poor adhesion force between OPEFB and the matrix, which formed cavities that will affect the hardness result.

Pickering *et al.* (2016) stated that the fibre dispersion also affected the properties of NFC, especially for composite made with short fibre. This is because of higher tendency of fibre agglomeration, which later affect the bonding between fibre and matrix. In addition, the presence of cavities which influenced the adhesion force also reduced the composite hardness.

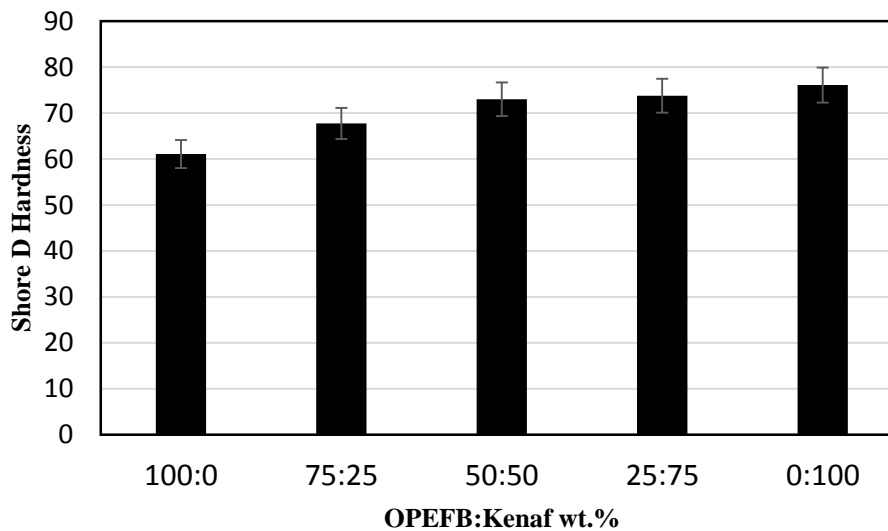


Figure 5: Shore D hardness of OPEFB / kenaf composites at varying fibre ratio.

### 3.2.3 Impact Strength

Figure 6 shows the results for impact tests conducted. The maximum impact strength (2.35 J/m) among the HNFC was obtained at 25:75 OPEFB / kenaf ratio, which is 23% higher compared with neat kenaf/HDPE composites. The addition of more OPEFB fibre into the HNFC formulation also caused declination energy absorption property. Furthermore, all HFNC formulation showed higher impact strength performance compared with neat kenaf/HDPE and neat OPEFB/HDPE composites.

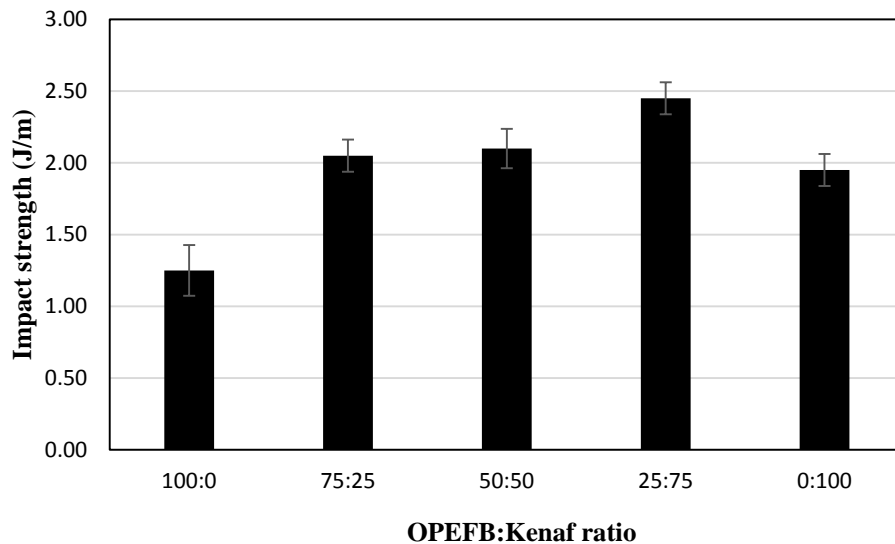


Figure 6: The impact energy of OPEFB / kenaf composites at varying fibre ratio.

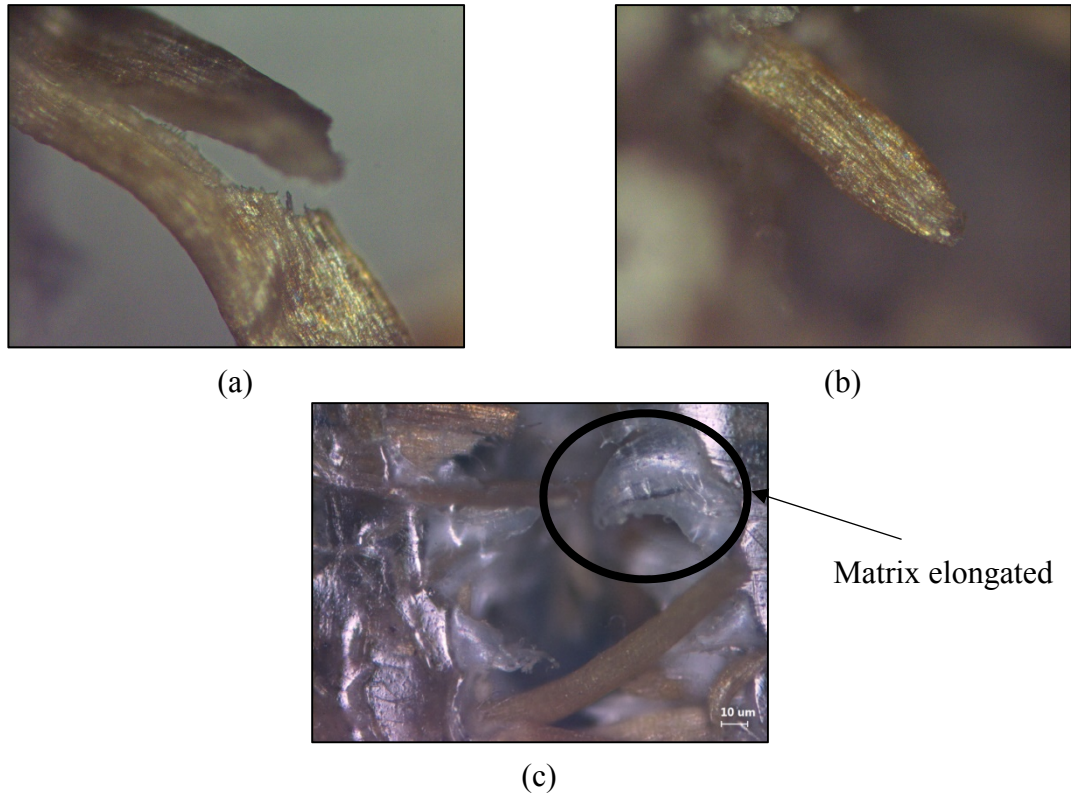
Figure 7 shows the failure condition for the impacted samples. Samples with complete break (Figure 7a) were obtained for all hybrid formulations, while samples with partial break (Figure 7b) were found for neat OPEFB/HDPE and neat kenaf / HDPE composites.



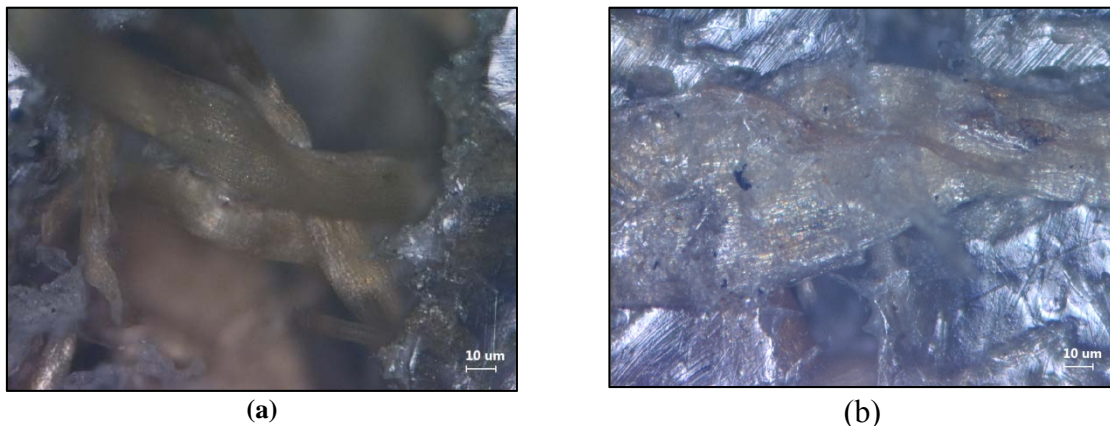
Figure 7: Izod impact samples after the test; (a) complete break; (b) partial break.

### 3.3 Morphological Analysis

Further morphological analysis was also performed on the samples with complete break after the impact test as shown in Figure 8. From the observation, the failure to the samples were caused by the fibre tearing, fibre pull out and matrix cracking. In matrix cracking mode, it can be seen the HDPE matrix has elongated and broke afterwards. In addition, morphological analysis was also performed for neat kenaf/HDPE and neat OPEFB / HDPE composites having partial break samples which clarify the failure occurred on the HDPE matrix as shown in Figure 9.



**Figure 8: The optical microscope analysis on complete break samples; (a) OPEFB fibre tearing (b) fibre pull out (c) matrix cracking.**



**Figure 9: The optical microscope analysis on partial break samples; (a) neat OPEFB fibre (b) neat kenaf fibre.**

#### 4. CONCLUSION

Several notable conclusions from this study are described as follows:

- i. The HNFC with 50:50 and 75:25 of OPEFB / kenaf ratio have comparable specific density, and is higher than 25:75 OPEFB / kenaf ratio.
- ii. The HNFC with 75:25 and 25:75 of OPEFB / kenaf ratio both showed maximum water absorptivity after immersed for 240 h.
- iii. The Shore D hardness and impact strength were found maximum at 25:75 OPEFB / kenaf ratio.
- iv. The flexural strength of HNFC was optimum at 25:75 of OPEFB / kenaf ratio, while the flexural modulus was optimum at 75:25 OPEFB / kenaf fibre ratio.

- v. The optical microscopy analyses found that the fracture occurred due to fibre tearing, fibre pull-out, and matrix cracking.
- vi. Hybrid formulation of 25:75 OPEFB / kenaf fibre ratio showed the optimum physical and mechanical properties for potential use in suitable product development applications.

## ACKNOWLEDGEMENT

The authors would like to acknowledge Universiti Teknikal Malaysia Melaka (UTeM) for providing financial support through UTeM research grant (PJP/2015/FKM(3A)/S01409). The authors also wish to thank Kilang Kelapa Sawit Kempas, Malaysia and Lembaga Kenaf dan Tembakau Negara, Malaysia for supplying the raw materials used in this study, as well as the Centre of Advanced Research on Energy (CARE), UTeM and Advanced Manufacturing Centre (AMC), UTeM for the use of the equipment.

## REFERENCES

- Abdul Aziz, N.F., Ibrahim, A., Ahmad, Z. & Dahan, R. (2016). Flexural properties of compression moulded kenaf polyethylene composite. *J. Teknol.*, **78**: 105–110.
- Abdul Khalil, H.P. S.P.S., Issam, A.M.M., Ahmad Shakri, M.T.T., Suriani, R. & Awang, A.Y.Y. (2007). Conventional agro-composites from chemically modified fibres. *Ind. Crops Prod.* **26**: 315–323.
- Akil, H.M., Omar, M.F., Mazuki, A.A. M., Safiee, S., Ishak, Z.A.M. & Abu Bakar, A. (2011). Kenaf fiber reinforced composites: A review. *Mater. Des.i* **32**: 4107–4121.
- Alavudeen, A., Rajini, N., Karthikeyan, S., Thiruchitrabalam, M. & Venkateshwaren, N. (2015). Mechanical properties of banana/kenaf fiber-reinforced hybrid polyester composites: Effect of woven fabric and random orientation. *Mater. Des.*, **66**: 246–257.
- ASTM International (1970). *ASTM D790 - Standard Test Methods for Flexural Properties of Unreinforced and Reinforced Plastics and Electrical Insulating Materials, Annual Book of ASTM Standards*. ASTM International, West Conshohocken.
- ASTM International (2010a). *ASTM D256 - Standard Test Methods for Determining the Izod Pendulum Impact Resistance of Plastics, Annual Book of ASTM Standards*. ASTM International, West Conshohocken.
- ASTM International (2010b) *ASTM D570 - Standard Test for Water Absorption of Plastics, ASTM Standards*. ASTM International, West Conshohocken.
- ASTM International (2016a) *ASTM D2240 - Standard Test Method for Rubber Property - Durometer Hardness, Annual Book of ASTM Standards*. West Conshohocken: ASTM International.
- ASTM International (2016b) *ASTM D4052 - Standard test method for density, relative density, and API gravity of liquids by digital density meter*. Edited by ASTM International. West Conshohocken: ASTM International.
- ASTM International (2017). *ASTM D790 - Standard Test Methods for Flexural Properties of Unreinforced and* ASTM International, West Conshohocken.
- Dhakal, H.N., Zhang, Z.Y., Bennett, N., Lopez-Arraiza, A. & Vallejo, F J. (2014). Effects of water immersion ageing on the mechanical properties of flax and jute fibre biocomposites evaluated by nanoindentation and flexural testing. *Comp. Mater.*, **48**: 1399–1406.
- Dhakal, H., Zhang, Z. & Richradson, M. (2007). Effect of water absorption on the mechanical properties of hemp fibre reinforced unsaturated polyester composites. *Comp. Sci. Technol.*, **67** : 1674–1683.
- Espert, A., Vilaplana, F. & Karlsson, S. (2004). Comparison of water absorption in natural cellulosic fibres from wood and one-year crops in polypropylene composites and its influence on their mechanical properties. *Compos. Part A.*, **35**: 1267–1276.
- Gururaja, M.N. & Rao, H. (2012). A review on recent applications and future prospectus of hybrid composites. *Inter. J. Soft Comput. Eng.*, **1**: 2231–2307.
- Hadi, M., Basri, A., Abdu, A., Junejo, N. & Hamid, H.A. (2014). Journey of kenaf in Malaysia : A

- review. *Acad. J.*, **9**: 458–470.
- Hanan, F., Jawaid, M. & Md Tahir, P. (2018). Mechanical performance of oil palm/kenaf fiber-reinforced epoxy-based bilayer hybrid composites. *J. Nat. Fibers*, In press.
- Hamma, A., Kaci, M., Mohd Ishak, Z.A. & Pegoretti, A. (2014). Starch-grafted-polypropylene/kenaf fibres composites. Part 1: Mechanical performances and viscoelastic behaviour. *Compos. Part A.*, **56**: 328–335.
- Holbery, J. & Houston, D. (2006). Natural-fiber-reinforced polymer composites in automotive application. *JOM*. **58** (11): 80–86.
- Jawaid, M., Abdul Khalil, H.P.S. & Abu Bakar, A. (2010). Mechanical performance of oil palm empty fruit bunches/jute fibres reinforced epoxy hybrid composites. *Mater. Sci. Eng.*, **527**: 7944–7949.
- Jawaid, M., Abdul Khalil, H.P.S. & Abu Bakar, A. (2011). Woven hybrid composites: Tensile and flexural properties of oil palm-woven jute fibres based epoxy composites. *Mater. Sci. Eng.*, **528**: 5190–5195.
- Jawaid, M., Abdul Khalil, H. P. S., Noorunnisa Khanam, P. and Abu Bakar, A. (2011). Hybrid composites made from oil palm empty fruit bunches/jute fibres: Water absorption, thickness swelling and density behaviours. *J. Polym. Environ.*, **19**: 106–109.
- Khoshnava, S.M., Rostami, R., Ismail, M., Rahmat, A. R., & Ogunbode, B. E. (2017). Woven hybrid biocomposite: Mechanical properties of woven kenaf bast fibre/oil palm empty fruit bunches hybrid reinforced poly hydroxybutyrate biocomposite as non-structural building materials. *Construct. Build. Mater.*, **154**: 155-166.
- Kureemun, U., Ravandi, M., Tran, L.Q.N., Teo, W.S., Tay, T.E. & Lee, H.P. (2018). Effects of hybridization and hybrid fibre dispersion on the mechanical properties of woven flax-carbon epoxy at low carbon fibre volume fractions. *Compos. Part B*, **134**: 28–38.
- Mansor, M.R., Sapuan, S., Zainudin, E., Nuraini, A. & Hambali, A. (2013). Stiffness prediction of hybrid kenaf/glass fiber reinforced polypropylene composites using rule of mixtures (ROM) and rule of hybrid mixtures (RoHM). *J. Polym. Mater.*, **30**: 321-334.
- MPIC (Ministry of Plantation Industries and Commodities) (2015). *Laporan Tahunan MPIC 2015*. Ministry of Plantation Industries and Commodities (MPIC), Malaysia.
- MPOB (Malaysian Palm Oil Board) (2016). *Oil Palm Estates, January – December 2016*. Malaysian Palm Oil Board (MPOB), Malaysia.
- Pickering, K.L., Efendy, M.G.A. & Le, T.M. (2016). A review of recent developments in natural fibre composites and their mechanical performance. *Compos. Part A.*, **83**: 98–112.
- Ramesh, M. (2016). Kenaf (*Hibiscus cannabinus* L.) fibre based bio-materials: A review on processing and properties. *Prog. Mater. Sci.*, **78–79**: 1–92.
- Radzi, A.M., Sapuan, S.M., Jawaid, M. & Mansor, M.R. (2018). Mechanical performance of roselle/sugar palm fiber hybrid reinforced polyurethane composites. *BioResources*, **13**: 6238-6249.
- Razak, N.W.A. & Kalam, A. (2012). Effect of OPEFB size on the mechanical properties and water absorption behaviour of OPEFB/PPnanoclay/PP hybrid composites. *Procedia Eng.*, **41**: 1593–1599.
- Saba, N., Paridah, M.T., Abdan, K. & Ibrahim, N.A. (2016a). Dynamic mechanical properties of oil palm nano filler/kenaf/epoxy hybrid nanocomposites. *Construct. Build. Mater.*, **124**:133–138.
- Saba, N., Paridah, M.T., Abdan, K. & Ibrahim, N.A. (2016b). Effect of oil palm nano filler on mechanical and morphological properties of kenaf reinforced epoxy composites. *Constr. Build. Mater.*, **123**: 15–26.
- Sanjay, M. & Yogesha, B. (2017). Studies on natural/glass fiber reinforced polymer hybrid composites: An evolution. *Mater. Today: Proc.*, **4**: 2739–2747.
- Satyanarayana, K.G., Arizaga, G.G.C. & Wypych, F. (2009). Biodegradable composites based on lignocellulosic fibers-An overview. *Prog. Polym. Sci.*, **34**: 982–1021.
- Shuhimi, F.F., Abdollah, M.F.B., Kalam, M.A., Hassan, M. & Amiruddin, H. (2016). Tribological characteristics comparison for oil palm fibre/epoxy and kenaf fibre/epoxy composites under dry sliding conditions. *Tribol. Int.*, **101**: 247-254.
- Singh, N., Hui, D., Singh, R., Ahuja, I.P.S., Feo, L. & Fraternali, F. (2017). Recycling of plastic solid

- waste : A state of art review and future applications. *Compos. Part B.*, **115**: 409–422.
- Sreekala, M. S., George, J., Kumaran, M. G. and Thomas, S. (2002). The mechanical performance of hybrid phenol-formaldehyde-based composites reinforced with glass and oil palm fibres. *Compos. Sci. Technol.*, **62**: 339–353.
- Sumathi, S., Chai, S.P. & Mohamed, A.R. (2008). Utilization of oil palm as a source of renewable energy in Malaysia. *Renew. Sustain. Ener. Rev.*, **12**: 2404–2421.
- Wambua, P., Ivens, J. & Verpoest, I. (2001). Some mechanical properties of kenaf/polypropylene composites prepared using a film stacking technique. *13<sup>th</sup> Inter. Conf. Compos. Mater.* Beijing, China: The Chinese Society for Composite Materials and China Universities Alumni Association, pp. 1–9.
- Yahaya, R., Sapuan, S.M., Jawaid, M., Leman, Z. & Zainuddin, E.S. (2018). Review of kenaf reinforced hybrid biocomposites: Potential for defence applications. *Current Analytical Chem.*, **14**: 226-240.



# INDENTATION BEHAVIOUR OF ECO-FRIENDLY FIBRE METAL LAMINATES IN DIFFERENT STACKING CONFIGURATIONS

Fadzila Hussain<sup>1</sup>, Sivakumar Dhar Malingam<sup>1\*</sup>, Mohd Ahadlin Mohd Daud<sup>1</sup>, Siva Irulappasamy<sup>2</sup> & Maciej Klósak<sup>3</sup>

<sup>1</sup>Fakulti Kejuruteraan Mekanikal, Universiti Teknikal Malaysia Melaka (UTeM), Malaysia

<sup>2</sup>Centre for Composite Materials, Kalasalingam Academy of Research and Education, India

<sup>3</sup>Universiapolis, Technical University of Agadir, Agadir, Morocco

\*Email: sivakumard@utem.edu.my

## ABSTRACT

*The use of natural fibre reinforced polymer composite in fibre metal laminate (FML) is the current interest. The potential and performance of FML based on natural fibre have been investigated. This paper investigated the effect of different stacking configurations (2/1, 3/2 & 4/3) subjected to quasi-static indentation test for oil palm empty fruit bunch fibre metal laminates (OPFML). This study used aluminium 6061 as a laminate skin and oil palm empty fruit bunch fibre reinforced polypropylene composites as a laminate layer. A motorised hydraulic moulding test press machine was used in this study to bond the FML panels at 155 °C, 1 kg/cm<sup>2</sup> and 4 min and for composites fabrication at 185°C, 35 kg/cm<sup>2</sup> and 8 min. Experiments were performed using a 12mm diameter hemispherical indenter with a constant strain rate of 1.0 mm/s. The indentation behaviour of OPFML panels were presented based on the peak load, maximum displacement, energy absorption and specific energy absorption (SEA) values. The results show that the highest stacking configuration, OPFML 4/3 has the highest value of the peak load, energy absorption and specific energy absorption due to the stiffer behaviour. From this study, it is found that the failure mode of quasi- static indentation test showed the damaged on aluminium and composite layers. Therefore, this study concludes that the stacking configuration influenced the indentation behaviour of OPFML panels.*

**Keywords:** *Quasi-static; indentation test; fibre metal laminate; oil palm fibre; natural fibre.*

## 1. INTRODUCTION

Fibre metal laminate (FML) is a laminate system with combination of metal plies and composite sheets. According to Ferrante *et al.* (2016), the key to FML is to combine superior fatigue resistance of composite materials with plastic behaviour and durability of metals. Their development is mainly due to the need to improve poor fatigue resistance of aluminium alloys through the use of alternate stacking of thin high strength metal sheet bonded together with alternating fibre reinforced composite layers. In history, the contemporary FML composite layers applied in aerospace industries are mainly based on the thermoset matrix and synthetic reinforcements. However, thermoset matrix requires long processing cycle during composite curing process and synthetic reinforcement have some environmental issues (Cortes, 2014). Hence, the requirement for sustainable material with low processing cycle in FML fabrication improvement is paramount. Replacing thermoset composite material with thermoplastic has contributed significantly to FML fabrication improvement. Thermoplastic based composite is primarily an option for FML composite laminates because this material is able to shape in a shorter processing time and can be moulded and bonded to the metal skin (Cortes & Cantwell, 2005).

Due to the sustainability characteristics of natural fibres such as lightweight, biodegradable, less abrasive and carbon dioxide neutral, the properties of natural fibre reinforced thermoplastic composites have been widely studied (Thakur *et al.*, 2014). Ahmad *et al.* (2015) asserted that recently many companies improve the reinforcement from mineral product or fibre glass with natural fibre for various parts based on thermoplastic composite in cars manufacturing. The current trend of replacement of synthetic fibre with natural fibre in polymer composite can also be extended to the FML field. Therefore, the mechanical behaviour of FML based on natural fibre reinforced thermoplastic composite has been investigated extensively. Santiago *et al.* (2017) had studied the impact response of thermoplastic fibre metal laminates (TFMLs) based on aluminium 2024-T3 and self-reinforcement polypropylene. It has been shown that TFMLs can absorb up to 75% more impact energy than conventional FMLs at low levels of deformation when the areal density of the material is taken into consideration. Examples for TFMLs based on natural fibres, is the use of hemp, basalt and flax fibre reinforced polypropylene composites as a FML composite layers in the investigation on tensile and impact properties of environmental-friendly materials (Kuan *et al.*, 2011) while Ng *et al.* (2017) used kenaf fibre reinforced polypropylene composites as a laminate layer to investigate the density and tension-tension fatigue performance of FMLs. Similarly, Sivakumar *et al.* (2016) used oil palm empty fruit bunch fibre reinforced polypropylene composite as a FML laminate layer in their investigations on impact behaviour of a novel oil palm fibre reinforced metal laminate system.

In recent years, the fibre metal laminate panel's mechanical properties subjected to quasi-static and impact loading have been widely concentrated and studied. In the study of the effect of impact energy division over repeated low-velocity impact on fibre metal laminates, a primary estimation of required energy for penetrating the FML specimens under impact loadings was done through quasi-static punch test (Kashani *et al.*, 2015). It was found that the penetration energy was equal to 25 J. Kathiravan *et al.* (2017) had studied the effects of stacking configuration on the response of tensile and quasi-static penetration to woven kenaf/glass hybrid composite metal laminate. It was obtained that the properties of tensile and quasi-static penetration of FMLs decreased as the content of kenaf fibres in the laminates increases. Fan *et al.* (2010) conducted experiment on FML based on aluminium alloy and glass fibre reinforced epoxy composite for both quasi-static and impact loadings. Both of the testing showed that increasing the laminate number from 2/1 to 4/3 increased the perforation resistance, as does increasing the thickness of the composite layer. Zhou *et al.* (2015) conducted quasi-static indentation test in their studies on loading rate effects in the perforation resistance of fibre metal laminates based on three different aluminium alloys (7075-O, 6061-O and 6061-T6) and a woven glass fibre reinforced epoxy with various configurations. Similarly, it was also shown that the value of specific energy absorption increases in passing from a 2/1 to a 3/2 to a 4/3 FML. However, no significant differences between various stacking configurations were shown when the failure mode of each configuration shows the similar pattern. Sivakumar *et al.* (2017) investigated the quasi-static indentation behaviour of kenaf bast fibre reinforced polypropylene metal laminates (KFML) with 2/1 configuration. It was found that the FML reinforced with treated kenaf fibre recorded an average of 19% increments in energy absorption and 4% increments in maximum load compared to FML reinforced with untreated kenaf fibre.

Yu *et al.* (2018) studied aluminium alloy-carbon fibre reinforced plastic (CFRP) bilayer plates under quasi-static and impact loading. It was found that the qualitative perforation mechanism in the CFRP layers was sensitive to the boundary condition but was not affected by the presence of the metallic layers in both quasi-static and ballistic tests. Romli *et al.* (2018) investigated failure behaviour of aluminium/CFRP laminates with varying fibre orientation in quasi-static indentation test. It has been found that increasing of crosshead speed would increase the damaged surface area, and a laminate increased with thickness was accompanied by decreasing degree of laminate deformation and occurrence of delamination between the individual composite layers and delamination on the metal-composite interface. Jakubczak & Bienias (2016) studied a comparison of correlations between static and dynamic loads of aluminium-glass and aluminium-carbon laminates. It was found that significant differences in

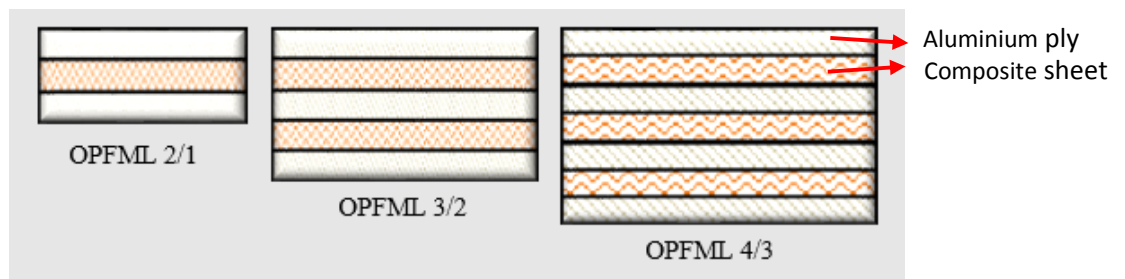
destruction scale have been denoted despite significant matching of load – displacement curves for static and dynamic tests of aluminium/carbon fibre reinforce polymer (CFRP) laminates. In this paper, quasi-static indentation tests were carried out on oil palm empty fruit bunch fibre metal laminates (OPFML) with various stacking configurations.

## 2. METHODOLOGY

### 2.1 Fabrication of FML

In this study, the OPFML were based on 6061 aluminium alloy plies with thickness of 0.5mm and the natural fibre reinforced thermoplastic composite sheets with thickness of 1.0mm. The composite material was fabricated from 30wt% oil palm empty fruit bunch fibre as a reinforcement and polypropylene as a matrix with 3% of Maleic anhydride grafted polypropylene (MAPP) as a coupling agent. The composite material was also heated in temperature of 185°C, pressure of 35 kg/cm<sup>2</sup> for 8 min followed by fast cooling to room temperature in a picture frame mould (200mm x 200mm x 1mm) using motorised hydraulic hot press machine. Then, the OPFML were laminated by stacking the appropriate number of aluminium plies and composite sheets resulting in varying stacking configurations (2/1, 3/2 and 4/3) as shown in Figure 1. Based on the figure, OPFML 2/1 consisted of two aluminium plies and one composite sheet, OPFML 3/2 consisted of three aluminium plies and two composite sheets and OPFML 4/3 consisted of four aluminium plies and three composite sheets. Aluminium also acts as a laminate skin and would always be on the outer layer in laminates.

There are two important processes in fibre metal laminate fabrication which are the surface treatment and bonding process. To provide an efficient bonding, the sand paper with 80 grit size was used for aluminium surface treatment in this study. The bonding process of OPFML consists of a few steps. Firstly, to remove any contaminant on materials during bonding process, the aluminium plies and composite sheets were cleaned with ethanol before the layers were assembled in a steel preparation plate. Then, the OPFML was bonded using a motorised hydraulic moulding test press machine at pressure 1 kg/cm<sup>2</sup> and temperature 155 °C for 4 min followed by fast cooling pressing at the same pressure. In addition, a modified polypropylene film adhesive was used to bond both materials resulting in final laminate of different thickness between 2mm to 5mm based on the stacking configuration. Finally, the OPFML panel will be cut into square size of 100mm x 100mm using shearing machine. This size is in accordance with ASTM D6264-98 for quasi-static indentation test of composite materials.



**Figure 1: The schematic diagram of OPFML with various stacking configurations.**

## 2.2 Quasi-Static Indentation Test

The OPFML panels were performed using universal testing machine 100kN, Instron model 5282 according to ASTM 6264-98. Oil palm empty fruit bunch fibre metal laminates specimen with dimension of 100mm x 100mm with different stacking configurations of 2/1,3/2 and 4/3 system were prepared, respectively. The OPFML panels were clamped in a rectangular steel jig with hole diameter of 70 mm and Hemispherical indenter with a diameter of 12.7mm as shown in Figure 2 to indent the panels. The loading in these tests were controlled by displacement with a constant crosshead velocity of 1 mm/min. The contact load and displacement were recorded by a dedicated computer attached to the test machine and the absorbed energy was then utilised to ascertain the specific perforation energy through normalizing the measured energy by the areal density of the target. The test is stopped when the load and displacement curve reached at the peak for a maximum load value. This is because the OPFML panels were indent at the maximum load. This is proven when the indent sound at aluminium skin on indentation side of OPFML panels (Figure 3) was heard during testing. Therefore, the indentation behaviour of each OPFML panels will be discussed focusing on maximum load variables in this study.

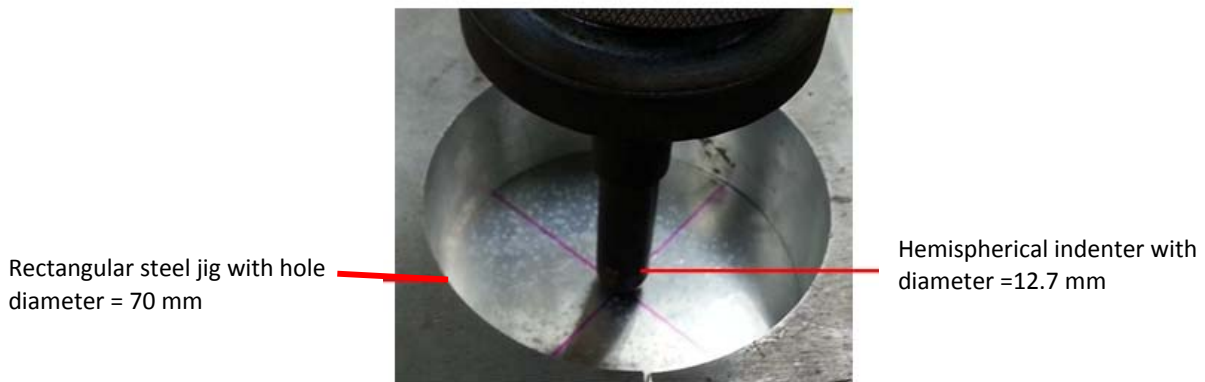


Figure 2: Quasi-static indentation test setup: the indenter and rectangular steel jig with hole.

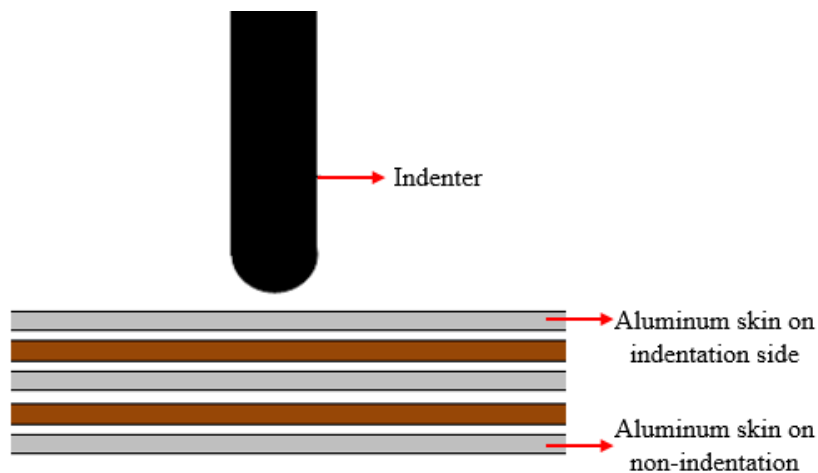


Figure 3: The indentation process of FML panels.

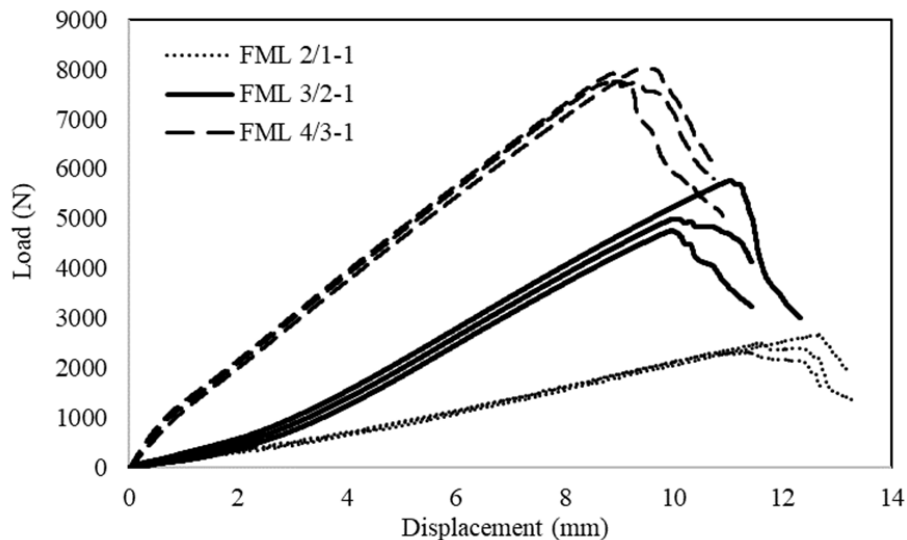
### 3. RESULTS AND DISCUSSION

The indentation response of varying stacking configuration of OPFML panels under the load-displacement curve, the value of energy absorption and specific energy absorption was analysed. Table 1 presents the summary of the mechanical properties for different stacking configurations of OPFML investigated in this study which was subjected to quasi-static indentation test.

**Table 1: Summary of parameters of quasi-static indentation test.**

Stacking Configuration	Average Peak load (N)	Average Displacement at peak load (mm)	Average Energy absorption (J)	Average Specific energy absorption (Jm <sup>2</sup> /kg)
OPFML 2/1	2482.67±173.85	11.76±0.82	15.43±1.08	3.77±0.27
OPFML 3/2	5169.84±527.37	10.34±0.59	32.05±1.66	4.96±0.25
OPFML 4/3	7897.88±131.07	9.13±0.31	50.03±0.76	5.78±0.08

Figure 4 shows typical load-displacement curve subjected to quasi-static indentation test of OPFML panels based on difference stacking configurations. The experiment was repeated three times for each stacking configuration. The results yielded that all curves showed similar features with the load increasing to the peak before decreasing as the indenter indented through the laminates thickness. Similar trends are apparent for all stacking with the peak load increased rapidly as the numbers of stacking increased. The peak load of 4/3 stacking configuration was higher than others due to stiffness behaviour.



**Figure 4: Load - displacement curve of quasi-static indentation test of FMLs panels with difference stacking configurations.**

Figure 5 shows the average peak load under quasi-static indentation test of each stacking configuration. Clearly, the higher stacking configuration exhibited higher average peak load with 7897.88 N while the lower stacking configuration exhibited lower average peak load with 2482.67 N. It is evident that the increasing number of stacking configuration could improve the indentation performance of FMLs based on natural fibre. The different percentage of average peak load for FML 2/1 compared with others was 51.97% less than FML 3/2 and 68.56% less than FML 4/3. These results prove that the values of peak load increase as the numbers of stacking configuration increase due to the stiffest behaviour in which the higher stacking configuration, 4/3 is the stiffest and requires the highest load to indent. Furthermore, increasing the stacking configuration also increases the thickness of FMLs. Similar finding was also observed by Zhou *et al.* (2015) during the quasi-static indentation test of fibre metal laminates with different stacking configurations and shown that the peak load increasing rapidly as the overall laminate thickness increases. Figure 6 shows the average maximum displacement of FMLs based on stacking configuration. The maximum displacement decreased as the stacking configuration increased with 11.76mm of FMLs 2/1, 10.34 mm of FMLs 3/2 and 9.13 mm of FMLs 4/3. The maximum displacement of FMLs 2/1 was higher than 12.1% of FMLs 3/2 and 22.36% of FMLs 4/3. This result indicated that the lower stacking configuration of 2/1 required the highest maximum displacement during indentation process. The condition was because of the lower stiffest behaviour.

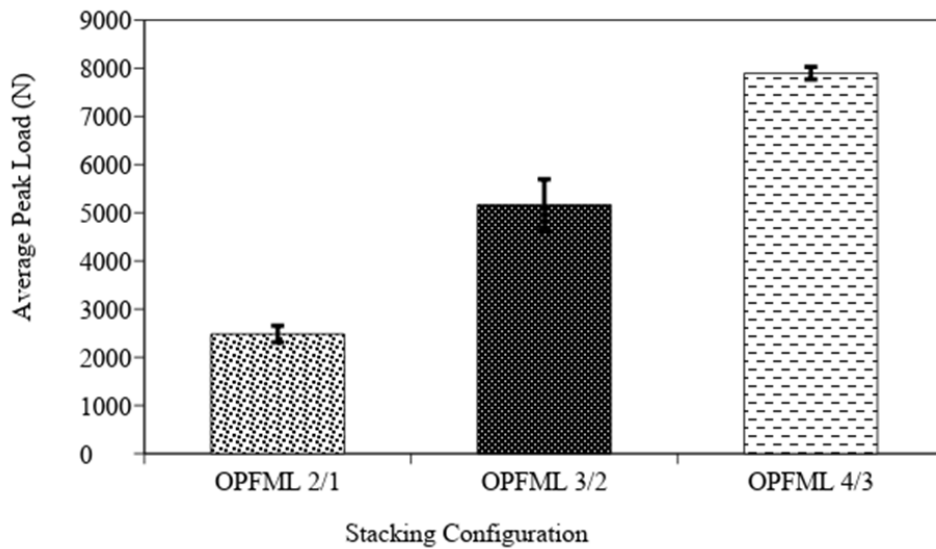
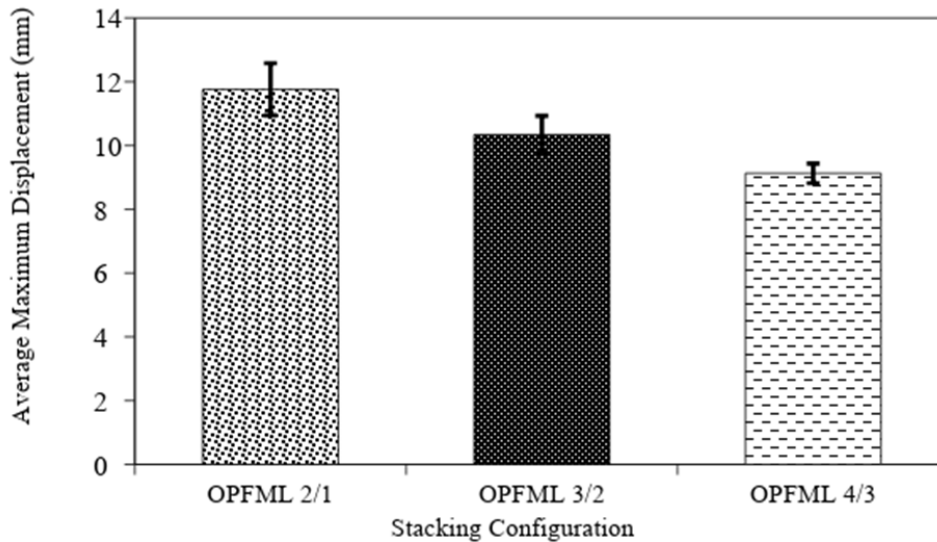


Figure 5: Average peak load of quasi-static indentation test of OPFML.



**Figure 6: Average displacement at peak load of quasi-static indentation test of OPFML.**

#### 4.2.2 Energy Absorption and Specific Energy Absorption

The energy absorption of OPFML panels under quasi-static loading was determined by measuring the area under the curve of load-displacement up to the peak load. The value of energy absorption for each laminates is presented in Figure 7. The results yielded that the energy absorption increased as the numbers of stacking configuration increased. Clearly, the energy absorption of the OPFML 4/3 was 35.9% higher than OPFML 3/2 and 69.2% higher than OPFML 2/1 values. Hence, the increase in energy was linearly proportionate with numbers of stacking configuration. In details, OPFML 4/3 offered a superior performance due to the stiffer behaviour and required higher energy absorption to complete the indentation process.

Figure 8 presents the specific energy absorption (SEA) values of the various OPFML panels investigated here. From the figure, it is clear that the trend of graph is similar with energy absorption whereby the SEA also increased as the stacking configuration increased. Similarly, the OPFML 4/3 offered the higher levels of specific energy absorption with 5.78 Jm<sup>2</sup>/kg values as compared to the OPFML 3/2 with 4.96 Jm<sup>2</sup>/kg and OPFML 2/1 with 3.77 Jm<sup>2</sup>/kg. Evidently, the highest stacking configuration offered the most impressive energy absorbing-characteristics during indentation process for these type of laminates. In other words, the specific energy absorption is directly proportionate with energy absorption values.

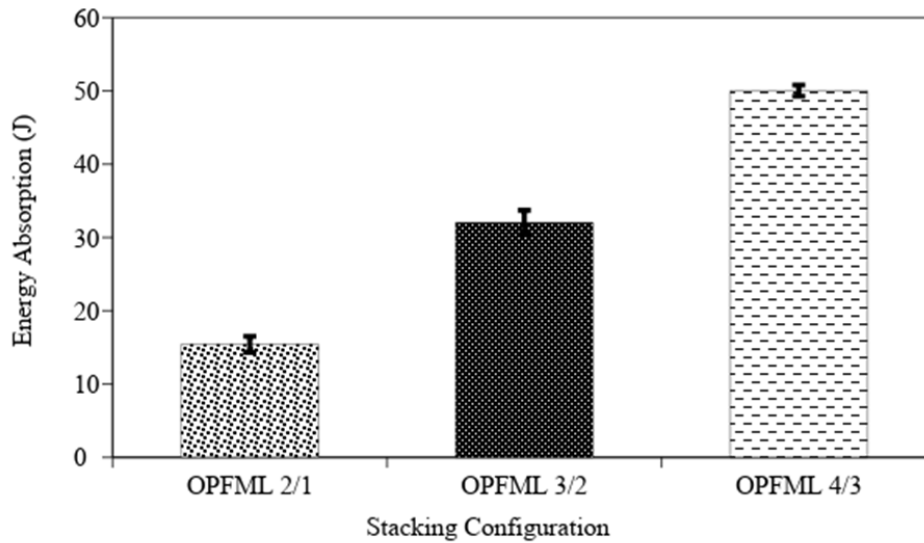


Figure 7: The variation of energy absorption of quasi-static samples.

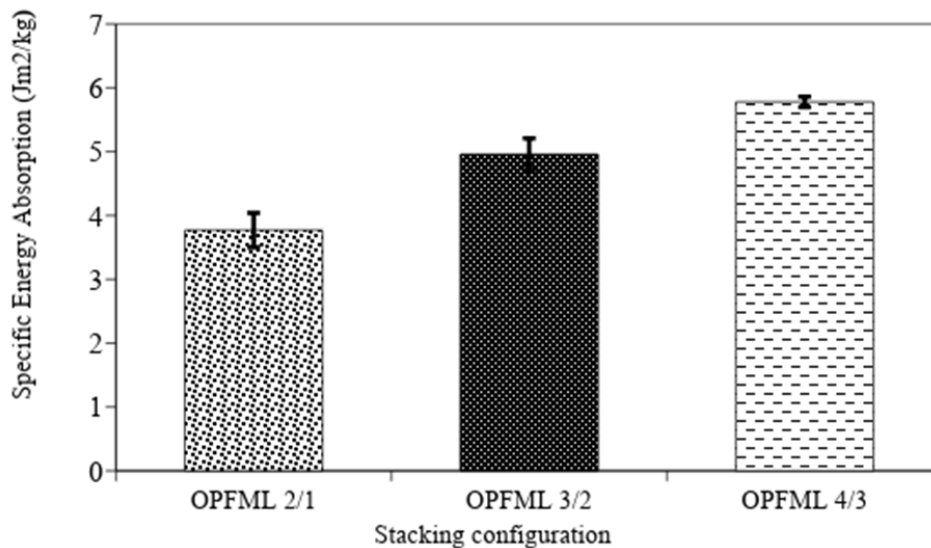


Figure 8: The variation of specific energy absorption of quasi-static samples.

#### 4.2.3 Failure Mode Subject to Quasi-Static Indentation Test

The failure modes of the quasi-static indentation test on the OPFML panels were investigated by examining the surface of indentation side and non-indentation side of the indentation damaged panels. Figure 9 shows the optical images of failure modes for each stacking configuration of OPFML panels subject to indentation and non-indentation side. From the figure, the indentation and non-indentation side of aluminium skins in OPFML 2/1, 3/2 and 4/3 exhibited similar trends with respect to the constant crosshead displacements, 1 mm/min. The first stage of indentation process began with the failures on the aluminium skins on indentation side of laminates. This condition proved when the cracks occurred with little tearing and exhibited plastic deformation on aluminium skins on the indentation side. Similarly



observed by Fan *et al.* (2010), who stated that the plastic deformation in the aluminium skins was close to the indentation zone. However, the different stacking configuration showed the different tearing size on the aluminium upper skins when the highest stacking configuration of OPFML panels studied here (OPFML 4/3) presented the larger aluminium tearing. Hence, the size of cracking increased as the stacking configuration increased.

Then, the indentation process continued until the second stage. In the second stage, the open-cracks failures including the matrix and fibres breakage of laminates composite layers and aluminium cracking of laminates skins occurred when the indenter went through the laminates thickness. This condition occurred because the laminates started to bend due to the maximum load that acted on it, resulting in the laminates obtaining a maximum bending. Then, there was an indentation on the aluminium skins of non-indentation side until the aluminium cracked. The figure 9 also shows open-cracks failure of the FML aluminium skins on non-indentation side. It showed that the highest stacking configuration (4/3) also produced the larger damaged area (in the red circle) during indentation process. Figure 10 shows the failure characteristic of OPFML panels under quasi-static indentation test such as aluminium cracking on laminates skins and some damaged on matrix and fibre in composite layers of OPFML panels. Clearly, the highest stacking configuration will make laminates suffer with more damages. Overall, the different stacking configurations of this type of OPFML panels produces different indentation values but similar trend of failure mode under static loading. These results give a good primary estimation for penetrating parameters required for further investigation on different stacking configurations of OPFML panels under dynamic loading.

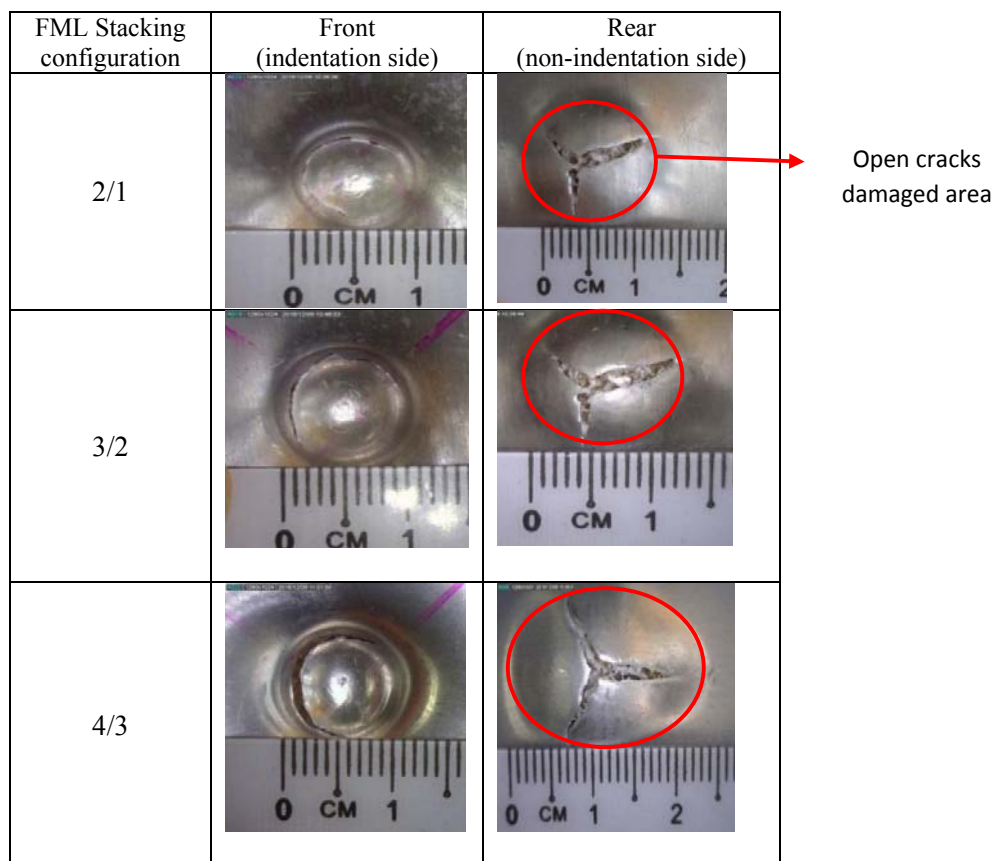


Figure 9: Quasi-static failure mode of FMLs 2/1, 3/2 and 4/3 stacking configuration.

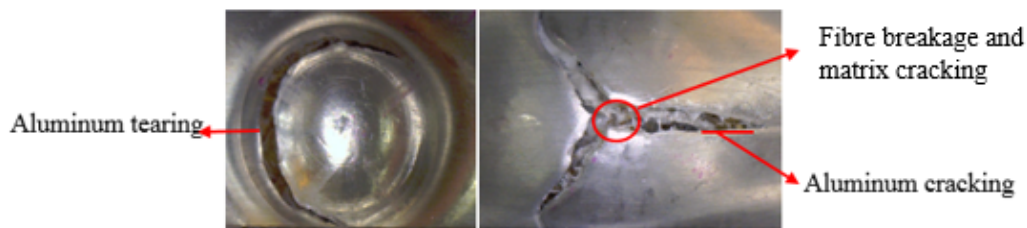


Figure 10: Quasi-static failure characteristics of FMLs panels.

#### 4. CONCLUSION

The indentation behaviour of fibre metal laminates based on aluminium alloy 6061 and oil palm empty fruit bunch fibre reinforced polypropylene composite (OPFML) with various stacking configurations have been investigated. From the results, several conclusions can be obtained. From the quasi-static indentation results, it can be concluded that the stacking configuration influences the indentation behaviour for this type of fibre metal laminate since the indentation parameter such as peak load, energy absorption and specific energy absorption increases as the stacking configuration increases. The failure modes of quasi-static indentation test samples show similar trend for each stacking configuration with aluminium tearing on the non-indentation side and matrix cracking and fibre breakage on the composite layer.

#### ACKNOWLEDGEMENT

The authors would like to thank Universiti Teknikal Malaysia Melaka (UTeM) for the continuous support of this research project. The authors also gratefully acknowledge support from Yayasan Sultan Iskandar Johor who helped fund part of this work.

#### REFERENCES

- Ahmad, F., Choi, H. & Park, M. (2015). A review: Natural fibre composites selection in view of mechanical, lightweight, and economic properties. *J. Macro. Mater. Eng.*, **300**: 10–24.
- Cortes, P. (2014). The fracture properties of a fibre metal laminate based on a self-reinforced thermoplastic composite material. *Poly. Comp.*, **35**: 427-434.
- Cortes, P. & Cantwell, W.J. (2005). The fracture properties of a fibre–metal laminate based on magnesium alloy. *Comp. Part B: Eng.*, **37**: 163-170.
- Fan, J., Cantwell, W. & Guan, Z. (2010). The low-velocity impact response of fibre-metal laminates. *J. Plastics Comp.*, **30**: 26–35.
- Ferrante, L., Sarasini, F., Tirillo, J., Lampani, L., Valente, T. & Gaudenzi, P. (2016). Low velocity impact response of basalt-aluminium fiber metal laminates. *Mater. Design*. **98**: 98–107.
- Jakubczak, P.A. & Bienias, J. (2016). Comparison of quasi static indentation and dynamics load of glass and carbon fibre aluminium laminates. *Aircraft. Eng. Aerospace. Tech.*, **88**: 404 - 410.
- Kashani, M., Sadhigi, M., Lalehpour, A. & Alderliesten, R. (2015). The effect of impact energy division over repeated low-velocity impact on fibre metal laminates. *J. Comp. Mater.*, **49**: 635–646.
- Kathiravan, S., Sivakumar, D., Ng, L.F. & Omar, B. (2017). The effects of stacking configuration on the response of tensile and quasi-static penetration to woven kenaf/glass hybrid composite metal laminate. *Poly. Comp.*, In press: doi:10.1002/pc.24691.

- Kuan, H., Cantwell, W.J. and Hazizan, M. & Santuli, C. (2011). The fracture properties of environmental-friendly fiber metal laminates. *J. Plastics Comp.*, **30**: 499–508.
- Ng, L.F., Sivakumar, D., Zakaria, K.A. & Selamat, M.Z. (2017). Fatigue performance of hybrid fibre metal laminate structure. *Int. Rev. Mech. Eng.*, **11**: 61–68.
- Romli, N.K., Rejab, M R M., Bachtiar, D., Siregar, J., Rani, M.F., Salwani, M.S. & Merzuki, M.N.M. (2018). Failure behaviour of aluminium/CFRP laminates with varying fibre orientation in quasi-static indentation test. *IOP Conf. Series: Mater. Sci. Eng.*, **319**: 1-7.
- Santiago, R., Cantwell, W. & Alves, M. (2017). Impact on thermoplastic fibre-metal laminates: experimental observations. *Comp. Struct.*, **159**:800-817.
- Sivakumar, D., Kathiravan, S., Selamat, M.Z., Said, M.R. & Sivaraos, S. (2016). A study on impact behaviour of a novel oil palm fibre reinforced metal laminate system. *ARPJ. Eng. Sci.*, **11**: 2483-2488.
- Sivakumar, D., Nisallini P., Omar B., Sivarao, S. & Selamat, M.Z. (2017). Quasi-static indentation behaviour of kenaf bast fibre reinforced metal laminate system. *Defence S&T Tech. Bull.*, **10**: 258-271.
- Thakur, V.K., Thakur, M.K. & Gupta, R.K. (2014). Review: Raw natural fibre-based polymer composites. *Int. J. Polym. Anal. Charact.* **19**: 256–271.
- Yu, B., Deshpande, V.S. & Fleck, N.A., (2018). Perforation of aluminium alloy-CFRP bilayer plates under quasi-static and impact loading. *Int. J. Impact Eng.*, **121**: 106-118.
- Zhou, J., Guan, Z.W., Cantwell, W.J., (2015). The influence of strain-rate on the perforation resistance of fibre metal laminates. *Comp. Struct.*, **125**:247-255.

# STUDY OF DELAMINATION FACTORS ON THE ABRASIVE WATER-JET DRILLING OF FIBRE METAL LAMINATES FOR MILITARY CARGO AIRCRAFT

Thirukumaran Manoharan<sup>1</sup>, Winowlin Jappes Jebbas Thangaiah<sup>1</sup>, Siva Irulappasamy<sup>1\*</sup>, Sivakumar Dhar Malingam<sup>2</sup> & Sandro Campos Amico<sup>3</sup>

<sup>1</sup>Centre for Composite Materials, Kalasalingam Academy of Research and Education, India

<sup>2</sup>Fakulti Kejuruteraan Mekanikal, Universiti Teknikal Malaysia Melaka (UTeM), Malaysia

<sup>3</sup>PPGE3M, Federal University of Rio Grande do Sul (UFRGS), Brazil

\*Email: isiva@klu.ac.in

## ABSTRACT

*Use of fibre metal laminates (FML) in military cargo aircrafts improves impact and fatigue resistance and decreases weight. Such aircraft assembly largely requires secondary processing, and the machining of hybrid materials such as FML is a great challenge. In particular, drilling causes harsh delamination due to severe vibrations during machining. This work investigates the effect of traverse speed on delamination applied to abrasive water-jet machining. The hybrid laminate, an alternate stacking of AA 7475 and E-glass fibre/epoxy laminas, is produced by compression moulding. Drilling was carried out using constant jet pressure and stand-off distance, with variable traverse speed (10, 20 and 30 mm/min). Delamination is evaluated through optical microscopy based on the internal damage caused around the edges. Three delamination models are analysed to assess the structural integrity of the FML. Traverse speed, variation in hardness between metal and composite, and their positioning affected the kerf taper in the machined volume. Electron microscopy revealed the mechanism behind material erosion and production of kerf taper, for the lower traverse speed produced less kerf taper and dimensional deviation but higher fibre fraying and delamination occurred.*

**Keywords:** *Fibre metal laminates (FML); abrasive water jet machining; kerf taper; delamination factor; erosion.*

## 1. INTRODUCTION

In defence aircrafts, fibre metal laminates (FML) are widely used due to their high and low velocity impact resistance, high fatigue strength, and enhanced mechanical fracture toughness and creep behaviour (Wu *et al.*, 2005). Resistance to multiple impacts and light-weight related benefits motivates the use of glass fibre reinforced aluminium stacking (GLARE<sup>TM</sup>) laminates in several military cargo aircrafts (C-5, C-17 and C-130) (Vlot *et al.*, 1999; Voegesang & Volt, 2000). The alternative stacking of fibre and metal can be classified according to materials, fibre orientation, thickness of plies and laminates, and number of each alternative lamina (Sinmazçelik *et al.*, 2011).

In the assembly line, secondary machining processes such as drilling, lapping and trimming were used to complete the process. Machining of FML (inter-cladding of fibre reinforced composites with metals) structures is a challenge in the aviation sector. Drilling is a primary machining process used to couple lapped structural members both in a permanent and/or temporary manner, but this cannot compromise the bear-ability limits of the structural members. Due to dissimilarities in subsequent layers, conventional

drilling of hybrid composites may be hard to achieve the dimensional requirements. In addition, the reinforcing and bulk matrix materials should be similarly removed (Liu *et al.*, 2012).

Conventional machining of fibre metal laminates may show unwanted characteristics such as delamination, peel-up and push down, fibre fraying, chips and tool wear, and hole surface damage (Thirukumaran *et al.*, 2018). Peel-up delamination was a primary defect when machining fibre reinforced structures. The tool cutting edge rounding (i.e., tool wear) was created to peel up delamination in laminate composites (entry and exit of the hole) (Faraz *et al.*, 2009). Delamination is one of the main defects observed in conventional machining of hybrid laminates, and may be seen as the deviation and detrition occurring from the drilled edges (Babu *et al.*, 2015; Bosco *et al.*, 2015). Uncut fibre portions, otherwise known as fibre fraying, also results from improper drilling (Ashrafi *et al.*, 2014). In order to control machining failure and poor hole quality, various machining issues have been investigated (Pawar *et al.*, 2015). Ramulu *et al.* (2015) reported greater surface roughness and delamination in computer numerical control (CNC) drilling of hybrid laminate structures, and suggested secondary processes to enhance drill quality. Use of a coated tool, production of pilot hole and micro finishing were some of the techniques that can be adopted to finish the drilling of hybrid laminates (Liu *et al.*, 2012; Thirukumaran *et al.*, 2018).

Later in the 1990s, researchers started to explore the suitability of unconventional machining processes for FML (Paul *et al.*, 2002; Liu *et al.*, 2012). Jensen *et al.* (2009) experimented with laser beam machining (LBM), which was found to be not suitable to cut polymer regions since the machining was done only on the metal. Ramulu *et al.* (2016) studied drilling of titanium / graphite FML using electrical discharge machining (EDM) and found that only conductive polymers are suitable, and reported excess material removing, cracking, interplay delamination, matrix burning and extrusion as disadvantages of this method. Abrasive water jet (AWJ) cutting is considered one of the most effective processes to machine hard and brittle materials, with better performance regarding thermal equilibrium and accuracy (Ma & Deam, 2006; Slawomir, 2014). The jet traverse speed has a major effect on surface finishing and kerf taper (Shanmugam *et al.*, 2009). This was ratified in the study of Ramulu *et al.* (2015), who investigates AWJ machining of Ti based FML, and concluded that when traverse speed needs to be increased, an increase in the abrasive flow rate can result in similar material removal rate.

Hence, it is now become unavoidable in processing engineering to select the unconventional machining method of machining to accommodate the high-performance materials into defence applications. By understanding the cons with conventional machining, researchers and engineers have started to transform the machining processes slowly towards unconventional. Especially in military aircrafts, reverting is the predominant joining process followed and which required so many numbers of drilling on the same panel. So that, this work focused the process parameter optimization to achieve flaw-less drilling using abrasive jet machine.

## **2. EXPERIMENTAL DETAILS**

### **2.1 Materials**

Aluminium 7475 alloy sheets supplied by The Coimbatore Metal Mart, Coimbatore/TN, India were used in this study. Chopped strand E-glass fibre mats were purchased from Nickunj, Chennai/TN, India, and epoxy 8109 resin with hardener HY 48 was supplied by Vasavibala Resins, Chennai/TN, India. Table 1 shows the characteristics of the raw materials and abrasive used (Garnet ~0.2  $\mu\text{m}$ ) in AWJ machining.

**Table 1: Raw material property.**

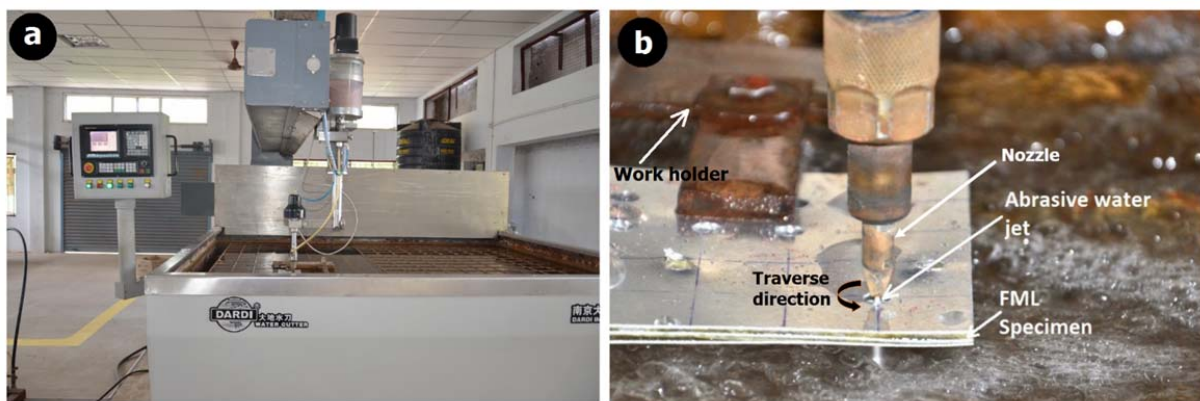
Indicator	Alloy	Polymer	Abrasive
Materials	AA7475	E-glass fibre/epoxy 8109+hardener HY 48	Garnet
Layer thickness (mm)	0.4	0.5	--
Density (g/cc)	2.81	2.54	4.12
Hardness	162 VHN	82 (Shore D)	7.5 (Mohs scale)
Modulus of elasticity (GPa)	70.3	10	248

## 2.2 Lamination Process

Fibre metal laminates were produced by stacking the AA 7475 alloy sheet intercalated with random oriented E-glass fibre/epoxy composite (GE). The AA 7475 surface was pre-cleaned with ethanol to remove impurities. Glass fibre / epoxy composites were prepared by simple lay-up process, i.e., pouring the formulated epoxy (1:2 of hardener) over the glass fibres. The whole set-up was then stacked into a mould (cavity of  $300 \times 130 \times 3$  mm), which was closed and clamped in a press at 18 MPa. The mould was heated to 75 °C and kept for 2 h. The temperature was then raised to 120 °C and maintained for 1 h. Finally, the mould was removed and allowed to cool to room temperature. After de-moulding, the samples were post-cured for 2 h at 60 °C.

## 2.3 Abrasive Water Jet Machining

An AWJ cutting machine-model DWJ1313-FB coupled to a high pressure (40 MPa) pump DIPS6-2230 (Figure 1) of DARDI International, Korea was used to produce the holes in the fabricated FML. The nozzle movements were numerically controlled.



**Figure 1: (a) The abrasive water jet machine unit. (b) Closer view of the machining process.**

Table 2 shows the machining parameters followed in this study. FML was mounted on the work holder of the AWJ machine (as shown in Figure 1b) and spatial coordinates and initial set-ups were done on the machine. The experiments were conducted at three traverse speeds, 10, 20 and 30 mm/min, with all other parameters constant, as shown in Table 2.

**Table 2: Machining parameters used in this study.**

Parameters	Value
Water jet pressure (MPa)	24
Abrasive flow rate (g/s)	2
Stand-of distance (mm)	2
Diameter of water jet nozzle (mm)	0.76
Abrasive material	Garnet
Grain size (µm)	0.2-0.315
Traverse speed (mm/min)	10, 20 and 30
Impact angle	90°

## 2.4 Internal and External Drill Quality Assessment

The quality of the drilled hole was assessed by observing fibre fraying (uncut fibre portion) and surface edge rounding distortions using a stereo microscope (Motic SMZ-168, Korea). The dimensional tolerance of the hole was verified using a coordinate measuring machine (TESA Technologies, Telford/UK). The magnitude of the kerf taper in the hole was calculated using the following equation:

$$Kerf\ taper = \left( \frac{D_t - D_b}{2t} \right) \quad (1)$$

where  $D_t$  - top drill diameter,  $D_b$  - bottom drill diameter and  $t$  - thickness of the laminate.

Material removal rate ( $MRR$ ) was calculated using the following equation:

$$MRR = h_t d_i v_f \quad (2)$$

where  $h_t$  - depth of penetration,  $d_i = \frac{D_t + D_b}{2}$  and  $v_f$  - traverse speed in mm/min.

Dimensional deviations for both jet entry and jet exit on the FML were calculated as  $D_a - D_m$ , where,  $D_a$  - actual diameter and  $D_m$  - diameter obtained after machining.

Fibre fraying ( $F_f$ ) was measured using the following equation:

$$F_f = \frac{A_f}{A_h} \quad (3)$$

where  $A_f$  - frayed fibre area and  $A_h$  - hole area.

## 2.5 Delamination Factor

Traverse speed governs the delamination models in fibre metal laminates. Drill damage was calculated in terms of the delamination factor ( $F_d$ ) obtained from the following equation:

$$F_d = \frac{D_{max}}{D_0} \quad (4)$$

where  $D_{max}$  - maximum diameter of delamination and  $D_0$  - nominal hole diameter.

The approach by Davim *et al.* (2007) was used to obtain an adjusted delamination factor ( $F_{da}$ ) in terms of crack damage:

$$F_{da} = F_d + \frac{A_d(F_d^2 - F_d)}{A_{max} - A_0} \quad (5)$$

where  $A_d$  is the total damage area,  $A_{max}$  is the area delimited by  $D_{max}$  and  $A_0$  is the area related to  $D_0$ .

The approach by Tsao *et al.* (2012) was used to measure the equivalent delamination factor ( $F_{ed}$ ) based on equivalent diameter for both damage and nominal diameter as shown in the following equation:

$$F_{ed} = \frac{D_e}{D_0} \quad (6)$$

where:

$$D_e = \left[ \frac{4(A_d + A_0)}{\pi} \right]^{0.5} \quad (7)$$

Delamination size ( $D_s$ ) was calculated as:

$$D_s = D_{max} - D_0 \quad (8)$$

### 3. RESULTS AND DISCUSSION

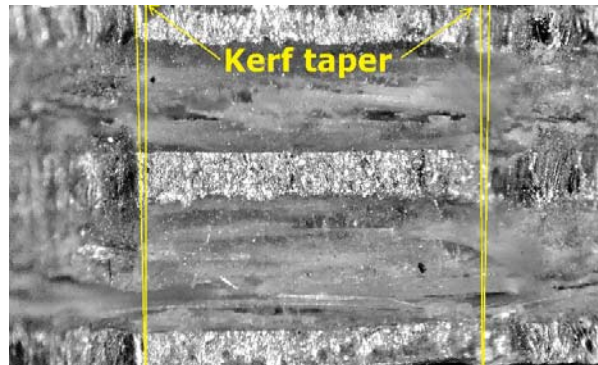
Table 3 shows the effect of traverse speed on the quality of the drills produced using AWJ cutting on the fabricated fibre metal laminates. It was observed that at higher traverse speed, significant variation in drill quality was recorded. Kerf taper also increased with the increase in traverse speed. In addition, at 10 mm/min, MRR was 148.13 mm<sup>3</sup>/min, with dimensional deviations at both the entry and the exit being 0.064 and 0.086 mm respectively. For the selected stand-of-distance (2 mm), the raise in traverse speed from 10 to 20 mm/min lead to an increase in MRR of ca. 98%. Such a drastic increase in MRR resulted in 33% increase in kerf taper. At 30 mm/min, the increase in MRR and kerf taper reached 194% and 266%, respectively, as compared to those at 10 mm/min.

**Table 3: Variation in drill quality parameters with jet traverse speed.**

Experiment No.	Traverse speed ( $T_s$ ) (mm/min)	Traverse time (s)	MRR (mm <sup>3</sup> /min)	Kerf taper	Dimensional deviations (mm)	
					Entry	Exit
1	10	90	148.13	0.003	0.064	0.086
2	20	45	294.14	0.004	0.104	0.132
3	30	31	435.75	0.011	0.156	0.224

For abrasive water jet machining of circular drills, kerf was one of the key studied factors. Figure 2 shows the kerf taper obtained in the AWJ machining of E-glass reinforced FML (3/2). At high traverse speed of the abrasive jet through the heterogeneous system, the projectiles (abrasive particles) may severely divert from their original path due to the drastic change in hardness of the alternate AA 7475 (162 VHN) and polymer composite layers in this FML stacking, yielding a high kerf taper. Micro-plowing, i.e., the loss of bonding between the smooth polymeric surface and the rough aluminium surface was also observed.

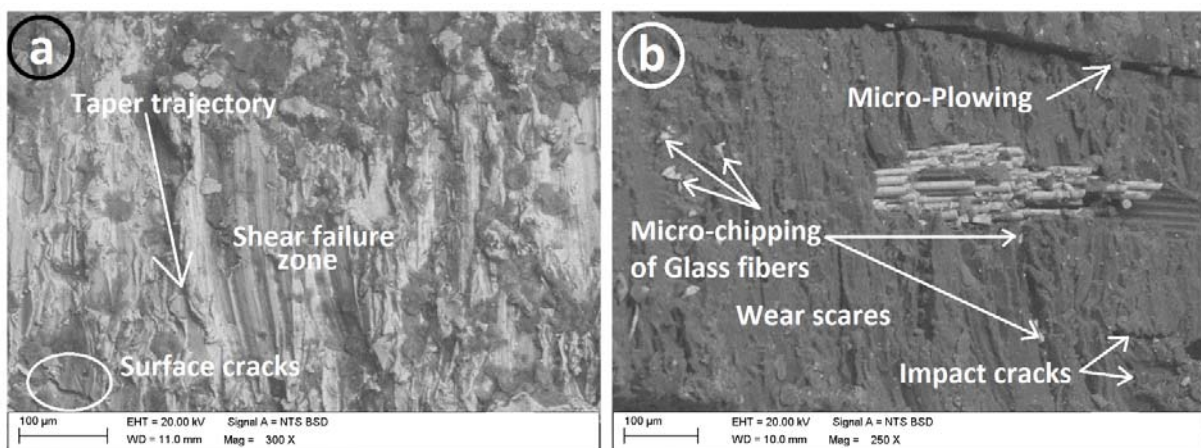




**Figure 2: Image of the kerf taper produced at 10 mm/min traverse speed.**

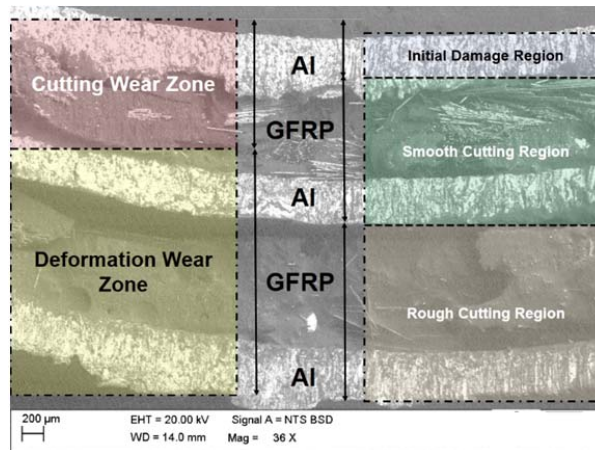
The surface machined at lower traverse speed (Figure 3(a)) shows more pronounced wear scars attributed to shear deformation in the AA 7475 alloy. In the composite layer, glass fibres were prone to brittle fracture and pull-out from the matrix (Figure 3(b)). For higher traverse speed, MRR increases since a larger number of abrasive particles impact a single spot, promoting patch removal of polymer material. Indeed, even though the abrasive flow rate was constant, the moment given to the abrasive and the short impinging time cause many energised particles to hit on a same place, increasing MRR. Furthermore, a narrower spread of water-jet over the drilling area and the bottom produced a lower angle.

Table 3 also shows that at low traverse speed, the deviation in drilling was minimum, i.e., the abrasive particles passing through the nozzle have enough time to wear out the targeted area, and almost near-net programmed profile can be obtained in both the entry and the exit surfaces. Perhaps the increase in traverse speed has a significant impact on projectile path as a result of the synergy in through the thickness hardness difference in FML (Ramulu *et al.*, 2015). Due to the water flow (wider) from the nozzle outlet, the bottom surface of the drill always displays higher dimensional deviation than the top one, which is observed by the kerf taper also. In addition, a two-fold increase in traverse speed from 10 to 20 mm/min led to an increase in dimensional deviation of 62.5 (top) and 53% (bottom), and a decrease in drilling time of 50%. A further increase in traverse speed to 30 mm/min led to an extra reduction in drilling time of 31%, with 143 (top) and 160% (bottom) increase in dimensional deviation.



**Figure 3: SEM images of surfaces machined at: (a) 10 mm/min and (b) 30 mm/min.**

Deflection of the AWJ produced wavy surface textures on the machined areas. Hence, the abrasive water jet energy caused the deviation in projectile trajectory that produced kerf taper. Such action is commonly classified into three zones (Figure 4). At the top, during the onset entry, in the Initial Damage Region (IDR), as identified by (Arola *et al.*, 1997), high energy abrasive particles attack the surface and sub-surface to promote machining at narrow direction. The energy of the jet and particles was much higher than at the drill onset. Material removal during AWJ machining comprised of plowing and rubbing, micro-chipping, and finally erosion. The shear force exerted with the resulting plastic deformation in the resin rich and in the aluminium regions were the predominant removal mechanism. Nonetheless, the abrasive particle impinging angle directly imparts material removal and controls all the above factors (Arola *et al.*, 1996, 1997).



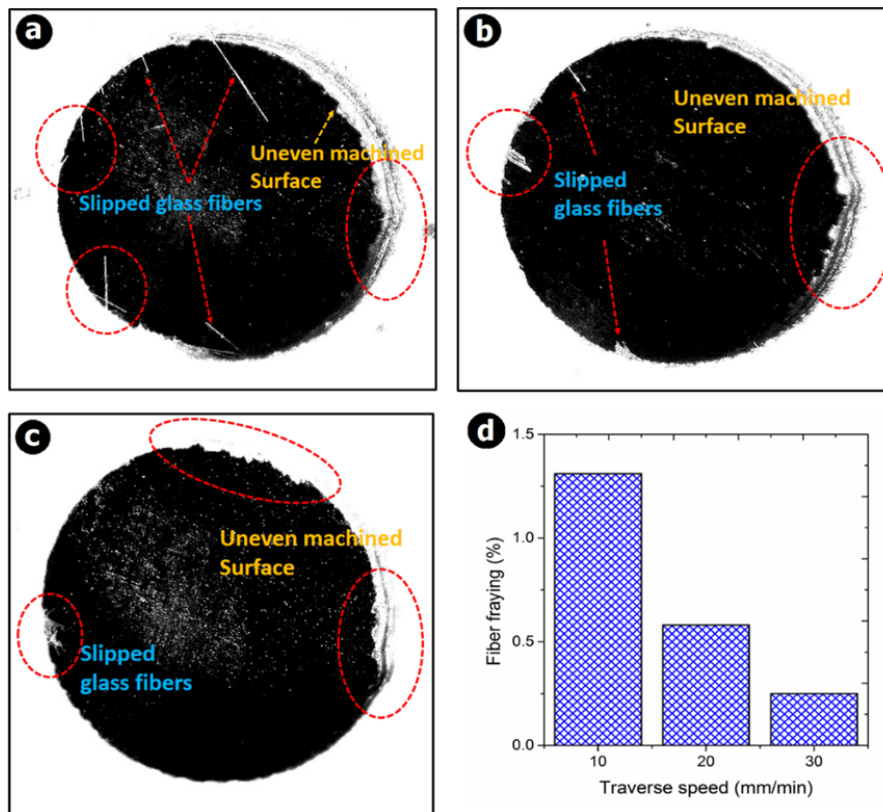
**Figure 4: Illustration of the wear micro-mechanism and damage zones.**

Erosion during AWJ machining of FML is purely referred to as the wear process. Such wear in the entire drill depth can be classified into entry “cutting wear zone” and exit “deformation wear zone”. During the onset of the machining process (at the entry), the abrasive particles hit the blank at an attack angle of  $90^\circ$ , where cutting wear was severe (Bellman & Levy, 1981). Next to the cutting wear zone, based on the traverse speed, particle attack angle becomes obtuse, between  $90^\circ$  and  $180^\circ$ , causing the removal of materials through deformation wear (Bitter, 1963a). Meantime, at the bottom of machined laminates, deformation zone also observed in this AWJ circular cutting action.

Bitter (1963b) reported that material removal rate in AWJ was not cutting-depth dependent, being mainly dependent on the shear induced abrasive machining at micro-level in conjunction with the cutting wear exerted. This is more pertinent to homogenous materials system, whereas for heterogeneous material systems such as FML, removal rate primarily depends on cutting depth and traverse speed. Indeed, Arola *et al.* (1997) later reported that MRR was directly controlled by traverse speed, which is attributed to the change in striking angle of the abrasive as a consequence of the change in hardness of subsequent layers in the FML. In the present work, MRR in E-glass reinforced FML (3/2) was highly dependent on traverse speed, reaching  $435 \text{ mm}^3/\text{min}$  at  $30 \text{ mm}/\text{min}$ , which is ca. 48% higher than at  $20 \text{ mm}/\text{min}$ .

Figures 5(a) - (c) shows optical micrographs of the machined hole, illustrating fibre fraying as a result of the AWJ machining of FML. At low traverse speed, un-machined or left-out blank portions, often referred to as fibre fraying, were more significant (Ashrafi *et al.*, 2014). This mechanism was more significant at  $10 \text{ mm}/\text{min}$  (Figure 5a), where fraying of glass fibre was 1.31% of the total removed area (Figure 5(d)).

Delamination was a severe damage experienced during drilling of laminated structures. In aircraft assembly, 60% of the rejection refers to delaminated composites (Hocheng *et al.*, 2005). Indeed, conventional drilling leads to severe delamination due to the significant vibration resulting from internal friction among contact areas (Sharma *et al.*, 2013). Unconventional machining techniques, on the other hand, are recognised as able to produce nearly flawless shapes. Nevertheless, fibre fraying and edge delamination are still reported in AWJ machining. Evaluation of delamination and its effect on the laminates are done through various methods. In experimental analysis, material removal rate governs the adjusted delamination factor (Rubio *et al.*, 2008).



**Figure 5: Traverse speed effect on fibre fraying produced in the hole machined at (a) 10, (b) 20 and (c) 30 mm/min, and (d) calculated values.**

The AWJ machining process is usually considered for impact fracture of the blank due to the water jet hitting the abrasive particles. At low traverse speed cuts, the particles impinging the resin as well as aluminium were attributed to the high sensitivity of the produced edge portions. On the other hand, at higher traverse speeds, drilling can occur with a reduced number of abrasive particles which significantly reduced edge damage, since the shear plane area was much smaller during higher traverse speed rather at lower traverse speed, which is influenced by edge damage, and thus, delamination would be larger. Figure 6 shows the delamination and damage area with corresponding curves comparing delamination factor models for E-glass reinforced FML (3/2) laminates. It can be seen that machined edge distortion at 10 mm/min (Figure 6a) was more pronounced than at 20 or 30 mm/min. For the former, erosion wear exerted during cutting of the ductile material led to severe plastic deformation and massive surface cracks.

Table 4 shows that the delamination factor has almost the same trend for all the test runs. The equivalent factor ( $F_{ed}$ ) was closer to the conventional factor ( $F_d$ ) than the adjusted factor ( $F_{da}$ ), and  $F_{ed}$  was always lower than  $F_{da}$ . The edge distortion and plastic deformation governs the propagation of delamination. Higher delamination factor  $F_{da}$  and  $F_{ed}$  were observed at higher  $A_d$ .

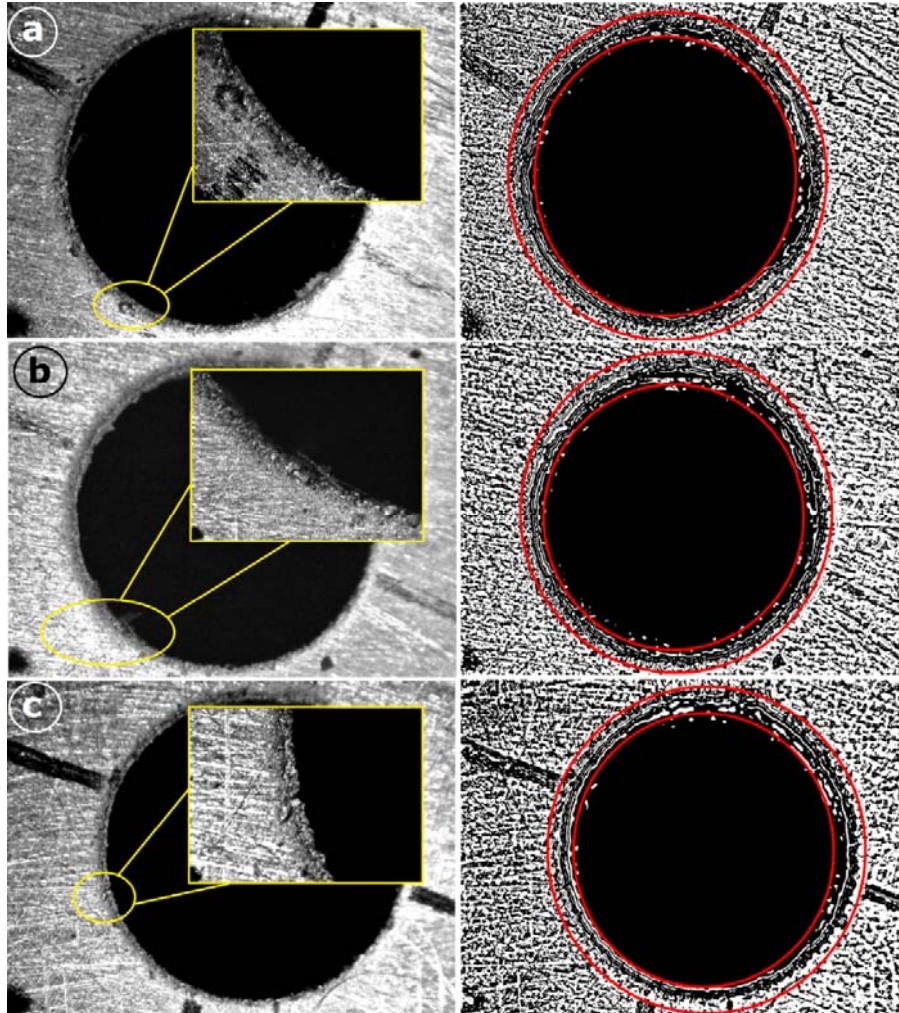


Figure 6: Indication of delamination when drilling at traverse speed of: (a) 10, (b) 20 and (c) 30 mm/min.

Table 4: Experimental results of delamination factor models.

Exp. No.	Traverse Speed (mm/min)	Delamination parameter			Delamination factor models			Delamination Size ( $D_s$ ) (mm)
		$D_{max}$ (mm)	$A_d$ (mm <sup>2</sup> )	$D_e$ (mm)	$F_d$	$F_{da}$	$F_{ed}$	
1	10	7	7.52	7.009	1.116	1.245	1.115	0.72
2	20	6.92	6.95	6.918	1.104	1.218	1.105	0.66
3	30	6.88	6.58	6.872	1.102	1.214	1.101	0.64

## 4. CONCLUSION

The drilling performance of E-glass reinforced FML machined using AWJ cutter was investigated in this work. Material removal rate, kerf taper, dimensional deviation, fibre fraying, delamination models and wear morphology were studied to address drilling quality. The produced drill hole was significantly influenced by the traverse speed. A common increasing trend was found for MRR, kerf taper and dimensional deviation for higher traverse speed. Fibre fraying significantly increased with lower traverse speed, being a direct indication of low drilling quality. Delamination and factors were the critical factors consider in drilling of E-glass reinforced FML. Traverse speed also governed the delamination factors, which were more significant at lower values (30 mm/min). Theoretical models were used to compare the findings. The equivalent factor ( $F_{ed}$ ) model yielded delamination values closer to the experimental ones, in comparison with the conventional factor ( $F_d$ ), and adjusted factor ( $F_{da}$ ) showed the largest deviations. In all, adoption of 30 mm/min traverse speed has the potential to generate near perfect drills in FML machined through AWJ.

## ACKNOWLEDGEMENT

The authors wish to thank the Department of Science and Technology (DST), India for the Fund for Improvement of Science and Technology Infrastructure in University and Higher Educational Institution (FIST) and the first author wishes to thank the Kalasalingam Academy of Research and Education, India for University Research Fellowship.

## REFERENCES

- Arola, D. & Ramulu, M. (1997). Material removal in abrasive waterjet machining of metals a residual stress analysis. *Wear*, **211**: 302–310.
- Arola, D., Ramulu, M. & Wang, D.H. (1996). Chip formation in orthogonal trimming of graphite/epoxy composite. *Compos. Part A: Appl. S.*, **27**: 121–133.
- Ashrafi, S.A., Sharif, S. & Farid, A.A. (2014). Performance evaluation of carbide tools in drilling CFRP-Al stacks. *J. Compos. Mater.*, **48**: 2071–2084.
- Babu, J., Sunny, T., Paul, N.A., Mohan, K.P & Davim, J.P. (2015). Assessment of delamination in composite materials : A review. *P. I. Mech. Eng. B: J. Eng.*, **230**: 1990–2003.
- Bellman, R. & Levy, A. (1981). erosion mechanism in ductile metals. *Wear*, **70**: 1–27.
- Bitter, J.G.A. (1963a). A study of erosion phenomena, Part-1. *Wear*, **6**: 5–21.
- Bitter, J.G.A. (1963b). A study of erosion phenomena, Part II. *Wear*, **6**: 169–190.
- Bosco, M.A.J. Palanikumar, K. Prasad, B.D. & Velayudham, A. (2015). Analysis on influence of machining parameters on thrust force in drilling gfrp-armor steel sandwich composites. *J. Compos. Mater.*, **49**: 1539–1551.
- Davim, J.P., Rubio, J.C. & Abrão, A.M. (2007). A novel approach based on digital image analysis to evaluate the delamination factor after drilling composite laminates. *Compos. Sci. Technol.*, **67**: 1939–1945.
- Faraz, A., Biermann, D. & Weinert, K. (2009). Cutting edge rounding : An innovative tool wear criterion in drilling CFRP composite laminates. *Int. J. Mach. Tool. Manu.*, **49**: 1185–1196.
- Hocheng, H. & Tsao, C.C. (2005). The path towards delamination-free drilling of composite materials. *J. Mater. Process. Tech.*, **167**: 251–264.
- Jensen, B.J., Cano, R.J., Hales, S.J., Alexa, J.A., Weiser, E.S., Loos, A. C. & Johnson, W.S. (2009). Fibre metal laminates made by the VARTM process. *17th Int. Conf. Compos. Mater.*, 27–31 July 2009, Edinburgh, Scotland.
- Liu, D.F., Tang, Y.J. & Cong, W.L. (2012). A review of mechanical drilling for composite laminates.

- Compos. Struct.*, **94**: 1265–1279.
- Ma, C. & Deam, R.T. (2006). A Correlation for predicting the kerf profile from abrasive water jet cutting. *Exp. Therm. Fluid. Sci.*, **30**: 337–343.
- Paul, S., Hoogstrate, A.M. & Van Praag, R. (2002). Abrasive water jet machining of glass fibre metal laminates. *P. I. Mech. Eng. B: J. Eng.*, **216**: 1459–1469.
- Pawar, O.A., Gaikhe, Y.S., Tewari, A., Sundaram, R. & Joshi, S.S. (2015). Analysis of hole quality in drilling GLARE fibre metal laminates. *Compos. Struct.*, **123**: 350–365.
- Ramulu, M., Pahuja, R., Hashish, M. & Isvilonanda, V. (2015). Abrasive waterjet machining effects on kerf quality in thin fibre metal laminate. *Proc. WJTA-IMCA Conf.*, New Orleans, pp. 2–4.
- Ramulu, M. & Spaulding, M. (2016). Drilling of hybrid titanium composite laminate (HTCL) with electrical discharge machining. *Mater.*, **9**: 746.
- Rubio, J.C., Abrao, A.M., Faria, P.E., Correia, A.E. & Davim, J.P. (2008). Effects of high speed in the drilling of glass fibre reinforced plastic : Evaluation of the delamination factor. *Int. J. Mach. Tool. Manu.*, **48**: 715–720.
- Shanmugam, D.K. & Masood, S.H. (2009). An investigation on kerf characteristics in abrasive waterjet cutting of layered composites. *J. Mater. Process. Tech.*, **209**: 3887–3893.
- Sharma, V., Kumar, V. & Kumar, H. (2013). Effects of Different Parameters on Delamination Factor of Glass Fibre Reinforced Plastic (GFRP). *Int. J. Manuf. Mater. Mech. Eng.*, **3**: 17–31.
- Sinmazçelik, T., Avcu, E., Özgür, M. & Çoban, O. (2011). A review : Fibre metal laminates, background, bonding types and applied test methods. *Mater. Design.*, **32**: 3671–3685.
- Slawomir, Z. (2014). Abrasive wear of fibre-metal composites based on fibreglass woven fabric layer. *Modern Tech. Ind. Eng.*, **837**: 290–295.
- Thirukumaran, M.I., Siva, I., Jappes, J.T.W. & Manikandan, V. (2018). Forming and drilling of fibre metal laminates – A review. *J. Reinf. Plast. Comp.*, **37**: 981–990.
- Tsao, C.C., Kuo, K.L. & Hsu, I.C. (2012). Evaluation of a novel approach to a delamination factor after drilling composite laminates using a core – saw drill. *Int. J. Adv. Manuf. Tech.*, **59**: 617–622.
- Vlot, A., Voegesang, L.B. & De Vries, T.J. (1999). Towards application of fibre metal laminates in large aircraft. *Air. Eng. Aero. Tech. Int. J.*, **71**: 558–570.
- Voegesang, L.B. & Vlot, A. (2000). Development of fibre metal laminates for advanced aerospace structures. *J. Mater. Process. Tech.*, **103**: 1–5.
- Wu, G. & Yang, J.M. (2005). The mechanical behavior of GLARE laminates for aircraft structures. *JOM*, **57**: 72–79.

# IDENTIFICATION OF HIGH LEVEL VIBRATION ON ROTOR BEARING SYSTEM USING EXPERIMENTAL DATA ANALYSIS

Yogeswaran Sinnasamy\*, Noor Aishah Sa'at, Hasril Nain, Ibrahim Tahir, Ahmad Subardi Mohd Wazir, Hanizah Kasmoni, Elizabeth Louisnaden & Khairul Anuar Ahmad

Science & Technology Research Institute for Defence (STRIDE), Ministry of Defence, Malaysia

\*Email: yoges.sinnasamy@stride.gov.my

## ABSTRACT

*In rotating machines, rolling element bearings are widely used in many applications, such as marine gear box and diesel engine. Vibration monitoring is highly capable to detect any abnormalities on bearings before failure occurs. In this paper, vibration measurement is utilised to detect the locations on rotor bearing systems that record the highest levels of vibration. Vibration spectrums captured on two units of healthy rolling element bearings in three different directions at various speeds were analysed, with the measurements found to have high level of accuracy. Based on the measurement procedure developed in this experimental work, condition monitoring (CM) for rotor-bearing systems can be developed in the future.*

**Keywords:** *Rolling element bearing; vibration monitoring; fundamental frequency; vibration spectrums; accuracy.*

## 1. INTRODUCTION

Rolling element bearings are widely used in naval and merchant ships to support main and auxiliary propulsion systems. In rotating machineries, these bearings are subject unbalanced forces generated in machines. This leads to different types of faults in the bearings and simultaneously leads to failure of rotating machinery (Khardersab & Shivakumar, 2018). A bearing fault can result in unscheduled maintenance and in extreme cases, plant shutdown. In fact, it was reported by Desavale & Mali (2016) that rolling element bearing faults account for almost 30% of faults in rotating machinery. These faults may be developed during longer run of bearing under certain conditions. Severe vibrations of bearing can even cause the entire system to function incorrectly and subsequently result in downtime of the system and financial loss to the user (Nistane & Harsha, 2016).

Condition monitoring (CM) is defined as the continuous evaluation of the health of a plant and its equipment throughout its service life. It is important to be able to detect faults while they are still developing. This is called incipient failure detection (Li *et al.*, 2012; Elamin, 2013). Meanwhile, failure is the termination of the ability to perform the required function, and fault is defined as a situation that exists after a failure (Elamin *et al.*, 2010). Incipient detection of diesel engine failures provides a safe operating environment and thus, it is becoming increasingly important to use comprehensive CM schemes for continuous assessment of the combustion and mechanical conditions of reciprocating machineries (Gu *et al.*, 2006).

Vibration is one of the most common parameters that is used for monitoring the health condition of equipment and certain type of machineries based on movement of associated components and supporting bases as per operational requirements. CM of bearing faults is typically implemented using experimental data based vibration analysis (Mehdi *et al.*, 2011; Desavale *et al.*, 2013). Gani & Salami (2004) demonstrated the various types of common rotating machinery faults that can be detected using vibration analysis.

In this paper, vibration measurement is utilised to detect the locations on rotor bearing systems that record the highest levels of vibration. Based on the measurement procedure developed in this experimental work, CM for rotor bearing systems can be developed in the future.

## 2. METHODOLOGY

### 2.1 Experimental Setup

This experimental study was conducted at the Vibration Lab, Maritime Technology Division (BTM), which is one of the divisions in the Science & Technology Research Institute for Defence (STRIDE). The study is conducted on a rotor bearing, which is a simple apparatus for simulation that can be utilised for the study vibration behaviour on rotating elements such as bearings. Figure 1 and Table 1 show the description of the rotor bearing, which consists of 1/7 HP alternating current (A.C.) induction motor, coupling and rotor shaft of 335 mm, which is supported by two identical ball bearings (pillow blocks). The gap between these bearings is 165 mm. The diameter of the rotor shaft is 10 mm. The rotor shaft is driven by the motor, with its controlled using a variable frequency drive (VFD), which is mainly used to increase or decrease the speeds of A.C. motor for up to 11,500 rpm.

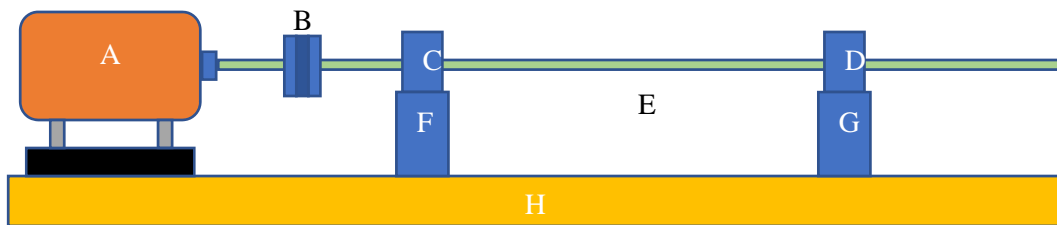


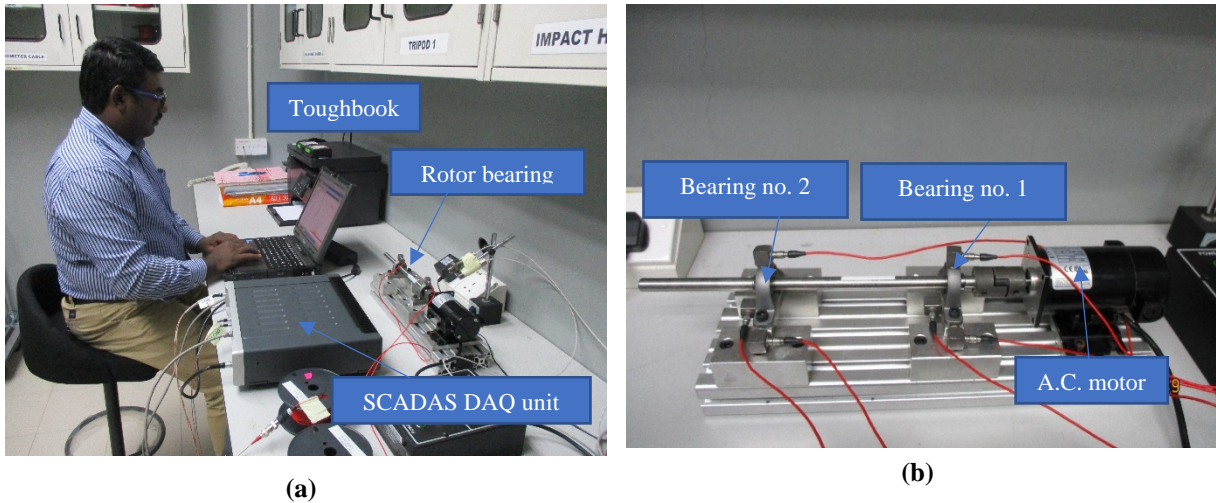
Figure 1: Line diagram of the rotor bearing. The descriptions for Locations A-H are given in Table 1.

Table 1: Description for each location on the rotor bearing shown in Figure 1.

Location	Description
A	A.C. Induction motor
B	Coupling
C	Pillow block no. 1
D	Pillow block no. 2
E	Rotor shaft
F	Bearing support no. 1
G	Bearing support no. 2
H	Main support board

Figure 2 shows the acquisition platform, which consists of a Toughbook (data recorder and analyser), data acquisition unit (SCADAS DAQ), RPM probe, accelerometers and the rotor bearing. A total of six accelerometers (vibration sensors) are used in this study. These accelerometers are commercially available integrated circuit piezoelectric (ICP) type, with sensitivity values ranging between 95.5 and 102.5 mV/g, which were recorded during calibration. These accelerometers are mounted on both bearings' housings using glue, as shown in Figure 3. This technique is used for temporary installation because the rotor bearing surface is not adequately prepared for stud mounting. Three sensors are mounted on each bearing in three directions (axial, vertical and transverse) and are connected to a data acquisition unit using high quality measurement cables integrated with the LMS Test. Lab software platform.



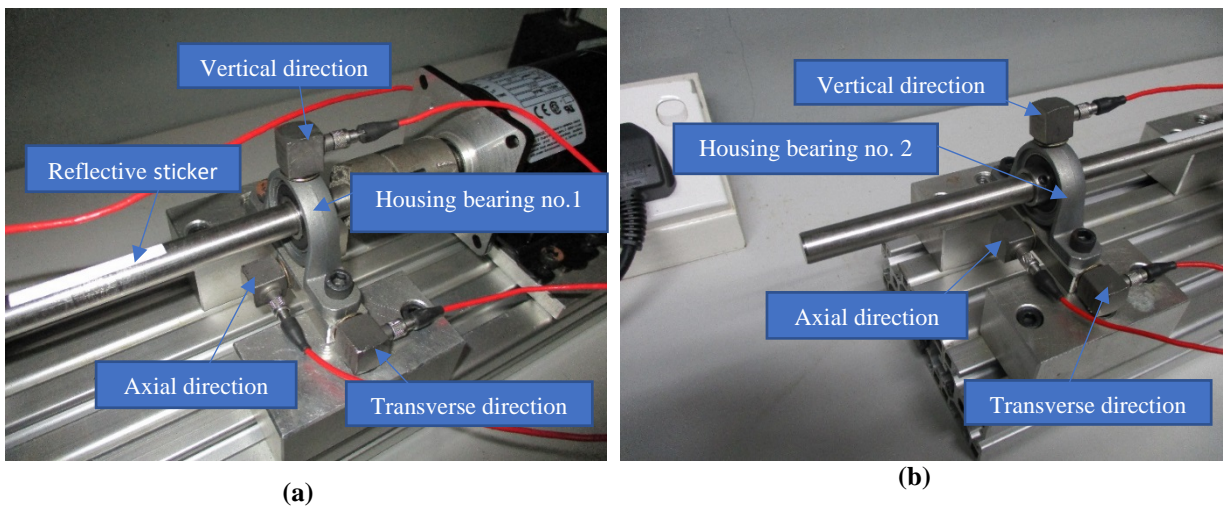


**Figure 2: Acquisition platform: (a) Measurement in progress (b) Rotor bearing.**

## 2.2 Measurement Procedure

Figure 3 shows the locations of the accelerometers and their directions on the rotor bearing. The measurements were performed at three shaft speeds; 3,000, 4,000 and 5,000 rpm. The duration for each measurement is 2 min. Table 2 shows the running rpm and frequency that was obtained by dividing the rpm value by 60 min, as shown in the following equation:

$$\text{Fundamental frequency, } f = \frac{\text{Shaft rpm}}{60} \quad (1)$$



**Figure 3: Accelerometer locations and directions: (a) Bearing no. 1 (b) Bearing no. 2.**

**Table 2: Calculated fundamental frequencies using Equation 1.**

Shaft speed (rpm)	Calculated fundamental frequency (Hz)
3,000	50.0
4,000	66.7
5,000	83.3

### 3. RESULTS & DISCUSSION

Figures 4-6 show the vibration spectrums on the housing surfaces of bearings no. 1 and no. 2 at the axial, transverse and vertical directions respectively, which are captured at the different shaft revolutions of the rotor bearing. Each figure consists of six vibration spectrums, which represent six different locations on the rotor bearing, particularly on both bearings' surfaces. The highest peak on the spectrum is known as the fundamental frequency or dominant frequency, which represents the running rpm of the rotor-shaft. Since all six peaks represent six different locations and directions on the rotor bearing overlapped, it is impossible to distinguish the vibration level among these peaks. Hence, the highest peak in the spectrum is identified as closest as possible to the fundamental frequency and is enlarged so that all the peaks and their vibration levels could be distinguished easily in accordance with the different colours that have been assigned to each spectrum. Based on comparison between these spectrums, it is found that the highest vibration is identified on bearing no. 2 in the transverse direction at 3,000, 4,000 and 5,000 rpm. Meanwhile, the lowest vibration is identified on bearing no. 1 in the vertical direction at 3,000 rpm. At 4,000 and 5,000 rpm, the lowest vibrations are found at two different locations, which are on bearing no. 2 in the vertical and axial directions.

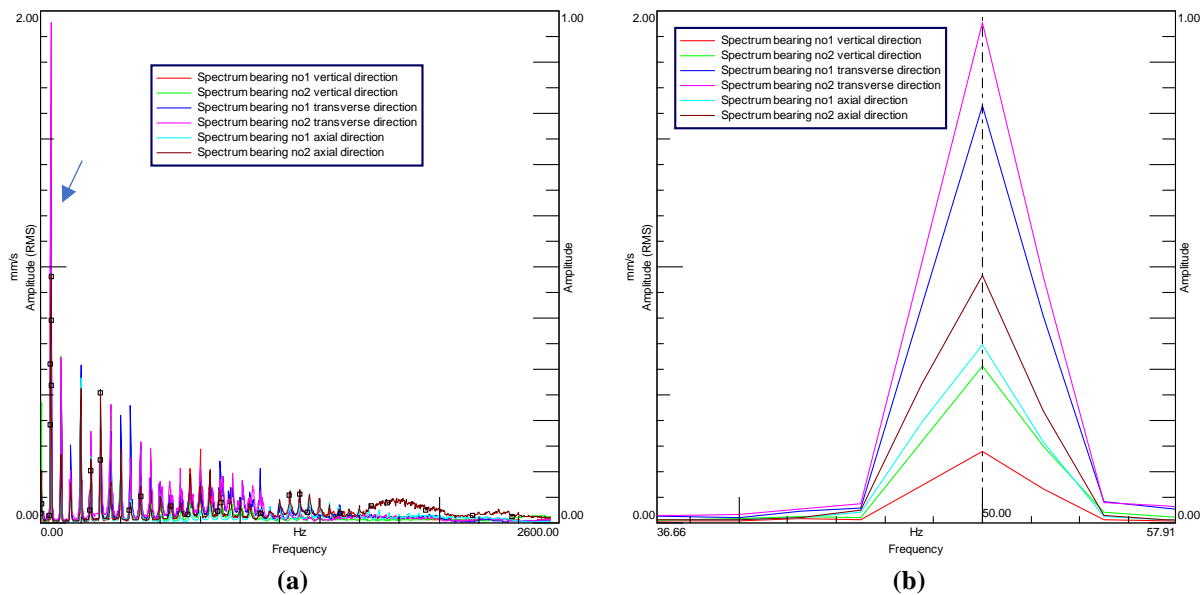


Figure 4: Vibration spectrums at 3,000 rpm: (a) Overall (b) Enlarged.

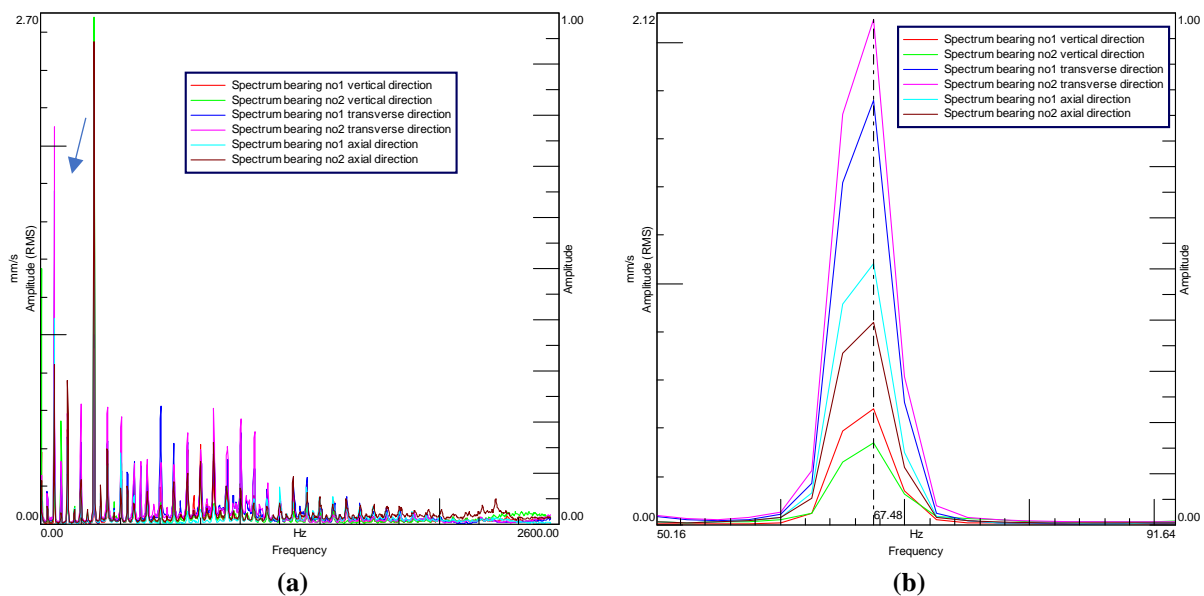
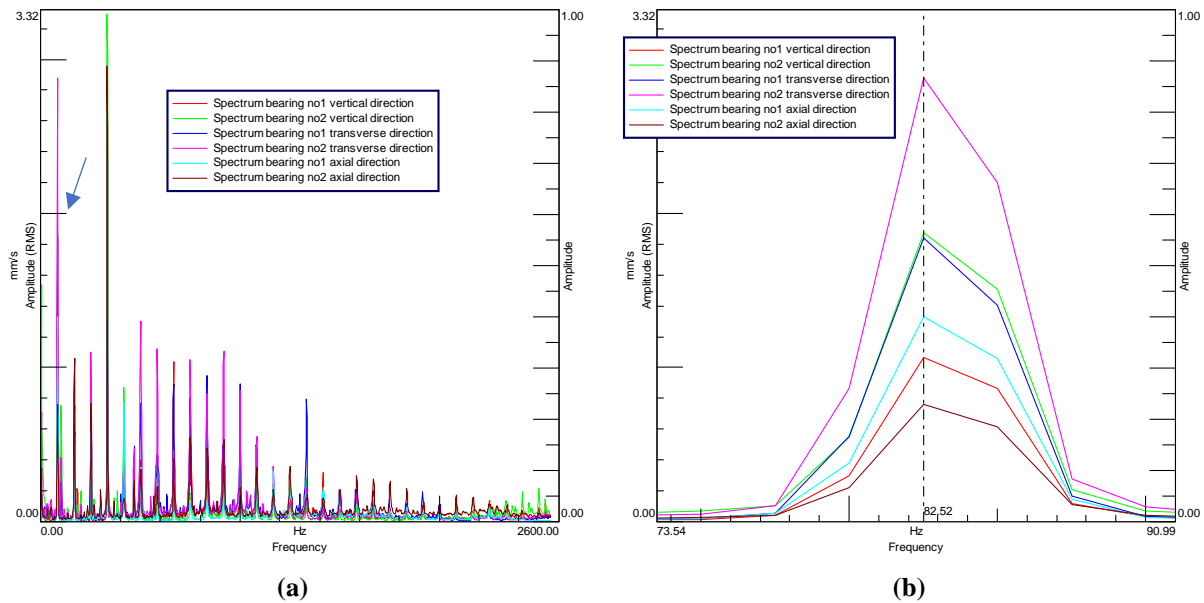


Figure 5: Vibration spectrums at 4,000 rpm: (a) Overall (b) Enlarged.



**Figure 6: Vibration spectrums at 4,000 rpm: (a) Overall (b) Enlarged.**

By referring to Figure 1, it shows that the location of the bearing no. 2 is closer to the end of rotor shaft, while the bearing no. 1 is closer to A.C. induction and coupling. Both of these bearings are supported by pillow blocks, which are tightened to the main support board using alley keys. Even though the differences among these locations are very close, it was found that the transverse direction on bearing no. 2 exhibited the highest vibration. This could be contributed by one or any combination of the most common symptoms, such as shaft misalignment, bearing imbalance or wobbling, and looseness of pillow support. Another factor that could lead to this finding could be the distance between bearing no. 1 and no. 2 from the induction motor. There is a possibility that wobbling exists due to the extra length of rotor shaft on bearing no. 2, which is hanging without any support.

Table 3 shows the accuracy values between the computed fundamental frequencies using Equation 1 and the fundamental frequency found on the enlarged vibration spectrums, as shown in Figures 4(b), 5(b) and 6(b). The slightest differences between calculated and actual values show that this experimental work performed at the highest level of accuracy. Pre-measurement tasks such as accelerometer selection based on sensitivity value, location and direction selection, calibration of accelerometers, conductivity check on measurement cables, and proper layout of the experimental apparatus can increase the accuracy level. These results could be considered as satisfactory and ultimately this measurement procedure could be applied in real applications for CM purposes.

**Table 3: Accuracy between calculated and actual fundamental frequency.**

Shaft speed (rpm)	Fundamental frequency (Hz)		Accuracy (%)
	Calculated	Actual	
3,000	50.0	50.0	100.0
4,000	66.7	67.5	99.2
5,000	83.3	82.5	99.2

Practically, the vibration spectrums recorded in this work could be used as a reference spectrum to compare vibration trending of the bearings in the future. Subsequently, this can be used to develop and enhance a CM programme to tackle any early failure symptoms before catastrophic failure occurs. In addition, vibration analysis on bearings could be applied to perform diagnosis of any failure symptoms and predict the lifespan of the bearings.

#### 4. CONCLUSION

In this paper, a vibration study on a rotor bearing at various levels of shaft revolution was performed using a multi-channel vibration data acquisition and analysis platform. The vibration level on each different location on bearings no. 1 and no. 2 on the rotor bearing were identified with high level of accuracy. The methodology developed in this study can be utilised to monitor the performance of real and in-site machineries, such as motors, pumps, compressors, gear boxes, diesel engines and bearings, periodically. In addition, this study can be improved by performing vibration study at higher levels of shaft revolutions, and different types or sets of bearings.

#### REFERENCES

- Desavale, R.G. & Mali, A.R. (2016). Detection of damage of rotor-bearing systems using experimental data analysis. *Procedia Eng.*, **144**: 195 – 201.
- Desavale, R.G., Venkatachalam, R. & Chavan, S.P. (2013). Antifriction bearings damage analysis using experimental data based models. *ASME J. Tribology*, **135**: 041105.
- Elamin, F. (2013). *Fault Detection and Diagnosis in Heavy Duty Diesel Engines Using Acoustic Emission*. PhD thesis, The University of Huddersfield, Huddersfield, UK.
- Elamin, F., Gu, F. & Ball, A. (2010). Diesel engine injector faults detection using acoustic emissions technique. *Modern Appl. Sci.*, **4**: 3-13.
- Gani, A. & Salami, M.J.E. (2004). Vibration Faults Simulation System (VFSS): A lab equipment to aid teaching of mechatronics courses. *Int. J. Eng. Ed.*, **20**: 61-66.
- Gu, F., Yesilyurt, I., Li, Y., Harris, G. & Ball, A. (2006). An investigation of the effects of measurement noise in the use of instantaneous angular speed for machine diagnosis. *Mech. Syst. Signal Proc.*, **20**: 1444-1460.
- Khardersab, A. & Shivakumar, S. (2018). Experimental investigation of the excitation forcing function in rotating machinery. *Procedia Manuf.*, **20**: 247-252.
- Li, Z., Yan, X., Guo, Z., Zhang, Y., Yuan, C. & Peng, Z. (2012). Condition monitoring and fault diagnosis for marine diesel engines using information fusion techniques. *Electron. Electr. Eng.*, **123**: 109-112.
- Mehdi, A., Rohani, B., & David, A. (2011). A new model for estimating vibration generated in the defective rolling element bearings. *J. Vib. Acoustics*, **133**: 1 – 8.
- Nistane, V.M. & Harsha, S.P. (2016). Failure evaluation of ball bearing for prognostics. *Procedia Techn.*, **23**: 179 – 186.

# MAGNETIC ASSESSMENT OF NEWLY INSTALLED ON BOARD DEGAUSSING SYSTEM

Abdul Rauf Abdul Manap<sup>1\*</sup>, Mohd Hambali Anuar<sup>1</sup>, Mahdi Che Isa<sup>1</sup>, Mohd Hazri Rahmat<sup>2</sup>, Roslan Slamatt<sup>1</sup>, Mohd Yusri Othman<sup>1</sup>, Hasril Nain<sup>2</sup>, Zuraini Abdul Manaf<sup>1</sup> & Muhammad Syauqat Abd Khalid<sup>2</sup>

<sup>1</sup>Magnetic Research & Treatment Centre

<sup>2</sup>Maritime Technology Division

Science & Technology Research Institute for Defence (STRIDE), Ministry of Defence, Malaysia

\*Email: abdulrauf@mod.gov.my

## ABSTRACT

*Ship degaussing (DG) is the process of reducing or canceling magnetic fields from a ship by applying an opposing field to it. The most practical and controllable ship DG process is to generate a magnetic field by passing a current through sets of loop coils around the ship. The challenge is to design and install a DG system on board the ship in order to compensate for the ship's magnetic signature to a specified target within a safe limit. In this paper, a brief concept of a ship's DG system and magnetic disturbance of ferromagnetic materials are briefly discussed. We will then qualitatively measure the magnetic field disturbance caused by a ship in Malaysian waters by carrying out ranging works, DG process and finally evaluate the performance of newly installed DG system. This study shows that the ranging process has been carried out successfully and the performance of the new DG system is evaluated based on the capability of the DG system to reduce the magnitude of ship's magnetic fields in the tropical region of Malaysian waters.*

**Keywords:** *Degaussing (DG); compensate; magnetic signature; silencing; magnetisation.*

## 1. INTRODUCTION

Outside the mariner's community, it is a little-known fact that ships become magnetised. Through a magneto-mechanical interaction, the hull of a ship slowly acquires its own particular magnetic signature from the mechanical stress of being used plus being constantly in the Earth's magnetic field. The magnetic disturbance caused by a ship in the local Earth's magnetic field could be resolved into two main effects. The first, known as permanent magnetic field, is the ship's own magnetic field that is acquired over time, while the other one is called an induced magnetic field, which is the result of interaction between the ship's materials and the magnetic field at the location and orientation of the ship at that moment time (Bekers & Lepelaars, 2013). Most commercial and naval ships are constructed from steel material and their existence disturbs the Earth's magnetic field, making them susceptible to magnetic influenced sea mines. To avoid detection by sea mines and magnetic anomaly detectors (MADs), naval and sometimes civilian ships need to be camouflaged from magnetic detectors (Holmes, 2008; Poteete, 2010). For ferromagnetic ships, the resultant magnetic field will be dependent on the handling of the magnetic materials used in its construction, and the location or locations of its construction. This signature will then change gradually over time depending on the ship's usage and transits made (MOD, 2004).

Reducing the magnetic signatures of a ship will minimise the effectiveness of sea mines in shallow water (Holmes, 2006). The ship's magnetic signature reduction affects the signature amplitude, making it necessary to increase actuation sensitivity of shallow-water sea mines to meet the operational target within the effective radius of explosive charge. However, if sea mines have increased sensitivity to counter the reduction of the target ship's magnetic signature, then

minesweeping systems is more practical (Holmes, 2008; Vermeulen, 2018). One of the ways to reduce the magnetic signature of a ship is by installing a degaussing (DG) system on board.

Magnetic signature is a key element of operational capability of most of the naval surface ships and studies have shown that it can be predicted and validated in the laboratory (Varma, 2014). The primary goal of magnetic signature analysis and prediction is to reduce the likelihood of detection and thereby increase survivability of ships in the operational field (Zhang *et al.*, 2010; Chengbao & Daming, 2012). On board DG was pioneered as a means of countering sea mines, which were ever present danger in the confined water during World War II in Europe between the Allies, the Soviets and Germany (BHE, 2011). The UK is the first country to develop a DG system during that war owing to a result of a total 44 British ships being sunk in the English Channel by the magnetic bottom mine threats, in between September 1939 to January 1940 (Schoeffel, 1952).

Basically, DG equipment consists of a three-axis mast mounted magnetometer, a computer controller and a power amplifier cubicle for supplying all the DG loops. At the beginning of the design, the aim is only to compensate permanent and induced ship's magnetisation in three orthogonal components, which are *M* axis (vertical), *L* axis (longitudinal horizontal) and *A* axis (athwartship horizontal). Nowadays, there are two types of DG system installation in use, which are open loop DG (OLDG) and closed loop DG (CLDG) systems (Zahir *et al.*, 2005).

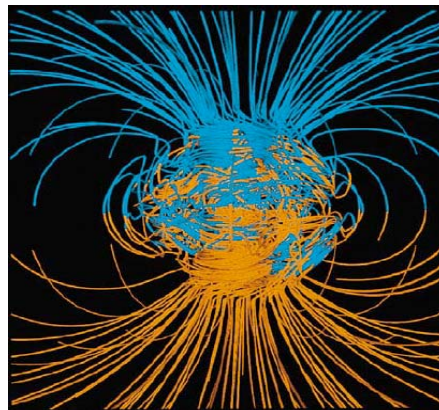
This system needs an adjustment process for the loops to minimise the ship's signature to a specified target. This process is named as the first of class calibration ranging. The process requires a ship to go through a measurement for obtaining the undegaussed signature and DG loop effect (NSTM, 1992). It is more efficient to set fine-tuning for a DG system by ranging (Holmes, 2008). Commonly the ranging is taken at specified shore-based DG calibration facilities known as magnetic ranging and deperming facilities. This facility consists of two major parts, which are ranging and treatment. Ranging is to measure with two sensor arrays consisting of five tri-axial magnetometers arranged along the two Earth magnetic axes North / South (N/S) and East / West (E/W). The treatment part is to deperm the ship's hull with a few set loops arranged on underwater structures (ECA, 2018). In the underwater electromagnetic scientific community, most researchers have standardised on using the right handed rectangular coordinate system (*x*, *y*, *z*) for sensor reference and orientation, where *x* is the ship's longitudinal axis with positive towards the bow, *y* is the ship's athwartship axis with positive in the starboard direction and *z* is the vertical axis with positive downwards (Lucas & Richards, 2015). The process of treatment is important for ships at different scales. In deperming, the ship is tightly wrapped in the horizontal direction by copper wire and alternative reducing magnetic field is applied to that coil (Griffiths, 2014). The applied field changes the domain orientation until all domains of the object are randomly oriented and their average magnetisation approaches zero (Sonal *et al.*, 2018).

The aims of this paper are to highlight in brief the magnetic disturbance caused by ferromagnetic ship, introducing an on board DG system structure, carry out magnetic ranging and finally to check the performance of a newly installed DG system, especially in the tropical region of Malaysian waters.

## **2. MAGNETIC DISTURBANCE ON FERROMAGNETIC SHIPS**

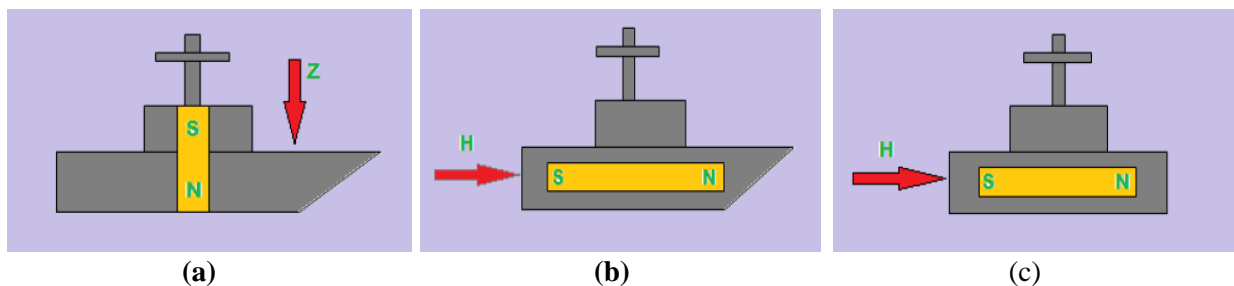
A ferromagnetic source can be divided into two components, known as permanent and induced magnetisation. Permanent magnetism is produced during construction. It will change over time due to natural decay caused by changing exciting force, refits, violent shocks to ship's structure due to bombing, collision, or other cases. Induced magnetism is from the ferrous content of the ship (permeability), the Earth's magnetic field, and the shape and orientation of the ship in magnetic field. A material is classified as ferromagnetic if its magnetic permeability is very high, which causes the material to act as a magnet in the presence of the Earth's magnetic field. The material becomes a stronger magnet when it has higher permeability and / or is in a stronger Earth's magnetic field. Induced magnetism is also altered if the ship has changed its shape and orientation (Hasril *et al.*, 2013).

The Earth's magnetic field can be equated to a huge bar magnet, the North Pole of the bar magnet is known as the South Geomagnetic Pole and the South Pole as the North Geomagnetic Pole, as shown in Figure 1 where inward and outward directed field lines are in blue and yellow respectively, and extend to about two Earth radii from the core (Source: PSC, 1996). The positions of the North and South Geomagnetic Poles in 2015 are  $80.37^\circ$  N  $72.63^\circ$  W and  $80.37^\circ$  S  $107.37^\circ$  E respectively (Thébault, 2015). The magnetic field lines run from the South Geomagnetic Pole to the North Geomagnetic Pole and in specified equatorial waters are inclined at an angle of about  $0.035^\circ$  upward from the horizontal. The strength of the total magnetic field in equatorial waters is about 40,490 nT (nanoTesla) with a yearly variation of about 10.8 nT (NOAA, 2014). A ship's magnetic field is produced mainly by the ferromagnetic materials used in the construction of the ship hull, internal structure, machinery and auxiliary items, which are magnetised in the Earth's magnetic field, producing a local magnetic disturbance, regardless of the ship's movement (Razicichanu, 2004). Therefore, it is important to understand the effect of the Earth's magnetic field's presence in equatorial waters in order to lessen its detectability by sea mines.



**Figure 1: Three dimensional computer simulation of the Earth's magnetic field (Source: Glatzmaier & Roberts, 1995).**

For the purpose of DG, it is convenient to represent the magnetic field of a ship by imaging three magnets placed perpendicular to each other, as shown in Figure 2. The magnetic fields of these three magnets are respectively termed as the vertical magnetic (VM) field, longitudinal magnetic (LM) field and athwartship magnetic (AM) field. Traditionally, VM, LM and AM consist of permanent and induced magnetic fields for each ship.



**Figure 2: Magnetic fields of a ship: (a) Vertical magnetic (VM) field (b) Longitudinal magnetic (LM) field (c) Athwartship magnetic (AM) field (Source: Sardono *et al.*, 2017).**

Thus, a ship conventionally has six components of magnetism, which are permanent vertical magnetism (PVM), induced vertical magnetism (IVM), permanent longitudinal magnetism (PLM), induced longitudinal magnetism (ILM), permanent athwartship magnetism (PAM) and induced athwartship magnetism (IAM), as depicted in Figure 3.

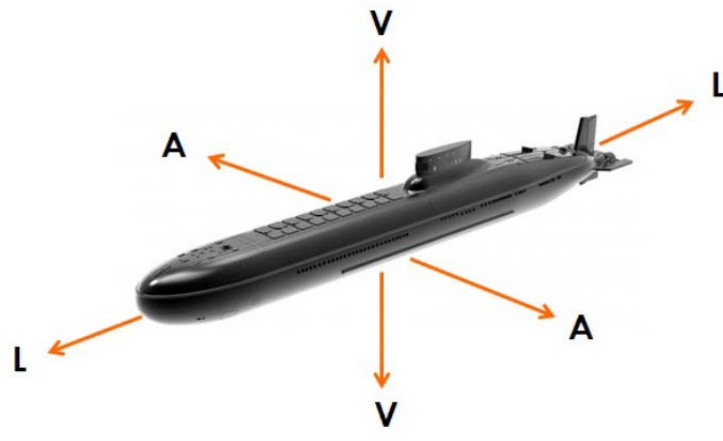


Figure 3: Coordinate system of a ship's magnetisation (Source: Sardono *et al.*, 2017).

As mention before, magnetic disturbance can be resolved into two components; induced and permanent. Each component can be further resolved into the three axes; *M* axis (vertical), *L* axis (longitudinal horizontal) and *A* axis (athwartship horizontal). Commonly the axes of induced magnetisation are proportional to the Earth's magnetic field. At the specific area in the equatorial region, generally the Earth's magnetic fields are pointing to the North (41,444.7 nT), West (79.9 nT) and upwards (4,501.9 nT) (NOAA, 2018).

### 3. DG SYSTEM

A DG system installed on board of a ship is mainly aimed to counteract or compensate the ship's magnetic field as much as possible. Theoretically, the condition with very low magnetic signature can be achieved in which a magnetic influence device such as sea mines could not detect the presence of the ship. However, in real situations, ship's magnetic field cannot be completely eliminated as the DG process only decreases the vulnerability of a ship from magnetic weapons. Basically, an on board DG system consists of the equipment shown in Figure 4.

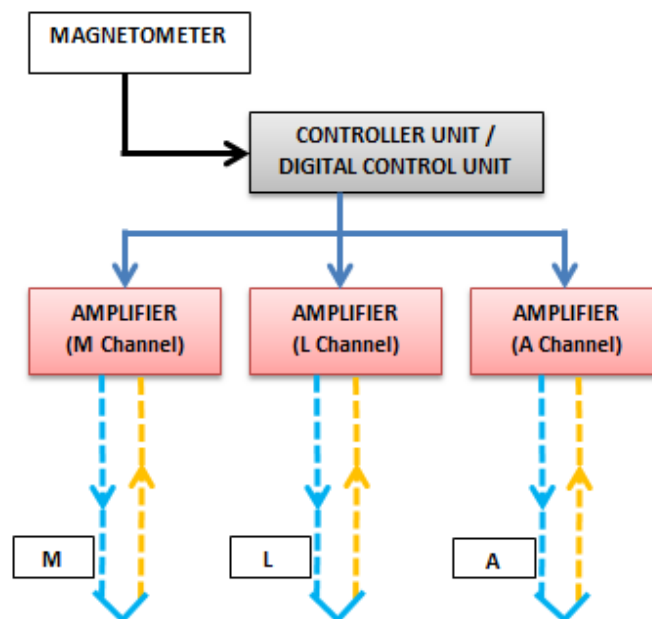


Figure 4: On board DG system structure.



### 3.1 Magnetometer

The magnetometer head is mounted on an alignment fixture at mast, which ensures that the axes are aligned with the ship's axes. The system normally runs automatically by continually sensing the magnitude and polarity of the Earth's magnetic field along the ship's three axes and sends this information to the controller unit. After the first installation, the magnetometer must be put through the zeroing process, where the magnetometer must be compensated for the effect of the ship's DG coil fields, induced and permanent magnetisation.

### 3.2 Controller Unit

The controller unit usually comes with embedded software to run mathematical computations to calculate the required induced current demands to minimise the ship's magnetic signature if the ship changes its heading.

### 3.3 Power Amplifiers

The power amplifiers function to drive a three axis ( $M$ ,  $L$  and  $A$ ) coiling system by supplying current to these DG coils. Each current has two components, induced and permanent. In the normal mode, the induced current component in a particular axis is proportional to the Earth's field along that axis as measured by the magnetometer while the permanent current component in any axis is a fixed bias whose magnitude is chosen during magnetic ranging.

### 3.4 DG Coils

DG cable loop coils are evenly distributed along the ships in three axes as shown in Figure 5 and supplied by current to produce magnetic fields that are, as nearly as possible, opposite to the magnetic fields produced by the ship's magnetisation (NSTM, 1992).

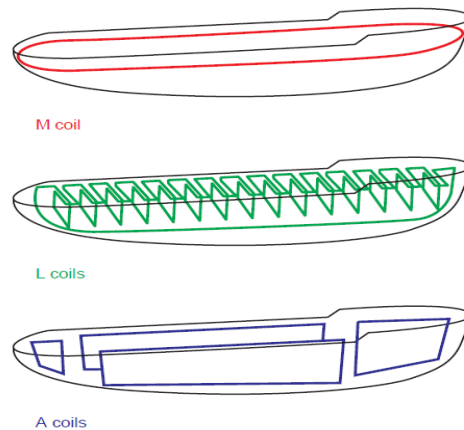


Figure 5: A schematic of the basic ship on board DG coils (Source: Zahir *et al.*, 2005).

### 3.5 DG System Installation

Generally, there are two types of existing DG systems, namely OLDG and CLDG. Both systems are used by commercial and naval ship. The conventional one is the OLDG system. This system assumes the ship's permanent magnetisation is constant even though the magnitude of ship's permanent magnetisation will change over time since the ship's ferromagnetic hull and auxiliary equipment experience a lot of mechanical stress as it sails within the Earth's magnetic field (Holmes, 2008). This means, from time to time, the permanent current settings have to be recalculated to account for drifts in the permanent magnetisation. The OLDG system of ships should go through periodic ranging to ensure that the system is effective within the period of time (Zahir *et al.*, 2005).

For the past 15 years, CLDG has emerged as a new solution for magnetic signature management, as it is a standalone system can dynamically sense the changes in the local magnetic field environment and directly respond to implement real time compensatory measures (Henocq *et al*, 2003). When operating, the CLDG system is capable to continually monitor changes in ship's permanent magnetisation while sailing and automatically adjust the permanent current settings to maintain the magnetic signature at specified target. The flow of the CLDG process is as shown in Figure 6.

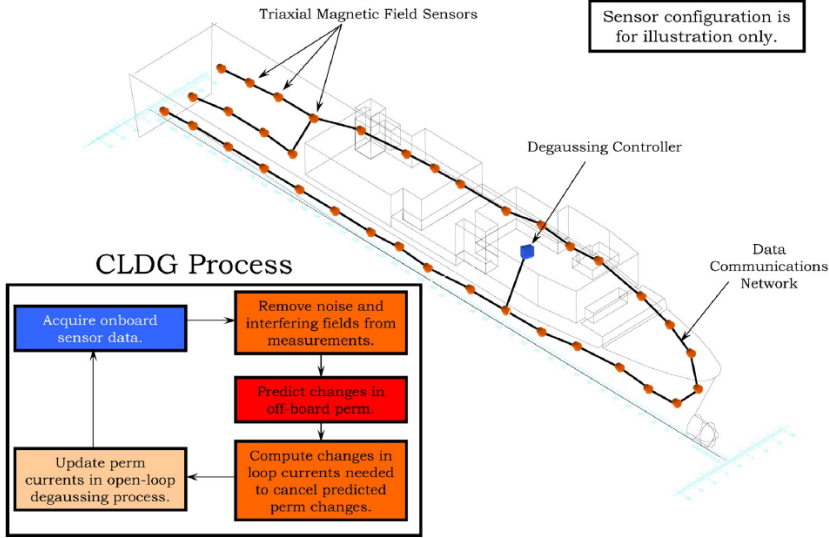


Figure 6: CLDG concept (Sources: Holmes, 2008).

4. MAGNETIC RANGING PROCEDURE

The purpose of magnetic ranging is to adjust and control certain parameters in order to achieve the targeted magnetic signature. The parameters to be considered are induced currents, permanent currents and number of DG loop turns. The ship will be navigated on inter-cardinal headings with DG system in off and on conditions (North-west, NW & South-east, SE) to measure the ship's undegaussed and degaussed signatures respectively. The inter-cardinal heading concept is shown in Figure 7.

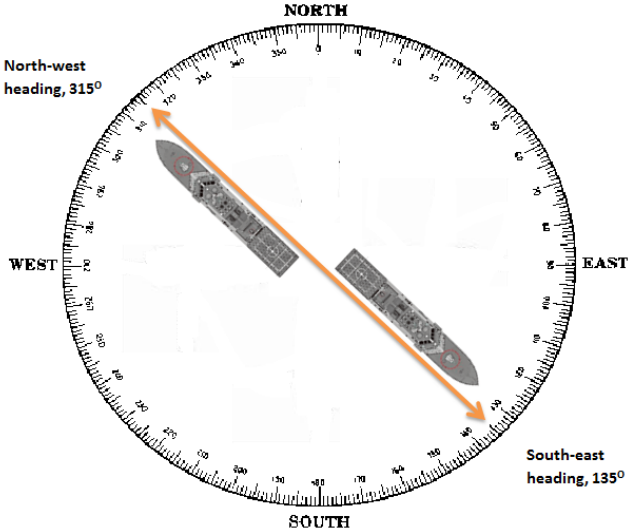
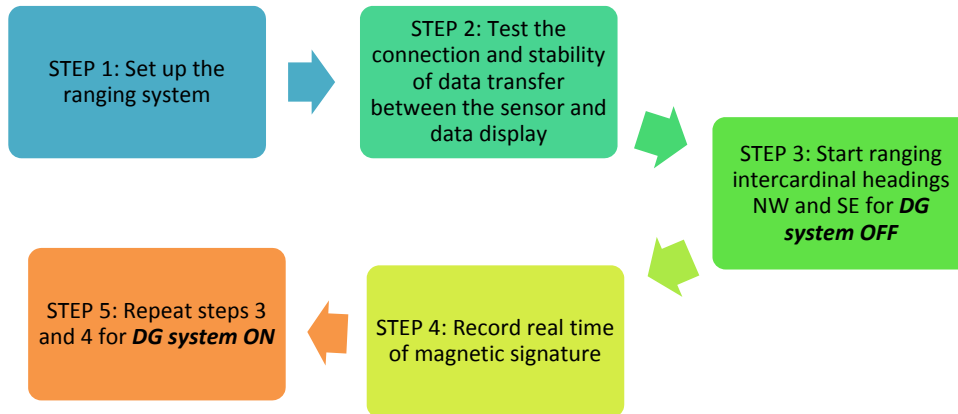


Figure 7: Inter-cardinal heading concept during magnetic ranging procedure.

The required loop turns are set by estimating the required number of loop turns, and induced and permanent DG currents. If the DG loop turns have been adjusted during ranging, the DG coils compensation shall be updated. The ship's degaussed signature is measured again. Upon completion of the ranging process, the induced and permanent current settings, and loop turns in each loop are recorded.



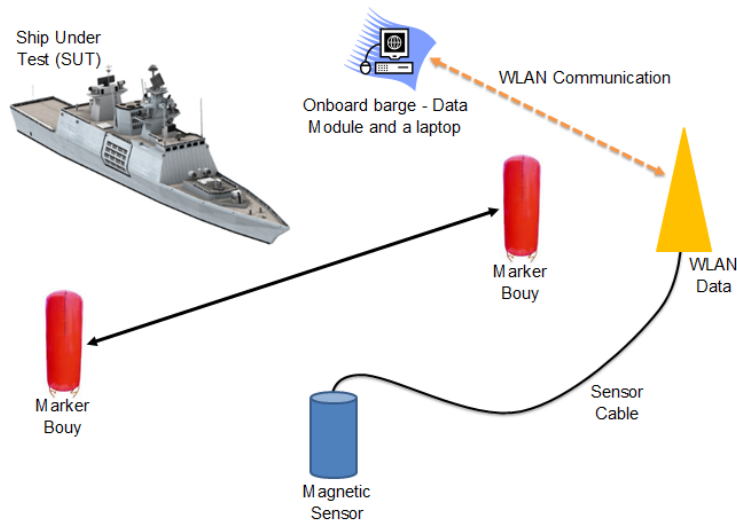
**Figure 8: Ranging process flow.**

Before the ranging process is started, a magnetic sensor is deployed in an identified area near Teluk Belanga, Pangkor (4.28° N, 100.56° E) as shown in Figure 10 at 15 m depth below sea level.



**Figure 9: Location of the magnetic ranging (4.28° N, 100.56° E).**

The underwater cable of the sensor will be connected to the control equipment that is located on the barge. Two buoys will be deployed within the ranging areas as a marker, where the distance between the buoys is estimated to be about 40 to 60 m. The ship will pass over the magnetic sensor within the buoys and then the magnetic signature of ship will be recorded. The ship under test (SUT) will be moving from NW to SE and SE to NW headings with a constant speed of 6 knots in order to get the primary magnetic signature. The DG system on board should be in OFF condition to obtain the primary ship magnetic signature, which will be analysed by the ranging control equipment. The analysis process will estimate the DG coil turn and current ampere that need to be adjusted on the on board DG system for magnetic compensation. Finally, the ranging process is performed with the DG system in ON condition with adjusted coil turn and ampere current. The ship's headings and movement is similar as the DG OFF condition. The schematic diagram of ranging procedure (ON and OFF) is shown in Figure 10.



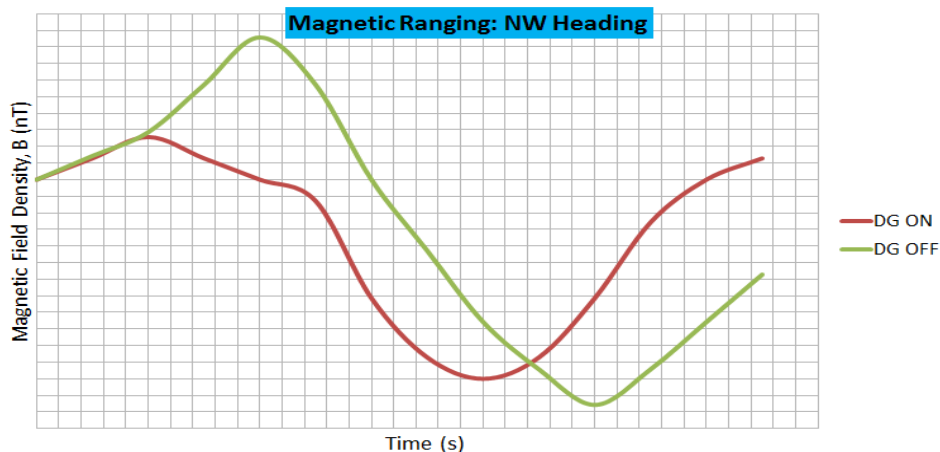
**Figure 10: Setup of the ranging system by deploying underwater magnetic sensor at the 15 m depth, and connecting the sensor cable with sensor and wireless data communication.**

## 5. RESULTS AND DISCUSSION

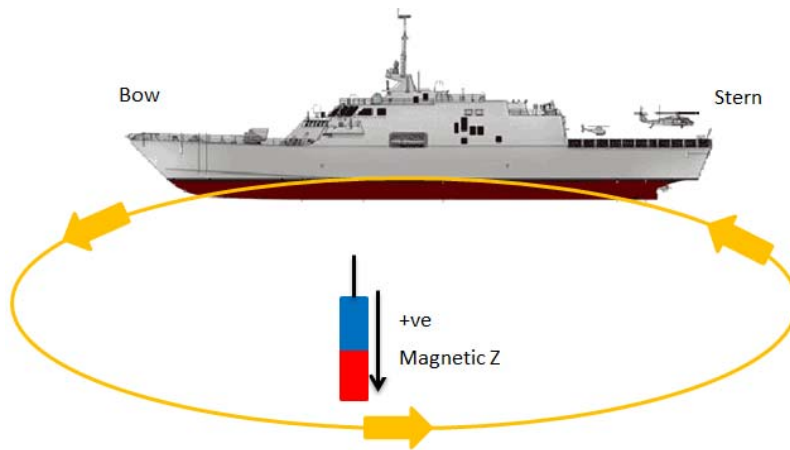
In this study, four datasets have been recorded during the ranging procedure, which are two datasets on undegaussed signature (OFF) and two data on degaussed signature (ON) for both NW and SE headings. Analysis of the magnetic signature will bases on vertical ( $z$ ) magnetic sensor, where its orientation is positive downward (Figure 5). The magnetic signature can be divided into two components. The first is permanent magnetisation, which is a function of the ship’s size, material, location and orientation during construction. It can be minimised at the time of deperming. The second one is induced magnetisation, which is dependent on the current geographical position and orientation of the ship in the Earth’s magnetic field.

### 5.1 NW Heading, $315^\circ$

Figure 11 shows the magnetic signature of the ship before (OFF) and after (ON) the DG system was operated during the ranging for the NW heading. Further analysis shows that the ship’s signature characteristic can be classified as LM. Since the sensor orientation is positive downward, the sensor indicates that the LM produced by the ship is positive towards the bow and negative towards the stern. Figure 12 shows the illustration of the formation of LM.



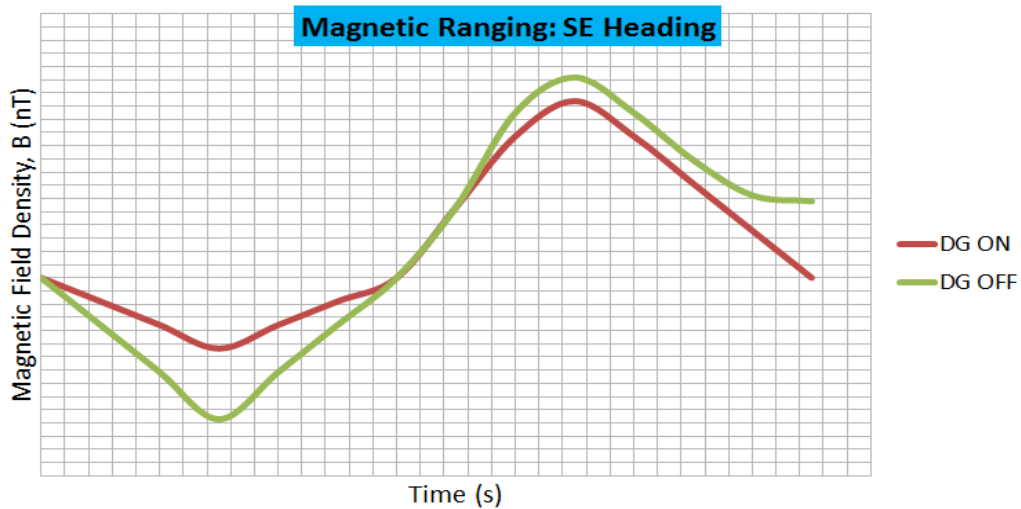
**Figure 11: Recorded ship’s magnetic signature for the NW heading ( $315^\circ$ ).**



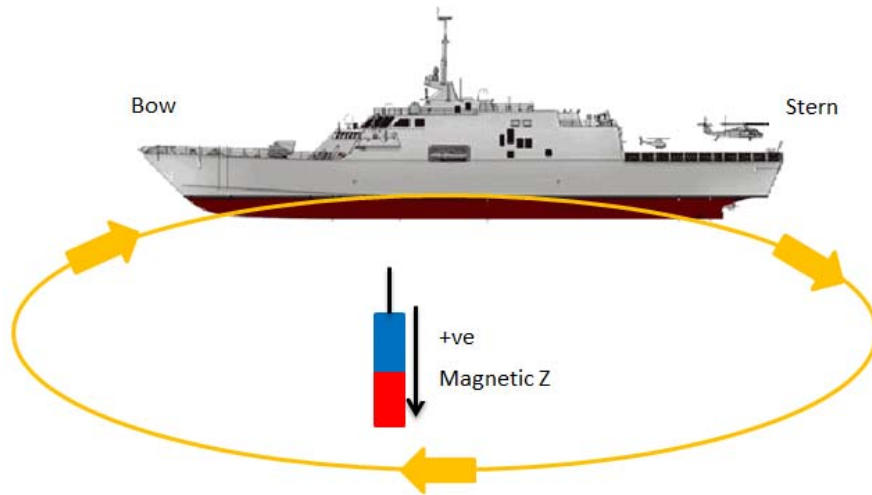
**Figure 12: Illustration of LM field signature produced by the ship for the NW heading referring to magnetic sensor Z.**

## 5.2 SE Heading, 135°

Figure 13 shows the magnetic signature of the ship before (OFF) and after (ON) the DG system was operated during the ranging for the SE heading. The ship's signature characteristic can also be classified as LM. The sensor indicates that the LM produced by ship is negative towards the bow and positive towards the stern. Figure 14 shows an illustration of the formation of LM.



**Figure 13: Recorded ship's magnetic signature for the SE heading (135°).**



**Figure 14: Illustration of LM field signature produced by ship for the SE heading referring to magnetic sensor  $z$ .**

### 5.3 Discussion

The magnitude of the magnetic field in both headings recorded a decreasing value when the DG system is operated. This indicates the DG system is working properly by producing a magnetic field to compensate the magnetic field from the ship. Further signature analysis showed that when ship is moving in the NW heading NW, sensor  $z$  indicates that the LM produced by ship is positive towards the bow and negative towards the stern, while for the SE heading, sensor  $z$  indicates the LM produced by ship is positive towards the stern and negative towards the bow. This means that the magnetic field of ship is influenced by external field, which is the Earth's magnetic field. In the equatorial region, the biggest strength of the Earth's magnetic field component is pointing towards the north.

The ship's induced magnetisation represents the reaction of the ferromagnetic material to the ambient field, and is usually decomposed into components defined in a Cartesian coordinate system related to the ship:  $x$ -axis corresponding to the longitudinal ( $L$ ) direction,  $y$ -axis to the athwartship ( $A$ ) direction, and  $z$ -axis to the vertical ( $V$ ) direction perpendicular to both  $x$  and  $y$ . When the ship changes course from NW to SE, the  $z$ -component of the ship's magnetic field signature changes sign from positive to negative. By analysing the magnetic signatures of the ship in the NW and SE intercardinal courses, and then taking the difference between the NW and SE course pairs, it was found that the magnetic signature produced by the ship is ILM. At the same time, it can be concluded the qualitative value of the ship's induced magnetisation is more dominant than the ship's permanent magnetisation (Chengbao & Daming, 2012).

Modern DG systems are normally very sophisticated but they still rely on the assumption that the permanent magnetisation of a ship is well known for example, zero. Therefore, in conjunction with magnetic treatment, military ships are continuously degaussed when operated in mine risk areas. On board DG system and coils on board are supplied with a current to generate their own magnetic fields designed to oppose the ship's field at current location. In a modern surface ship, the currents must be changed automatically with geographical location and with the heading of the ship. Alternatively, active DG coils are built inside the ships during construction to provide the changes of magnetic field correction. The coils are constantly fed with electric current provided from unique computer-controlled generators to create an opposing magnetic field. That field is constantly matched with the ship's changing magnetic field during its sailing across the sea (Zahir *et al.*, 2005; Holmes, 2008; MOD, 2008).

## 6. CONCLUSION

The ferromagnetic fields of ships can be exploited by the magnetic influence sea mines and hence, DG systems shall be used to minimise or reduce the magnetic signature of ships. Based on the magnetic ranging procedure conducted in the equatorial region, the qualitative results from the magnetic measurement showed that the newly installed DG system is capable to reduce the magnetic signature of a designated ship. The magnetic signature from the ranging procedure also showed that the ship operated in equatorial waters produce a dominant induced LM rather than AM and VM. The magnetic ranging procedure setup in this study was found to be useful and suitable for the next scheduled routine process in order to monitor periodically the performance of the on board DG systems. This measured data is then used to determine the optimum setting for the DG system to compensate for the ship's magnetic signature. It is strongly recommended that any newly constructed ships are to be equipped with DG systems to ensure the changes of magnetic signature can be monitored, controlled and reduced to a safe level.

## ACKNOWLEDGMENT

The authors gratefully acknowledge the support from STRIDE's management, through the Vehicle Mobility and Equipment & System Cluster under the Tropical Testing Programme Initiative. We also thank our colleagues from the Magnetic Research & Treatment Centre who provided insight and expertise that greatly assisted the study and comments that greatly improved the manuscript.

## REFERENCES

- Bekers, D. & Lepelaars, E. (2013). Degaussing system design optimization. *8<sup>th</sup> Int. Marine Electromag. Conf. (MARELEC 2013)*, Hamburg, 16-19 July 2013, pp. 16-19.
- BHE (Bright Hub Engineering). (2011). *The Core Theatre of WWII - War in Europe between the Allies, the Soviets, and Germany* Available online at: [http://www.brighthubengineering.com/marine-history/124799-some-famous-eropean-ships-and-battles-of-wwii/#imgn\\_2](http://www.brighthubengineering.com/marine-history/124799-some-famous-eropean-ships-and-battles-of-wwii/#imgn_2) (Last access date: 7 September 2017).
- Birsan, M. (2008). *Prediction of the Ship's Permanent Magnetisation*. Technical Memorandum, Defence R&D Canada, Ottawa, Ontario, Canada.
- Chengbao, G. & Daming, L. (2012). Prediction of magnetic signatures of ship's induced vertical magnetisation. *IEEE 6<sup>th</sup> Int. Conf. Electromag. Field Problems Appl. (ICEF 2012)*, Dalian, 19-21 June 2012.
- ECA Group (ECA) (2018). *Overrun Deperming Station* Available online at: <https://www.ecagroup.com/en/solutions/overrun-deperming-station> (Access Date: 31 May 2018).
- Glatzmaier, G.A. & Roberts, P.H. (1995). *A Three-Dimensional Self-Consistent Computer Simulation of a Geomagnetic Field Reversal*. Institute of Geophysics and Planetary Physics and the LDRD program, Los Amos.
- Griffiths, D. J. (2014). *Introduction to Electrodynamics*. Harlow Pearson, UK.
- Hasril, N., Mahdi, C.I., Mohd Moesli, M., Nik Hassanuddin, N.Y., Mohd Subhi, D.Y. & Irwan, M.N. (2013). Management of naval ships' electromagnetic signatures: A review of sources and countermeasures. *Defence S&T Tech. Bull.*, **6**: 93-110.
- Henocq, H. Toniuzzi, J.L, Coulomb, C. Chadebec, O. & Bongiraud, J.P. (2003). Advanced studies in closed loop degaussing. *Electromag. Silencing Symp. (EMSS)*.
- Holmes, J.J. (2006). *Exploitation of a Ship's Magnetic Field Signatures*. Morgan & Claypool, US.
- Holmes, J.J. (2008). *Reduction of a Ship's Magnetic Field Signatures*. Morgan & Claypool, US.
- Lucas, C.E. & Richards, T.C. (2015). *A Novel Technique for Modeling Ship Magnetic Signature*. Defence Research and Development Canada.
- MOD (Ministry of Defence) (2004). *DEF STAN 81-130: The Transportation, Handling, Storage and Packaging of Magnetically Sensitive Equipment*. Ministry of Defence, UK.

- MOD (Ministry of Defence) (2008). *DEF STAN 02-612 Issue 2: Guide to the Design of Ferromagnetic Signature Control System and Degaussing*. Ministry of Defence, UK
- NOAA (National Oceanic and Atmospheric Administration) (2014). *International Geomagnetic Reference Field* Available online at: <https://www.ngdc.noaa.gov/IAGA/vmod/igrf.html> (Access Date: 7 September 2017).
- NOAA (National Oceanic and Atmospheric Administration) (2018). *Magnetic Field Estimated Values* Available online at: <https://www.ngdc.noaa.gov/geomag-web/?model=igrf#igrfwmm> (Access Date: 21 September 2018).
- NSTM (Naval Ship's Technical Manual) (1992). *Chapter 475 Magnetic Silencing*. Naval Sea System Command, US.
- Poteete, S. (2010). *Navy's N-Layer Magnetic Model with Application to Naval Magnetic Demining*. Master Thesis, Department of Oceanography, University of Washington, US.
- PSC (Projects in Scientific Computing) (1996). *When North Goes South* Available online at: <http://www.psc.edu/science/Glatzmaier/glatzmaier.html> (Access Date: 7 September 2017).
- Razicheanu, A., Ionita, V. & Gavrilla, H. (2004). *Methods of Reducing the Ship's Magnetic Signature*. National L Symposium of Theoretical Electrical Engineering (SNET), Romania.
- Sardono, S., Juniarko, P., Eddy Setyo, K. & Anggela, W.K. (2017). Study of calculation of degaussing system for reducing magnetic field from submersible vehicle. *Int. J. Mar. Inno Res.*, **1**:68-75.
- Schoeffel, M. F. (1952). *A Short History of Degaussing*. Bureau of Ordinance, NAVORD OD 8498, Washington D. C., US.
- Sonal, J., Sampada, A. & Ratan, S. (2018). Analysis of anhysteretic demagnetisation procedure of under-water vehicles. *J. Eng. Prac. Fut. Tech. (JEpFT)*, **1**: Sr. No. 2.
- Thébault, E. (2015). *International geomagnetic reference field: The 12th generation*. *Earth Planets Space*, **67**: 79.
- Varma, R.A.R. (2014). Design of degaussing system and demonstration of signature reduction on ship model through laboratory experiments. *Phys. Proc.* **54**: 174-179.
- Vermeulen, A. F. (2018). Coastal border control using magnetic field signatures. In Monsuur, H., Jansen, J.M. & Marchal, F.J. (Eds), *NL ARMS Netherlands Annual Review of Military Studies 2018*. T.M.C. Asser Press Publisher, The Hague, pp. 249-269.
- Zahir, A.D., Hutt, D.L. & Richards, T.C. (2005). *Maritime Electromagnetism and DRDC Signature Management Research*. Defence R&D Canada (DRDC), Atlantic, Canada.
- Zhang, W., Xu, J. & Cheng, J. (2010). Analysis of ship magnetic field surveying based on two Tri-axial Magnetic Sensors. *IEEE Int. Conf. Comput. Mechatron. Contr. Electron. Eng.* (ICCMCEE 2010), Changchun, 24-26 August 2010.



# EFFECT OF LOW FREQUENCY EXCITATION FOR CRACK DETECTION USING NONLINEAR VIBRO-ACOUSTIC MODULATION METHOD

Tino Hermanto<sup>1</sup>, Ruztamreen Jenal<sup>1,2\*</sup>, Abd. Rahman Dullah<sup>1,2</sup>, Azma Putra<sup>1,2</sup> & Nor Salim Muhammad<sup>1,2</sup>

<sup>1</sup>Faculty of Mechanical Engineering

<sup>2</sup>Centre for Advanced Research on Energy (CARE)  
Universiti Teknikal Malaysia Melaka (UTeM), Malaysia

\*Email: ruztamreen@utem.edu.my

## ABSTRACT

*This paper investigates the effect of three different low frequency excitations on a centre cracked aluminium plate using the nonlinear vibro-acoustic modulation (VAM) method. The plate was hung with cords to provide free boundary condition. A mechanical shaker and piezoelectric transducer were used to provide simultaneous interaction between low frequency excitation and high frequency inputs respectively. The modal analysis was validated by finite element model simulation. Fourteen excitation locations under the crack were tested. The surface deflection was measured using scanning laser Doppler vibrometer. Surface deflections and R-values were used to determine the most effective frequency mode and excitation location. The experimental results show that the first vibration mode frequency produces the most significant effect on defect detection. The most effective locations for excitations are at the centre near the crack line and at the edge of plate.*

**Keyword:** *Nonlinear vibro-acoustic modulation (VAM); laser Doppler vibrometer; fatigue crack; piezoelectric (PZT) transducers; wave modulation.*

## 1. INTRODUCTION

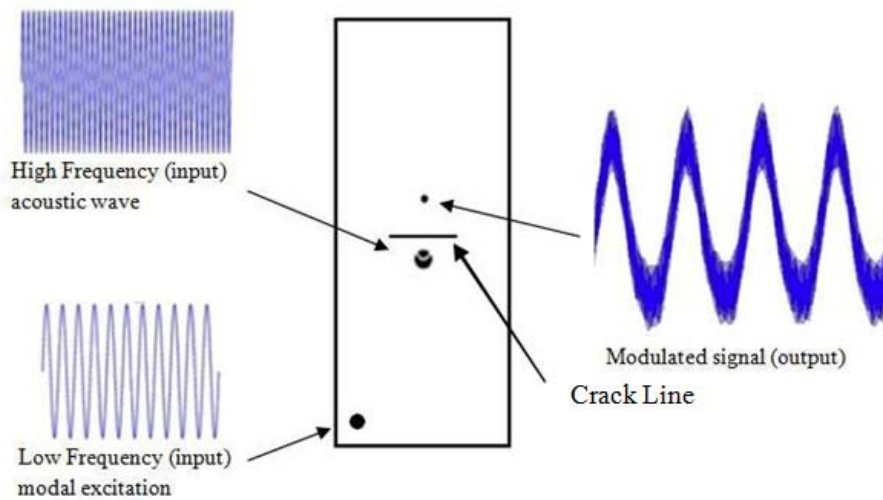
Vibro-acoustic modulation (VAM) is a test that introduces high and low frequency signals into a test specimen simultaneously. The VAM technique is discussed a lot in the literature, with an overview given in Pieczonka *et al.*, (2016). It involves piezoelectric (PZT) transducers that provide high frequency continuous waves generation and mechanical shakers for low frequency vibration excitation (Zaitsev *et al.*, 2003, 2005; Duffour *et al.*, 2006; Donskoy *et al.*, 2007). The interaction of the waves with the presence of non-uniformity of the structure such as cracks, debonding and fatigue defects produce nonlinear wave interaction effect, such as sidebands around the high frequency signal peaks. As reported by Parsons & Staweszewski (2006), piezoelectric excitation with surface-bonded low profile PZT transducers is suitable for crack detection based on nonlinear acoustics. Donskoy & Sutin (1998) found that even a rather weak crack can also lead to an anomalously high level of nonlinearity. Nonlinear acoustic techniques have been introduced as an effective approach to overcome the limitations of linear acoustic techniques (Broda *et al.*, 2012). There are many literature sources on the aspects of nonlinearities involved in VAM, both theoretically and numerically described by Donskoy & Sutin (1998) and Kober & Prevorovsky (2014). Geng *et al.* (2016) theoretically studied thermal effects on the vibro-acoustic characteristics of simply supported and clamped plates. Li & Li (2015) carried out analytical studies on the vibration and sound radiation of composite plates.

The first applications of VAM for structural damage detection were related to cracks in metals. These applications include fatigue crack detection in steel (Duffour *et al.*, 2006), fatigue cracks in aluminium (Straka *et al.*, 2008, Tszeng, 2013; Lim *et al.*, 2014), aircraft fuselage panels (Zagrai *et al.*, 2008) and railway wheel disks (Zaitsev *et al.*, 2011). More recently, the technique has been applied to detect barely visible impact damage in laminated composites (Chrysochoidis *et al.*, 2011, 2014), composite sandwich panels with a Nomex honeycomb core (Klepka *et al.*, 2012), and composite airframe components (Zagrai *et al.*, 2004). Other applications include crack detection in concrete (Payan *et al.*, 2010) and glass (Jenal & Staszewski, 2010). In addition, Sutin & Johnson (2005) mentioned a successful application of VAM to stress corrosion cracks in steel pipes, bonding quality assessment in titanium, and thermoplastic plates used for aerospace applications.

In most researches, the modulation phenomenon is usually studied in the frequency domain, where the modulating effect is manifested by the presence of sidebands around the main peak at high frequencies (Van Den Abeele & De Visscher, 2000). Current studies usually regard the ratio of the sidebands and main peak as a damage index to indicate the presence of cracks. Duffour *et al.* (2006) addressed on averaging the amplitude of the sidebands over a wide ultrasonic frequency to eliminate the dependence of the sensitivity of VAM on ultrasonic frequency. Hu *et al.* (2010) found that the damage index calculated in the spectrum domain may lead to false indications about the damage severity and modulation processes. However, it still showed non-ideal correlation between crack size and strength of modulation. Matteo *et al.* (2009) demonstrated that small fatigue cracks can be detected by increasing the amplitude level of modulation and successfully detected cracks in solid structure. Martowicz *et al.* (2012) presented a simulation study of the generation of frequency mixing components in a cracked aluminium plate with the use of peridynamics.

The sideband intensity correlates to the presence of damage. However, the sideband intensity is also influenced by the energy of the low frequency vibration mode generated during the test and discussion to address this phenomenon is lacking. This paper presents experimental results to show the effect of low frequency excitation in nonlinear vibro-acoustic test for crack detection.

The method considered in this study is based on a combined VAM of an intensive low frequency excitation and high frequency wave. These two excitations are introduced to the structure simultaneously (Figure 1). The number of sidebands and amplitude depends on the intensity of modulation and strongly related to damage severity.

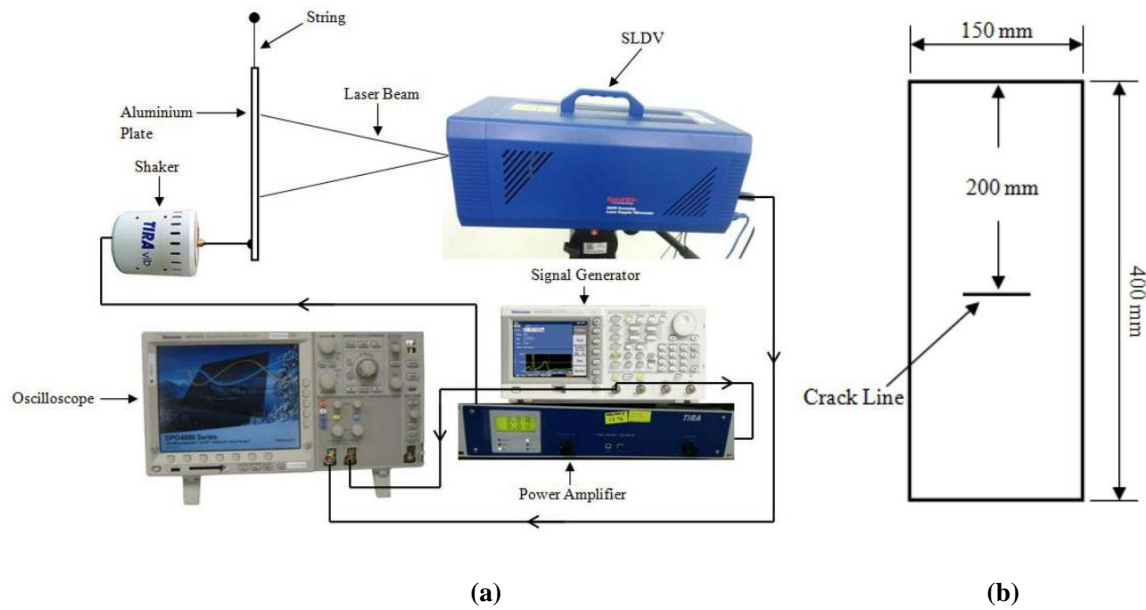


**Figure 1: Schematic layout demonstrating the principle of VAM.**

## 2. METHODOLOGY

### 2.1 Modal Analysis

Modal analysis was performed to determine the modal parameters, such as natural resonant frequencies and mode shape of a cracked plate. The test plate was a 35 mm centre cracked Al-2024 aluminium plate having dimensions of 400 mm x 150 mm x 2 mm. The schematic diagram of the experimental modal analysis is shown in Figure 2. The excitation signal was generated using a Tektronix AFG 3022 signal generator and amplified by a TIRA type BAA 60 power amplifier. The excitation was introduced to the plate using a TIRA GmbH type S 50018 mechanical shaker. The responses of the plate were measured using a single head scanning laser Doppler vibrometer (SLDV) and recorded into a Textronix DPO 4032 oscilloscope. The input parameters in the experiment are shown in Table 1.



**Figure 2: (a) Experimental set up for the modal test. (b) Front view of test plate.**

**Table 1: Input parameters for the modal test.**

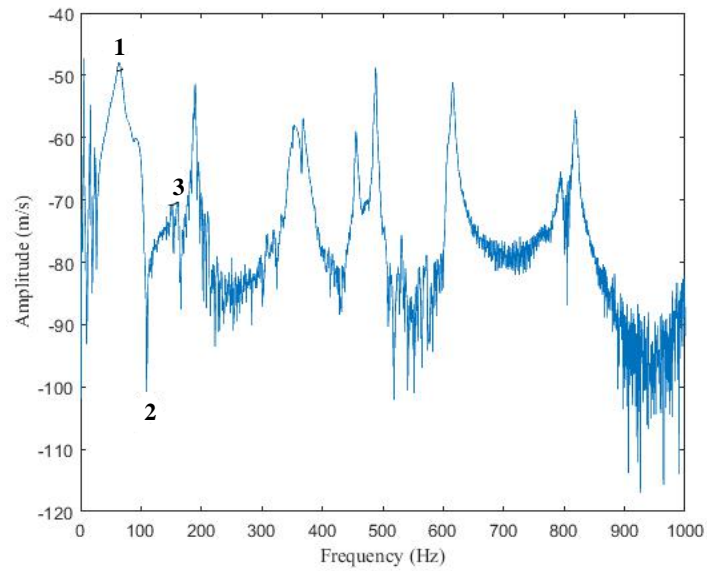
Item	Parameter
Signal : Sweep sine	1-2000 Hz
Sweep time	2 s
Amplitude	5 Vpp
Sampling size	20 kS/s

Figure 3 shows the results of the frequency response function (FRF) for the plate using single point measurement. The figure shows some peaks that can be identified as the vibration mode frequency for the plate. The three vibration mode frequencies from the figure are 65, 109, and 168.5 Hz, which are identified as vibration modes 1, 2, and 3 respectively. Vibration mode 2 appears slightly in the plot because the plate responses depend on the location of excitation and response measurement. If the plate is excited in a nodal area, the response peaks would not appear or would appear only slightly in the FRF.

In order to validate the measurement results, finite element method (FEM) was performed by modelling the plate as quadrilateral continuum shell (SC8R) elements. The steady-state dynamic analysis procedure was applied to obtain the linearised response of the plate at harmonic frequency excitation.

Figure 4 shows three mode shapes and surface deflection results from the FEM simulation and experiment. The mode shapes in the experiment show similar trend with those from the simulation. The resonant frequencies for experiment are 65, 109 and 168.5 Hz for first, second and third modes respectively. The resonant frequencies values for the simulation are 66, 106 and 184 Hz for the first, second and third modes respectively. However, the resonant frequencies differ by 1.5 to 9.2%, which could be due to the non-uniformity of the experimental plate. The validated experiments resonant frequencies were then used as the input frequencies in the low frequency excitation in the nonlinear vibro-acoustic test.

Theoretically, the maximum vibration responses could be produced when the point of excitation is located at the maximum point of deflection from the above modal test. In the above modal analyses, the maximum deflection points are shown in red. Table 2 shows the effective excitation locations for the three different vibration mode frequencies. From the table, a common location to produce the most effective vibration responses is at the corner edge of the plate.



**Figure 3: Frequency response function (FRF).**

FE simulation			
	Mode 1 (66 Hz)	Mode 2 (106 Hz)	Mode 3 (184 Hz)
Experiment			
	Mode 1 (65 Hz)	Mode 2 (109 Hz)	Mode 3 (168.5 Hz)

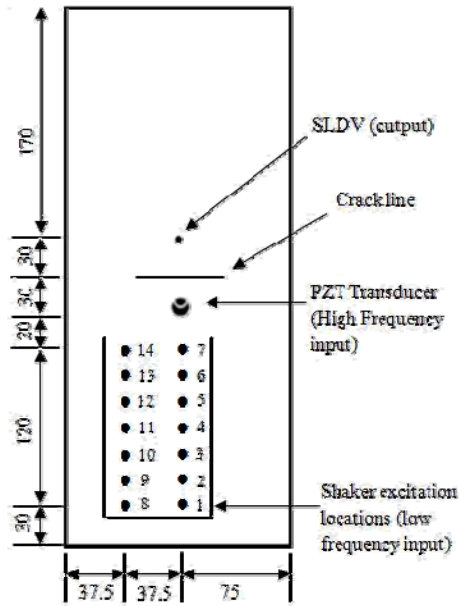
**Figure 4: Mode shapes of the aluminium plate from the simulation and experimental results.**

**Table 2: The effective excitation location for different vibration modes.**

Vibration mode frequency	Effective location
First vibration mode	Both short edges
Second vibration mode	Corner edges
Third vibration mode	Both short edges

## 2.2 Nonlinear VAM Test

Figure 5 shows the schematic diagram of the aluminium plate with locations of the stinger shaker and PZT transducer to provide the low frequency excitation and high frequency input respectively. The PZT transducer to induce 60 kHz high frequency signal was attached 30 mm below the crack line. The stringer shaker excitation location was arranged in two columns with seven points at each column. The first column is located at the centre of the plate (excitation points 1-7) with each point separated at interval of 20 mm. The second column (excitation points 8-14) was arranged at 37.5 mm gap with the first column. The lowest point of each column was 30 mm from the short edge of the plate. As in the experimental modal test, the vibration response was measured using the SLDV.



Note : All dimensions in mm

Figure 5: The schematic diagram of the excitation location on the test plate.

The plate was excited at its resonant frequencies, i.e., at 65, 109 and 168.5 Hz. Figure 6 shows the velocity of the plate in time domain measured by the SLDV for each frequency. These were then transformed into frequency domain using the Fast Fourier Transform (FFT).

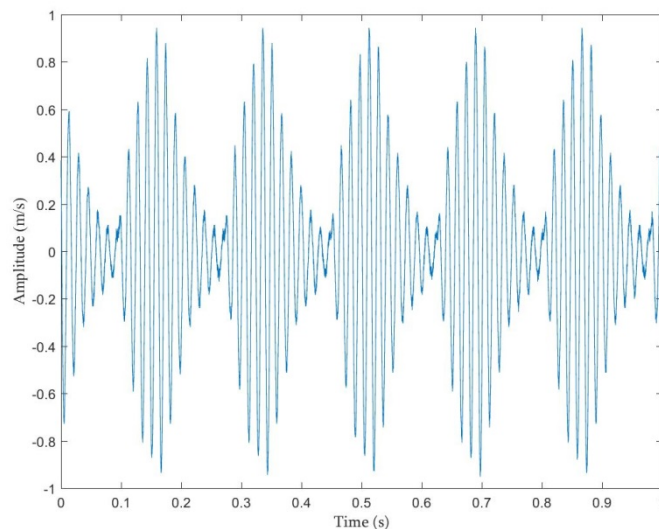


Figure 6: Power spectrum of the low frequency at 65 Hz in time domain.

Figure 7 shows the frequency spectrum amplitude of the 60 kHz high frequency signal modulated with 65 Hz low frequency. It can be observed that the side peaks presented besides the centre frequency 60 kHz has the frequency spacing of the low frequency excitation. In order to measure the intensity of the sideband, the ratio of the amplitude of the first sideband frequency against that of centre frequency is used. The ratio is given as:

$$R = \frac{A_1 + A_2}{A_0} \quad (1)$$

where  $A_0$  is the centre frequency, and  $A_1$  and  $A_2$  are the first sideband amplitudes before and after the centre frequency.

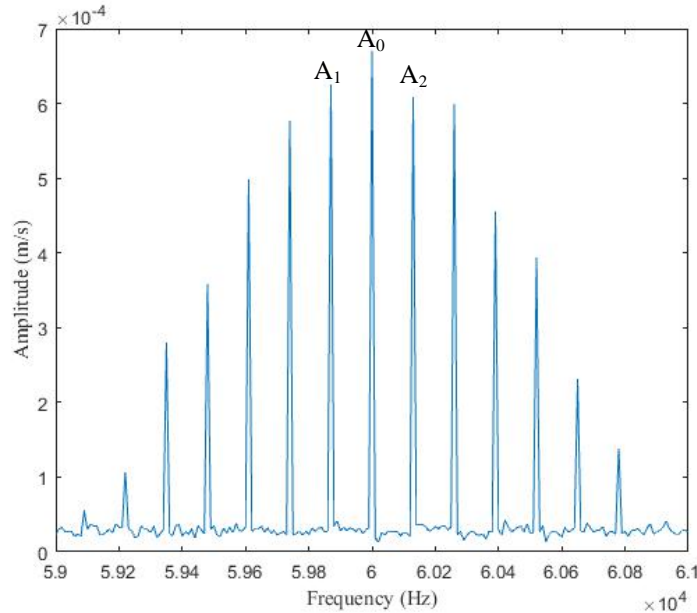


Figure 7: Power spectrum of the high frequency signal at 60 kHz in frequency domain.

### 3. RESULTS & DISCUSSION

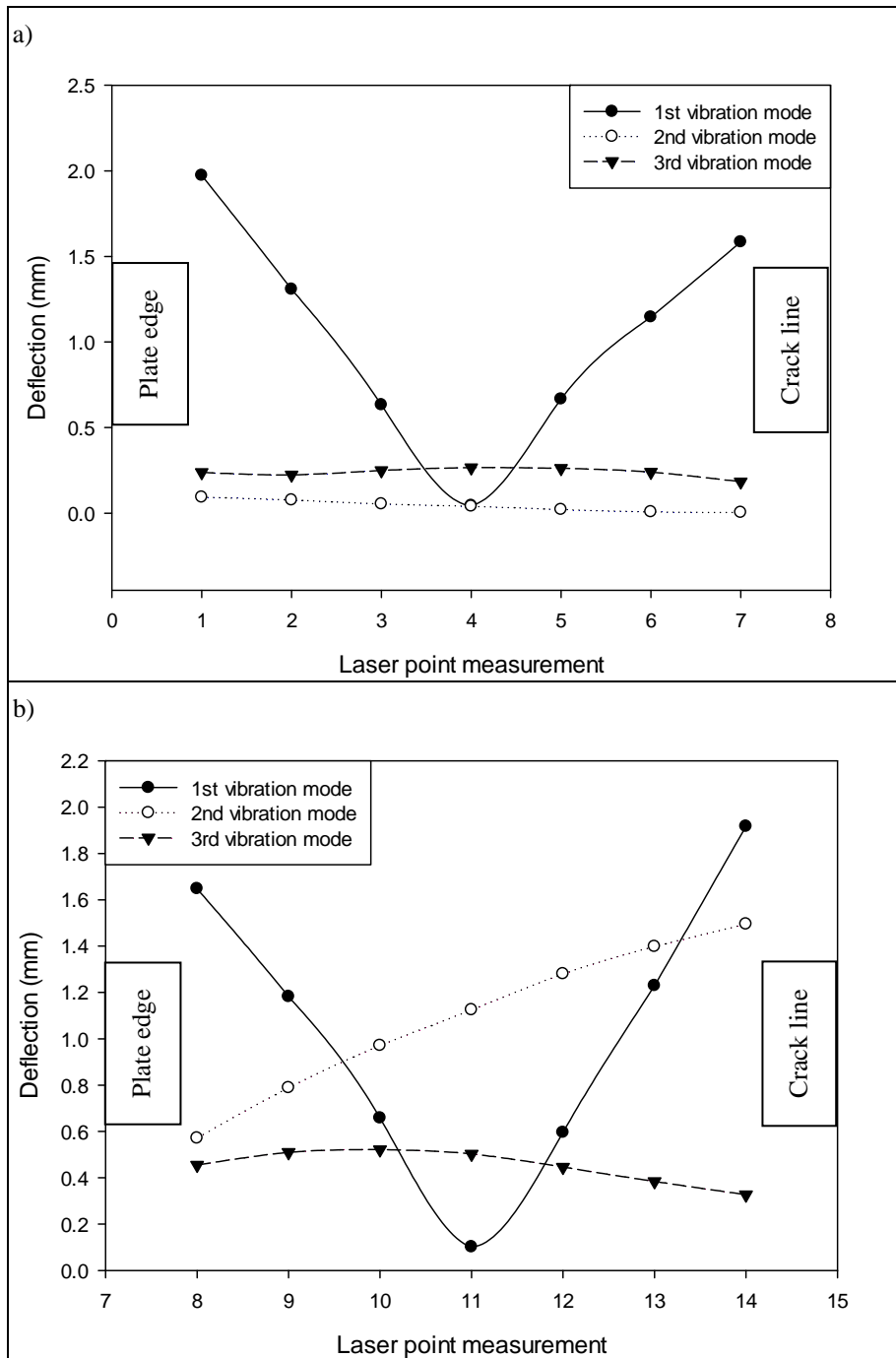
The results in this section were obtained from the modal test methodology output of the vibration responses due to a single frequency excitation measured at points 1 to 14. Figure 8 shows the first vibration mode frequency performed as well as the corresponding mode shapes.



Figure 8: Example of the first mode shape of the aluminium plate.

#### 3.1 Surface Deflection

Figure 9 shows the surface deflections against the first, second and third vibration mode frequency excitations at (a) points 1 to 7 and (b) points 8 to 14. The first vibration mode frequency (65 Hz) produced similar graph patterns in both graphs. The highest deflection for the first vibration mode excitation happened at plate edge (points 1 and 8) and near the crack line (points 7 and 14). Meanwhile, the minimum deflection happened at points 4 and 11. Thus, points 4 and 11 are considered as the anti-nodal points of the plate. In the second vibration mode frequency (109 Hz) excitation responses, there was no significant deflection at points 1 to 7, but the surface deflection steadily increased from points 8 to 14. There was no significant deflections at all the measured points for the third vibration frequency (168.5 Hz) excitation responses.



**Figure 9: Graphs of surface deflections at (a) points 1 to 7 and (b) points 8 to 14 when the plate was excited at a single point by the three vibration mode frequencies.**

### 3.2 R-value

Figure 10 show the  $R$ -values of first, second and third vibration mode frequency excitations at the shaker excitation locations. From Figure 10, the first vibration mode excitation shows the highest  $R$ -value as compared to the other vibration mode excitation with the maximum value at plate edge and near crack line, while the minimum value is at the centre of the measured points. This result is related to the excitation at nodal and anti-nodal points respectively.

Due to higher degree non-linearity, in the second and third vibration mode frequency excitations, there are no significant trending that could be related with the excitation locations. However, the  $R$ -values are lower than the values from the first vibration mode excitation at most of the excitation locations due to low surface deflections. From the figure, the first vibration mode excitation at the nodal point will produce the effective nonlinear wave interaction effect on  $R$ -value. However, the other vibration mode excitations also produce the nonlinear effect but do not show any significant location.

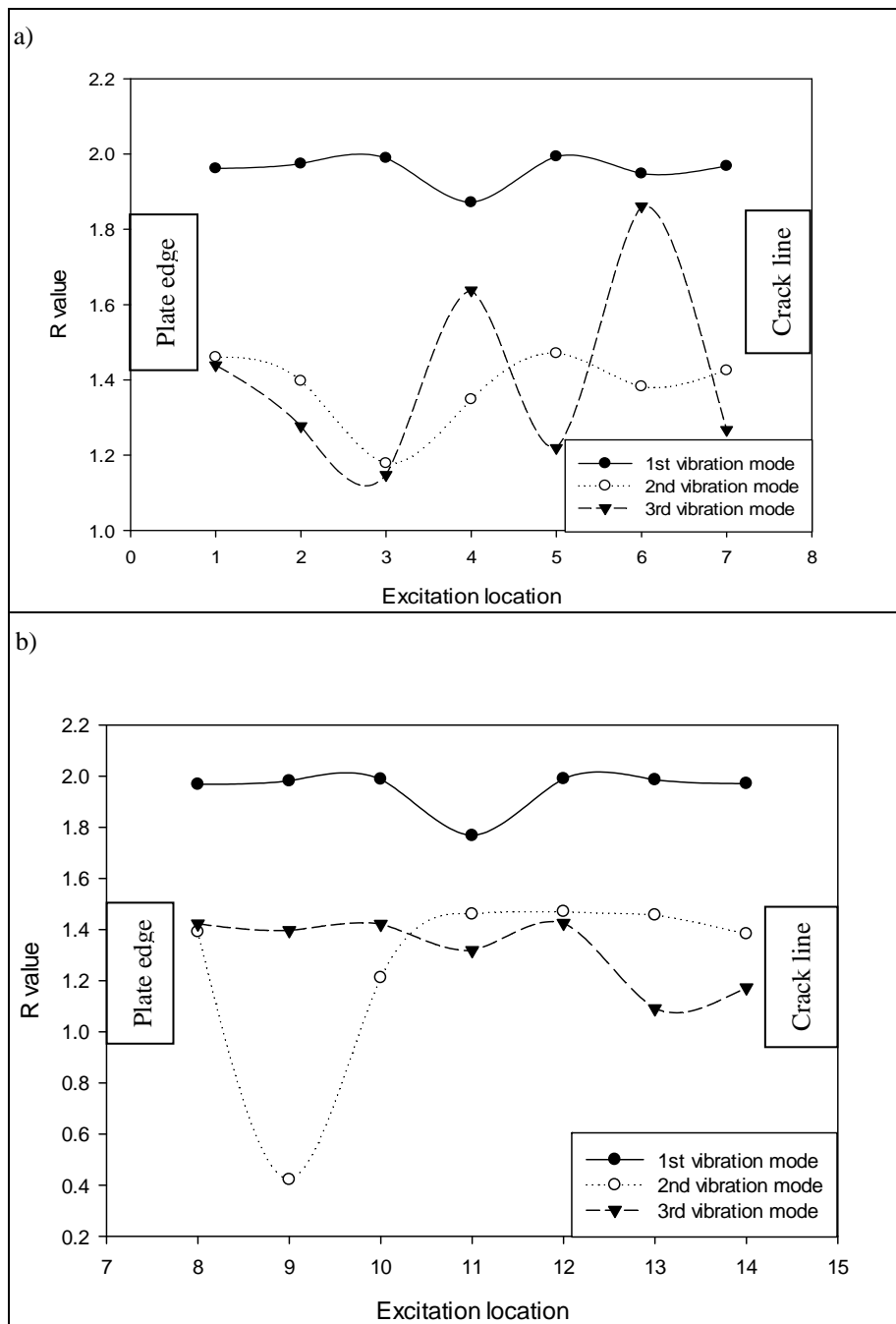


Figure 10: Graphs of  $R$ -value against excitation locations at (a) points 1 to 7 and (b) points 8 to 14, for the three vibration mode frequencies.



#### 4. CONCLUSION

The nonlinear acoustic test was carried out on the aluminium plate with three different low frequency excitations at 14 locations to study the crack detection effectiveness. From the Figure 9, the trends of the plot differ between vibration modes. The first vibration mode frequency excitation produced the most significant effect on the plate responses. The response varied across the plate area with the highest and lowest surface deflections being at the nodal area (point 1) and anti-nodal point (point 4) respectively. Although, the second and third vibration mode frequency excitation did not show any trending, it did produce significant plate responses.

The experimental results showed that the first vibration mode excitation produced significant effect on  $R$ -value. The second and third vibration mode excitations also produce significant effect on the  $R$ -value, but the excitation location was not significantly affected. As the first vibration mode shows the highest non-linear wave interaction, it is considered as the most effective mode for fatigue crack detection, while the most effective excitation locations are at the centre and edge of the plate.

#### ACKNOWLEDGEMENT

Authors would like to acknowledge Universiti Teknikal Malaysia Melaka (UTeM) for the Zamalah awarded to the first author.

#### REFERENCES

- Broda, D., Staszewski, W., Martowicz, A., Uhl, T. & Silberschmidt, V. (2014). Modelling of nonlinear crack-wave interactions for damage detection based on ultrasound-a review. *J. Sound Vibration*, **333**: 1097 – 1118.
- Chrysochoidis, N.A., Assimakopoulou, T.T. & Saravanos, D.A. (2014). Nonlinear wave structural health monitoring method using an active nonlinear piezoceramic sensor for matrix cracking detection in composites. *J. Intell. Mater. Syst. Struct.*, **26**: 2108-2120.
- Chrysochoidis, N.A., Barouni, A.K. & Saravanos, D.A. (2011). Delamination detection in composites using wave modulation spectroscopy with a novel active nonlinear acousto-ultrasonic piezoelectric sensor. *J. Intell. Mater. Syst. Struct.*, **22**: 2193–2206.
- Donskoy, D.M. & Sutin, A. (1998). Vibro-acoustic modulation nondestructive evaluation technique. *J. Intell. Mater. Syst. Struct.*, **9**: 765-771.
- Donskoy, D., Zagrai, A., Chudnovsky, A., Golovin, E. & Agarwala, V. (2007). Damage assessment with nonlinear vibro-acoustic modulation technique. *International Design Engineering Technical Conferences and Computers and Information in Engineering Conference*. Proc. ASME DETC2007-34697, pp. 1949-1956.
- Duffour, P., Morbidini, M. & Cawley, P. (2006). A study of the vibro-acoustic modulation technique for the detection of cracks in metals. *J. Acoust. Soc. Am.*, **119**: 1463.
- Geng, Q. & Li, Y. (2016). Solutions of dynamic and acoustic responses of a clamped rectangular plate in thermal environments, *J. Vib. Contr.*, **22**:1593-1603.
- Hu, H.F., Staszewski, W.J., Hu, N.Q., Jenal, R.B. & Qin, G.J. (2010). Crack detection using nonlinear acoustic and piezoceramic transducers-instantaneous amplitude and frequency analysis. *Smart Mater. Struct.*, **19**: 065017.
- Jenal, R. B. & Staszewski, W. J. (2010). Crack detection in glass plates using nonlinear acoustics with low-profile piezoceramic transducers. *Health Monitoring of Structural and Biological Systems*. Proc. SPIE **7650**: 765030.
- Klepka, A., Staszewski, W.J., Jenal, R.B., Szewdo, M., Iwaniec, J. & Uhl, T. (2012). Nonlinear acoustics for fatigue crack detection– experimental investigations of vibro-acoustic wave modulations. *Struct. Health Monit.*, **11**: 197–211.
- Kober, J. & Prevorsevsky, Z. (2014). Theoretical investigation of nonlinear ultrasonic wave modulation spectroscopy at crack interface. *NDT E Int.*, **61**: 10–15.
- Lim, H. J., Sohn, H., Desimio, M., Brown, K. & Derriso, M. (2014). Reference-free fatigue crack detection using nonlinear ultrasonic modulation under various temperature and loading conditions. *Mech. Syst. Signal Process.*, **45**: 468–478.

- Li, W. & Li, Y. (2015) Vibration and sound radiation of an asymmetric laminated plate in thermal environments. *Acta Mech. Solida Sin.*, **28**: 11-22.
- Martowicz, A., Pawel, P. Staszewski, W.J. & Uhl, T. (2012). Modelling of nonlinear vibro-acoustic wave interaction in cracked aluminium plates using Local Interaction Simulation Approach. *Sciences and Engineering*. Proc. ECCOMAS, pp. 5420-5429.
- Matteo, S., Staszewski, W.J. & Jenal, R.B. (2009). Structural damage detection using ultrasonic wave modulation with low-profile piezoceramic transducers. In Kundu, T. (Ed.) *Health Monitoring of Structural and Biological Systems*. Proc. SPIE, **7295**: 72950J-72950J-9.
- Parsons, Z. & Staweszewski, W.J. (2006). Nonlinear acoustic with low-profile piezoceramic excitation for crack detection in metallic structures. *Smart Mater. Struct.*, **15**: 1110-1118.
- Payan, A., Garnier, V. & Moysan, J. (2010). Potential of nonlinear ultrasonic indicators for nondestructive testing of concrete. *Adv. Civ. Eng.*, **Vol. 2010**:1–8.
- Straka, L., Yagodzinsky, Y, Landa, M & Hänninen, H. (2008). Detection of structural damage of aluminum alloy 6082 using elastic wave modulation spectroscopy. *NDT E. Int.*, **41**: 554–563.
- Sutin, A. M. & Johnson, P. (2005). Nonlinear elastic wave NDE II. Nonlinear wave modulation spectroscopy and nonlinear time reversed acoustics. *AIP Conf. Proc.*, **760**: 385
- Pieczonka, L., Martowicz, A. & Staszewski, W. (2016). Nonlinear vibroacoustic wave modulations for structural damage detection: An overview. *Optical Eng.*, **55**: 1.
- Tszeng, T.C. (2013). Modulation spectroscopy of acoustic waves in solids containing contact-type cracks. *J. Vib. Acoust.*, **135**: 064504-064504-6.
- Van Den Abeele, K. & De Visscher, J. (2000). Damage assessment in reinforced concrete using spectral and temporal nonlinear vibration techniques. *Cem. Concr. Res.*, **30**: 1453–64.
- Zagrai, A., Donskoy, D. & Lottiaux, J. (2004). N-Scan®: new vibromodulation system for crack detection, monitoring and characterization. *AIP Conf. Proc.*, **700**:1414–1421.
- Zagrai, A., Donskoy, D., Chudnovsky, C. & Golovin, E. (2008). Micro and macroscale damage detection using the nonlinear acoustic vibro-modulation technique. *Res. Nondestr. Eval.*, **19**: 104–128.
- Zaitsev, V.Y., Matveev, L.A. & Matveyev, A.L. (2011). Elastic-wave modulation approach to crack detection: comparison of conventional modulation and higher-order interactions. *NDT E. Int.*, **44**: 21–31.
- Zaitsev, V.Y., Gusev, V. & Castagnède, B. (2003). Thermoelastic mechanism for logarithmic slow dynamics and memory in elastic wave interaction with individual cracks. *Phys. Rev. Lett.*, **90**: 075501-075504.
- Zaitsev, V.Y., Gusev, V.É., & Nazarov, V.E. (2005). Acoustic wave—crack interaction: mechanism of nonlinear elastic and inelastic dynamics at different time-scales. *Acoust. Phys.*, **51**: S67-S77.

# ENHANCEMENT OF DEFECT SIGNATURE FOR ACOUSTIC WAVE SOURCE LOCATION FROM TWO WAVE MODES IN PIPE

Nor Salim Muhammad<sup>1</sup>, Ahmad Fuad Ab Ghani<sup>2</sup>, Rokhmadi<sup>1,3</sup>, Abd Rahman Dullah<sup>1</sup> & Azma Putra<sup>1</sup>

<sup>1</sup>Faculty of Mechanical Engineering, Universiti Teknikal Malaysia Melaka (UTeM), Malaysia

<sup>2</sup>Faculty of Engineering Technology, Universiti Teknikal Malaysia Melaka (UTeM), Malaysia

<sup>3</sup>Center for Nuclear Reactor Technology and Safety, National Nuclear Agency of Indonesia, Indonesia

\*Email: norsalim@utem.edu.my

## ABSTRACT

*Simulated waves are used to evaluate a technique for acoustic wave source location in pipes. Acoustic waves that are collected from five sensors are used to determine the direction of incoming source and determine the location of corrosion defects in a pipe. Longitudinal L(0,2) and flexural F(1,3) modes are used to detect acoustic waves from corrosion activities. The difference in time of arrival is used to estimate the location of the corrosion defects in the pipe. Although the computed distance is slightly different than the actual location, the technique indicated potential for its further improvement in structure health monitoring.*

**Keywords:** *Structure health monitoring; acoustic emission; signal enhancement; source location.*

## 1. INTRODUCTION

Structural health monitoring in aircrafts, power plants and petrochemical industries has been taken seriously to avoid any operational failures that could lead to loss of production and life (Anghileri *et al.*, 2005; Gao & Rose, 2009; Heimbs *et al.*, 2014; Mazal *et al.*, 2014; Jones *et al.*, 2015). At the same time, non-destructive inspection techniques such as computer radiography, phased arrays, ultrasonic guided wave and acoustic emission are among the techniques that are increasingly addressed in the industries to detect the presence of defects over large areas including plates and pipe structures. A study on army airframe also indicates possibilities to immediately alert the flight crews to structural damage, such as matrix cracking and delamination, as they occur to allow corrective actions before any catastrophic failure (Marantidis *et al.*, 1994; Prosser *et al.*, 1995, Okafor *et al.*, 2005; Eaton *et al.*, 2012; Mazal *et al.*, 2014; Leinov *et al.*, 2016).

Recently, the use of ultrasonic guided wave and acoustic emission are seen to be useful for inspection over the underground pipes or insulated pipelines. This is due to the ability of the techniques that utilise the acoustic wave propagation to detect and locate defects in the pipe structures (Nair & Cai, 2010; Eaton *et al.*, 2012; Mostafapour & Davoudi, 2013). The use of ultrasonic guided waves will excite an initial pulse that will propagate along the waveguide and a part of the elastic wave will be reflected from the defect in the structures (Rose, 2014). On the other hand, the use of acoustic emission is only based on listening to the generated acoustic wave from the corrosion activity around the defect areas. The use of acoustic emission is seen to save the cost of equipment compared to the use of the guided wave technique because of no excitation for the initial pulse.

However, there are also difficulties where the reference trigger is not available from the equipment to record the specific waveforms that possibly contain the defect signatures. The collected acoustic waves contain very broad frequency bandwidth that might occur at low level of continuous oscillation due to stress concentration or elastic deformation and high level of burst signal caused by crack formation or corrosion activities (Nair & Cai, 2010; Eaton *et al.*, 2012; Mostafapour & Davoudi, 2013).

Moreover, we believe the use of acoustic wave propagation from cracks and delaminations in an appropriate manner can determine the locations of the defects in structures in industries and military equipment. Therefore, we initiated a study to identify the direction and location of acoustic waves using the collected waves from five sensors on a pipe.

## **2. SIMULATION AND SIGNAL PROCESSING**

Signal processing is concerned on the operations performed on signals that consist of a number of mathematical operations as specified by a software program (Proakis & Manolakis, 1996). The algorithmic operations are carried out for noise reduction, signal enhancement, and extraction of the information through operations including filtering, averaging, fast Fourier and wavelet transforms (Mostafapour & Davoudi, 2017). The signal processing in this study is aimed to obtain the defect information using enveloped curves and enhanced signals of the generated acoustic waves from corrosion activities in pipes. Waveforms from finite element method (FEM) are used in order to avoid complex wave propagation at the initial stage of our study.

### **2.1 Modes Selection in Pipe**

Acoustic wave propagation in aluminium media is often used in studying wave propagations in carbon steel due to the lighter mass that allows to perform experimental work easily. Wave mode propagation in aluminium pipe for our study had been computed using the CIVA guided wave module, which is a software that developed in France by the CEA-LIST and its partners. Calculation of the wave mode propagation allows us to select the suitable wave mode for monitoring corrosion defects in pipe. Potential wave modes that propagate at lower frequency than 100 kHz in aluminium pipe with dimension of 100 mm external diameter and 6 mm thickness are shown in Figure 1, which consists of longitudinal  $L(0,1)$  and  $L(0,2)$  modes as well as flexural  $F(n,m)$  mode (Rose, 2014; Leinov *et al.*, 2016). At the same time,  $L(0,2)$  shows higher velocity than  $F(1,3)$  and selection of the mode propagation at different wave velocity has advantage to decouple defect information from complex wave propagations (Rose, 2014). Therefore, we decided to utilise the velocity of  $L(0,2)$  and  $F(1,3)$  in this study to estimate the location of corrosion defect from the enhanced defect signature that generated from the area of defect.

### **2.2 Simulation of Acoustic Wave Generation in Pipe**

A straight pipe model with a corrosion defect is shown in Figure 2. It simulates acoustic wave generation from corrosion activities in the aluminium pipe with length of 8 m. The pipe model used tetrahedral and hexahedral types of meshes for the calculation in defect and intact regions respectively. The mode is meshed at size of 4 mm with total of approximately 300,000 elements. Five acoustic sensors are placed on the pipe in a straight line at common distance of 100 mm between the sensors with the centre of the measurement placed at 3 m from the left end of the pipe. The sensor's location was preferred to avoid complex wave propagation from the reflected waves that may occur on the left end of the pipe. The corrosion process is simulated by a traction force at the right end of the pipe that uses five cycles of tone

burst signal (Salim *et al.*, 2018) at 40 kHz. The possible acoustic waves collected from the five sensors are shown in Figure 3.

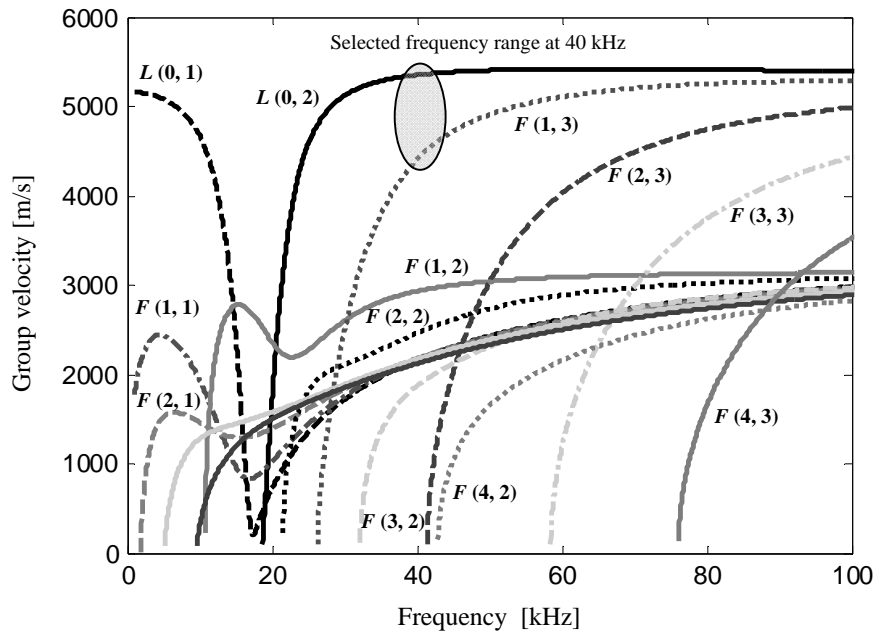


Figure 1: Dispersion curves of the aluminium pipe (at 6 mm thickness).

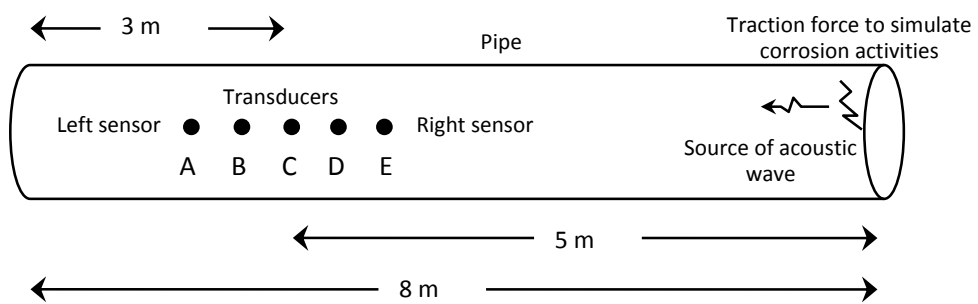
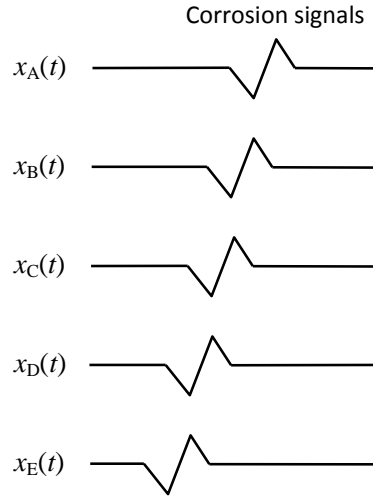


Figure 2: Model of acoustic wave generation in the pipe.



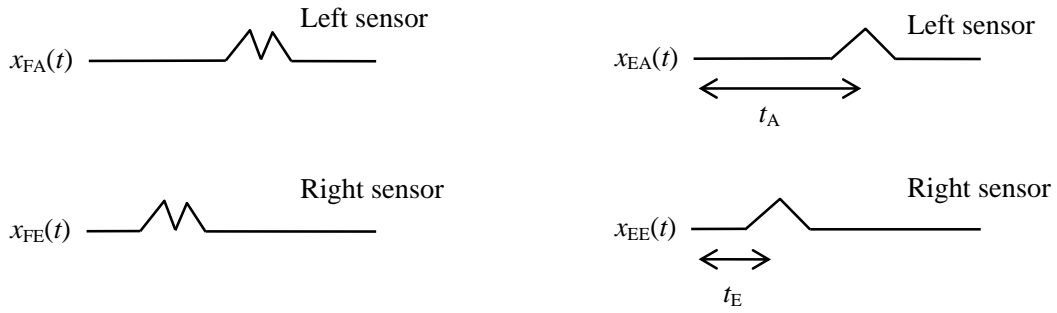
**Figure 3: Collected signals from five sensors at 40 kHz.**

### 2.3 Direction Identification of the Source of Acoustic Wave

The direction of the wave source is important to be determined in order to process the collected signals for enhancement of the defect signature accordingly. The collected waves from most right and left sides of the pipe are shown in Figure 3 as  $x_A(t)$  and  $x_E(t)$ , respectively. Generally, the acoustic signals are likely to come from the right or left side of the sensors (Eaton *et al.*, 2012; Mostafapour & Davoudi, 2013) and two different signal processing schemes will be applied for the different directions of the acoustic sources in the pipe. Therefore, arrival times of the significant wave packets for the most left and right sensors are necessary to be evaluated at the beginning of the signal processing in order to determine direction of the generated wave source in pipe.

The time of arrivals of the wave packets for the most left and right sensors are determined based on enveloped curves that processed from the collected waveforms as in Figure 4. The processing includes calculations of full waves with band pass filter (Proakis & Manolakis, 1996) between 20 to 80 kHz, which are indicated as  $x_{FA}(t)$  and  $x_{FE}(t)$  in Figure 4(a). The results are then passed to a low pass filter at 15 kHz to obtain the enveloped curves of  $x_{EA}(t)$  and  $x_{EE}(t)$  in Figure 4(b). The evaluated time of arrivals of the significant peaks from the left and right sensors are indicated as  $t_A$  and  $t_E$  in Figure 4(b).

The shorter time of arrival of the significant peaks of the enveloped curves is used to determine the direction of the acoustic source in the pipe (Eaton *et al.*, 2012). It is because of linear relationship between the travel time and distance from the sensors. Consequently, the acoustic source will be on the right side when the time of arrival at the right sensor shows the shortest travel time and if otherwise the direction of the acoustic source is on the left side of the sensors.



(a) Full waves of the signals from the left and right sensors (band pass filter 20 to 80 kHz)

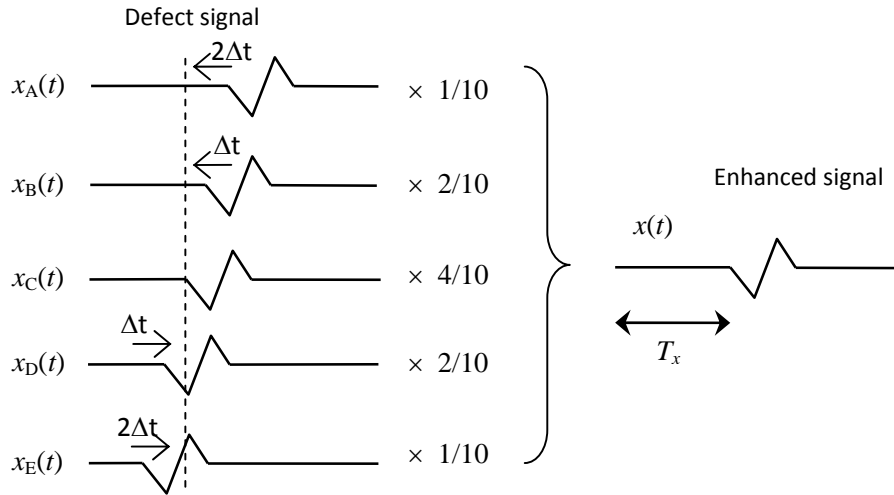
(b) Enveloped curves of the signals from the left and right sensors (low pass filter 15 kHz)

**Figure 4: Measurement of the arrival time.**

## 2.4 Enhancement of the Wave Packet Based on the $L(0,2)$ and $F(1,3)$ Modes

Signal enhancements in ultrasonic are also found in previous studies to increase visibility of the defect echo in ultrasonic inspections (Kim *et al.*, 2006; Salim *et al.*, 2009). Figure 5 shows signal enhancement when the acoustic source is detected on the right side of the pipe. The figure shows that a significant wave packet was collected from the right sensor in  $x_E(t)$ , which had arrived earlier than the wave packet that was collected from the left sensor in  $x_A(t)$ .

The waves of  $x_A(t)$ ,  $x_B(t)$ ,  $x_D(t)$ , and  $x_E(t)$  are shifted by  $\Delta t$  and  $2\Delta t$ , so that the component of  $L(0,2)$  or  $F(1,3)$  modes of the collected waves will be arranged in phase to the component in  $x_C(t)$ . The amplitudes of the waves are then weighted by  $\frac{4}{10}$ ,  $\frac{2}{10}$  and  $\frac{1}{10}$  as in the Figure 5 to represent the contribution of the collected waves for the enhanced defect signature in pipe. The weighted values are selected to high contribution from centre of the sensors and the contribution is reduced as the waves collected away from the centre. The collected waveforms are used to enhance the signature of defect in the final waveform  $x(t)$  based on the velocity of  $L(0,2)$  and  $F(1,3)$  modes. The time of arrival for the wave packet in the final waveform, which indicated as  $T_x$ , is used to calculate the difference in time of arrivals of the modes and estimate location of the corrosion from centre of the sensors.



**Figure 5: Enhancement of the acoustic waves.**

### 3. RESULTS AND DISCUSSION

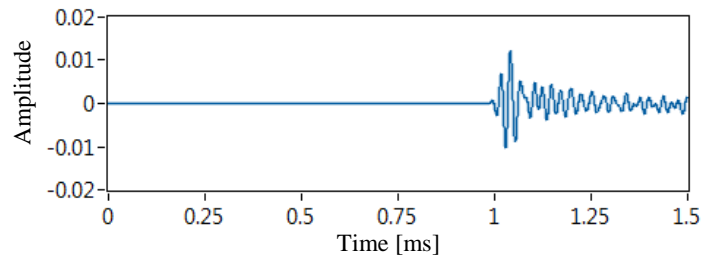
#### 3.1 Collected Signals

The simulation of corrosion activities in the straight pipe showed acoustic wave generation as represented in Figure 6. The horizontal axis of the graphs shows the travel time of the acoustic wave but vertical axis of the graphs do not represent any physical quantity. The collected signals from sensors at 40 kHz showed almost similar wave packet but with different time of arrivals at locations of A, B, C, D, and E as in  $x_A(t)$ ,  $x_B(t)$ ,  $x_C(t)$ ,  $x_D(t)$ , and  $x_E(t)$ . The minimum time of arrival can be observed in  $x_E(t)$  from the collected signal at E that is located near the acoustic source while the maximum time of arrival was obtained in  $x_A(t)$  from the sensor at A which was located at the furthest distance from the acoustic source (Eaton *et al.*, 2012; Mostafapour & Davoodi, 2017).

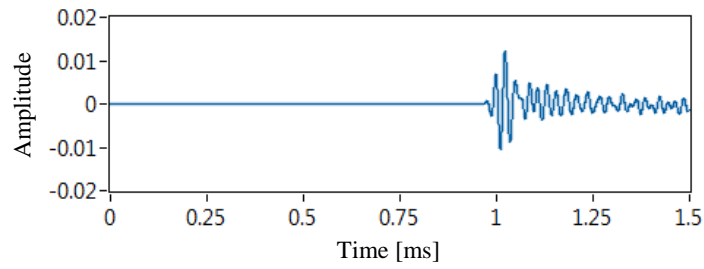
#### 3.2 Expected Direction of Acoustic Source in Pipe

The difference in time of arrival is used in this study to identify the location of the corrosion activities that generated the acoustic waves (Prosser *et al.*, 1995; Mazal *et al.*, 2014). At the same time, the collected signal from the most right and left sensors are used to determine the direction of the acoustic source, as in Figures 6(a) and 6(e).

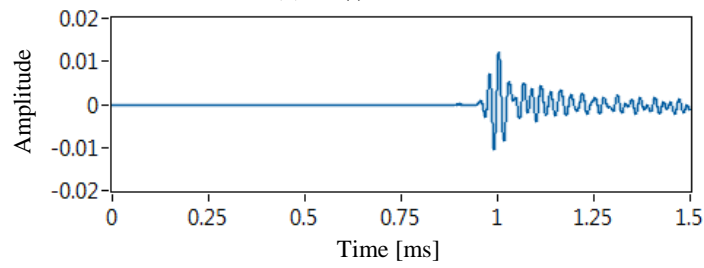




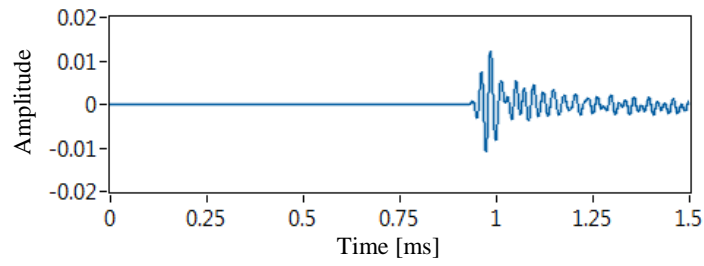
(a)  $x_A(t)$  at location A



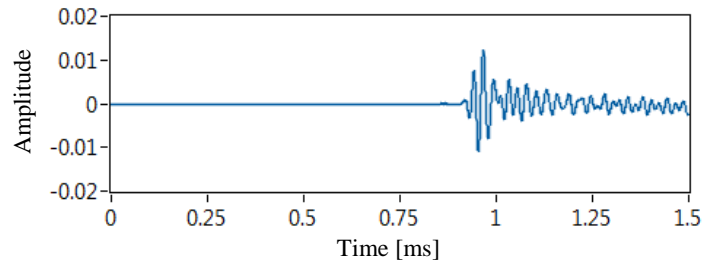
(b)  $x_B(t)$  at location B



(c)  $x_C(t)$  at location C



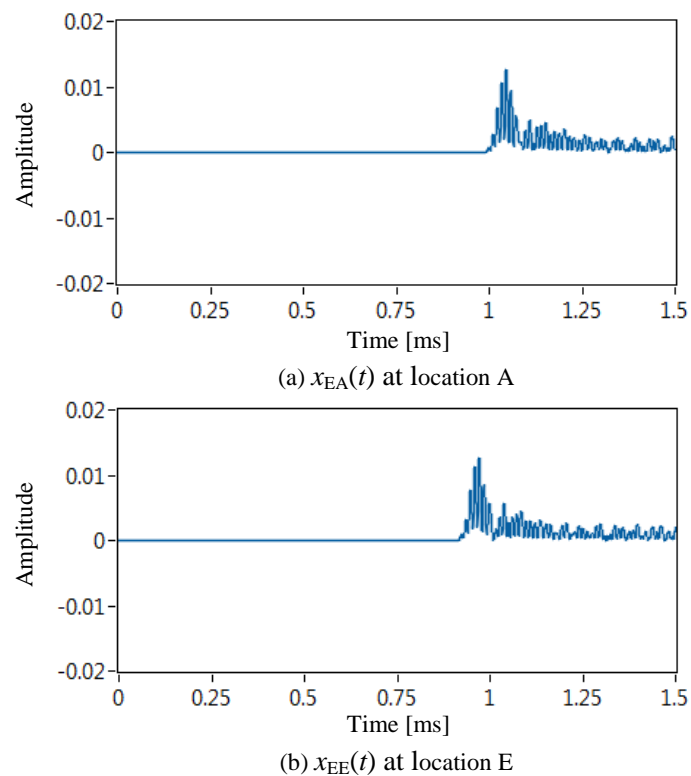
(d)  $x_D(t)$  at location D



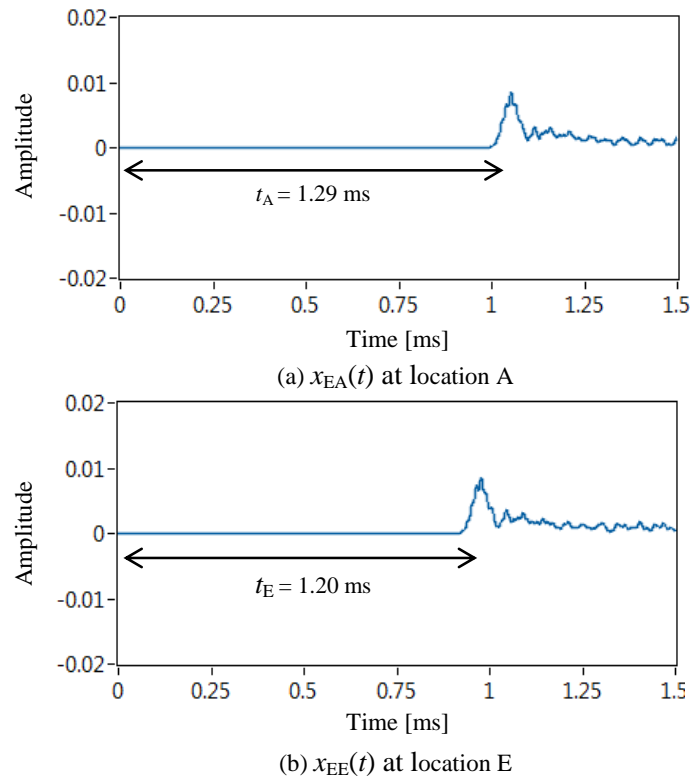
(e)  $x_E(t)$  at location E

**Figure 6: Collected acoustic waves at the five locations.**

The full waves and their enveloped curves that are obtained from the signal processing are shown in Figures 7 and 8 respectively. Band pass filter of 20 to 80 kHz is used to reduce noise during calculation of full waves for the signals from the most right and left sensors. The final enveloped curves for the full waves are obtained by the use of low pass filter at 10 kHz as shown in Figure 8. The use of peak detector in a LabVIEW program detected the arrival of peaks in  $x_{EA}(t)$  and  $x_{EE}(t)$  at 1.29 and 1.20 ms, respectively. Since the time of arrival in  $x_{EE}(t)$  at E is shorter than for  $x_{EA}(t)$  at A, the distance to the acoustic source of E is closer than that of A. In other words, the acoustic source is located on the right side of the pipe as described in Figure 2.



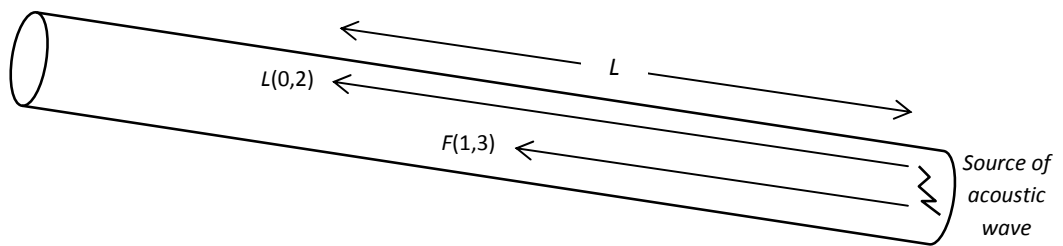
**Figure 7: Computed full waves (20 to 80 kHz of band pass filter).**



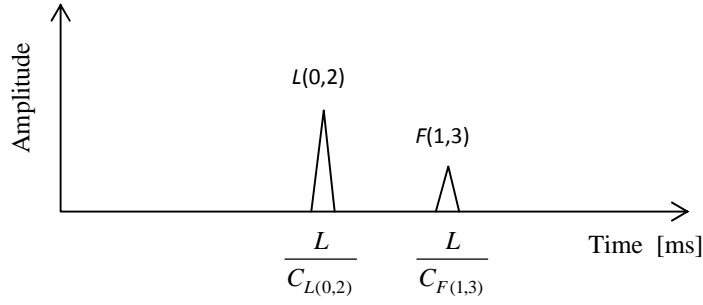
**Figure 8: Enveloped curves of the computed full waves (15 kHz of low pass filter).**

### 3.3 Location of Corrosion Defect in the Pipe

The location of defect can be determined based on the difference in time of arrival of the propagation modes in pipe (Ebrahimkhanlou & Salamone, 2017). The dispersion curves in Figure 2 show that  $L(0,2)$  and  $F(1,3)$  modes have slightly different velocities at frequency of around 40 kHz. Moreover, the two modes are also separated at the frequency from the velocities of the other modes. The mode propagations in can be illustrated as in Figures 9 and 10, where  $L(0,2)$  is propagating ahead of  $F(1,3)$  mode.



**Figure 9:  $L(0,2)$  and  $F(1,3)$  mode propagations in the pipe.**



**Figure 10: Expected time of arrivals for the  $L(0,2)$  and  $F(1,3)$  modes.**

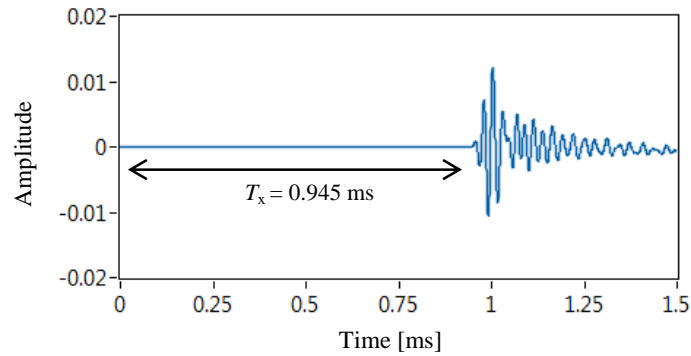
Since the time of arrival for  $F(1,3)$  is longer than for  $L(0,2)$ , as in Figures 9 and 10, the calculation of the location of defect is carried out based on the difference between time of arrivals for the  $F(1,3)$  and  $L(0,2)$  modes, as in Equations 1 to 2, where  $C_{L(0,2)}$  and  $C_{F(1,3)}$  are the group velocities of the modes, and  $L$  is the distance from the centre of the sensors to the source of the acoustic wave.

$$\Delta t = \frac{L}{C_{F(1,3)}} - \frac{L}{C_{L(0,2)}} \quad (1)$$

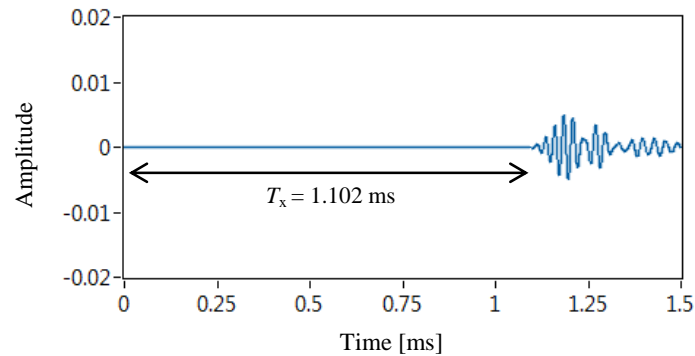
$$L = \frac{\Delta t}{\frac{1}{C_{F(1,3)}} - \frac{1}{C_{L(0,2)}}} \quad (2)$$

The time of arrival for the  $L(0,2)$  is obtained from the signature of the corrosion defect, which was enhanced by using the direction of the acoustic source and the velocity of  $L(0,2)$  at 5,400 m/s. The enhanced acoustic wave  $x(t)$  is shown in Figure 11, which indicates the time of arrival for  $L(0,2)$  at approximately 0.945 ms.

The use of digital band pass filter in Figure 12 shows the waveform for the frequency content of 30 to 50 kHz, which is enhanced at the  $F(1,3)$  mode velocity of 4,500 m/s, as shown in the dispersion curves. The filtered waveform indicates the arrival of the wave packet at approximately 1.102 ms to the centre of the sensors. The results indicate difference in time of arrival of approximately 0.157 ms and predicts the corrosion activities at about 4.4 m from the centre of the sensors. Although there is a difference between the estimated and actual location of defect in pipe, the observations on the two modes can be used in predict the location of corrosion activities in pipes.



**Figure 11: Enhanced acoustic signal  $x(t)$  at velocity of 5,360 m/s (without digital filter).**



**Figure 12: Enhanced signal  $x(t)$  at velocity of 4,410 m/s (band pass filter at 30 to 50 kHz).**

#### 4. CONCLUSION

The location of source of acoustic wave in a straight pipe had been determined using a passive acoustic wave technique. The direction of the source is determined from the enveloped curves of the most right and left sensors, while the distance from the centre of the sensors to location of the source is computed from the difference between time of arrivals of the enhanced  $F(1,3)$  and  $L(0,2)$  modes. The enhanced  $F(1,3)$  and  $L(0,2)$  modes are obtained from enhancement of the collected signals based on their group velocities and a band pass filter. The calculated location shows almost good result to the actual location and indicates possible implementation of fixed point corrosion monitoring for the passive wave technique in real applications on structure health monitoring.

#### ACKNOWLEDGMENTS

This work is supported by Universiti Teknikal Malaysia Melaka (UTeM) and the Ministry of Education (MOE) under research grants FRGS/1/2014/TK01/FKM/02/1/F0211, FRGS/2/2013/TK01/UTEM/02/F0171, and ERGS/1/2013/FKM/TK01/UTEM/02/01/E00014.

#### REFERENCES

- Anghileri, M., Castelleti, L.M.L. & Tirelli, M. (2005). Fluid–structure interaction of water filled tanks during the impact with the ground. *Int. J. Impact Eng.*, **31**: 235-54.
- Eaton, M.J., Pullin, R. & Holford, K.M. (2012). Acoustic emission source location in composite materials using Delta T Mapping, *Composites Part A*, **43**: 856-863.
- Ebrahimkhanlou, A. & Salamone, S. (2017). Acoustic emission source localization in thin metallic plates: a single-sensor approach based on edge reflections, *Ultrasonics*, **78**: 134-145.
- Gao, H. & Rose, J.L. (2009). Ice detection and classification on an aircraft wing with ultrasonic shear horizontal guided waves. *IEEE Trans. Ultrason. Ferroelectr. Freq. Control*, **56**: 334-344.
- Heimbs, S., Nogueira, A.C., Hombergsmeier, E., May, M. & Wolfrum, J. (2014). Failure behaviour of composite T-joints with novel metallic arrow-pin reinforcement. *Compos. Struct.*, **110**: 16-28.
- Jones, R., Peng, D., Huang, P., & Singh, R.R.K. (2015). Crack growth from naturally occurring material discontinuities in operational aircraft. *Procedia Eng.*, **101**: 227-234.
- Kim, C., Zemp, R.J. & Wang, L.V. (2006). Intense acoustic bursts as a signal-enhancement mechanism in ultrasound-modulated optical tomography, *Opt. Lett.*, **31**: 2423-2425.

- Leinov, E., Lowe, M.J.S. & Cawley, P. (2016). Investigation of guided wave propagation in pipes fully and partially embedded in concrete, *J. Acoust. Soc. Am.*, **140**: 4528-4539.
- Marantidis, C., Way, C.B.V. & Kudva, J.N. (1994). Acoustic-emission sensing in an on-board smart structural health monitoring system for military aircraft, *Proc. SPIE Conf.*, **2191**: 258-264.
- Mazal, P., Vlastic, F. & Bartkova, D. (2014). Application of acoustic emission for identification of differences in fatigue damage of selected materials for power plants, *Key Eng. Mater.*, **627**: 313-316.
- Mostafapour, A. & Davoudi, S. (2013). Analysis of leakage in high pressure pipe using acoustic emission method, *Appl. Acoust.*, **74**: 335-342.
- Mostafapour, A. & Davoudi, S. (2017). A method for acoustic source location in plate-type structures, *Mech. Syst. Sig. Process*, **93**: 92-103.
- Nair, A. & Cai, C.S. (2010). Acoustic emission monitoring of bridges: Review and case studies, *Eng. Struct.*, **32**: 1704-1714.
- Okafor, A.C., Singh, N. & Enemuoh, U.E. (2005). Design, analysis and performance of adhesively bonded composite patch repair of cracked aluminum aircraft panels. *Compos. Struct.*, **71**: 258-270.
- Proakis, J.G. & Manolakis, D.G. (1996). *Digital Signal Processing*. Prentice-Hall, Inc, Upper Saddle River, New Jersey.
- Prosser, W.H., Jackson, K.E. & Kellas, S. (1995). Advanced waveform-based acoustic emission detection of matrix cracking in composites, *Mater. Evaluat.*, **53**: 1052-1058.
- Rose, J. L. (2014). *Ultrasonic Guided Waves in Solid Media*, Cambridge University Press, Cambridge.
- Salim, M.N., Alnadhari, A.S.S, Ramlan, R., Dan, R.M., Jenal, R. & Nor, M.K.M. (2018). Effect of nickel foil width on the generated wave mode from a magnetostrictive sensor, *Defence S&T Bull.*, **11**: 36 - 48.
- Salim, M.N., Hayashi, T., Murase, M. & Kamiya, S. (2009), Visualization and modal analysis of guided waves from a defect in a pipe. *Jpn. J. Appl. Phys.*, **48** : 07GD6-GD6-5.

# FOOD SECURITY AND PROPER NUTRITION: A PUBLIC HEALTH AND HUMANITARIAN PRIORITY IN PRE- AND POST-CBRN EVENTS

Stefania Moramarco

Department of Biomedicine and Prevention, University of Rome Tor Vergata, Italy

Email: stefania.moramarco@gmail.com

## ABSTRACT

*The use of chemical, biological, radiological, and nuclear (CBRN) agents during armed conflicts, as an act of terrorism or when accidents involve them, is a threat to any society. In recent years, the occurrence of different kind of disasters and emergencies has risen worldwide, resulting in large numbers of communities affected, causing victims, food crisis, refugees and people displaced. CBRN events can have devastating impacts on the four dimensions of food security (availability, access, utilization and stability) and health (morbidity and mortality patterns), impacting health services and living environment. As a direct result, impaired or jeopardized nutritional status of population is likely to occur, feeding a vicious circle of malnutrition and outbreaks of infectious diseases, ending into famine and mortality. When the access to and the use of natural resources – i.e. food, water, land – are restricted, people start to move to seek for safer environment and stability to survive, increasing the number of refugees and people displaced. Those vulnerable people are directly dependent of food aids, and much more exposed to food insecurity and outbreaks of infectious diseases, especially in crowded refugee camps. Ensuring proper nutrition, health services and secure environment after exposure to CBRN events is therefore a difficult task that needs consideration throughout the world. On the other hand, food access is a key aspect to conflict escalation and terrorism: famine and starvation create the basic conditions for discontent and extremism, increasing the risk of further CBRN attacks around the world. Food war includes the use of hunger as a weapon in active conflict, leading to food insecurity and increased need of humanitarian and health assistance. Therefore, the right to food access, secure and safe, and more generally to proper nutrition, is one of the public health and humanitarian priorities to be considered and not underestimated by CBRN advisors both pre-and post-CBRN events.*

**Keywords:** CBRN events; food security; humanitarian aids; nutrition; public health.

## 1. INTRODUCTION

It is indisputable that after chemical, biological, radiological, and nuclear (CBRN) events, such as those occurring during armed conflicts, massive losses in all the aspects of a civil society occur (Ciparisse *et al.*, 2016; Malizia & 2013/2014 CBRNe Masters Group, 2016; Abate *et al.*, 2016). As a multi-dimensional phenomenon, food security is one of the first sectors affected. In 1996, during the World Food Summit, the Food and Agriculture Organization-FAO claimed that “food security exists when all people, at all times, have physical, social and economic access to sufficient, safe and nutritious food that meets their dietary needs and food preferences for an active and healthy life”. Countries affected by CBRN events especially during armed conflicts show higher levels of chronic and acute food insecurity and undernutrition: food production is disrupted through destruction and plundering of crops, livestock and food reserves; economic investments are discouraged; occupation is suppressed; food exchanges are interrupted; human capital is destroyed. These kinds of situations push food prices higher in both local and international markets. National military allocations inevitably draw investments away from sustainable development and redirect people from peaceful to destructive pursuits (Messer *et al.*, 2002). Most of the population become unable to meet their daily needs, due also to high food prices and food shortages. Those conditions can last even long after, especially when protracted armed conflicts occur, because assets have been destroyed, people killed or displaced, environment damaged, with health, education and social services shattered (FAO, 2002). In addition, food can be also used as a weapon against population. An example was Iraq, where in 2016,

production levels continued to fall as a large part of the cereal production belt was directly under the control of rebel forces, affecting access to agriculture inputs, cereal harvest and post-harvesting activities.

Beyond such devastation, the armed conflict directly impact on the supply of health services and can indirectly cause biological threats, such as epidemics of infections that spread through vulnerable populations. Many of the countries with internal conflicts experienced severe outbreaks of cholera in 2017, such as Yemen, Democratic Republic of Congo, South Sudan, Borno state in Nigeria and Somalia, which raised the levels of malnutrition. When displacements occur, it is more difficult to contain and treat diseases, which perpetuate the rise of malnutrition level in the population (FSIN, 2018).

On the other hand, food insecurity can be one of the root causes triggering and exacerbating conflicts and related consequences. As an example, the 2011 protests across North Africa and the Middle East were in part a response to higher food and energy prices (Perez, 2013). Protracted crises area are most likely in food insecurity area, generating a vicious cycle in which significant proportions of the population are acutely vulnerable to hunger, diseases and disruptions to livelihoods over prolonged periods. For example, 7 years of civil war in the Syrian Arab Republic have led to massive losses in all the sectors, from human capital to socio-economic drivers. FAO currently identifies 19 countries with a protracted crisis situation, with 14 of these being in this category since 2010. Almost all have experienced periods of low-intensity conflicts combined with periods of higher-intensity wars (FAO *et al.*, 2017).

Most of the time those countries do not have the capacity to respond alone to such massive emergencies (WHO, 1999), but request humanitarian assistance, defined as an emergency situation where significant external assistance and resources are required and where a multi-sectoral response is needed, with the engagement of a wide range of international actors and experts (IASC, 2007). In 2017, almost 124 million people across 51 countries and territories faced crisis levels of acute food insecurity and required urgent humanitarian actions, with specific regards for populations living in conflict area of north-east states of Nigeria, South Sudan, Somalia and Yemen (FSIN, 2018). The 2017 UN World Humanitarian report stated that 38 extremely violent political conflicts were ongoing in 2016, increasing the number of refugees and people forcibly displaced: 65.6 million people globally. Most of the world's refugees came from Afghanistan, Somalia, South Sudan, Sudan and Syria. The global number of internally displaced persons-IDPs (40.3 million) continued to be approximately double the number of refugees (22.5 million). Of these countries, the number of refugees from South Sudan increased the most, growing by 64% during the second half of 2016 (UNOCHA, 2017). It is estimated that displaced people spend an average of more than 17 years in camps or with host communities (Von Grebmer *et al.*, 2015).

Therefore, since a CBRN event can be both a direct or indirect threat to any civil society, CBRN advisors should not neglect that food security, proper nutrition, food aid and health services are the minimum essential standards to be ensured to the population in pre and post-CBRN events.

## **2. FOOD SECURITY IN POST-CBRN EVENTS**

### **2.1 Problem Statement**

The first short-term effect of a CBRN event during armed conflicts is loss in human lives. In 2016, 70% of deaths and injuries resulting from explosive weapons were civilian. In populated areas it reached 92%. The use of explosive weapons also results in explosive remnants of war (ERW), which pose a continuing lethal threat, and a major obstacle to reconstruction and the return of displaced persons. In 2016, 86% of deaths and injuries from mines and ERW were civilian (UNOCHA, 2017), but humanitarian aid workers are also exposed to the same risks. Despite the international humanitarian law prohibits attacks, harassment, intimidation and arbitrary detention of humanitarian relief personnel, the global number of aid workers killed, injured, assaulted and arrested increased in 2016 compared with 2015. In 2016, the greatest number of incidents of aid workers killed, injured or kidnapped occurred in Syria, with at least 132 documented incidents. Of the documented weapons used in incidents where aid workers got involved, the use of explosive weapons experienced the greatest increase between 2015 and 2016, moving from 38 to 133 incidents (UNOCHA, 2017). It is clear that attacks against aid workers indirectly affect access to health care



for civilians. Furthermore, in some armed conflicts, health and humanitarian facilities have become targets: clinics have been destroyed, access to hospital restricted, water treatment plants turned to rubble, vaccines and other lifesaving drugs intentionally blocked from reaching civilians. An example has happened in Syria and neighbouring countries where the onset of the civil war led to the complete deterioration of the health infrastructure through the wide destruction of facilities, the shortage in health care personnel and medicines, the lack of secure routes and transportation (Sharara & Kanj, 2014).

Simultaneously, a major emergency results in lack of adequate and safe food and proper nutrition. Impact can be direct (affecting directly food stocks and productive assets) or indirect (driven by economic, social, political and institutional changes). Food security can be threatened from short to long-term by disruption of normal livelihoods and workforce, limited delivery of health and nutrition services, discouragement of economic investments, dependence on emergency aids, displacement and rise in numbers of migrants in both neighbourhood and more distant countries. Access to food or relief foods starts to be scarce: crops can be destroyed and households' movement towards fields restricted, so that farmers are forced to relocate. This highly impacts on food production, trade and access (United Nations, 1993), especially when CBRN events occur in countries mostly based on agriculture. It crowds out normal economic activity such as food production, destroys infrastructure and cuts off access to food supplies, with blocking of food access often used as a tool of political terror (Messer *et al.*, 2002; Collier *et al.*, 2003). Within the households, purchasing power decreases, as well as access to water and fuel for cooking, negatively affecting food preparation, feeding practices and food allocation, all of which contribute to extreme acute food insecurity. Moreover, the increase in military spending and the domestic use of military force will lead to deterioration of food security (Scanlan & Jenkins, 2001).

In these precarious conditions of food shortage, the nutritional emergency suddenly occurs with impaired or jeopardized nutritional status of the population, increased risk of malnutrition and famine. In 2016, the prevalence of undernourishment in countries affected by conflicts was almost 4% higher than countries not affected by conflicts: 489 million out of a total of 815 million chronically undernourished in 2016. This difference is even more pronounced for children: almost 122 million of chronically under age five malnourished children live in countries affected by conflict, with 6% difference in average prevalence between conflict and non-conflict affected countries.

It is also important to consider that a CBRN event can occur accidentally in those emergency contexts, as direct consequence of poor public health strategy, response and services during armed conflict. Medical infrastructures are usually crippled, health system is paralyzed, and the access to facilities is restricted or when referring to crowded refugee camps, infectious diseases and outbreaks could spread quickly, becoming a threat both inside the country and across borders. The infectious diseases worsen even more the already compromised nutritional status of the people affected, with excessive mortality becoming almost inevitable. In Yemen, for example, the targeting of hospitals, clinics, water treatment plants, and sanitation facilities has caused the largest cholera outbreak in the world, with 5,000 new infections every day, more than 200,000 people infected, and 1,300 died before the end of 2017. Refugees and internally displaced persons are particularly vulnerable to risk of infectious disease outbreaks and epidemics, especially in crowded refugee camps with unhygienic conditions (Brinkman & Hendrix, 2011). For example, in the aftermath of the Rwanda crisis in 1994, outbreaks of cholera caused at least 48,000 cases and 23,800 deaths within one month in the Goma refugee camps in Congo.

## **2.2 The Role of CBRN Advisors**

Throughout the last decades, International Organizations (World Health Organization-WHO, United Nations High Commissioner for Refugees-UNHCR, The United Nations Children's Fund-UNICEF, and World Food Programme-WFP) and several non-governmental organizations (NGOs, such as Medecins Sans Frontieres-MSF) have published manuals and guidelines to assist those concerned with preparing for emergencies (WHO, 1999; WHO, 2000; MSF, 1995). "Preparedness" requires that CBRN advisors have knowledge to be effectively ready and capable to respond to those disasters, by guaranteeing the minimum humanitarian and health standards for the affected population.

The Sphere Project Handbook (2001), launched by a group of NGOs, the Red Cross and Red Crescent movement, is a manual designed for humanitarian workers to respond to different situations including natural disasters, conflict, slow and rapid-onset events, rural and urban environments, and complex political emergencies in all countries. This handbook establishes minimum standards for delivering interventions in different contexts (including food and nutrition), with particular regards to the most vulnerable and exposed people, especially when displaced, and refugees. Early identification and caring of the most vulnerable group is in fact essential during first response. Safety nets, by giving basic income support to individuals who were casualties of certain risks, are critical instruments that can mitigate the effect of short-term spikes in food prices on food insecurity, helping to prevent violent conflict and contribute to long-term development (ILO, 2003).

At the beginning of 2013, UN International Agencies and different partners launched the Nutrition Cluster Handbook aimed to provide those involved in nutrition coordination at different levels (i.e. UN agencies, NGOs, national authorities, donors and affected communities) with relevant tools, guidance, information and resources to support their roles in facilitating predictable, coordinated and effective preparation for, and responses to, nutrition needs in humanitarian emergencies. The handbook aims to be applicable across a range of country contexts and different types of emergency, providing guidance in relation to emergency preparedness, activation of the emergency response, and transition out of the emergency phase (The Global Nutrition Cluster, 2013).

In the initial stages of any disaster, there is instability, acute shortage, and mass movement of people, with victims totally dependent on aid. For example, the international humanitarian assistance in the four countries most affected by famine (Nigeria, South Sudan, Somalia and Yemen), contributed to prevent deterioration in food security and nutrition. However, in 2017, almost 32 million food-insecure people were reported to be still in need of urgent assistance across the same four countries (FSIN, 2018). Critical gaps in emergency preparedness result in a cascade of failures, such as interruptions in the chain of delivery for food, water, medicine, and other primary supplies. There are often inevitable delays in evaluation, planning, donations, transport, and formation of distribution system (Singh, 2010). Delayed actions will severely threaten and increase the risk of malnutrition, disease and death. CBRN advisors should be ready to consider and manage the emergence of food insecurity after CBRN events, at short and long-term, trying to facilitate access to food aids and health assistance for curing the malnourished, promoting adequate distribution of food, preventing malnutrition among the most vulnerable. Rapid nutrition assessment followed by systemic surveys and continued monitoring of nutritional conditions (surveillance) are basic activities to food relief programs and further plan (MSF, 1995). Distribution of cooked or ready-to-use food is usually the first short-term measurement, but for longer-term plans there are a lot of aspects to consider other than merely food distribution, such as the availability of necessary arrangements of hygienic environments to prepare and dish out food, or culturally appropriate practices that might not cause offence.

### **3. FOOD SECURITY IN PRE-CBRN EVENTS**

#### **3.1 Problem Statement**

Despite the causes of conflicts are multiple and complex, price spikes in food and civil unrest are correlated. With the increasing level of hunger and undernutrition in countries in fragile situations and those affected by conflicts, it is imperative to have a clearer understanding of the relationship between hunger, conflicts and peace (FAO *et al.*, 2017). In fragile states where socio-economic instability exists, food insecurity can both trigger armed conflicts. Examples of this can be seen throughout history: in 2011, the Arab Spring, which toppled governments in Tunisia, Egypt and Libya, had in food price (sugar, oil, and flour) a consistent motivating factor. The protests in Tunisia, which signaled the start of the Arab Spring domino effect, were initially demonstrations against high bread prices. While public outrage over high food prices was not the only cause, it is actually perceived as an important one (Maystadt *et al.*, 2012). Moreover, a situation of food insecurity contributes both to protract armed conflicts. This is what happened in the Horn of Africa in the 1970s, 1980s, and 1990s, when droughts devastated the already food-insecure and politically-oppressed populations, triggering chronic famines into civil wars.

On the other hand, food can be used as leverage during conflicts: food war is a concept which includes the use of hunger as a weapon in active conflict and leading as a consequence to food insecurity and need of humanitarian assistance. During the so called “Age of Extremes” from World War I to the end of the Cold War, calamitous famines were caused by totalitarian systems and wartime leaders routinely used starvation as a weapon. Combatants frequently use hunger as a weapon: they use siege to cut off food supplies and productive capacities, starve opposing populations into submission, and hijack food aid intended for civilians (Messer *et al.*, 2002). An example is the Ethiopian famines of the 1980s, where the food insecurity of the victims was part of a deliberate Ethiopian state policy of forced resettlement of the opposition, using the food aid selectively as a political tool to reward followers and let others starve (Clay *et al.*, 1988). Hunger can often be a critical element, and rebel groups can offer an alternative livelihood to protect household food security through incentives and promises of improved conditions (FAO *et al.*, 2017). Despite the description of food insecurity as leading to conflict, it is not the whole story, as famine and starvation create and feed the conditions for extremism. Terrorist organizations like al-Qaeda have used food insecurity to recruit and promote their political objectives. As the food crisis worsens, countries such as Somalia, Pakistan, Syria, Nigeria, Iraq, Libya, Lebanon, Egypt, and many others will become more at risk to terrorism and political instability (American Security Project, 2017), a major concern not only for countries directly affected but also a worldwide threat. Famine and starvation create a vicious cycle for conflict, extremism and terrorism that increases the risk of CBRN deliberate attacks or indirect events around the world. Swaminathan (1994) claims that “hunger anywhere threatens peace everywhere”. Despite limited knowledge in regards to the role that food security and nutrition can play in preventing or mitigating conflicts and in potentially contributing to sustaining peace, there is no doubt that a peaceful and stable environment in every country is a fundamental condition for the attainment of sustainable food security (FAO, 2016). It is highly unlikely that food security will improve until there is a resolution to the conflict. Considering things from this prospective, the right to food security could be a key for prevention of armed conflicts, CBRN attacks and their related events.

### **3.2 The Role of CBRN Advisors**

In case of any food emergency, data preparedness is essential to prevent CBRN events. “Preparedness” refers to a minimum set of information standards, tools, sources, partnerships and forums to enable effective and immediate information management. It allows management and use of information immediately following an emergency. Countries that face ongoing emergencies are more likely to have some level of data preparedness, though it is also important to address this issue in countries prone to natural disasters or with a high risk of future crisis (The Global Nutrition Cluster, 2013). There are several systems, databases, and software for early warning of state of food security, such as the FAO GIEWS, the US FEWS NET and the WFP mVAM. Improved early warning and response tools, with technically-advanced use of geographic information systems and satellites plus on-the-ground informants, are part of a deliberate international political strategy to prevent food insecurity and consequent famine, infectious disease outbreaks and civil disruption.

The FAO Global Information and Early Warning System (GIEWS) classifies and regularly updates the list of countries requiring external assistance for food, dividing them into three categories according to the predominant driver: countries with an exceptional shortfall in aggregate food production and supplies, widespread lack of access to food and severe localized food insecurity.

The Famine Early Warning Systems Network (US FEWS NET) is a leading provider of early warning and analysis on acute food insecurity, created in 1985 by the US Agency for International Development (USAID). The NET provides monthly reports and maps detailing current and projected food insecurity; timely alerts on emerging or likely crises.

Both the GIEWS and FEWS NET are based on the Integrated Food Security Phase Classification (IPC). IPC is a set of standardized tools intended to provide a ‘common currency’ for classifying the severity and magnitude of food insecurity emergencies. It is based on a consensus-building process to provide decision makers with a rigorous analysis of food insecurity along with objectives for response in both emergency and development contexts. IPC describes the severity of food emergencies, with five-phase scale to help

governments and other humanitarian actors quickly understand a crisis (or potential crisis) and take action (Figure 1).

PHASE 1 Minimal	More than four in five households (HHs) are able to meet essential food and nonfood needs without engaging in atypical, unsustainable strategies to access food and income.	
PHASE 2 Stressed	Even with any humanitarian assistance at least one in five HHs in the area have the following or worse: Minimally adequate food consumption but are unable to afford some essential non-food expenditures without engaging in irreversible coping strategies.	
PHASE 3 Crisis	Even with any humanitarian assistance at least one in five HHs in the area have the following or worse: food consumption gaps with high or above usual acute malnutrition OR are marginally able to meet minimum food needs only with accelerated depletion of livelihood assets that will lead to food consumption gaps.	<b>URGENT ACTION REQUIRED</b>  <b>!</b>  Phase classification would likely be worse without current or programmed humanitarian assistance.
PHASE 4 Emergency	Even with any humanitarian assistance at least one in five HHs in the area have the following or worse: large food consumption gaps resulting in very high acute malnutrition and excess mortality OR extreme loss of livelihood assets that will lead to food consumption gaps in the short term.	
PHASE 5 Famine	Even with any humanitarian assistance at least one in five HHs in the area have an extreme lack of food and other basic needs where starvation, death, and destitution are evident. Evidence for all three criteria (food consumption, acute malnutrition, and mortality) is required to classify Famine.	

**Figure 1: IPC area phase classification (Source: FEWS NET, 2017).**

The WFP Mobile Vulnerability Analysis and Mapping (WFP mVAM) is a real-time food security delivering data system through mobile technology. It is currently a tool for monitoring food security through phone calls to key informants and households. Respondents are asked short questions on demographics, market prices, food availability, food assistance, household food consumption and nutrition, negative coping strategies, and primary food sources. Respondents are also given the opportunity to report on the food security situation in their households and communities.

The WFP mVAM and the FAO GIEWS initiated a joint project in 2009 and developed the Shock Impact Simulation Model (SISMod) to assess the food security situation in low-income food deficit countries. SISMod is a macroeconomic modelling system which brings new possibilities to allow timely quantitative assessments on the ex-ante and ex-post impact of various types of shocks (market, economic, climatic) on livelihood and food security. It identifies and profiles the vulnerable groups, and estimates to what extent they are in need, providing early estimates of the impacts of shocks before field assessments are carried out, informing the initial development of response scenarios. For example, in 2015 it was used to model most likely scenario for the conflict in Yemen in the near future. The model predicted that the depth of hunger for 2016 would have increased by 110%, and the food-insecure population would have reached 16.6 million, 47% more than before the crisis and up by 2.5 million compared to the latest IPC. The worst-case scenario estimated that the food-insecure population would have been increased by 89%, leaving 21 million people (77% of the population) food insecure, with the depth of hunger tripling: not so far from recent data of 60% of the entire population reported at the beginning of 2017.

## **4. EVIDENCES FROM THE FIELD**

### **4.1 The Case of South Sudan**

In 2018, South Sudan's civil war entered its fifth year. Armed conflict is destroying rural livelihoods, forcing many farmers to relocate, decimating assets, deepening poverty and increasing the vulnerability of millions of people (FAO *et al.*, 2017). Since the start of the conflict, almost 2 million people have been internally displaced, and another 2 million have sought refuge in neighbouring countries with more than 230,000 people sheltering in UN countries (Human Right Watch, 2017). The delivery of health and nutrition services have been disrupted, several aid agencies have been forced to relocate. The Government has declared the state of emergency: emergency humanitarian assistance continues to be delivered to around 2.5 million people a month and this assistance is preventing more extreme outcomes in many areas, although the reach of assistance is under 50% of the estimated population in need.

The UN described South Sudan as one of the world's most dangerous places for aid workers: at least 83 killed since the conflict started in December 2013, 16 in 2017 (Human Right Watch, 2017). Despite an agreement for the Cessation of Hostilities (COH) was signed in December, armed conflicts continue in most of the area. Crisis (IPC Phase 3) and Emergency nutrition (IPC Phase 4) outcomes persisted in all regions of South Sudan in January 2018, with some households declaring famine, with serious risk of Catastrophe (IPC Phase 5) in a worst-case scenario of an extended absence of humanitarian assistance. In fact, it is expected most households to deplete their stocks three months earlier than was typical in pre-crisis years. Famine (IPC Phase 5) has occurred with at least 20% of households having extreme lack of food.

#### **4.2 The Case of Syrian Arabic Republic**

The Syrian crisis has entered the seventh years, claiming hundreds of thousands of lives and injuring countless civilians. It is a complex, internationalized conflict, with various armed groups in control of much of the country. Food security in Syria has plummeted since the beginning of the conflict in 2011. Formerly a vibrant middle-income economy, 85% of the population now live in poverty, of which 69% live in extreme poverty, meaning they are unable to cover their basic needs, including food (UNOCHA, 2016). Numbers of people already declared food-insecure or those at risk of food insecurity rise day after day. In 2016, an estimated 6.7 million people were acutely food insecure and in need of urgent humanitarian assistance, while the prevalence of acute malnutrition was at increased levels in most areas (7 %). Over the course of 2017, an average of 5.2 million people benefitted from UN food assistance on a monthly basis. Years of conflict have had a cumulative destructive effect on the economy, infrastructure, agricultural production, food systems and social institutions. Many food markets are controlled by powerful groups, leading to steadily increasing prices: in the besieged city of Deir Ezzur, a bag of sugar has reached the cost of over US\$450. These have resulted in people adopting negative coping strategies: some 50% of Syrian households have reduced the number of daily meals and more than 30% have restricted the consumption of adults to prioritize children (FSIN, 2018). Families are forced particularly to cut out protein-rich and dairy products from their diets, and most have to reduce portion sizes, eating only one or two meals a day (FAO *et al.*, 2017). The overall food consumption deteriorated in the first half of 2018, where 30% of the surveyed Syrian households (almost one in three) reported poor and borderline food consumption. At governorate level, the sharpest increase in inadequate food consumption was seen in Dar'a, from 21% in May to 40% in June (WFP Syria, 2018).

As safety nets were not provided for these farmers, the only recourse for most became migration to urban areas. As a results, the largest increases in food insecurity numbers were reported for the governorates of Quneitra, Dar'a, Damascus, Idleb and Aleppo, all affected by large population movements since late 2015 due to an escalation of conflict, as well as by market price changes and food shortages. In mid-2016, Aleppo alone registered a 24% increase in the number of people at risk of food insecurity. Particularly acute food insecurity conditions among people living in besieged and hard-to-reach areas, where food supplies are extremely limited and where the population largely relies on food assistance. In late September 2016, the humanitarian and security situation in Eastern Aleppo City (EAC) became extremely worrying following an unprecedented escalation of violence: the number of civilian casualties increased drastically as well as damaged civilian infrastructure, including hospitals. Humanitarian aids could not have access to the EAC or provided assistance since July 2016: in November 2016 an estimated 275,000 people were trapped inside EAC (FSIN, 2017).

Concerns for hunger and malnutrition are growing nationwide since it can affect anyone, from the thousands of people still trapped in the besieged enclave, to people who managed to leave. In fact, since 2011, there has been a continuous exodus of Syrians seeking to escape the conflict: more than 6 million people remain displaced inside the country, with another 5 million Syrian refugees living in the nearest countries (Egypt, Iraq, Jordan, Lebanon, Turkey). The majority of Syrian refugees in the five main host countries rely on humanitarian assistance to meet their basic needs, and assistance is their primary source of food. After almost seven years of displacement, assessments reveal an alarming deterioration in refugee food security. In Lebanon, 36% of refugees are food insecure; in Turkey almost 30%; in Egypt 61% of households are severely economically vulnerable; in Jordan 72% of Syrian refugees are either food insecure or vulnerable to food insecurity (FAO *et al.*, 2017).

### 4.3 The Case of Iraq

Although in December 2017 the Government of Iraq declared victory over the Islamic State of Iraq and the Levant -ISIL, the impact of the protracted conflict on food insecurity remains severe: 3.2 million people are facing hunger, especially those depending on agriculture for their livelihoods (FAO *et al.*, 2017). Conflict has damaged the food security of the Iraqi population in different ways: the loss of assets, disruption to livelihoods and lack of employment opportunities represent the major drivers. People were forced to abandon farms, damaging harvests, equipment, supplies, livestock, seeds, crops and stored food. Infrastructures such as water supplies for agricultural and domestic use have been damaged or destroyed. A large part of the cereal production belt is now directly under the control of rebel forces, affecting access to agricultural activities. In addition to food shortages, the escalating conflict has caused severe fuel scarcity, damaging market functionality and sustaining higher local prices, limiting food access for the most vulnerable. Families report limited livelihood opportunities, which reduce their purchasing power and restricts their access to the social safety net that entitles Iraqis to receive rations of flour, rice and cooking oil from the government. Heavy contamination of retaken areas with unexploded ordnance and improvised explosive devices poses immediate and long-term risks for the environment and the people.

According to WFP's mVAM monitoring system, food insecurity is higher in districts affected by conflict and displacement: since violence erupted, over 3 million people have become internally displaced. Most IDPs are in camps to the east and south of Mosul in Ninewa, Erbil and Anbar governorates and in host communities. Employment and livelihood opportunities are more challenging for people living inside camps compared to those in host communities. The International Organization for Migration in Iraq estimates that, since the start of the crisis in 2014, more than 3 million were displaced (IOM Iraq, 2017). As of 31 August 2018, there are more than 4 million Iraqis -670 thousand families- who have returned to their home location and still nearly 2 million IDPs -320 thousand families identified (IOM Iraq, 2018).

Humanitarian needs will remain severe, particularly for displaced families inside and outside the camps, for vulnerable residents of retaken communities and people fleeing intense fighting. Meanwhile, security issues will continue to hamper access for humanitarian assistance to those in need, further diminishing their food security. Vulnerable residents of newly retaken areas are also expected to face severe shortages of basic goods and medical services (FAO *et al.*, 2017). In the long term, access to agricultural land will be reduced by the high number of unexploded ordnance and mines laid by ISIL, even in liberated areas. Violent clashes between Iraqi and Kurdish forces could escalate even more in the territories disputed between the Kurdistan Region of Iraq (KRI) and the Iraqi central government in Baghdad. The potential for localized violence will remain until Iraqi authorities and the Kurdistan Regional Government resolve the status of the contested territories and the disputes over oil revenues. The planned humanitarian response for 2018 includes assisting up to 400,000 newly or repeatedly displaced people fleeing asymmetric attacks and unstable areas, but it is highly likely that additional people will require humanitarian assistance (FSIN, 2018).

### 4.4 The Case of Yemen

Since the breakout of conflict in Yemen in March 2015, over 10,000 people have been killed, approximately 4,000 of them civilians, and more than 3 million Yemenis are internally displaced as of January 2017 (IPC, 2017). The Yemen ongoing conflict is having devastating effects on food security, population displacement, economy, agricultural- including for the fisheries and livestock sectors, disruption of infrastructure, services, markets and livelihoods. The conflict-induced crisis has been devastating for the country, aggravating the already fragile socio-economic context and causing unprecedented levels of undernutrition. Before the outbreak of the conflict, more than 50% of the Yemeni population was already living under the national poverty line, but after the beginning of the conflict, the entire social protection system has collapsed, with a suspension of safety nets to 1.5 million beneficiaries through the Social Welfare Fund since 2015 (WFP, 2016). A 20% increase in food insecurity has been registered from June 2016 and a 47% from June 2015 (IPC, 2017), with an estimated 17 million people experiencing severe food insecurity in March 2017 (IPC Phases 3 and 4) and requiring urgent humanitarian assistance. An additional 8.2 million people were estimated to be in Phase 2 Stressed in 2016 (FSIN, 2017).

The Yemen Emergency Food Security and Nutrition Assessment (WFP/FAO/UNICEF Joint EFSNA, 2016) confirmed that acute malnutrition was at alarming levels in 2015, with 10 out of the 22 governorates classified under emergency phase IPC 4. The last FAO Yemen country report (2017) claims that more than 60% of households have adopted strategies such as reducing portions, eating less favoured foods or skipping meals altogether; more than 80% of Yemenis are in debt, and more than 50% of households are buying food on credit. Chronic child undernutrition (stunting) has been a serious problem for a long time, but acute undernutrition (wasting) has peaked in the last three years, reaching above the emergency threshold of 15% (FAO *et al.*, 2017).

The alarming level of food insecurity is expected to deteriorate further: Yemen relies on imports for more than 90% of its staple foods, but port infrastructure, essential for ensuring food imports and humanitarian assistance, are seriously threatened by the worsening conflict. Restrictions coupled with fuel shortages have reduced the availability of essential commodities. The annual inflation rate has increased to over 30%, pushing average consumer prices 70% above pre-crisis levels. With both urban and rural communities relying on markets on a daily basis, increases in the cost of food, cooking fuel, water and medicine heavily undermine food access and utilization. The nutrition situation has been aggravated by the dramatic breakdown of the health care system and its infrastructure: an outbreak of cholera and other epidemics started in 2016 has affected several governorates and was still continuing in 2017 (WHO, 2015).

## 5. CONCLUSION

Ensuring food security is a complex and timely operation, often underestimated or taken too late into consideration in pre and post-CBRN events. Eliminating hunger is not just a moral imperative: it also makes economic sense, have impact on political stability, nationally and internationally and can be one of the key to prevent CBRN events.

Unfortunately, up to now food security has not been at the centre of the conversation as to how to prevent and deal with CBRN events, therefore this matter will continue to be a critical issue. In all the countries where conflicts will be the primary drivers of food security crises during 2018, in addition to direct loss of life, disruption of agricultural production, trade and market is expected, requiring the intervention of even more humanitarian assistance. Moreover, vulnerable people will continue to be internally displaced and to seek refuge in neighbouring countries increasing the risk of malnutrition and infectious diseases outbreaks, especially when overcrowding occurs.

Considering this complex context, well trained CBRN advisors, with specific competence in nutrition and public health, are essential for prevention, management and restoration of unintentional and intentional food security and health related CBRN events. This opens the door to a necessary and concrete debate among the experts in the field, since CBRN advisors need to be prepared and set specific strategy for early recovery by guaranteeing the minimum humanitarian and health standards, and also to reduce future risks in all different scenarios involving food security in pre and post-CBRN events.

## REFERENCES

- Abate, A., Sassolini, A., Ludovici, G. M., Gaudio, P., Ciparisse, J.F., Cenciarelli, O., Gallo R., Carestia M.C., Di Giovanni D., Iannotti A., Strigari L., Palombi L., Bellecci C. & Malizia, A. (2016). The local effects of a global disaster: Case study on the Fukushima radiological emergency management in Italy. *Defence S&T Tech. Bull.*, **9**: 126-133.
- American Security Project (2017). *Food Insecurity is a Counterterrorism Problem*. Available online at: <https://www.americansecurityproject.org/food-insecurity-is-a-counterterrorism-problem> (Last access date: April 2018)
- Brinkman, H.J. & Hendrix, C.S. (2011). *Food Insecurity and Violent Conflict: Causes, Consequences, and Addressing the Challenges*. World Food Programme (WFP), Rome.
- Ciparisse, J.F., Malizia, A., Poggi, L.A., Cenciarelli, O., Gelfusa M., Carestia, M.C., Di Giovanni,D., Mancinelli, S., Palombi, L., Bellecci, C. & Gaudio, P. (2016). Numerical simulations as tool to predict

- chemical and radiological hazardous diffusion in case of nonconventional events. *Model. Sim. Eng.*, **Vol. 2016**: 6271853
- Clay, J., Steingraber, S. & Niggli, P. (1988). *The Spoils of Famine: Ethiopian Famine Policy and Peasant Agriculture*. Cultural Survival: Cambridge, Massachusetts.
- Collier, P., Elliot, L., Hegre, H., Hoeffler, A., Sambanis, N. & Reynal-Querol, M. (2003). *Breaking the Conflict Trap: Civil War and Development Policy*. Oxford University Press, Oxford.
- FAO (2002). Food, security, justice and peace. *World Food Summit*, 10-13 June 2002, Rome.
- FAO (2016). *Peace, Conflict and Food Security What do we know about the linkages?* Food and Agriculture Organization (FAO), Rome.
- FAO, IFAD, UNICEF, WFP & WHO (2017). *The State of Food Security and Nutrition in the World 2017: Building Resilience for Peace and Food Security*. Food and Agriculture Organization (FAO), Rome.
- FAO (2017). *Yemen Situation Report, February 2017*. Food and Agriculture Organization (FAO), Rome.
- FEWS NET (2017). *Overview of the Integrated Phase Classification (IPC)*. Famine Early Warning Systems Network (FEWS NET), Washington D.C.
- FSIN (2017). *Global Report on Food Crisis 2017*. Food Security Information Network (FSIN), Food Security Information Network (FSIN), Saskatchewan, Canada
- FSIN (2018). *Global Report on Food Crisis 2018*. Food Security Information Network (FSIN), Food Security Information Network (FSIN), Saskatchewan, Canada.
- Human Right Watch (2017). *World Report 2018: Events of 2017*. Human Rights Watch, New York.
- IASC (2007). *Operational Guidance on Designating Sector/Cluster Leads in Major New Emergencies*. Inter-Agency Standing Committee (IASC), Geneva.
- ILO (2003). *Social Protection: A Life Cycle Continuum Investment for Social Justice, Poverty Reduction and Sustainable Development*. International Labour Office (ILO), Geneva.
- IOM Iraq (2017). *Integrated Location Assessment II – Part 1: Thematic Overview*. International Organization for Migration (IOM), Le Grand-Saconnex, Switzerland.
- IOM Iraq (2018). *Displacement Tracking Matrix DTM Round 102*. International Organization for Migration (IOM), Le Grand-Saconnex, Switzerland.
- IPC (2017). *Republic of Yemen: IPC Analysis - Summary of Findings*. Intergrated Food Security Phase Classification (IPC), Geneva.
- Malizia, A. & 2013/2014 CBRNe Masters Group (2016). Disaster management in case of CBRNe events: an innovative methodology to improve the safety knowledge of advisors and first responders. *Defense Secur. Anal.*, **32**: 79-90.
- Maystadt, J.F., Tan, T. & Breisinger, C. (2012). Does food security matter for transition in Arab countries? *IFPRI Discussion Paper 01196*. International Food Policy Research Institute, Washington D.C.
- Messer, E., Cohen, M.J. & Marchione, T. (2002). Conflict: A cause and effect of hunger in environmental change and security program, *ECSP Rep.*, **7**: 1–20.
- MSF (1995). *Nutrition Guidelines*. Medecins Sans Frontieres (MSF), Brussels.
- Perez, I. (2013). *Climate Change and Rising Food Prices Heightened Arab Spring*. Available online at: <https://www.scientificamerican.com/article/climate-change-and-rising-food-prices-heightened-arab-spring> (Last access date: May 2018).
- Scanlan, S.J. & Jenkins, J.C. (2001). Military power and food security: A cross-national analysis of less-developed countries, 1970–1990. *Int. Stud. Q.*, **45**: 159–187.
- Sharara, S., & Kanj, S. (2014). War and Infectious Diseases: Challenges of the Syrian Civil War. *Plos One*
- Singh, S.N. (2010). Nutrition in emergencies: Issues involved in ensuring proper nutrition in post-chemical, biological, radiological, and nuclear disaster. *J. Pharm. Bioallied Sci.*, **2**: 248–252.
- Swaminathan, M.S. (1994). *Uncommon Opportunities: An Agenda for Peace and Equitable Development*. Report of the International Commission on Peace and Food, London.
- The Global Nutrition Cluster (2013). *Nutrition Cluster Handbook: A Practical Guide for Country-Level Action*. United Nations Children's Fund (UNICEF), Geneva.
- The Sphere Project (2001). *Humanitarian Charter and Minimum Standards in Disaster Response*. The Sphere Project, Geneva
- United Nations (1993). *World Economic Survey, 1993*. United Nations, New York.
- UNOCHA (2016). *Humanitarian Needs Overview 2017: Syrian Arab Republic*. United Nations Office for the Coordination of Humanitarian Affairs (UNOCHA), New York.
- UNOCHA (2017). *World Humanitarian Data and Trends*. United Nations Office for the Coordination of Humanitarian Affairs (UNOCHA), New York.



- Von Grebmer, K., Bernstein, J., de Waal, A., Prasai, N., Yin, S., & Yohannes, Y. (2015). *2015 Global Hunger Index: Armed Conflict and the Challenge of Hunger*. International Food Policy Research Institute (IFPRI), Washington, D.C.
- WFP (2016). *Fighting Hunger Worldwide: Special Focus Yemen*. World Food Programme (WFP), Rome.
- WFP/FAO/UNICEF Joint EFSNA (2017). *Yemen Emergency Food Security and Nutrition Assessment: Concept Note*. World Food Programme (WFP), Rome.
- WFP Syria (2018). Syria mVAM Bulletin 26: June 2018. <https://docs.wfp.org/api/documents/WFP-0000073848/download/>. Accessed October 2018
- WHO (1999). *Community Emergency Preparedness: A Manual for Managers and Policy-Makers*. World Health Organization (WHO), Geneva.
- WHO (2000). *The Management of Nutrition in Major Emergencies*. World Health Organization (WHO), Geneva.
- WHO (2015). Health system in Yemen close to collapse. *Bull. WHO*, **93**: 670 - 671.

## FIRST RESPONDER CBRN - 9-LINER POCKET RESPONSE CARD

Patrick Wengler<sup>1\*</sup>, Orlando Cenciarelli<sup>1,2</sup>, Gian Marco Ludovici<sup>1</sup>, Andrea Duggento<sup>3</sup>, Maria Guerrisi<sup>3,4</sup>, Andrea Malizia<sup>1,3</sup> & Pasquale Gaudio<sup>1,2</sup>

<sup>1</sup>International Master Courses in Protection against CBRNe Events, University of Rome Tor Vergata, Italy

<sup>2</sup>Department of Industrial Engineering, University of Rome Tor Vergata, Italy

<sup>3</sup>Department of Biomedicine and Prevention, University of Rome Tor Vergata, Italy

<sup>4</sup>Università Cattolica Nostra Signora del Buon Consiglio, Tirana, Albania

\*Email: wengler\_patrick@vo.lu

### ABSTRACT

The nine lines or points related to Chemical, Biological, Radiological and Nuclear agents (CBRN) pocket response card represents a quick form that the operator can entirely fill with critical information of his investigation during the 5-10 first minutes after his arrival on the scene. The idea is, that, in a very short time, all the necessary information will be shared directly with other emergency services or emergency management services, so that everybody is aware of what they are dealing with, and what kind of equipment and personnel needs to be deployed or dispatched. This card is intended to implement a harmonized model of information flow between first responders, being able to act more quickly in prevention, first aid, and managing the incident at the scene, whether it is an act of terrorism, traffic accident or standard industrial incident. The card will be available for different emergency services, such as police, fire department, civil protection units and emergency first responders. This will help to integrate the different missions that every single emergency management system (EMS) unit has to cover.

**Keywords:** Chemical, Biological, Radiological and Nuclear (CBRN); Hazardous Material (HAZMAT); response card; first responder; emergency management system (EMS).

### 1. INTRODUCTION

Looking at the developing threats of Chemical, Biological, Radiological and Nuclear (CBRN) / Hazardous Material (HAZMAT) incidents (Interpol, 2017), it is important for first responders to have basic knowledge of CBRN / HAZMAT response and the related possible complications. Moreover, first responders should also have basic knowledge of decontamination and personal protective equipment (PPE). With adequate basic knowledge of CBRN / HAZMAT response, the adoption of the CBRN / HAZMAT 9-liner pocket response card and a minimal amount of training, first responders would be capable of communicating in a fast and easy way the required information for an appropriate action plan and the right dispatch of units during a CBRN / HAZMAT incident.

During an incident or attack occurring with CBRN agents, having the right information at an early stage is crucial (Garcia *et al.*, 2011), since it involves the agent implicated in the event, and to determine if it is a terrorist attack or just an accident. At the same time, it will also specify which protective equipment needs to be worn for first responders rushing in. In this regard, to better analyze the difference between deliberate attack or accident in a CBRN incident, it is important to define what are CBRN threats (CEEP, 2017).

CBRN agents are weaponized or non-weaponized chemical, biological, radiological and nuclear agents that if used for terrorist purposes could cause extensive damage to both the population and

infrastructure. Weaponized materials can be used to create conventional weapons (e.g., bombs), improve and enhance existing explosives (e.g., mixtures of fuels and fertilizers), or advanced and enhanced conventional weapons (e.g., dirty bombs) (Cavallini *et al.*, 2014). Generally, non-weaponized materials are classified as Dangerous Goods (DG) or HAZMAT, and can include contaminated food, livestock and crops (Pellegrino *et al.*, 2012). An accidental CBRN incident may result from human error, tainted food products, technological failure or a natural disaster, and may include spills, leaks or airborne releases. These accidents are usually identified as DG (dangerous goods) or HAZMAT incidents (Pellegrino *et al.*, 2012). Contrarily, intentional releases of hazardous materials are deliberate criminal acts, such as for example: purposeful dumping of chemicals or radioactive waste by industries to avoid regulatory requirements, or any kind of terrorist acts using CBRN agents (Santella & Steinberg, 2011). Despite the fact that the response to a CBRN incident whether intentional or accidental always remains the same, intentional CBRN incidents also imply special conditions related to territorial responsibility, public security and international relations (Coppola, 2006). Whether accidental or intentional, the impact of a CBRN event can be significant.

The necessary information gathered during CBRN / HAZMAT events may come from various sources, such as intelligence services or any other civilian emergency response unit (Jalalzai, 2016). Most of the time, the first person on the scene (referred to as the first responder) has no special equipment or training to deal with a CBRN / HAZMAT incident (HENDON, 2017). While arriving on scene, the first responder receives a basic set of information from the dispatcher. Frequently, arriving on the scene, the first responder realizes that the information received is not complete and important parts are missing. This usually happens because the citizen who called in was in shock or in fear, and missed out on communicating important information. The CBRN / HAZMAT 9-liner pocket response card will contribute to overcome these problems and it will help the first responders to gather all necessary information and be able to:

- i) Protect himself correctly;
- ii) Communicate important information;
- iii) Create, adapt security perimeter;
- iv) If possible, and necessary, evacuate and rescue citizens.

This paper will discuss on the items in the response card and their importance, as well as the training and knowledge required by first responders to fill up the card.

## **2. CBRN RISKS**

### **2.1 Chemical**

A chemical is considered hazardous if it has high levels of toxicity, flammability, and reactivity, causing potential damage to organs and tissues. Exposure to these substances can occur via inhalation, skin contact, ingestion or injection. Hazardous chemicals (e.g., toxic industrial chemicals - TICs) that may be dispersed in environment accidentally include petroleum substances (e.g., gasoline, liquid, natural and gases) and those used at industrial level (e.g., pesticides and chlorine) (Michałowicz & Duda, 2007). Chemical weapons released deliberately are often classified according to their effect on organisms. Nerve gases (e.g., SARIN, VX, and VR) enter the body through skin contact or inhalation, attacking the nervous system (Ganesan *et al.*, 2010). Lung irritants (e.g., chlorine and phosgene) are inhaled and cause serious damage to the respiratory system. Vesicants (e.g., mustard gas) damage the skin, and if they are absorbed can also affect other areas of the body. Depending on the severity and duration of exposure, the effects may include temporary illness or injury, permanent complications or death (Ganesan *et al.*, 2010).

## **2.2 Biological**

Biological warfare agents (BWA) achieve their intended effects due to the dispersion in the environment of microorganisms (e.g., viruses and bacteria) or toxins, and the consequent possibility to cause a communicable disease in affected people (except for toxins, which are not infectious) (Cenciarelli *et al.*, 2013). These events include natural spread of an infectious disease (e.g., influenza and SARS epidemics, or Ebola virus disease outbreak in West Africa in 2014) (Cenciarelli *et al.*, 2015), accidental dispersion of an agent (e.g., an accident in a laboratory where normally an agent is used), or intentional release as a terrorist act (e.g., letters containing anthrax spores, USA 2001) (Ludovici *et al.*, 2015). The main characteristic of the biological agents is their capacity to multiply in a host over time. The disease that ensues is the result of interaction between the biological agent, host (including the immune status of the host) and the environment (e.g., sanitation and population density) (Eisenberg *et al.*, 2007). Intentional release of aggressive biological agents aims to strike a large number of people, causing serious illnesses and spreading infections (Ludovici *et al.*, 2015).

## **2.3 Radiological**

Radiological risks occur due to exposure to excessive doses of harmful radiation (open sources). External radiation occurs when the radioactive material, in liquid or powder form, enters into contact with the skin or the clothes of the individual, while the internal contamination occurs with the ingestion / inhalation of radioactive substances (Rojavin *et al.*, 2011). Accidental radioactive sources include natural underground reserves (e.g., uranium or radon gas) or leakage from facilities storing radioactive waste (e.g., spent fuel from nuclear power plants) (Barnett *et al.*, 2006). In contrast, intentional releases may result from the radiological dispersal devices (RDDs), (e.g., dirty bombs), which trigger explosions that disperse radioactive material in the environment; or radiological exposure devices (REDs), which do not cause explosions but are hidden sources of radioactivity designed to unknowingly expose people to radiation (Barnett *et al.*, 2006). The effects of radiation on health depend on many factors, including the source, amount of emitted radiation and exposure duration. Significant exposure concentrated in a short time can cause acute radiation illness and even death. Instead, low long-term exposures (e.g., during working life) increases the likelihood of developing chronic diseases, including various forms of cancer (Scott, 2004).

## **2.4 Nuclear**

Nuclear accidents are those that directly result from the detonation of a nuclear device or from accidents that may occur in a nuclear power plant (e.g., Chernobyl and Fukushima), and the related release of large amounts of energy, resulting in the dispersion of a large amount of radiation, pressure, and heat (Bushberg *et al.*, 2007). Nuclear accidents have the potential to cause catastrophic loss of lives and destruction of infrastructure (Will, 2011). Fortunately, nuclear weapons that various terrorist groups could obtain are relatively small, because of the great difficulties in obtaining a substantial quantity of radioactive material (Ferguson, 2005).

## **2.5 Psychological Warfare Related to a Terror Attack**

A terrorist attack can be defined as any kind of incident that aims to terrorize and spread fear into the population. The intentional use of CBRN materials may create great panic and fear and the population may become violent while trying to survive. Such scenarios imply massive casualties to civilian life and property (Crenshaw, 2011; Kiras, 2014).

### 3. CBRN / HAZMAT 9-LINER POCKET RESPONSE CARD

The CBRN / HAZMAT 9-liner pocket response card is firstly directed to law enforcement officers, who have no specialized training on CBRN / HAZMAT. Since it is crucial to receive all the needed information as fast as possible during a CBRN / HAZMAT event, this paper includes a description of the card that could be used to help gather all essential information to evaluate the situation. Thanks to this simple card, the emergency response dispatcher will be able to delegate the right and necessary units to the incident / attack. The response card (Figure 1) may be used for various emergency management system (EMS) services. The distinction can be made upon the color on the upper part of the chart (Table 1).

Figure 1: The 9-liner response card.

Table 1: Color of the card and emergency services related.

Color	Service
Dark Blue	Police
Red	Firefighters
Orange	Civil Protection
Clear Blue	Health Emergency Services
Green	Military

The first line in the card is important to know the exact time when the incident happened. This could be very useful to perform calculations on spreading or mutation of the agent over time, or the level of intoxication that could be present. At the same time, this information may be used later on for police investigations and report writing. The second line indicates where the agent was found or released. This would help to know how to control the contaminated area or the eventual need for packing

equipment. This information will also be used to make the necessary calculations on what the dispersion zones could be, facilitating the elaboration of an evacuation plan.

The third line is devoted to the agent that has been used if the conducted investigation was a success. This will help in using the adequate PPE and the right medical response. If the agent is unknown because there are no labels present giving some indications, the box unknown on the chart may be ticked. However, the chart also offers the possibility to insert the signs and symptoms observed, in case some characteristic of the agent's effect could help to define the agent implicated. This information is important so that the right decontamination product can be chosen and applied. The fourth line indicates the number of casualties. This will help to dispatch enough ambulances, and also give the hospitals enough time to prepare for large amounts of patients. If the first responder is unable to investigate the agent that was used while observing and writing down observed symptoms, the medical personnel has time to advise and prepare accordingly to the agent involved with antidotes or medical counter measures. Not only will this information help medical personnel to be prepared from a logistical point of view, it also gives the required information for choosing the right level of PPE for the response.

The fifth and sixth lines include important information that need to be communicated. Depending on what area the incident happened, the weather may have greater implications on the incident. This will help, together with all the other accumulated information, to calculate the contaminated zone, evacuation zones and perimeter security that needs to be set in place; PPE that needs to be handed out; and what information should be given to the citizens to protect themselves. Knowing the three different states of agents (solid, liquid and gas), every product has its own boiling point (BP), where it may change its physical characteristics. Depending on the temperature present, and the known agent or product involved, the necessary actions can be taken to avoid the boiling being reached to prevent further damage, or health and safety issues for the surrounding areas.

The seventh line is a reminder to write down who was contacted and gave orders, so that later on when the report needs to be written, the correct person of contact (POC) is written down. This will help to make it easier for the follow-up. The eighth line gives an indication of which units were involved. This may help in administrating afterwards the right information, debriefing or request to the right unit. The ninth point is designed on the principle of the sandbox. The first responder can draw in all the related information, and make adequate changes as soon as they appear. In doing so, the first responder always has the information up to date, and is able to provide at any moment the right ones. This point is like a sandbox, where all the additional information is drawn on the 3-layer zone system, including wind direction, staging area, distance of the spill / contamination, decontamination line, emergency line and decontamination corridor.

#### **4. TRAINING & KNOWLEDGE NEEDED FROM EMS OPERATORS TO FILL IN THE RESPONSE CARD**

The training required for operators would be a very short and time-saving education, getting them all the basic knowledge they need, using the referenced material, such as the Emergency Response Guidebook (ERG) (Brown & Dunn, 2007), helping them to select the right PPE (personal protective equipment), since the safety of the operator on scene comes first (PAHMS, 2016). The selection of the right PPE can avoid contamination, and secure the health and safety of the operator.

**Defining zones.** Getting to know the 3-layer zone system, (N. J. S. P., 2016) and what would be set in place for contaminated casualties, the operator could not just only send in the correct information but also prepare the zone depending on weather conditions (Reason, 2016).

**Predicting the weather in sight.** The operator would receive basic knowledge on assessing the wind from the ground by having some very low-cost wind measurement tools. Basic knowledge on wind

strength measurements while observing its surroundings by using, for example, Swiss military weather kit (Gasic *et al.*, 2009).

**Hazardous material.** The training and education needed for the operator are basic knowledge of the different dangerous goods regulations classes (DRG) (PAHMS, 2016) and their health and safety issues they can face in any kind of accident or incident. (N. J. S. P., 2016).

## 5. CONCLUSION

The 9-liner pocket response card presented in this work and the right training dedicated to it would be a very good basic knowledge for operators responding to any kind of CBRN / HAZMAT incident, by being able to do very a quick and correct scene assessment, and setting up the needed security and safety parameters. This card and its combined training would be a strong tool to helping to save and protect lives quicker and faster in cost effective manner.

## REFERENCES

- Barnett, D.J., Parker, C.L., Blodgett, D.W., Wierzba, R.K. & Links, J.M. (2006). Understanding radiologic and nuclear terrorism as public health threats: preparedness and response perspectives. *J. Nucl. Med.*, **47**: 1653-1661.
- Brown, D.F. & Dunn, W.E. (2007). Application of a quantitative risk assessment method to emergency response planning. *Comput. Oper. Res.*, **34**: 1243-1265.
- Bushberg, J.T., Kroger, L.A., Hartman, M.B., Leidholdt, E.M., Miller, K.L., Derlet, R. & Wraa, C. (2007). Nuclear/radiological terrorism: emergency department management of radiation casualties. *J. Emerg. Med.*, **32**: 71-85.
- Cavallini, S., Bisogni, F. & Mastroianni, M. (2014). Economic impact profiling of CBRN events: focusing on biological incidents. *Arch. Immunol. Ther. Exp.*, **62**: 437-444.
- CEEP (2017). *What is CBRN?* Centre for Excellence in Emergency Preparedness (CEEP), Ontario.
- Cenciarelli, O., Pietropaoli, S., Malizia, A., Carestia, M., D'Amico, F., Sassolini, A., Di Giovanni, D., Rea, S., Gabbarini, V., Tamburrini, A., Palombi, L., Bellecci, C. & Gaudio, P. (2015). Ebola virus disease 2013-2014 outbreak in West Africa: an analysis of the epidemic spread and response. *Int. J. Microbiol.*, **Vol. 2015**: 769121.
- Cenciarelli, O., Rea, S., Carestia, M., D'Amico, F., Malizia, A., Bellecci, C., Gaudio, P., Gucciardino, A. & Fiorito, R. (2013). Bioweapons and bioterrorism: a review of history and biological agents. *Defence S&T Tech. Bull.*, **6**: 111-129.
- Coppola, D.P. (2006). *Introduction to International Disaster Management*. Elsevier, Amsterdam.
- Crenshaw, M. (2011). *Explaining Terrorism*. Routledge, Abingdon Oxon, Oxfordshire
- Eisenberg, J.N.S., Desai, M.A., Levy, K., Bates, S.J., Liang, S., Naumoff, K. & Scott, J.C. (2007). Environmental determinants of infectious disease: a framework for tracking causal links and guiding public health research. *Environ. Health Perspect.*, **115**: 1216-1223.
- Ferguson, C.D., Potter, W.C. & Sands, A. (2005). *The Four Faces of Nuclear Terrorism*. Routledge, Abingdon, UK.
- Ganesan, K., Raza, S.K. & Vijayaraghavan, R. (2010). Chemical warfare agents. *J. Pharm. Bioallied Sci.*, **2**: 166.
- Garcia, A.F., Rand, D. & Rinard, J. (2011). *IHS Jane's CBRN Response Handbook*. IHS Global, Englewood, Colorado.
- Gasic, B., Moeckel, C., MacLeod, M., Brunner, J., Scheringer, M., Jones, K.C. & Hungerbühler, K. (2009). Measuring and modelling short-term variability of PCBs in air and characterization of urban source strength in Zurich, Switzerland. *Environ. Sci. Technol.*, **43**: 769-776.
- HENDON (2017). *Patrol Response to Hazardous Materials*. Available online at: [http://www.hendonpub.com/resources/article\\_archive/results/details?id=1331](http://www.hendonpub.com/resources/article_archive/results/details?id=1331) (Last access date: 8 February 2017).

- Interpol (2017). *CBRNE*. Available online at: <https://www.interpol.int/Crime-areas/CBRNE/CBRNE> (Last access date: 8 February 2017).
- Jalalzai, M.K. (2016). *Fixing the EU Intelligence Crisis: Intelligence Sharing, Law Enforcement and the Threat of Chemical, Biological and Nuclear Terrorism*. Algora Publishing, New York.
- Kiras, J.D. (2014). *The Globalization of World Politics, 6<sup>th</sup> Ed.*, Oxford University Press, Oxford.
- Ludovici, G.M., Gabbarini, V., Cenciarelli, O., Malizia, A., Tamburrini, A., Pietropaoli, S., Carestia, M., Gelfusa, M., Sassolini, A., Di Giovanni, D., Palombi, L., Bellecci, C. & Gaudio, P. (2015). A review of techniques for the detection of Biological Warfare Agents. *Defence S&T Tech. Bull.*, **8**: 17-26.
- Michałowicz, J. & Duda, W. (2007). Phenols—sources and toxicity. *Pol. J. Environ. Stud.*, **16**: 347-362.
- N. J. S. P. (2016). *Hazardous Material Technician*. New-Jersey: State Police Hazardous Material Response Unit (HMRU). Available online at: <http://www.njsp.org/division/homeland-security/hazardous-materials-response.shtml> (Last access date: 16 August 2016).
- PAHMS. (2016). *Emergency Response Guidebook*. Department of Transportation, US
- Pellegrino, F., Psinakis, T.J., Morrissey, R., D'italia, R., Vinciguerra, E.J., Tupper, K. J. & Bruzzi, M.C. (2012). *U.S. Patent, No. 8,154,399: Method of Operating a Networked CBRNE Detection System*. U.S. Patent and Trademark Office, Washington, DC.
- Reason, J. (2016). *Managing the Risks of Organizational Accidents*. Routledge, Abingdon, UK.
- Rojavin, Y., Seamon, M.J., Tripathi, R.S., Papadimos, T.J., Galwankar, S., Kman, N., Cipolla, J., Grossman, M.D., Marchigiani, R. & Stawicki, S.P. (2011). Civilian nuclear incidents: An overview of historical, medical, and scientific aspects. *J. Emerg. Trauma Shock*, **4**: 260-272.
- Santella, N. & Steinberg, L.J. (2011). Accidental releases of hazardous materials and relevance to terrorist threats at industrial facilities. *Emergency*, **8**: 53.
- Scott, B.R. (2004). Health risks from high-level radiation exposures from radiological weapons. *Radiat. Prot. Manage.*, **21**: 9-25.
- Will, R.C. (2011). *Costs, Risks, and Myths of Nuclear Power: NGO World-wide Study on the Implications of the Catastrophe at the Fukushima Dai-ichi Nuclear Power Station*. Women's International League for Peace and Freedom, Geneva.



# IDENTIFICATION OF SPIKING CHEMICALS RELATED TO THE CHEMICAL WEAPONS CONVENTION IN WATER SAMPLE DURING AN INTERLABORATORY COMPETENCY TEST

Faris Rudi, Hidayah Aziz, Norliza Hussein, Norhayaty Zahari, Shalwa Abu Bakar & Shamsul Ismail

Science Technology Research Institute for Defence (STRIDE), Ministry of Defence, Malaysia

\*Email: faris.rudi@stride.gov.my

## ABSTRACT

*An overview of approach, standard procedure and results following the participation in the 6<sup>th</sup> Organisation for the Prohibition of Chemical Weapons (OPCW) Chemical Weapons Convention (CWC) Chemical Analysis Competency Testing (CCACT) are presented. CCACT is an initiative from OPCW to assist state party laboratories to build the latter's capacity in preparing for the Proficiency Test (PT). With an aim to join the PT, the Science and Research Institute for Defence's (STRIDE) Chemical Analysis Laboratory participated in the CCACT in 2018 to detect and identify chemical weapons for environmental analysis certification. Identification of chemical weapons is challenging not only because these chemicals are unstable and very toxic, but the analysis and the interpretation of results are required to be at a certain level of competency for all participating laboratories. As a general guideline a sample has to be analysed by at least two different analytical techniques, and at least one of these techniques use spectrometry. All these spiking chemicals from the given water sample was found which are Quinuclidin-3-ol and 2, 2-Diphenyl-2-hydroxyacetic acid classified as Schedule 2 precursor or reactant of chemical weapons, and Methyl-diethanolamine (MDEA) classified as Schedule 3 precursor or reactant of chemical weapons.*

**Keyword:** *Chemical Weapons Convention (CWC) Chemical Analysis Competency Testing (CCACT); Proficiency Test (PT); spiking chemicals; water samples; chemical weapons.*

## 1. INTRODUCTION

Despite the ongoing calls to disarm and ban the use of Chemical Weapons (CW) except for peaceful purposes, the threats that have emerged into a new form nowadays are rather alarming. The use of CW to cause harm began approximately a hundred years ago when chlorine gas was used in 1914-1918 during World War I (Fitzgerald, 2008). The greenish-yellow cloud that smells like bleach instantly irritates the eyes, nose, throat and lungs of those exposed to it, and at high concentration, chlorine gas would be fatal due to asphyxiation. In World War I, approximately 1,000 soldiers were reported dead just a few minutes after the gas was released. The use of the chemical weapons did not stop there. With the advance of new technologies and knowledge, new toxic chemical weapons were created, such as sarin and VX. Recently, the half-brother of the North Korean President was assassinated at the Kuala Lumpur International Airport 2 (KLIA2) on 13 February 2017, having apparently been attacked with a chemical. According to the Government of Malaysia, the chemical used was VX (OPCW Executive Council, 2017a). These chemical warfare agents are now becoming more available especially to non-state actors to inflict harm to the intended targets or victims (Szinicz, 2005).

Chemical weapons, including toxic chemicals and their precursors, are prohibited (in types and quantities) for use in munitions and devices as well as any equipment specifically designed to cause death or other

harm through toxic properties of those toxic chemicals, which would be released as a result of the employment of such munitions and devices (OPCW Technical Secretariat, 1997a). People, soil, water, air or any material that come into contact with chemical weapons may be contaminated with chemical warfare agents and are sampled for environmental analysis, while traces of degradation products of chemicals weapons which are found in urine, faeces, mucous membranes, etc. are sampled for biomedical analysis (Plamboeck *et al.*, 2016).

The Organisation for the Prohibition of Chemical Weapons (OPCW) has established the Chemical Weapons Convention (CWC), which came into force on 29 April 1997 as an international body that prohibits the production, stockpiling, transfer and use of chemical weapons (OPCW Technical Secretariat, 1997a). At present, the Convention has been signed by 193 countries or known as state parties, representing almost 98% of the world population. The Technical Secretariat is a body of the OPCW that executes the CWC internationally. It also facilitates all laboratories that intend to participate in Proficiency Test (PT) seeking to become a designated laboratory (DL) for analysis of environmental samples related to the CWC (Meier, 2013).

As a member of Malaysia’s National Authority (NA), STRIDE is one of the technical agencies that is responsible for Schedule 1 Chemicals of Malaysia’s CWC Act. Besides that, STRIDE plays a key role in detecting and analysing samples for determination of the presence of Schedule 1 Chemicals. As member of NA, STRIDE shall fulfil the obligations towards the implementation of the National CWC Act 2005 (Act 641) and the International CWC Convention. STRIDE is currently developing its capability as the national defence laboratory in analysis and providing assistance to the NA for verification functions (National Authority Chemical Weapons Convention Malaysia, 2008) .

The Science and Research Institute for Defence’s (STRIDE) Chemical Analysis Laboratory participated in the 6th Chemical Weapons Convention Chemical Analysis Competency Test (CCACT) in 2018 to detect and identify chemical weapons for environmental analysis certification. The objective of this paper is to report the spiking chemicals found related to the CWC during the (CCACT).

## 2. SCHEDULE OF CHEMICALS AND COMPETENCY TESTING

### 2.1 Schedule of Chemicals under the CWC

The toxic chemicals that have been used as chemical weapons can be categorised into several types, such as nerve, choking, blood or blister agents. These toxic chemicals are then classified into three schedules under the CWC (OPCW Technical Secretariat, 1997a), as shown in Table 1.

**Table 1: Schedule of chemicals under the CWC (Source: OPCW Technical Secretariat, 1997a).**

<i>Schedule of Chemicals</i>	<i>Definition</i>
Schedule 1	Includes those that have been used or can be used as chemical weapons that have very limited / few or no use for peaceful purposes.
Schedule 2	Primarily precursor for Schedule 1 and have some uses for industrial purposes.
Schedule 3	Produced mainly by industries for purposes not prohibited by CWC, but still can possess a threat by becoming a precursor for Schedule 2 and Schedule 1.

## 2.2 CWC Chemical Analysis Competency Testing (CCACT)

CCACT is a competency test introduced by the Technical Secretariat in 2015 to assist laboratories in building their capacities and preparing for the PT (OPCW Executive Council, 2015). The OPCW provides a database for spiking chemicals for the CCACT, but none for the PT. By participating in this competency building programme, we hope that our laboratory can build the capability to take the PT in the future and maybe one day, become one of the centres of excellence for chemical weapons laboratory in South the East Asian region.

In terms of the conditions for DL status, a participating laboratory needs to successfully achieve grades of AAA or AAB in the last three consecutive tests. Grade A indicates that the laboratory manages to identify all spiking chemicals with no reporting error, while grade B is awarded to laboratories that missed a spiking chemical or reporting an error. Laboratories that received more than one B or lower grades are suspended, and are not eligible to receive or perform sample analysis of chemical weapons on behalf of OPCW. This PT scheme is strict and has zero tolerance for false positive results. A laboratory that accidentally reports false positive spiking chemicals will fail the test, and lose its DL status. Besides the PT scheme, the laboratories must be accredited from a recognised international accreditation body to maintain the DL status (OPCW, 1997a).

Identification of spiking chemical weapons in the PT is one of the most difficult analytical challenges. Furthermore, some of the spiking chemicals are not found in the conventional database. Hence it requires the laboratory to have synthesis expertise to identify spiking chemicals. OPCW DL laboratories have the capabilities to perform chemical synthesis to produce authentic standards for spectra analytical data-matching, especially when spectra are unavailable in commercial database libraries.

For the CCACT, samples collected by an inspection team in the course of an investigation for alleged use of chemical weapons. Then, the OPCW laboratory receives the samples, and control and blank samples of appropriate matrices are prepared. The contents of scheduled compounds are unknowns with low concentration which is less than 10 ppm. The results and report should be submitted to OPCW laboratory within 15 days after receiving the samples (OPCW, 1997c)

The analysis report includes the results with the sample chemical name, structural formula, Chemical Abstracts Service (CAS) number, appropriate structural information, data from analytical databases, sample preparation details, chromatograms, spectra, etc. At least two independent analysis techniques, with at least one being a spectrometric technique should give consistent results (Konopski *et al*, 2014). The NIST MS library is one of the commercial database of analytical information. Besides that, the OPCW creates and updates a database of chemical schedules under the CWC, known as the OPCW Central Analytical Database (OCAD), which is available to all State Parties of the Convention (Mesilaakso, 2005). The OCAD features over 6,000 mass spectra, 5,200 retention indices, 1,400 NMR spectra and 1,000 IR spectra. In October 2017, the OPCW Executive Council approved the first set of non-schedule chemicals for the inclusion in the OCAD (OPCW Executive Council, 2017b). Only spiking chemicals and or their degradation products are to be reported. Reporting other chemicals not relevant to the test aims will constitute failure of the test taken or risk of false positive results. Table 2 shows the acceptable performance criteria of laboratories in CCACT.

**Table 2: Guideline for acceptable performance criteria of laboratories participating in the PT (adapted from OPCW, (1997c)).**

Acceptable Performance Criteria	
(a)	Analysis of test samples and reporting of test results should be carried out within the set time frame (15 calendar days starting from the day the samples arrive at the particular participant laboratory site).
(b)	Identification of chemicals should be based on at least two different analysis techniques preferably spectrometric (e.g. EI-IMS, CI-MS, LC-MS, IR, NMR) with consistent results.
(c)	All analytical data supporting the identifications (chromatographic and spectrometric data) must be annexed to laboratory report.
(d)	The laboratory must indicate on which basis the chemicals are identified (comparison with data on standard chemicals, data in analytical base or interpretation of spectra).
(e)	The laboratory must describe sample preparation and analytical methods in detail or make reference to accessible Recommended Operating Procedure (ROPs), or Standard Operating Procedure (SOPs) or to the validated procedures according to quality assurance / quality control (QA/QC) regime of the laboratory. All deviations from the procedure will have to describe in details.
(f)	The identified chemicals must be reported with sufficient structure information, including at least the structural formula, CAS registry number (if available) and chemical name, and preferably the CWC Schedule-, IUPAC, or CA name. If IUPAC and CA names are not available, a name from which the structure can be derived should be included.
(g)	Only chemicals relevant to the aims of the test should be reported.
(h)	False positive results must not occur. Any chemicals that is not contained in or that could not be formed in the sample matrix will constitute a false positive result. Reporting any false positive result will constitute failure of the Proficiency Test.

### 3. METHODOLOGY

#### 3.1 Procedures for OPCW CCACT

The procedure and criteria for acceptable performance of laboratories and conduct of the OPCW PT was documented in 1997 (OPCW, 1997b, c) and summarised in Table 2 (Hulst *et al.*, 2002). OPCW also provides four valid procedures for the CCACT, which includes the Standard Operating Procedure (SOP) for the CCACT, Work Instruction for the Preparation of Samples, Evaluation of Results and Reporting of Results of the CCACT for participating laboratories guideline (OPCW Technical Secretariat, 2017b, c, d, e).

#### 3.2 Sample Preparation

The main reference for the sample preparation of the water sample was sourced from a collection of the Recommended Operating Procedures (ROPs) for Sampling and Analysis in the Verification of Chemical Disarmament or known as the Blue Book. The ROPs were written by The Finnish Institute for Verification of the Chemical Weapons Convention (VERIFIN) and these guidelines are updated based on new recommendations (Paula, 2011). Our laboratory took the method from this book and made some adjustments in the procedure and the chemical used. Water sample for this 6<sup>th</sup> CCACT was prepared by OPCW laboratory and arrived at our laboratory on 22 May 2018. The test scenario from OPCW indicated that the sample was from a puddle of water and three sets of water samples were given of which were 25 ml respectively. Three sets of sample comprise of a blank, control and sample were send to STRIDE was analysed by a team of five scientists. All solvents used for this test were of analytical grade. The derivatisation agent, N,O-Bis (trimethylsilyl)trifluoroacetamide (BSTFA) was bought from Sigma-Aldrich and was used for polar chemicals to facilitate GC-MS analysis for improvement of sensitivity and selectivity. The water for preparing solvent was ultrapure (Atrium Pro Ultrapure Water System, Sartorius)

and all glassware used for this competency test was new to prevent any cross contamination during sample preparation of analysis.

A total of 5,000  $\mu\text{l}$  of water sample was evaporated to dryness using rotary evaporator (45 °C, 35 mbar) and then silylated with 400  $\mu\text{l}$  of BSTFA. Derivatisation was carried out for 30 min at 60 °C, and the derivatised sample was then allowed to cool for 30 min before injecting to the instrument. The other 1,000  $\mu\text{l}$  of water sample was evaporated to dryness using rotary evaporator and then dissolved in 400  $\mu\text{l}$  1% triethylamine in methanol prior to 5 min of sonicating.

It was then evaporated to dryness again and silylated with 50  $\mu\text{l}$  of BSTFA and addition of 50  $\mu\text{l}$  acetonitrile. Derivatisation was conducted for 30 min at 60 °C. The solvent blank was also prepared for these two water sample methods. The water sample after preparation and derivatisation was analysed for the presence of spiking chemicals related to the CWC using GC-MS (Agilent 7890A GC, Agilent 5975C Inert XL MSD). GC-MS is mainly used to identify and analyse volatile chemical warfare agents or non-volatile degradation products of chemical warfare agents after derivatisation.

#### 4. RESULTS AND DISCUSSION

Three spiking chemicals were found in water sample: Quinuclidin-3-ol, 2,2-Diphenyl-2-hydroxyacetic acid and Methyl-diethanolamine. The presence of these chemicals was confirmed with two analytical techniques, which were electron ionisation (EI) and refractive index (RI). For Quinuclidin-3-ol, the mass spectrum showed the peak molecular ion at  $m/z$  199, followed by a peak at  $m/z$  184 ( $[\text{M} - \text{CH}_3]^+$ ). The mass spectrum obtained is similar with OPCW Central Analytical Database (OCAD) with scoring match factor of 926 (Central OPCW, 1999). The requirement for reporting a chemical is the match factor must be at least 800. The presence of Quinuclidin-3-ol was also confirmed in the sample with RI of 1,271, while RI from OCAD is 1,267. The external standard was used for this RI technique where carbon series (C7-C30) and water sample were separately injected to the GC-MS. The difference of the calculated RI and RI from OCAD must be  $\pm 20$ .

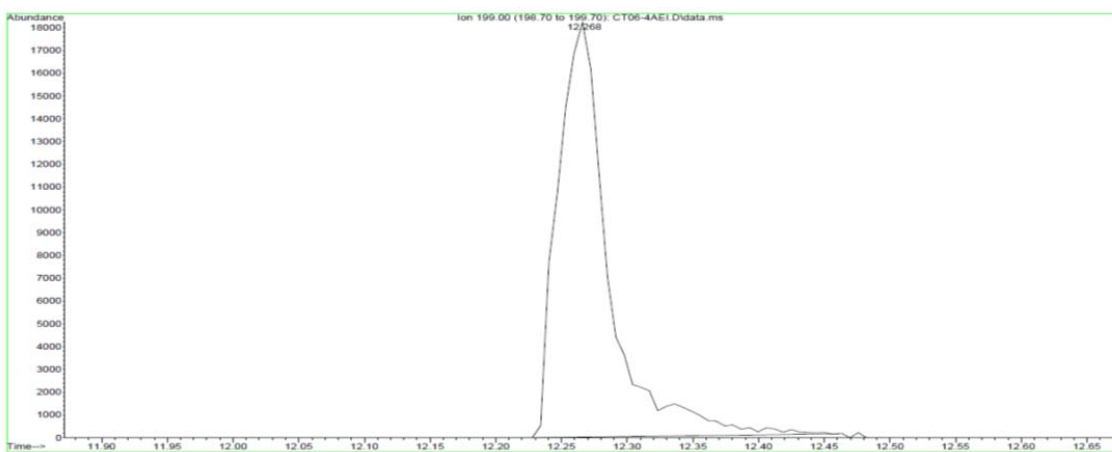
Figures 1 and 2 show the results of the mass spectrum of Quinuclidin-3-ol for the EI and RI techniques respectively in terms of extracted ion chromatogram (EIC). From the diagram, there was no carryover of the sample in the solvent blank, which indicates that instrument is free from contamination and the spiking chemical obtained was accurate. The mass spectrum for 2,2-Diphenyl-2-hydroxyacetic acid shows peak molecular ion at  $m/z$  372, The other peak presence was  $m/z$  357 ( $[\text{M} - \text{CH}_3]^+$ ) and base peak at  $m/z$  255. The result of this spiking chemical was supported by the RI technique, where the calculated RI was 1,916 and RI from OCAD is 1,908.

Figures 3 and 4 show the results for 2,2-Diphenyl-2-hydroxyacetic acid spectrum for the EI and RI techniques respectively. No carryover was found at both solvent blanks to indicate any contamination. The final spiking chemical found in this water sample was Methyl-diethanolamine (MDEA). MDEA was identified by the mass spectrum of its trimethylsilyl (TMS) by molecular ion peak at  $m/z$  263. The RI calculated for compound was 1,311 while the RI from OCAD is 1,314.

Figures 5 and 6 show the mass spectrum of MDEA for the EI and RI technique respectively. The summarised spiking chemicals found in this competency test are tabulated in Table 3.

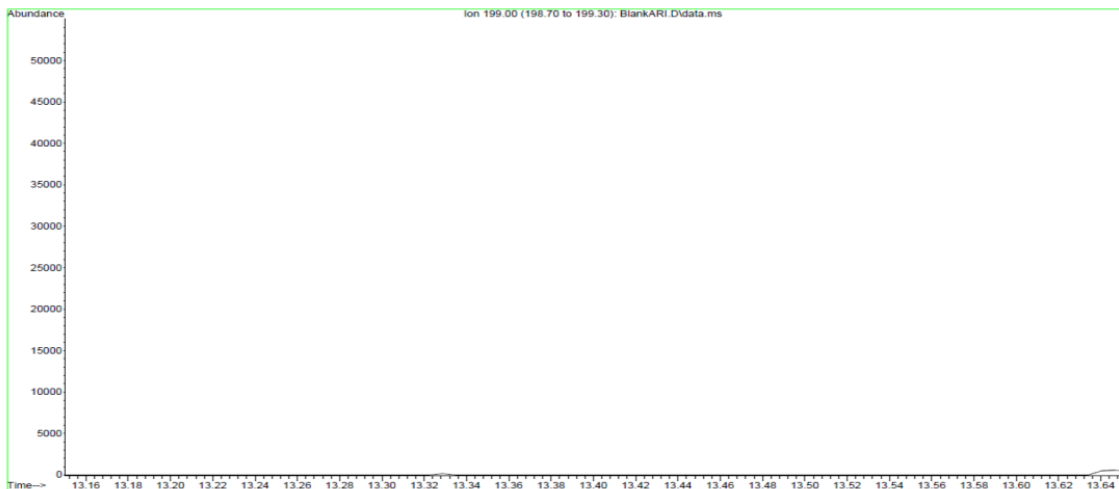


(a)

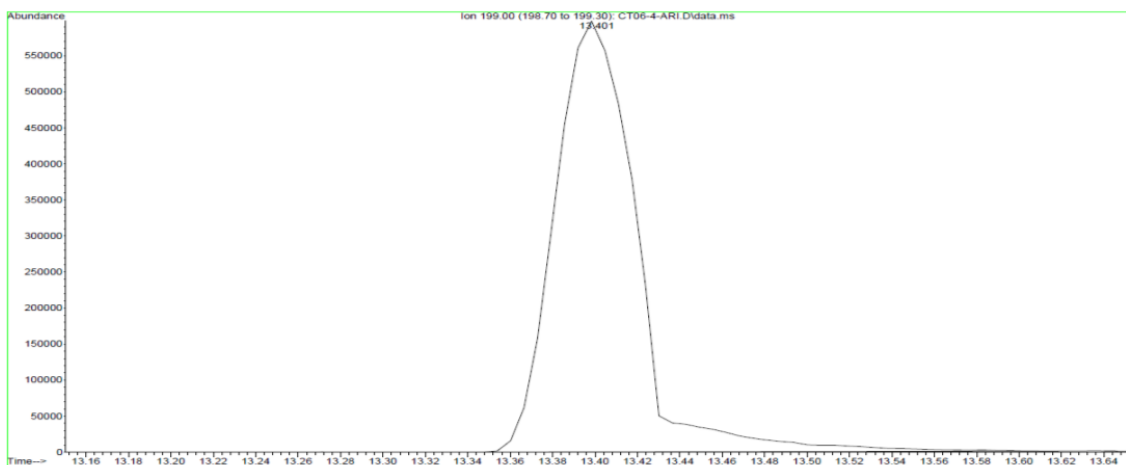


(b)

Figure 1: Mass spectrum of Quinuclidin-3-ol for the EI technique: (a) EIC of solvent blank. (b) EIC m/z 199 molecular ion.



(a)



(b)

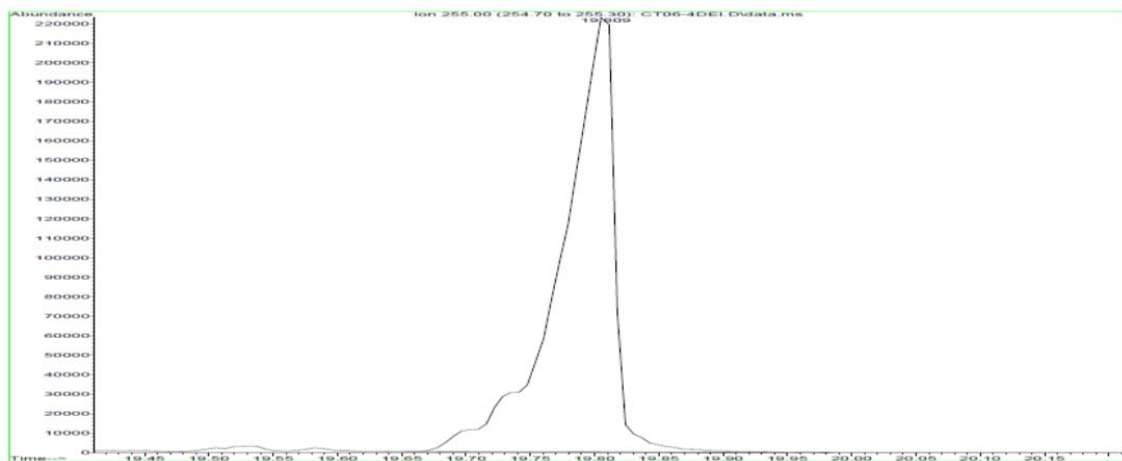


(c)

Figure 2: Mass spectrum of Quinuclidin-3-ol for the RI technique: (a) EIC of solvent blank. (b) EIC m/z 199 molecular ion. (c) Chromatogram of external series.



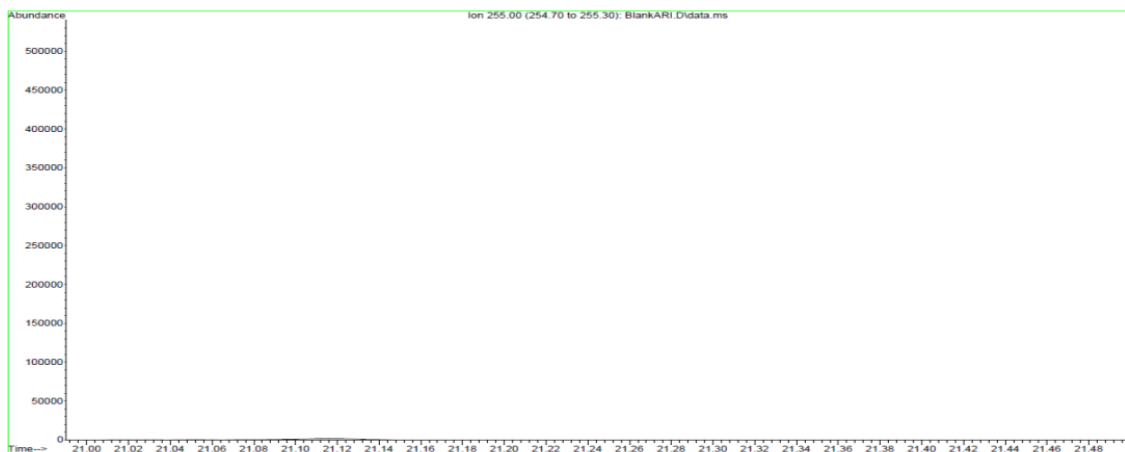
(a)



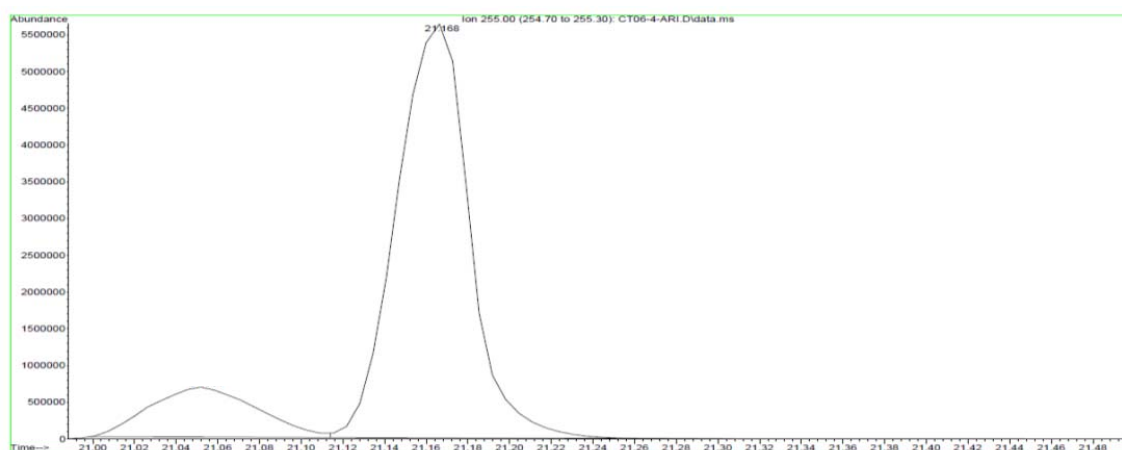
(b)

Figure 3: Mass spectrum of 2,2-Diphenyl-2-hydroxyacetic acid for the EI technique: (a) EIC of solvent blank.  
(b) EIC m/z 255 base peak.

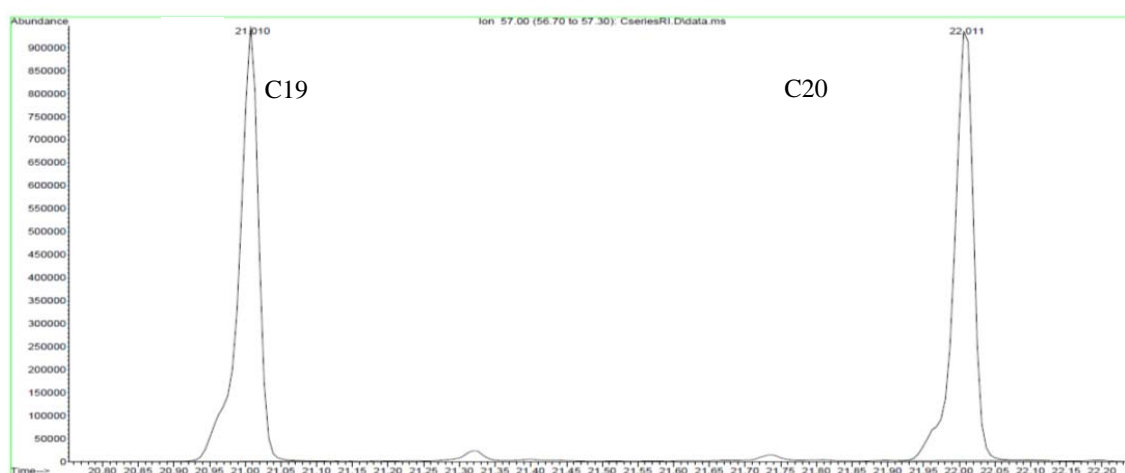




(a)



(b)

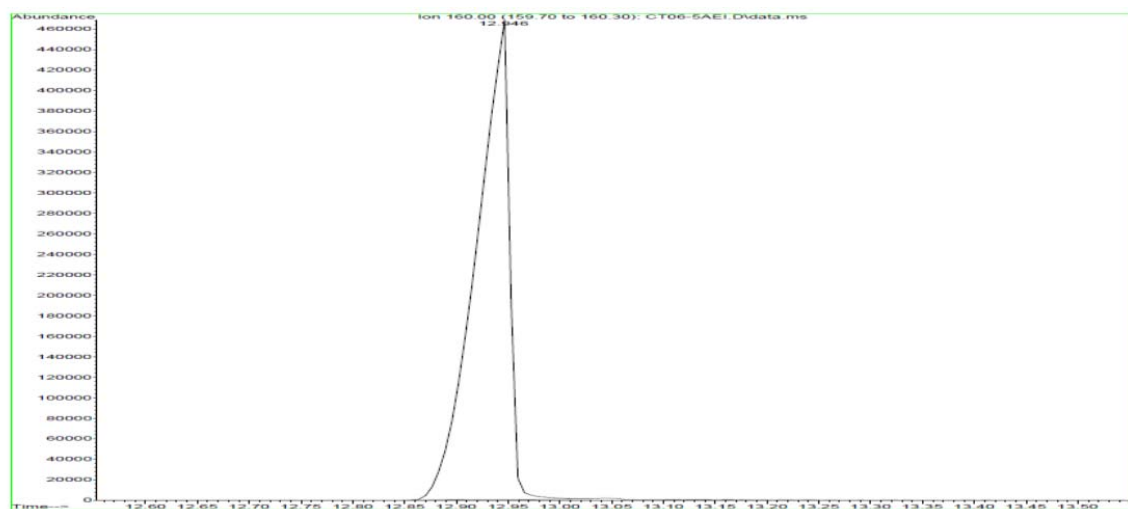


(c)

Figure 4: Mass spectrum of 2,2-Diphenyl-2-hydroxyacetic acid for the RI technique: (a) EIC of solvent blank. (b) EIC m/z 255 base peak. (c) Chromatogram of external series.



(a)

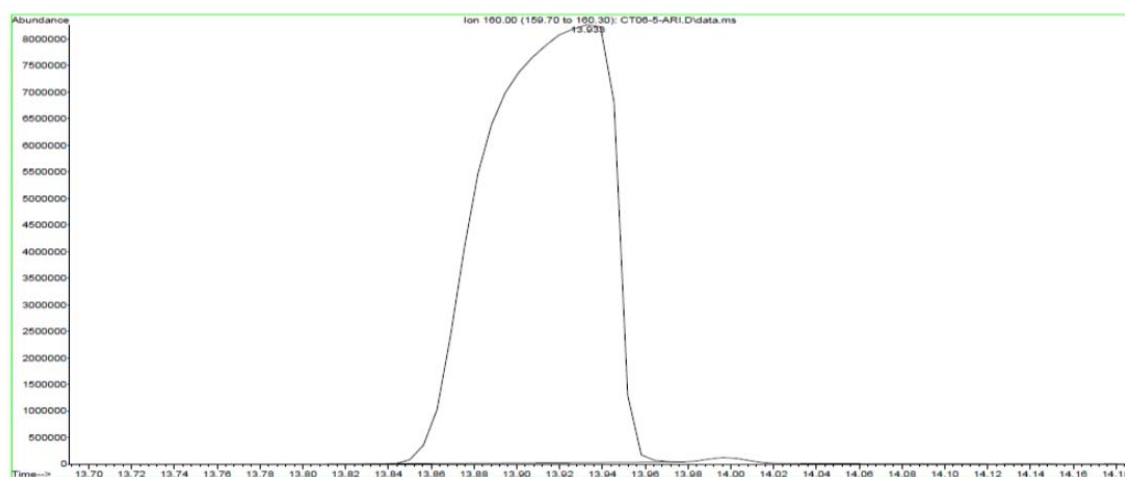


(b)

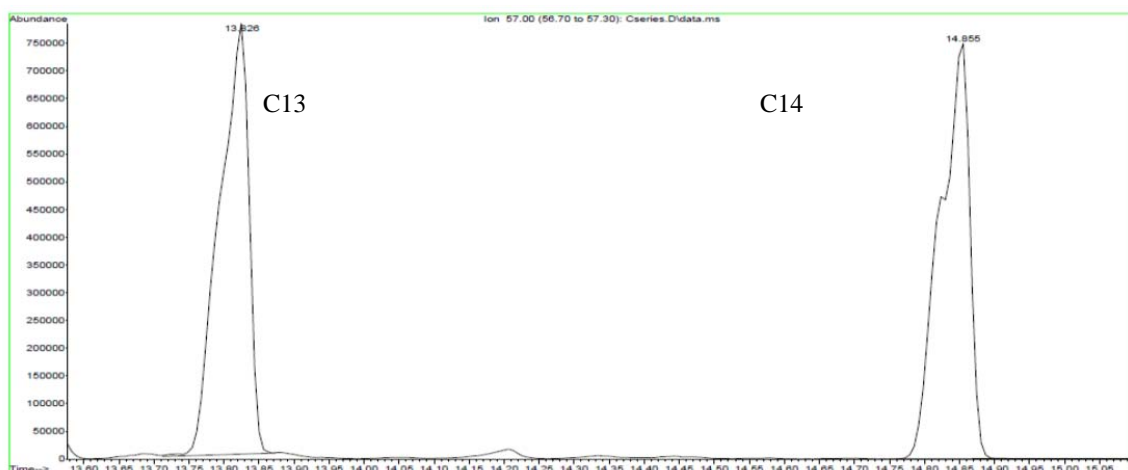
Figure 5: Mass spectrum of MDEA for the EI technique: (a) EIC of solvent blank. (b) EIC m/z 160 molecular ion.



(a)



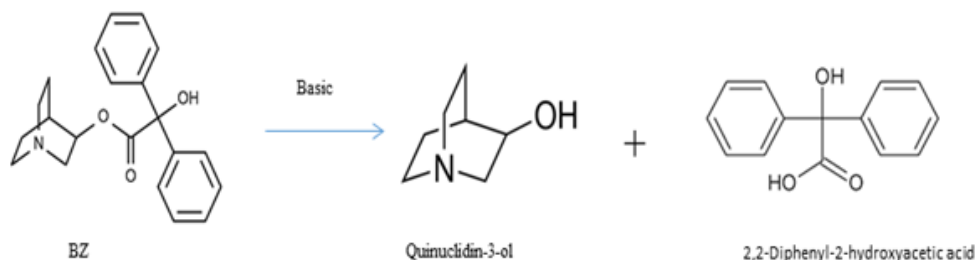
(b)



(c)

Figure 6: Mass spectrum of MDEA for the RI technique: (a) EIC of solvent blank. (b) EIC m/z 160 molecular ion. (c) Chromatogram of external series

Quinuclidin-3-ol and 2, 2-Diphenyl-2-hydroxyacetic acid are the degradation products by hydrolysis reaction of 3-quinuclidinyl benzilate (BZ). BZ is a type of an incapacitating agent of chemical weapons that act on the central nervous system by reversible blockade of muscarinic-type receptors in the cholinergic nervous system (Black & Muir, 2003). The hydrolysis reaction is shown in Figure 7.



**Figure 7: Hydrolysis reaction of BZ (adapted from Black & Muir, 2003).**

Meanwhile, MDEA is also a degradation product of nitrogen mustard bis(2-chloroethyl)methylamine (HN2) by hydrolysis in the presence of water. Mustard agents once received their name because the synthesis product had the smell of mustard oil (Andersen *et al.*, 2017). Nitrogen mustard is a type of vesicant or blistering agent of chemical weapons and is classified as Schedule 1 (Ohsawa & Seto, 2006).

**Table 3: Chemicals from spiking chemicals identified in the water sample**

Chemical name	Chemical structure	Cas number	Schedule	GC-MS	
				EI (m/z)	RI
Quinuclidin-3-ol		1619-34-7	2.B.09	199 [M] <sup>+</sup> 184,129	RI from compound = 1,271 RI from OCAD = 1,267
2,2-Diphenyl-2-hydroxyacetic acid		76-93-7	2.B.08	372 [M] <sup>+</sup> 357, 255	RI from compound = 1916 RI from OCAD = 1,908
Methyldiethanol amine (MDEA)		105-59-9	3.B.16	263 [M] <sup>+</sup> 248,160	RI from compound = 1311 RI from OCAD = 1,314

## 5. CONCLUSION

The analysis for identification of spiking chemical in water sample for CWC (CCACT) was completed within 15 days and the results of the relevant chemicals were reported to OPCW. The two identification techniques used which were EI and RI, were able to identify the spiking chemical. However, the RI technique is not good enough for PT. OPCW recommends that our laboratory consider using other spectrometry techniques such as chemical ionisation (CI), liquid chromatography- mass spectrometry (LC-MS) and nuclear magnetic resonance (NMR) in future.

## ACKNOWLEDGEMENT

The authors would like to thank the top management of STRIDE for the continuous support throughout this competency test. In addition, the authors would also wish to express their gratitude to researchers from Protection and Biophysical Technology Division (BTPB) that helped in sample preparation throughout this test. Furthermore, the authors would like to thank the Department of Chemistry Malaysia for the analytical training provided before this competency test.

## REFERENCES

- Andersen, H., Vecchio, L., Gazerani, S., P. & Arendt-Nielsen, L. (2017). Dose-response study of topical allyl isothiocyanate (mustard oil) as a human surrogate model of pain: hyperalgesia and neurogenic inflammation pain. *Biochem J.*, **158**: 1723-1732.
- Black, R. M. & Muir, B. (2003). Derivatisation reactions in the chromatographic analysis of chemical warfare agents and their degradation products. *J. Chromatogr. A*, **1000**:253-281.
- Hulst A. G., de Jong A. L., de Reuver L. P., van Krimpen S. H., van Baar B. L. M., Wils E. R. J., Kientz C. E. & Brinkman U. A. T. (2002). Identification of chemicals related to the Chemical Weapons Convention during an interlaboratory proficiency test. *Trends Anal. Chem.*, **21**: 116-130.
- Fitzgerald, G. J. (2008). Chemical Warfare and Medical Response during World War 1. *Am J Public Health N.*, **98**, 611-625.
- Konopski L., Liu P., Wuryani W. & Sliwakowski M. (2014). OPCW proficiency test: A practical approach also for interlaboratory test on detection and identification of pesticides in environmental matrices. *Sci World J*, **Vol. 2014**: 542357.
- Meier, U.C. (2013). Detection and identification of hydrolysis products of sulfur mustards at trace levels in environmental samples using liquid chromatography solid phase extraction combined with off-line nuclear magnetic resonance analysis. *J. Chromatogr. A*, **1286**: 159-165.
- Mesilaakso, M. (2005). *Chemical Weapons Convention Chemical Analysis-Sample Collection, Preparation and Analytical Methods*. John Wiley & Sons Ltd, New Jersey.
- Vanninen P. (2011). *Recommended Operating Procedures for Analysis in the Verification of Chemical Disarmament*. University of Helsinki, Helsinki.
- National Authority Chemical Weapons Convention Malaysia (NACWC) (2005). *Akta 641: Akta Konvensyen Senjata Kimia 2005*. Ministry of Foreign Affairs, Putrajaya.
- National Authority Chemical Weapons Convention Malaysia. (2008). *Work Manual: A Guideline to the Implementation of the Chemical Weapons Convention*. Ministry of Foreign Affairs, Putrajaya.
- Ohsawa, I. & Seto, Y. (2006). Determination of nitrogen mustard hydrolysis products, ethanolamines by gas chromatography- mass spectrometry after tert-butyldimethylsilyl derivatisation. *J. Chromatogr. A*, **1122**:242-248.
- OPCW (1997a). Proficiency testing leading to certification of designated laboratories. *Proceeding of the Decision of OPCW Conference of the State Parties*. doi:C-1/DEC.60. Organisation for the Prohibition of Chemical Weapons (OPCW), The Hague, Netherlands.
- OPCW (1997b). Criteria for acceptable performance of laboratories in proficiency testing. *Conference of the State Parties, (pp. C-1/DEC.62)*. Organisation for the Prohibition of Chemical Weapons (OPCW), The Hague, Netherlands.
- OPCW (1997c). Criteria for the conduct of OPCW proficiency testing. *Conferences of the State Parties, (pp. C-1/DEC.65)*. Organisation for the Prohibition of Chemical Weapons (OPCW), The Hague, Netherlands.
- OPCW Executive Council (2015). Report by Ambassador Robert P. Mikulak Facilitator for chemical industry and other Article VI issues. *Documents from the Seventy-Ninth Session of the Executive*

- Council*. Organisation for the Prohibition of Chemical Weapons (OPCW), The Hague, Netherlands.
- OPCW Executive Council (2017a). Decision Chemical Weapons Incident in Kuala Lumpur, Malaysia. *Documents from the Seventy-Ninth Session of the Executive Council.*, Organisation for the Prohibition of Chemical Weapons (OPCW), The Hague, Netherlands.
- OPCW Executive Council (2017b). Decision-Lists of new validated data on non-scheduled chemicals for approval by the Executive Council for inclusion in the OPCW Analytical Database. *Documents from the Seventy-Ninth Session of the Executive Council*. Organisation for the Prohibition of Chemical Weapons (OPCW), The Hague, Netherlands.
- OPCW Technical Secretariat (1997a). *Convention on the Prohibition of the Development, Production, Stockpiling and Use of Chemical Weapons and on their Destruction*. Organisation for the Prohibition of Chemical Weapons (OPCW), The Hague, Netherlands.
- OPCW Technical Secretariat (2017b). *Standard Operating Procedure for the Organisation of OPCW Proficiency Test*. Organisation for the Prohibition of Chemical Weapons (OPCW), The Hague, Netherlands.
- OPCW Technical Secretariat (2017c). *Work Instruction for the Preparation of Samples for OPCW Proficiency Test.*, (p. *QDOC/LAB/WI/PT02*). Organisation for the Prohibition of Chemical Weapons (OPCW), The Hague, Netherlands.
- OPCW Technical Secretariat (2017d). *Work Instruction for the Evaluation of the Results of OPCW Proficiency Test.*, (p. *QDOC/LAB/WI/PT03*). Organisation for the Prohibition of Chemical Weapons (OPCW), The Hague, Netherlands.
- OPCW Technical Secretariat (2017e). *Work Instruction for the Reporting of the Results of the OPCW Proficiency Test.*, (p. *QDOC/LAB/WI/PT04*). Organisation for the Prohibition of Chemical Weapons (OPCW), The Hague, Netherlands.
- Plamboeck A. H., Stoven S., Davidson R. D., Fykse E., Griffiths M., Nieuwenhuizen M., Rivier C. & van der Schans M. (2016). Laboratory analysis of CBRN-substances: Stakeholder networks as clue to higher CBRN resilience in Europe. *Trends Anal. Chem.*, **85**: 2-9.
- Szinicz, L. (2005). History of chemical and biological warfare agents. *Toxicol.*, **214**:167-181.

# DEFENCE SPENDING IN AN ERA OF UNCERTAINTY AND BUDGETARY CONSTRAINTS

Ananthan Subramaniam\*, Amirudin Sulaiman & Wong Wai Loong

National Defence University of Malaysia (UPNM), Malaysia

\*Email: ananthan@upnm.edu.my

## ABSTRACT

*In the light of current global economic crisis, defence budgets of most nations have experienced significant reductions. Malaysia, in particular faces momentous security challenges especially as it aspires to exert greater control on its vast land and maritime borders. Current defence and security operations, particularly in East Sabah, consume a sizeable amount of the defence spending. This leaves little financial resources to support its military's modernisation plan especially as it moves into a critical phase of its strategic transformation programme. This paper looks into the challenges of the defence planning during a period where demands for current operating expenditure are on the rise. Coupled with that, strategic shocks place an added strain on allocated budgets. A strategic choice in defence spending needs to be made between force readiness and force modernisation.*

**Keywords:** *Military; defence planning; defence spending; defence budget; force modernisation.*

## 1. INTRODUCTION

Planning is a function of management. Without appropriate planning, it would be impossible for organisations to achieve organisational goals. Likewise, defence organisations require strategic planning, both short term and long term, to fulfil their roles, tasks and responsibilities (Davis, 2000). According to Montgomery (2009), the purpose of defence planning is to ensure defence forces of a nation are prepared to react effectively to potential contingencies and eventualities in the future. These forces will require a wide range of operational capabilities ranging from scenarios of all-out war to operations under the context of military operations other than war (MOOTW). However, he also suggests that the likelihood of achieving such a level of preparation is near impossible. Gray (2008) provides an explanation for this impracticality as defence planning is basically undertaken in the realm of 'uncertainty'. As such it is almost impossible to predict and pre-empt the nature of contingencies that a nation might face. At the same time, the amount of resources a nation can make available for defence is often limited due to other competing needs such as social, health and education. Thus, defence planners are often faced with the difficult task of convincing financiers to provide the resources needed to develop forces for various unforeseen eventualities.

The objective of this paper is to discuss the challenges of Malaysia's defence spending in an uncertain security environment coupled with severe budgetary constraints. The paper will first discuss fundamental defence management issues and budget allocations. This will be followed by reviewing policy guidance provided by the National Defence Policy. The vagaries of the uncertain security environment will then be analysed in determining defence spending choices. It must be stressed that the overall intention of this paper is to create an awareness of issues pertaining to defence planning and spending. Analyses and proposals for planning approaches are not discussed here.

## **2. DEFENCE MANAGEMENT**

Defence spending falls under the wider scope of defence management. Eccles (1965 in Bland, 1999) explains that defence management is “the bridge between the economy of a nation and tactical operations of combat forces”. To appreciate this concept, one needs to understand that governments have a fundamental responsibility in ensuring their citizens well-being and their security. In order to fulfil this obligation, governments have to create the necessary conditions for generation of wealth and prosperity while ensuring the protection of such prosperity (Le Roux, 2004). Given this scenario, the economy of a nation has significant correlation with the capacity of defence forces to execute their tasks. The more professional a defence force, the greater it’s contribution to the economic prosperity of the nation. Likewise, a nation’s economic health can determine how well defence forces are trained and equipped to protect national interests. In this sense, defence management activities (defence spending) play a vital role in transforming scarce resources allocated by the government into military capability in accordance with the government guidance (Bland, 1999).

Often, decision makers at all levels from politicians to bureaucrats to senior commanders in the military, are faced with the dilemma of opportunity cost in utilising the limited resources. At the national level, policy makers need to weigh the competing demands between socio-economic development and modernisation of defence forces. This predicament in the selection of options between investment in defence and goods for public consumption is often referred to as the dichotomy of ‘guns and butter’ (Ananthan, 2017). Additionally, external technology suppliers and their governments can also influence major spending decisions. At the defence organisation level, pressures on spending priorities can emanate from inter-service rivalries, local suppliers and defence industry players (Wah, 1990). Whatever the influencing factors, defence planners must take into consideration the need to transform the allocated resources into effective military capability within the ambit of clearly defined and established defence policy.

## **3. DEFENCE STRATEGIC PLAN AND CAPABILITY DEVELOPMENT**

All defence planning has to start with guidance from defence policy. The current National Defence Policy (NDP) was released in 2010 (Ministry of Defence Malaysia, 2010). The NDP’s overriding principle for a comprehensive defence strategy is self-reliance. It goes on to outline national interests which need to be defended. These are categorised based on three distinct geographical areas; 1) the core land mass and territorial waters, 2) the EEZ which contains significant economic resources, and 3) the strategic waterways and airspace. The NDP thus calls for the Malaysian Armed Forces (MAF) to possess a “high degree of readiness” to defend and protect these interests against both domestic and external threats in either the conventional or non-conventional form (NDP, 2010). Given this demand, MAF has drawn up a force modernisation strategic blueprint, widely known as the 4<sup>th</sup> Dimension MAF (4D MAF) plan. This often quoted plan was formulated for execution from 2009 through to 2020 and beyond. This plan envisions the transformation of MAF into a fully integrated and balanced force based on ‘jointry’ and inter-operability among the three services. The plan has seen continued revision and currently serves as the guiding document for MAF’s force modernisation and procurement priorities (Affandi, 2017).

The MAF Headquarters’ approach in creating a modern fighting force is via the Capability-Based Planning method (MAF HQ, 2017). This method has been adopted by most modern defence forces in developing a wide range of military capability in a threat ambiguous environment. Capability-Based Planning (CBP) by definition is a system for long-term force structure planning under conditions of uncertainty “to provide capabilities suitable for a wide range of modern-day challenges and circumstances while working within an economic framework” (Davis, 2002). It enables defence organisations to determine capability needs, allocate resources within constraints and track activities and outcomes (RAND, 2016). This CBP approach has been used to prepare the 4DMAF strategic plan. It must be stressed though that the CBP approach helps identify a broad set of capabilities across wide-ranging scenarios and missions to deter and defeat adversaries in combat. However, a full



spectrum force needs to be equipped, trained and prepared for other non-combat missions such as peacekeeping, disaster relief, public order and other tasks assigned under the national blue ocean strategy (NBOS).

#### 4. STRATEGIC PLANS AND FISCAL REALITIES

Defence policies and force modernisation plans often encounter constrained budget allocations or unpredictable budgetary cuts. This often creates a predicament of ‘strategy resource mismatch’. Taylor and Waldman (2008) described this as a universal problem where policy ambitions face a resource imbalance. The vagaries of the economic environment often mean that resources cannot be allocated as planned. This situation then requires force developmental strategies to be continually reviewed, realigned and prioritised.

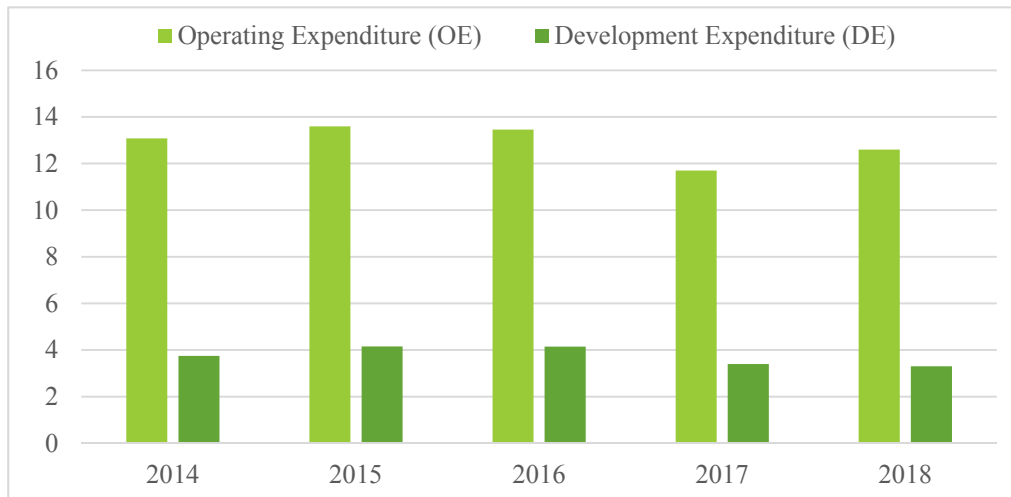
Like most countries in this region, Malaysia’s economy has been hit by the recent slump in global petroleum prices. Coupled with the depreciation of the national currency, the finances of the country have been roundly squeezed. Inevitably, this has repercussions on defence spending. In fact, the nation’s allocation for defence has not shown any significant increase in real terms in the last several years. It has been hovering around 1.6% of GDP and 6.25% of overall annual government expenditure (Ministry of Finance Malaysia, 2018). Data for years 2014 to 2018 indicates that the total defence budget has averaged RM 16.3 billion. The operating expenditure (OE) takes up the bulk of the allocation in the last five years at 77.5% while development expenditure (DE) accounts for 22.5% (see Table 1). Operating expenditure is mainly used for activities that are recurrent and continuous such as emoluments, pensions, maintenance, utilities, rentals, and grants. Development allocation is a non-recurrent expenditure that is essentially for procurement of capital weapon systems and infrastructure. The annual DE is allocated from the budget approved to implement development programmes and projects under the Five-Year Malaysia Plan (Economic Planning Unit, 2017)

**Table 1: Malaysia's Defence Budget Statistics from 2014 to 2018 in RM billion.**

	2014	2015	2016	2017	2018	Average
Operating Expenditure (OE)	13.079	13.595	13.457	11.700	12.600	12.886
% of Defence Budget	77.7	76.6	76.5	77.5	79.2	77.5%
Development Expenditure (DE)	3.751	4.150	4.145	3.400	3.300	3.689
% of Defence Budget	22.3	23.4	23.5	22.5	20.8	22.5%
Total Defence Budget	16.830	17.745	17.602	15.100	15.900	16.255
Total Government Budget	259.092	260.737	265.224	267.15	280.25	266.49
% Defence of Government Budget	6.50	6.81	6.64	5.65	5.67	6.25%
GDP	1012.449	1063.355	1108.227	1168.444	1228.822*	1088.119
% Defence of GDP	1.66	1.67	1.59	1.30	1.14*	1.56%

(Source: Ministry of Finance Malaysia, 2018) \*forecast

Figure 1 shows a graphical representation of data in Table 1. As can be seen, the allocations for both OE and DE have declined in the last two years when compared to budgets from 2014 to 2016. In terms of percentage of the defence budget, the allocation for DE has remained less the 25% over the last five years resulting in less opportunity to purchase capital assets (Caffrey, 2017). The increase in OE is quite significant. One of the major operating expenditure is personnel emolument which has amounted to 63.6% in 2017 (Ministry of Defence Malaysia, 2018). This can be expected to increase as salary scales and rank structures continue to be in the upward trend.



**Figure 1: Malaysia's Defence Budget from 2014 to 2018 in RM billion**  
**Source: Ministry of Finance Malaysia, 2018.**

## 5. SECURITY ENVIRONMENT AND DEFENCE SPENDING

At the global level, border security is fast becoming one of the biggest cause for concern for nation states. An analysis on current global security concerns suggest that security agencies of most governments the world over are facing tremendous challenges to effectively maintain control of the borders and protect resources within their territories (Nurkin, 2016). Similarly, Malaysia experiences significant challenges in protecting its extensive land and maritime borders<sup>1</sup> from encroachments and other forms of intrusions. As the only country in ASEAN that shares borders with six other member states, MAF and other security agencies of the nation are fully occupied with operations to deter and preventing crimes such as illegal border crossings, human and substance smuggling, illegal fishing, kidnap for ransom and piracy.

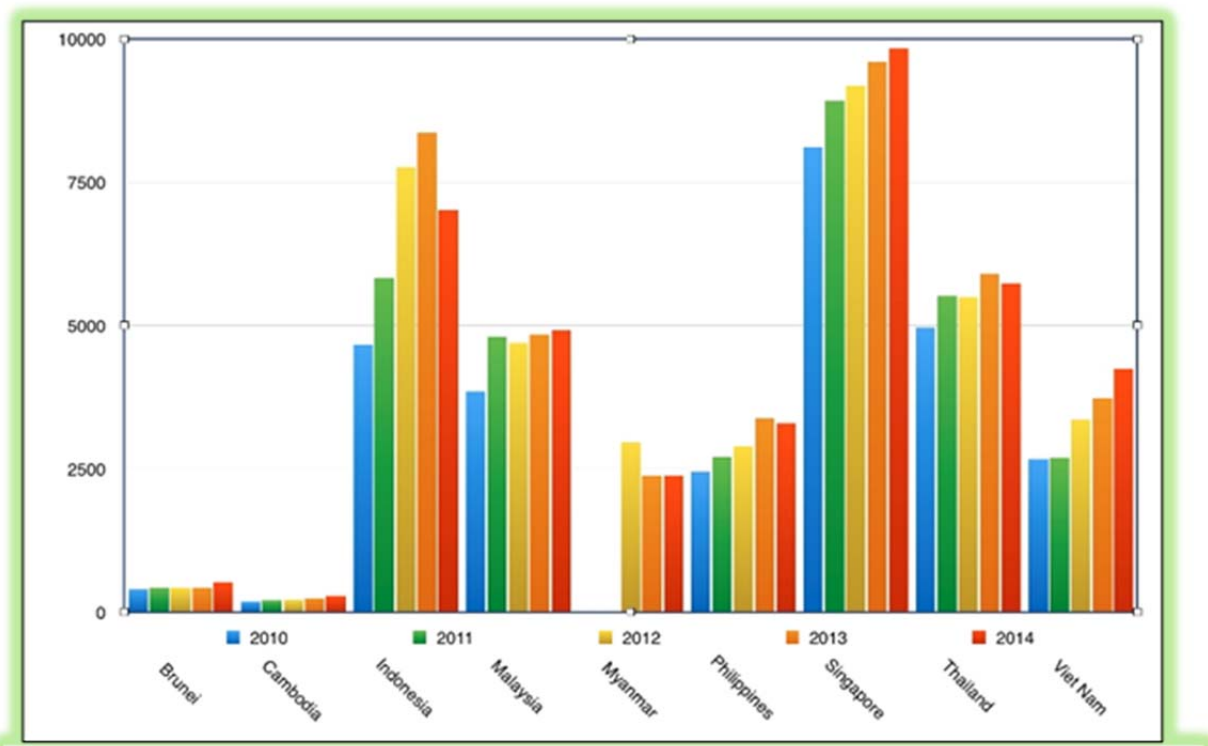
Davis (2000) suggests that uncertainty is an ever-present phenomena and simply preparing diligently for it will not eliminate it. As such, even though national security planners prepare security forces for a wide range of security challenges, it is almost impossible to predict and be fully prepared for all circumstances. Occasionally, these forces will have to encounter events which are classified as strategic 'surprises' or 'shocks' (Gray, 2014). A strategic shock can be defined as an event both of military or non-military nature, often with a low probability of occurrence but producing significant impact which requires decision makers to pay greater attention to future defence planning and spending (Anton, 2013).

Events in recent years reflect the magnitude of 'shocks' that has impacted the nation's wider security. Some of the major shocks requiring the involvement of MAF are as follows; Nipah virus pandemic in 1998, Sipadan kidnappings in 2000, Al-Ma'unah incident in 2000, Sultanate of Sulu forces incursion into Eastern Sabah in 2013, MH370 disappearance in 2014, and the East coast floods of 2014-15. Meanwhile minor shocks include such incidences as the Ambalat stand-off in 2005, the hijacking of Malaysia commercial vessels in the Straits of Malacca, the illegal landings of refugees in Langkawi, the findings of mass graves of illegal immigrants in Wang Kelian in 2015 and the Beting Patinggi intrusions by Chinese coastguard and fishing vessels in 2016. These shocks are unprecedented events which could not have been predicted by defence planners. Yet the MAF has to be thoroughly involved

<sup>1</sup> Land borders; Brunei 266 km, Indonesia 1,881 km, Thailand, 595 km and coastline; Peninsular Malaysia 2,068 km, East Malaysia 2,607 km [CIA. (2016). World Fact Book: Malaysia. <https://www.cia.gov/library/publications/the-world-factbook/geos/my.html>]

in support of other government agencies to tackle these security issues. When such events occur, a lack of contingency provisions in the current defence budget will mean funds available for other plans and requirements are diverted through realignment, reprioritised or even discarded entirely.

Defence forces constantly face the dichotomy between force modernisation and force readiness for current and anticipated operations (Pennie, 2001). While force modernisation plans requires large amounts of financial funding, the day to day operational tasks of maintaining peace and security consumes both training time and financial resources of MAF. For example, the aftermath of the Sulu Sultanate incursion into Sabah in 2013 saw the expansion and creation of new security organisations such as the Eastern Field Command in Kuching and ESSCOM in Lahad Datu. The formation of these organisations and building of infrastructure collectively increases the operating expenditure. These new budgetary demands significantly impact the ability of MAF to sustain existing military operations and development of future military capabilities.



**Figure 2: ASEAN countries military expenditures from 2010- 2014 in million U.S. dollar terms.**  
**Source: SIPRI dataset, graphic prepared by Abuza (2015).**

On the other hand, ASEAN nations have been steadily increasing their defence spending in recent years as shown in Figure 2. This increasing trend though has created a perception that member states are engaged in an arms race or a balancing of forces against each other. However, a detailed look at the defence equipment being procured by individual nations, suggest that these purchases have more likely been made to address threats to their territorial integrity and sovereignty especially in the South China Sea (Ribar, 2015).

In comparison with other member states such as Indonesia, Singapore, Thailand and Vietnam, Malaysia’s spending increase has not been significant. While Indonesia is just ahead of Singapore in the group of top 15 arms importing countries (Liang & Perlo-Freeman, 2017), Malaysia has had to be more pragmatic in its spending between current operational needs and force developmental aspirations given the fiscal realities in the past few years. Operational expenditure and purchase of equipment for forces engaged in countering the low level threat in Sabah and other non-traditional threats has taken precedents over the continued creation of conventional capabilities. According to

Dzirhan (2016), many of the planned development programmes have been either scrapped, shelved or scaled down due to budgetary constraints. Examples include the decision to purchase a lighter form of attack helicopters rather than high-end versions which had been on trial, the deferment in the formation of marine forces and the purchase of a multi-role support ship. To further offset procurement challenges, assets have been moved around between the tri-service organisations of MAF. Examples of which are movement of air defence weapons and transport helicopters and the redeployment of Hawk aircrafts to East Malaysia. By and large, the annual defence budget allocation for development expenditure is being disbursed for on-going programmes rather than new procurements.

## 6. CONCLUSION

The MAF contributes to Malaysia's wider national interests by working in concert with the Foreign Policy through the National Defence Policy. As a defence force, it is routinely required to complement security agencies due to its legacy and inherent capacity to carry out security operations in support of civilian authorities. MAF's aspiration of developing into a modern and credible war fighting force requires a greater focus on procurement of capital equipment, training and development of doctrine. However, due to uncertainty in the security environment and the various security challenges that are ever present, MAF has to be constantly involved in routine operations classified as operations other than war such as border security operations, humanitarian and disaster relief, and peacekeeping operations. Coupled with financial constraints and budgetary cuts, MAF's modernisation in accordance with its 4<sup>th</sup> Dimension Strategic Plan continues to be severely hampered. The government has to consider providing more development funding in both the 11th Malaysia Plan (2016-2020) and 12th Malaysia Plan (2021-2025) to ensure the modernisation of MAF progresses according to the planned trajectory.

## REFERENCES

- Abuza, Z. (2015). *Analyzing Southeast Asia's military expenditures*. Available online at: <http://cogitasia.com/analyzing-southeast-asias-military-expenditures/> (Last access date: 6 September 2018).
- Affandi, R.M. (2017). *Chief of Defence Force address to course 47/2017 at Malaysian Armed Forces Command and Staff College*. Transcript 25 August 2017.
- Ananthan, S. (2017). Management of defence resources. In Haslinda, A. (Ed.), *Management Theories and Practices*. UPNM Press, Kuala Lumpur, pp 111-120.
- Anton, S. (2013). Conceptual insights of strategic shock and strategic surprise. *Strat. Impact*, **1**: 58-67.
- Bland, D.L. (1999). *Issues in Defence Management*. McGill-Queens University Press, Kingston, Canada.
- Caffrey, C. (2017, October 27). *Malaysia announces 5.3% defence budget increase*. IHS Jane's Defence Industry. Available online at: <https://www.janes.com/article/75262/malaysia-announces-5-3-defence-budget-increase> (Last access date: 14 August 2018)
- Davis, P. K. (2000). Defense planning in an era of uncertainty : East Asian issues. In Crawford, N.W., & Moon, C. (Eds.), *Emerging Threats, Force Structures, and the Role of Air Oower in Korea*. RAND, Santa Monica, Ca, pp. 25–49.
- Davis, P.K. (2002). *Analytic architecture for capabilities-based planning, mission-system analysis, and transformation*. RAND, Santa Monica, California.
- Dzirhan, M. (2016). Procurement plans remains under funding pressure. *Def. Rev. Asia*, **10**: 10-13.
- Economic Planning Unit (2017) *Development planning*. Economic Planning Unit, Malaysia. Available online at: [http://www.epu.gov.my/en/helpdeskppp\\_a](http://www.epu.gov.my/en/helpdeskppp_a) (Last access date: 26 November 2017).
- Gray, C. S. (2008). Coping with uncertainty: Dilemmas of defense planning. *Comp. Strategy*, **27**: 324–331.

- Gray, C.S. (2014). *Strategy And Defence Planning: Meeting The Challenge Of Uncertainty*. Oxford, UK: Oxford University Press.
- Le Roux, L. (2004). The defence sector and the defence budget: Minimising costs and maximising benefits. In Chileshe, G., Chimanse, M., Ngoma, N., Lwando, P., & Mbewe, T. (Eds). *Civil–Military Relations in Zambia: A review of Zambia’s Contemporary CMR History and Challenges of Disarmament, Demobilisation and Reintegration*. Institute for Security Studies, Cape Town, South Africa.
- Liang, X. & Perlo-Freeman, S. (2017). *Corruption in the Indonesian Arms Business: Tentative Steps Towards an End to Impunity*. World Peace Foundation, Massachusetts.
- MAF HQ (2017). *Capability Management and Development in MAF*. Lecture at Armed Forces Staff College, Kuala Lumpur on 20 July 2017.
- Ministry of Defence Malaysia. (2010). *Malaysia’s National Defence Policy*. Kementerian Pertahanan Malaysia, Kuala Lumpur.
- Ministry of Defence Malaysia (2018). *Laporan Tahunan 2017*. Available online at: <http://www.mod.gov.my/ms/component/phocadownload/category/11-laporan-tahunan.html> (Last access date: 4 August 2018).
- Ministry of Finance Malaysia (2018). *GDP Statistical Table 2017/2018*. Available online at: [http://www.treasury.gov.my/pdf/economy/er/1718/st3\\_1.pdf](http://www.treasury.gov.my/pdf/economy/er/1718/st3_1.pdf) (Last access date: 4 August 2018).
- Montgomery, E.B. (2009). *Defense Planning for the Long Haul: Scenarios, Operational Concepts, and the Future Security Environment*. Available online at: <http://csbaonline.org/publications/2010/01/defense-planning-for-the-long-haul/> (Last access date: 27 June 2018).
- Nurkin, T. (2016). *The Future of Borders, Boundaries, Sovereignty and Security*. Available online at: from <http://www.janes.com/article/61362/security-the-future-of-borders-boundaries-sovereignty-and-security-es2016d3> (Last access date: 4 August 2018).
- Pennie, K. R. (2001). Strategic thinking in defence. *Canadian Mil. J.*, **3**: 21–28.
- RAND. (2016). *Capabilities Based Planning*. Available online at: <http://www.rand.org/topics/capabilities-based-planning.html> (Last access date: 4 August 2018).
- Ribar, M. (2015). *Explaining Southeast Asia’s Force Build-Up*. Available online at: <http://thediplomat.com/2015/01/explaining-southeast-asias-force-buildup> (Last access date: 6 September 2018).
- Taylor, C. & Waldman, T. (2008). *British Defence Policy Since 1997: Background Issues*. Research Paper 08/58, House of Commons Library, London.
- Wah, C.K. (Ed.) (1990). *Defence Spending in Southeast Asia*. Institute of Southeast Asian Studies, Singapore.

# DEMYSTIFYING SHIP OPERATIONAL AVAILABILITY: AN INNOVATIVE APPROACH FOR MANAGEMENT OF IN-SERVICE SUPPORT CONTRACTS

Al-Shafiq Abdul Wahid<sup>1\*</sup>, Mohd Zamani Ahmad<sup>2</sup>, Khairol Amali Ahmad<sup>3</sup>, Joshua P. Taylor<sup>4</sup>, Aisha Abdullah<sup>5</sup>, Al-Athirah Al-Shafiq<sup>6</sup>, Arifah Ali<sup>7</sup> & Keizo Kitagawa<sup>8</sup>

<sup>1,7</sup>Faculty of Mechanical Engineering, Universiti Teknologi Malaysia (UTM), Malaysia

<sup>2</sup>Institut Sultan Iskandar, Universiti Teknologi Malaysia (UTM), Malaysia

<sup>3</sup>Faculty of Engineering, National Defence University of Malaysia (UPNM), Malaysia

<sup>4</sup>Commander, US Navy, US Embassy, Malaysia.

<sup>5,6</sup>Enigma Technical Solutions Sdn. Bhd., Malaysia

<sup>8</sup>Captain, Japanese Maritime Self-Defence Force, Japan

\*Email: al\_shafiq@hotmail.com

## ABSTRACT

*Asset availability optimisation concepts have been studied in a multitude of industries for a few decades now. The defence industry is no exception, whilst traditionally navies worldwide were concerned in achieving targeted ship availability, nowadays budget and regulatory restrictions increase the burden for all stakeholders. Most concepts developed are applied to systems that do not have many interlinked and parallel operating sub-systems. Nevertheless, navy ships are complex assets and it appears no generic framework has yet been developed that is universally applicable. A key drawback is that historically, proposed efforts remained placed on complex mathematical calculations and estimates, which required not only sophisticated programmes but also limited the understanding to a few highly skilled professionals able to implement them. This has never been appealing to most practitioners as well as the majority of stakeholders who continuously complain about the gap between theory and practice. This paper proposes an innovative 4-step approach by demystifying ship operational availability involving both human and machinery/systems related factors. These factors called downtime influence factors (DIFs) are presented in a simplified 'bite-size' form for better understanding of the practitioners to enable them to appreciate their individual contribution towards improving the common goal achieving higher Ship Operational Availability.*

**Keywords:** *Demystifying ship availability; human and equipment factors; downtime influence factors (DIFs); severe DIFs; 4- step availability improvement.*

## 1. INTRODUCTION

Asset availability optimisation concepts have been introduced and studied at length and in depth in a multitude of industries for a few decades now. For industrial organisations, high asset availability has traditionally been linked to higher profits, while for the defence sectors high availability was viewed as a required performance measure or a targeted Operational Availability ( $A_o$ ) (OPNAVINST 3000.12A, 2003). However, in recent years, government agencies worldwide are increasingly subjected to higher risk compliance with a reducing defence budget. This is also the case for most navies that have to strike a balance to satisfy the various stakeholder requirements. Some navies have pioneered innovative concepts such as contracting for availability as a means to delegate some of the burden to their contractors, such as the Royal Navy in the UK (Tomkins, 2012) and Italian / French Navy through the FREMM Program (Dell'Isola & Vendittelli, 2015). Other navies such as Australia are studying how to achieve the

optimum Preventive Maintenance requirements to mitigate technical risks to an acceptable level, comply with regulations and policy and provide an acceptable level of Ao at the lowest Life Cycle Cost as studied by Hamilton (2016).

The Royal Malaysian Navy (RMN) alike its counterparts world-wide also strives to achieve high Ship Availability within a set budget, whilst achieving its vision of becoming a World Class Navy (RMN, 2017). Nevertheless, even those established navies such as USN, Dutch Navy, Royal Navy UK, Australian Navy have not been able yet to formulate a strategy that can be applied either to their own fleet or universally to improve availability whilst regulatory, quality or / and cost performance measurements are being imposed. In simple terms, there appears to be no generic “best suited methodology”. This is mostly due to the fact that naval vessels are complex assets and have to be viewed as system of systems with highly interlinked relationships. The term System of Systems (SoS) is used by the US Navy Research, Development and Acquisition (2006) in an Engineering Guidebook to describe an integrated force package of interoperable systems acting as a single system to achieve a mission capability.

In accordance to Reliability Analysis Centre (2004), operational availability is not just a function of design but also of maintenance policy, logistics system and other supportability factors. It can be improved by improving the design, improving the support, or both. As availability is a measure of maintenance performance (Parida & Kumar, 2009) , history has shown that efforts resulting in an increase of ship operational availability is commendable. Admiral Bowman was lauded by US Congress for his leadership in achieving an increase of 25% ship operational availability for the CVN21 aircraft carrier (US Congress, 2004). The key concept of the presented research is that Availability can be simply expressed as Uptime and can be formulated as “One minus Downtime” as derived from Hou Na *et al.* (2012). Basically, the lower the Downtime, the higher is the Availability.

Efforts in improving availability and implementing various independent strategies without identifying and understanding the underlying downtime influence factors (DIFs) could be futile as some of these DIFs may be the root cause to the resulting short, medium and long-term issues. Due to limited available data and research into naval ship DIFs, a literature review across various engineering disciplines on factors affecting Downtime and Operational Availability was carried out by the authors. The focus of the research is based around the RMN Patrol Vessels (PVs) that are currently being maintained through the In-Service Support (ISS) Contract between the Government of Malaysia (GoM) and Boustead Naval Shipyard (RMN, 2011). The ISS Contract covers Maintenance Services, Spare Parts, Training and Computer Support System for Maintenance.

This paper represents the latest instantiation of a series of evolving work by the authors, subsequent to Al-Shafiq *et al.* (2018) attempting to improve the methods and techniques used by various stakeholders worldwide in their attempt in improving their operational availability figures in general, with an immediate application to naval surface combatants. The main contributions include the consolidation of a multitude of DIFs related to human and equipment from various fields of research, the ranking of DIFs to identify the most troublesome factors, the application of multiple rounds of Delphi Methodology with Snowballing Technique to improve rigour of the study. The findings are introduced in a simplified ‘bite-size’ approach which can easily be appreciated by practitioners to enable them recognize their individual contribution towards improving the organization’s operational availability.

## **2. METHODOLOGICAL APPROACH TO THE RESEARCH**

### **2.1 Gap between Theory and Practice**

The authors agree with the findings of Dekker (1996) that many papers have been written for math purposes only. Mathematical analysis and techniques, rather than solutions to real problems, have been central to many papers in maintenance optimisation models. However, the mathematical results are not appealing to practitioners. Dekker (1996) continued by stating that it is astonishing how little attention is paid either to make results worthwhile or understandable to practitioners, or to justify models on real problems or to consider data problems.

The authors further agree with Dekker (1996) that companies are not interested in publication and that many good ideas have been developed in industry, but only a small amount has appeared in scientific literature. To have academics study industrial problems, they have to be exposed to them and be rewarded if they solve them. Although academic freedom is a great thing, it does not force academics to tackle industrial problems. Therefore, companies should stimulate researchers by offering them problems and allowing them to analyse and publish their results. Dekkers (1996) also reiterated that sometimes if approaches are successful, companies are afraid of losing a competitive edge by publishing their findings. A competitor might use information disclosed in a scientific paper to develop a competing product or otherwise gain commercial advantage or to discredit the product claims of the company making the disclosure (National Research Council, 2003). Furthermore, scientific literature focuses on new aspects and thus, the tenth application of a model will not be published. Therefore, the authors have embarked on the journey of bridging the knowledge gap between academics and practise, with the hope that the published study would benefit all, academics and practitioners alike.

### **2.2 Identification of the Downtime Influence Factors**

The identification of research variables begins with a thorough review of over 700 literatures concerning downtime elements that affects the availability of naval vessels, and downtime of equipment and systems from various fields of research. Subsequently a further literature review was conducted in determining other relevant data to the study from various stakeholders including copies of the ISS contract, historical records of vessel condition, home base of vessel (location), vessel operations area, mission schedule, availability of maintenance support facilities, availability of spares support, logistical support, infrastructure, availability of Original Equipment Manufacturers (OEM) and specialists, availability of special tools and test equipment, funding approval period, budget and cash flow status, and management organisation structure.

All pertinent information relevant to the scope of the current ISS contract includes Planned Maintenance or Preventive Maintenance (PM), Corrective Maintenance (CM), provision of spares, computer support, engineering support, training and Integrated Logistics Support (ILS) were collected. Other relevant information beyond the ISS contract but relevant during the implementation of ISS activities such as the RMN Administrative Order for the execution of ISS, was also collected for study. The generic list of variables consisted of close to 100 variables, most of which were believed by the researcher to be similar in meaning and interpretation. In order to reduce the list and pool into a more manageable number of groups with relevant terms for better understanding for future stages, a Focus Group Discussion was conducted.

A 7-Stage modified sequential Delphi approach into identifying the DIFs for the RMN ISS for patrol vessels (PV) was carried out as summarised in Table 1 and presented by Al-Shafiq *et al.* (2017a, b). The objective was to discover and better understand the unavailability causes and to highlight as well as to prioritise the areas of improvement. A panel of 30 professionals directly



involved in naval ship maintenance was selected and their expert opinion was sought via various questionnaires. In the subsequent stage, five Top Management Experts as proposed via Snowballing Technique in earlier rounds were used to validate and confirm the findings.

**Table 1: The seven stages of the Delphi study.**

Research Stage	Phase, Expert Group & Delphi Round	Activity and Results
Stage 1 Focus Group Discussion (FGD)	Phase 1 Expert Group 1	<ul style="list-style-type: none"> <li>Focus Group Discussion conducted.</li> <li>50 DIFs pooled from various literatures across various engineering fields.</li> </ul>
Stage 2 Delphi Round 1	Phase 1 Expert Group 1	<ul style="list-style-type: none"> <li>30 experts identified for survey.</li> <li>50 DIFs confirmed by experts.</li> <li>Weightage of severity (probability versus likelihood of occurrence) through risk analysis obtained.</li> </ul>
Stage 3 Delphi Round 2	Phase 1 Expert Group 1	<ul style="list-style-type: none"> <li>Same 30 experts surveyed.</li> <li>Consensus from previous rounds achieved.</li> <li>Severe DIFs identified with probability of likely (4 and above) and impact (4 and above).</li> <li>Snowballing to identify top management experts conducted.</li> <li>Selection criteria of top management experts.</li> </ul>
Stage 4 Delphi Round 3	Phase 2 Expert Group 2 (Top Management)	<ul style="list-style-type: none"> <li>5 top management experts selected and surveyed.</li> <li>Confirmation of 50 DIFs.</li> <li>Weightage of severity to identify 15 most severe DIFs.</li> </ul>
Stage 5 Delphi Round 4	Phase 2 Expert Group 2 (Top Management)	<ul style="list-style-type: none"> <li>Same 5 top management experts surveyed.</li> <li>Consensus from top management experts achieved.</li> <li>Reconfirmation of Severe DIFs.</li> <li>15 most severe DIFs ranked.</li> </ul>
Stage 6 Delphi Round 5	Phase 3 Expert Group 2 (Top Management)	<ul style="list-style-type: none"> <li>Same 5 top management experts surveyed.</li> <li>Confirmation of DIFs that impact ship availability from KPI impact assessment.</li> </ul>
Stage 7 Delphi Round 6	Phase 3 Expert Group 2 (Top Management)	<ul style="list-style-type: none"> <li>Same 5 top management experts surveyed.</li> <li>Consensus from top management experts achieved.</li> </ul>

Table 2 summarises the 50 categories of DIFs as supported by literatures from various fields and Focus Group Discussion (FGD) involving the 30 experts.

**Table 2: Summary of 50 DIFs and the relevant literature.**

S/No	DIFs for Ship Operational Availability	Authors of literatures from various fields
1	Equipment and Systems – Hull and Design	(GAO, 1981), (GAO, 1982), (GAO, 2014a), (GAO, 2014b), (GAO, 2014c), (Rosenberger & Pointner, 2015), (Dell'Isola & Vendittelli, 2015), (Forsthoffer, 2005), (Bloch&Geitner, 2012), (Jardine <i>et al.</i> , 1993), (Allred, 1995), (IAEA, 2005), (Prasertrunguang & Hadikusumo, 2009), (Glorian & Spiegelberg, 1998), (Dhillon, 2002), (Papavinasam, 2013), (Al-Najjar, 1998), (Nepal & Park, 2004), (WEC, 1991), (Balafas <i>et al.</i> 2010), (Odeyinde, 2008), (Lazakis <i>et al.</i> , 2010), (Sinnsamy <i>et. al.</i> , 2017).
2	Equipment and Systems – Main Propulsion	
3	Equipment and Systems – Electrical	
4	Equipment and Systems – Weapon Systems including guns and missiles	
5	Equipment and Systems – Auxiliaries	

6	Equipment and Systems – Outfittings	
7	Maintenance Policy - Priority on Type of Maintenance	(Dell'Isola & Vendittelli, 2015), (GAO, 2014b), (GAO, 2014c), (Sullivan, 2011), (Driessen <i>et al.</i> 2010), (Stackley, 2009), (Dhillon, 2002), (Edwards <i>et al.</i> , 1998), (Jonsson, 1997), (Gits, 1994), (Ford <i>et al.</i> , 2013), (GAO, 1982), (Jardine <i>et al.</i> , 1993), (Al-Najjar, 1998), (Marquez & Gupta, 2005), (Colosi <i>et al.</i> , 2010), (Pascual <i>et al.</i> , 2006), (Park <i>et al.</i> , 2010), (Nepal & Park, 2004), (Goossens, 2015), (Jazouli & Sandborn, 2011), (Stambaugh & Barry, 2014), (Pan <i>et al.</i> , 2012), (Reliability Analysis Centre, 2004), (Boyle <i>et al.</i> , 2011), (Farajiparvar, 2012), (U.S. Navy, 2014).
8	Awareness of Importance of Maintenance / Attitude – including hiding problems from becoming official.	(Leva & McDonald, 2013), (GAO, 1982), (Bloch & Geitner, 2012), (Morris & Sember, 2008), (Jonsson, 1997), (Marquez & Gupta, 2005), (Banaitiene & Banaitis, 2012), (Attwater <i>et al.</i> , 2014), (Mafini & Dubihlela, 2013), (Obeng-Odoom & Amedzro, 2011), (Zahedi-Seresht <i>et al.</i> , 2014), (Chang, 1999), (Blaikie, 1993).
9	Maintenance Budget Allocation	(Dell'Isola & Vendittelli, 2015), (Sullivan, 2011), (Dhillon, 2002), (Dhillon, 2002), (Lock, 2014), (GAO, 2014), (GAO, 2014b), (Commission on Wartime Contracting, 2011), (Jardine <i>et al.</i> , 1993), (Stambaugh & Barry, 2014), (Nepal and Park, 2004), (Jonsson, 1997), (Dekker, 1996), (GAO, 1982), (Walker, 2005), (Bateson, 1985), (Kazi, 2005), (Swanson, 2001), (Henry & Bil, 2015), (Garel, 2013), (Romzek & Johnston, 2002), (Apte <i>et al.</i> , 2008), (Yuan, 2016), (Atkinson, 1999), (Pascual <i>et al.</i> , 2008), (Stambaugh & Barry, 2014), (Eckstein, 2016), (Erwin, 2014), (Balafas <i>et al.</i> , 2010), (Odeyinde, 2008), (Zahedi-Seresht <i>et al.</i> , 2014)
10	Information Management	(GAO, 1982), (Ford <i>et al.</i> , 2013), (Bloch & Geitner, 2012), (Jonsson, 1997), (Ljungberg, 2009), (Belkhamza & Wafa, 2012), (U.S. Congress, 1986), (RAND, 1996), (IAEA, 2005), (Jardine <i>et al.</i> , 1993), (Dekker <i>et al.</i> , 1998), (GAO, 2002), (Mathew <i>et al.</i> , 2006), (Harz, 1981)
11	Preventive Maintenance	(Rosenberger & Pointner, 2015), (Driessen <i>et al.</i> , 2010), (Dhillon, 2002), (Bloch & Geitner, 2012), (Edwards <i>et al.</i> , 1998), (Pecht, 2009), (Jonsson, 1997), (IAEA, 2005), (Gits, 1994), (Dell'Isola & Vendittelli, 2015), (Pogačnik <i>et al.</i> , 2015), (Marquez & Gupta, 2005), (Katsikas <i>et al.</i> , 2014), (Kadry, 2013), (Alabdulkarim <i>et al.</i> , 2004), (Pan <i>et al.</i> , 2012), (Mathew <i>et al.</i> , 2006), (Marais <i>et al.</i> , 2013), (Popovic <i>et al.</i> , 2011)
12	Corrective Maintenance	(GAO, 1981), (Driessen <i>et al.</i> , 2010), (Dhillon, 2002), (Jonsson, 1997), (Cooke & Paulsen, 1997), (Ross, 2009), (Dell'Isola & Vendittelli, 2015), (Pogačnik <i>et al.</i> , 2015), (Kadry, 2013), (Chang, 1999), (Marais <i>et al.</i> , 2013), (Schreiber, 2007), (Deris <i>et al.</i> , 1999), (Eti <i>et al.</i> , 2004), (Weibull, 2017)
13	Predictive Maintenance	(Dell'Isola & Vendittelli, 2015), (Dhillon, 2002), (Bloch & Geitner, 2012), (Edwards <i>et al.</i> , 1998), (Cooke & Paulsen, 1997), (Swanson, 2001), (Marquez & Gupta, 2005), (Katsikas <i>et al.</i> , 2014), (Popovic <i>et al.</i> , 2011), (Offenbeek & Vos, 2016).
14	Emergency Repair & Docking	(Houtum & Kranenburg, 2015), (Pizam, 2010), (Telsang, 2007), (GAO, 2005), (Dhillon, 2002), (Jonsson, 1997), (Kowalski, 2002).

15	Equipment Technology / System Complexity	(Dell'Isola & Vendittelli, 2015), (McNamara <i>et al.</i> , 2015), (Jonsson, 1997), (Psenka, 2008), (Ross, 2009), (Pecht, 2009), (Kobbacy & Murthy, 2008), (Dean, 2003), (Walsh, 2014), (Darnall & Preston, 2010), (Deris <i>et al.</i> , 1999), (Glorian & Spiegelberg, 1998), (Xia <i>et al.</i> , 2012), (Ford <i>et al.</i> , 2013), (Dhillon, 2002), (Blaikie, 1993), (Marquez & Gupta, 2005), (Mavris, 2007)
16	Scheduling Issues	(Persson & Stirna, 2015), (Wilson, 2015), (Wilson, 2014), (Peters, 2014), (Bawa, 2009), (Kerzner, 2013), (Burford, 2012), (Banaitiene & Banaitis, 2012), (Badiru, 2009), (Colosi <i>et al.</i> , 2010), (Park <i>et al.</i> , 2010), (Odeh & Battaineh, 2002), (Darabaris, 2006), (Deris <i>et al.</i> , 1999), (GAO, 1981), (Xia <i>et al.</i> , 2012), (Dhillon, 2002), (Miau & Holdaway, 2013), (Pogačnik <i>et al.</i> , 2015), (Atkinson, 1999), (Marquez & Gupta, 2005), (Nepal & Park, 2004), (Pan <i>et al.</i> , 2012), (Jonsson, 1997), (Marais <i>et al.</i> , 2013), (Dekker <i>et al.</i> , 1998), (Swanson, 2001)
17	Maintenance of Special Tools, Test Equipment	(Dell'Isola & Vendittelli, 2015), (Pecht, 2009), (Dhillon, 2002), (GAO, 1982), (Atkinson, 1999), (Staub-French & Nepal, 2007), (Harz, 1981), (Mathew <i>et al.</i> , 2006)
18	Availability of Facilities	(Dell'Isola & Vendittelli, 2015), (Rosenberger & Pointner, 2015), (Banaitiene & Banaitis, 2012), (GAO, 1981), (Denman, 1999), (GAO, 2015b), (IAEA, 2005), (Dhillon, 2002), (GAO, 1982), (Deris <i>et al.</i> , 1999), (Henry & Bil, 2015), (Pogačnik <i>et al.</i> , 2015), (Nepal and Park, 2004), (Harz, 1981), (Balafas <i>et al.</i> , 2010), (Darabaris, 2006)
19	Spares Availability	(McNamara <i>et al.</i> , 2015), (Dell'Isola & Vendittelli, 2015), (Rosenberger & Pointner, 2015), (Banaitiene & Banaitis, 2012), (Driessen <i>et al.</i> , 2010), (Gits, 1994), (RAND, 1996), (Denman, 1999), (Dhillon, 2002), (GAO, 1982), (GAO, 1981), (Jardine <i>et al.</i> , 1993), (Marquez & Gupta, 2005), (Colosi <i>et al.</i> , 2010), (Nepal and Park, 2004), (Harz, 1981), (Balafas <i>et al.</i> , 2010), (Sandborn, 2013)
20	Obsolescence Issues	(Allman, 2015), (Dell'Isola & Vendittelli, 2015), (Mequignon & Haddou, 2014), (Moir & Seabridge, 2012), (Finch, 2012), (Bartels <i>et al.</i> , 2012), (Clavareau & Labeau, 2009), (Adriaansen, 2004), (National Research Council, 1993), (Driessen <i>et al.</i> , 2010), (Stambaugh & Barry, 2014), (Colosi <i>et al.</i> , 2010), (Nepal and Park, 2004), (Ladetto, 2015), (Sandborn, 2013), (Berkok <i>et al.</i> , 2013), (Freeman & Paoli, 2015), (Benedetto, 2014b), (Erkoyuncu <i>et al.</i> , 2015), (Rojo <i>et al.</i> , 2009)
21	Design and Design Change Issues	(Rosenberger & Pointner, 2015), (Dell'Isola & Vendittelli, 2015), (Papavinasam, 2013), (Xia <i>et al.</i> , 2012), (Dhillon, 2002), (GAO, 1982), (Abowitz & Toole, 2010), (Bloch & Geitner, 2012), (Jonsson, 1997), (Dekker, 1996), (Pecht, 2009), (Coles <i>et al.</i> , 2003), (Smith, 2005), (Temple & Collette, 2013), (Sullivan, 2011), (Australian National Audit Office, 2001), (Psenka, 2008), (Al-Najjar, 1998), (Stambaugh & Barry, 2014), (Ridgway <i>et al.</i> , 2009), (Marquez & Gupta, 2005), (Pascual <i>et al.</i> , 2006).

22	Knowledge Management incl Training, Knowledge and Skills	(Dell'Isola & Vendittelli, 2015), (GAO, 2014a), (Bloch & Geitner, 2012), (Pecht, 2009), (Ross, 2009), (Dollschneider, 2010), (152), (Dhillon, 2002), (Swanson, 2001), (Najjar, 1998), (Glorian & Spiegelberg, 1998), (Jonsson, 1997), (U.S. Congress, 1986), (GAO, 1982), (Lock, 2014), (Goh & Yip, 2014), (Comission on Wartime Contracting, 2011), (GAO, 2002), (Glorian & Spiegelberg, 1998), (Al-Shammari, 2009), (Henry & Bil, 2015), (Apte <i>et al.</i> , 2008), (Atkinson, 1999), (Colosi <i>et al.</i> , 2010), (Nepal and Park, 2004), (Harz, 1981), (Balafas <i>et al.</i> , 2010), (Pascual <i>et al.</i> , 2006), (Bianchetti, 2012)
23	Availability of OEM Expert Support	(Dell'Isola & Vendittelli, 2015), (IAEA, 2005), (Dhillon, 2002), (U.S. Congress, 1986), (Stackley, 2009).
24	Availability of Local vendor support	(Dell'Isola & Vendittelli, 2015), (More, 2013), (IAEA, 2005), (Dhillon, 2002), (Denman, 1999), (GAO, 1982), (Palvia <i>et al.</i> , 1996), (Karampelas, 2005).
25	Complexity and efficiency of existing contract	(Xia <i>et al.</i> , 2012), (USN 2012), (McNamara <i>et al.</i> , 2015), (Pecht, 2009), (Pascual <i>et al.</i> , 2006), (Offenbeek & Vos, 2016), (Balafas <i>et al.</i> , 2010), (Price, 2013), (Wiggins, 1985), (Stackley, 2009).
26	Capability of Customer performing Maintenance	(Dell'Isola & Vendittelli, 2015), (Banaitiene & Banaitis, 2012), (Driessen <i>et al.</i> , 2010), (Dearden et al. 1999), (Dollschneider, 2010), (Gibson, 2013), (Al-Shammari, 2009), (Jonsson, 1997), (Ayyub, 2000), (GAO, 1982), (Berkok <i>et al.</i> , 2013), (Mokaya & Kittony, 2008), (Harz, 1981), (Morris & Sember, 2008), (Obeng-Odoom & Amedzro, 2011).
27	Morale & Attitude of Customer involved in Maintenance	
28	Morale & Attitude of Contractor involved in Maintenance	(Jonsson, 1997), (GAO, 1982), (U.S. Congress, 1986), (Leva & McDonald, 2013), (Bloch & Geitner, 2012), (Morris and Sember, 2008), (Banaitiene & Banaitis, 2012), (Obeng-Odoom & Amedzro, 2011), (Attwater <i>et al.</i> , 2014), (Odeh & Battaineh, 2002), (Rendon, 2009), (Rendon & Snider, 2008).
29	Efficiency of Processes, Procedures and reporting structure include Finance	(Dell'Isola & Vendittelli, 2015), (Sullivan, 2011), (Dillon, 2002), (Lin <i>et al.</i> , 2015), (Thai, 2004), (Burford, 2012), (Odeh & Battaineh, 2002), (Foerst, 2010), (Goh & Yip, 2014), (McIntosh, E&Y, 2003), (Bloch & Geitner, 2012), (Jardine <i>et al.</i> , 1993), (Edwards <i>et al.</i> , 1998), (GAO, 1982), (Harz, 1981), (Bianchetti, 2012).
30	Ship Operational/sailing schedule	(RAND, 2006), (House of Commons Defence Committee, 2006), (Popovic <i>et al.</i> , 2011), (Marais <i>et al.</i> , 2013)
31	Non-Commonality of Equipment issues	(Driessen <i>et al.</i> , 2010), (Chang, 1999)
32	Non-Redundancy of Equipment	(Driessen <i>et al.</i> , 2010), (Dekker, 1996), (U.S. Congress, 1986), (Rosenberger & Pointner, 2015), (Nannapaneni <i>et al.</i> , 2014), (Lin <i>et al.</i> , 2015), (Staub-French & Nepal, 2007), (More, 2013), (Marquez & Gupta, 2005), (Pascual <i>et al.</i> , 2006)
33	High Turnover of maintenance supervisors.	(Chitram, 2008), (Dhillon, 2002), (Tan <i>et al.</i> , 2002), (Lowry <i>et al.</i> , 2006), (Mathew <i>et al.</i> , 2006), (Mokaya & Kittony,

34	High Turnover of maintainers	2008), (Thomas, 2013), (Mafini & Dubihlela, 2013), (GAO, 2014c), (Belkhamza & Wafa, 2012), (Price, 2013), (Parliament UK, 2008), (Wang <i>et al.</i> , 2010)
35	Different location of ships	(RMN, 2011), (Dhillon, 2002), (GAO, 2015), (Golding & Griffis, 2003), (Lu <i>et al.</i> , 2010), (Skoko <i>et al.</i> , 2013).
36	Statutory requirements	(IAEA, 2005), (WEC, 1991), (Goh & Yip, 2014), (Marquez & Gupta, 2005), (Glorian & Spiegelberg, 1998), (Lock, 2014)
37	Cashflow Shortages	(Banaitiene & Banaitis, 2012), (IAEA, 2005), (GAO, 1982), (GAO, 1981), (GAO, 2014a), (GAO, 2014c), (Denman, 1999), (U.S. Navy, 2012), (Lock, 2014), (GAO, 2014b), (Glorian & Spiegelberg, 1998), (IAEA, 2005)
38	Government Requirements and Policies (i.e. EEP, Offset etc),	(MOF, 2011), (TDA, 2010-2017), (Berkok <i>et al.</i> , 2013), (Bil & Mo, 2013), (Rendon, 2009), (Lee & Dobler, 1971), (Moe, 1984), (Romzek & Johnston, 2002)
39	Variation Order and Contract Change	(Banaitiene & Banaitis, 2012), (Lock, 2014), (Apte <i>et al.</i> , 2008), (Carter, 2015), (Odeh & Battaineh, 2002), (Rendon, 2009), (Thai, 2004), (Rendon & Snider, 2008), (GAO, 2009), (Rendon, 2009), (Rendon, 2009b), (Humbert & Mastice, 2014), (Price, 2013), (Romzek & Johnston, 2002).
40	Ageing /Aging of Equipment	(Mathew <i>et al.</i> , 2006), (Ladetto, 2015), (Glorian & Spiegelberg, 1998), (Colosi <i>et al.</i> , 2010), (Garel, 2013), (Marquez & Gupta, 2005), (Keller <i>et al.</i> , 2002), (Stambaugh & Barry, 2014), (Pascual <i>et al.</i> , 2006), (Park <i>et al.</i> , 2010), (Mafini & Dubihlela, 2013), (Offenbeek & Vos, 2016), (Davis, 2014), (Boonstra <i>et al.</i> , 2008), (Bianchetti, 2012), (Rendon, 2009), (Nepal and Park, 2004), (Chang, 1999), (Rendon & Snider, 2008)
41	Force Majeure	(RMN, 2011), (IAEA, 2005) (Nepal & Park, 2004),
42	Accidents & Hazards	(IAEA, 2005), (Reuvid, 2012), (Driessen <i>et al.</i> , 2010), (Twigge-Molecey and Price, 2013), (Banaitiene & Banaitis, 2012), (Bawa, 2009), (U.S. Bureau of Mines, 1998), (Ridgway <i>et al.</i> , 2009), (Nepal and Park, 2004), (Mathew <i>et al.</i> , 2006), (Soares, 2014), (Mahaffey, 2014), (Deodatis <i>et al.</i> , 2013), (Berkok <i>et al.</i> , 2013), (Rendon, 2009), (Ceric, 2011), (Stambaugh & Barry, 2014), (Sawyer, 1997), (Rendon & Snider, 2008)
43	Extraordinary Price Escalations (Spares, Consumables, Equipment)	(Banaitiene & Banaitis, 2012), (Lock, 2014), (Driessen <i>et al.</i> , 2010)
44	Pilferage, Theft & Fraud & Cheat	(McAfee & Champagne, 1994), (Hayes, 2014), (Doig, 2012), (Taska & Barnes, 2012), (Foerst, 2010), (U.S. Congress, 1986), (McIntosh E&Y, 2003), (Commissioning on Wartime Contracting, 2011), (GAO, 2015).

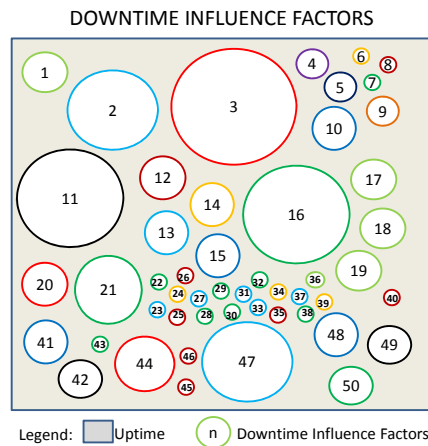
45	OLM, ILM, DLM - Overlap of maintenance duties (contractual) and impact if not performed	(U.S. Navy 2012), (Xia <i>et al.</i> , 2012), (Jonsson, 1997), (GAO, 1982), (Henry & Bil, 2015), (Balafas <i>et al.</i> , 2010), (Ford <i>et al.</i> , 2013), (Deris <i>et al.</i> , 1999), (Crane & Livesey, 2003), (Lim <i>et al.</i> , 2013), (Offenbeek & Vos, 2016), (Sword, 2010).
46	Contract Management across a wide range of stakeholders with conflicting interests	(Lock, 2014), (Gracht, 2012), (Wilkinson, 2009), (Chermack & Nimon, 2008), (Aven & Korte, 2003), (Rendon, 2009), (Price, 2013), (Kwak & Smith, 2009), (Nasab <i>et al.</i> , 2015), (Zahedi-Seresht <i>et al.</i> , 2014), (Jardine <i>et al.</i> , 1993), (Ford <i>et al.</i> , 2013), (U.S. Navy, 2012), (Pogačnik <i>et al.</i> , 2015), (Atkinson, 1999), (Davis, 2014), (263), (Boonstra <i>et al.</i> , 2008), (Xia <i>et al.</i> , 2012), (Taska & Barnes, 2012), (Rendon & Snider, 2008), (Offenbeek & Vos, 2016)
47	Impact of Parallel Contracts to Schedule, Genuinity of Spares, Professionalism of Repair Team etc.	(Sahoo, 2013), (Wearne, 1993), (Lawson <i>et al.</i> , 1999), (Carter, 2013)
48	Supporting of the Vessel outside of home ports (e.g. issue on mob, availability of materials etc.)	(Dell'Isola & Vendittelli, 2015), (GAO, 2015), (Golding & Griffis, 2003), (Lu <i>et al.</i> , 2010), (Skoko <i>et al.</i> , 2013).
49	Exogenous factors (i.e. company profit margin, administrative costs, peripheral costs, support cost)	(Dell'Isola & Vendittelli, 2015), (Banaitiene & Banaitis, 2012), (IAEA, 2005), (Henry & Bil, 2015), (Staub-French & Nepal, 2007), (Darnall & Preston, 2010), (Mathew <i>et al.</i> , 2006)
50	Exogenous factors - Contract Concept (Total Maintenance Package against segregated orders without interrelationships) and based on recommendations	(Dell'Isola & Vendittelli, 2015), (RAND, 1996), (Keller <i>et al.</i> , 2002), (Rusi Defence System, 2012)

### 2.3 Ranking of the Severe Downtime Influence Factors

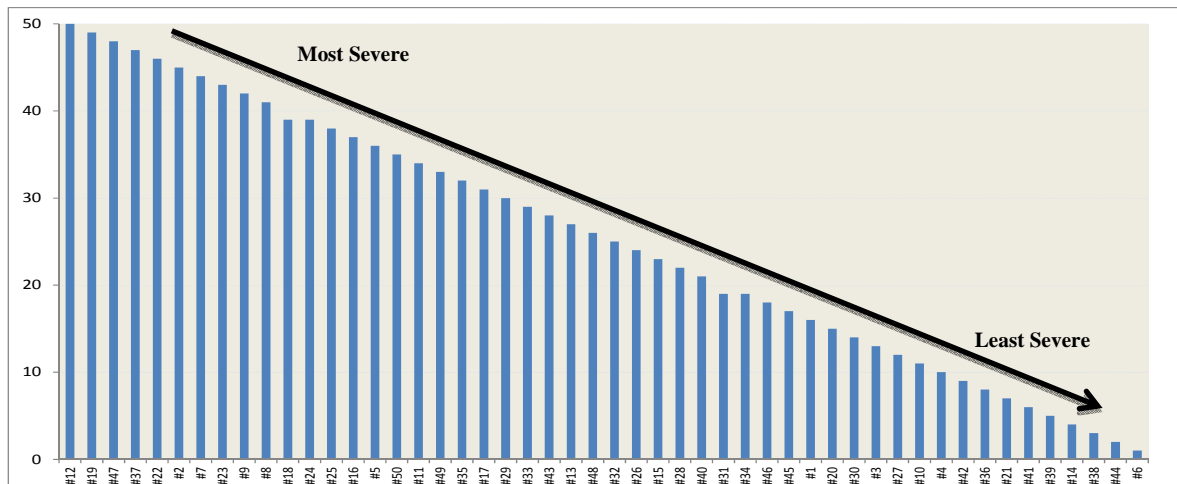
The simplified DIF model as shown in Figure 1 portrays the relationship between Uptime and Downtime (and availability) as well as the various DIFs that make up the Downtime, for the benefit of all levels of stakeholders.

Nevertheless, the sizes of the individual DIFs are yet to be determined at this stage. Figure 2 graphically represents the ranking of DIFs from most to least severe based on Delphi rounds. This new perspective introduced by the authors clearly shows that by reducing Downtime through either reducing the number of DIFs or reducing the size of the DIFs, the Availability (Uptime) will consequently be increased.

Further research is expected to focus on prioritisation of DIFs based on Risk Assessment methodology and reducing the 50 identified DIFs to those DIFs classified as “High Impact” and “Likely” to occur. In addition, each severe DIF is allocated a Severity Index (SI) that will enable contract managers and project managers to prioritise efforts, as exemplified in Figure 2.



**Figure 1: Conceptual diagram of the 50 DIFs.**



**Figure 2: the 50 Severe DIFs ranked from Most to Least Severe.**

## 2.4 Ranking of Downtime Influence Factors

A total of 15 DIFs were found to be severe based on the Risk Analysis as described in Table 1. An illustration of the derived 15 Severe DIFs impacting RMN Ship Operational Availability and the resulting reduced size of DIFs (improved availability) following improvement efforts by the various stakeholders is reflected in Figure 3.

The size of the sphere for each of the 15 Severe DIFs is proportionate to their Severity Index (SI) as presented in Al-Shafiq *et al.* (2017c). The higher the index, the bigger is the sphere and the more severe the DIF. For example, focusing attention and efforts on the most severe DIF which is “corrective maintenance” in order to reduce the size of this DIF, would result in a sizeable overall improvement in Uptime. An illustration of targeted efforts to improve availability for severe DIFs. “that are easily understood and relatable to any reader” are in Figures 4 and 5 respectively.

The availability dashboards illustrate the overall impact of the improvement based on cumulative efforts. The figures illustrate a small subset of efforts undertaken by the various stakeholders to improve the severe DIFs that encompass a multitude of possibilities that need to be carefully studied.

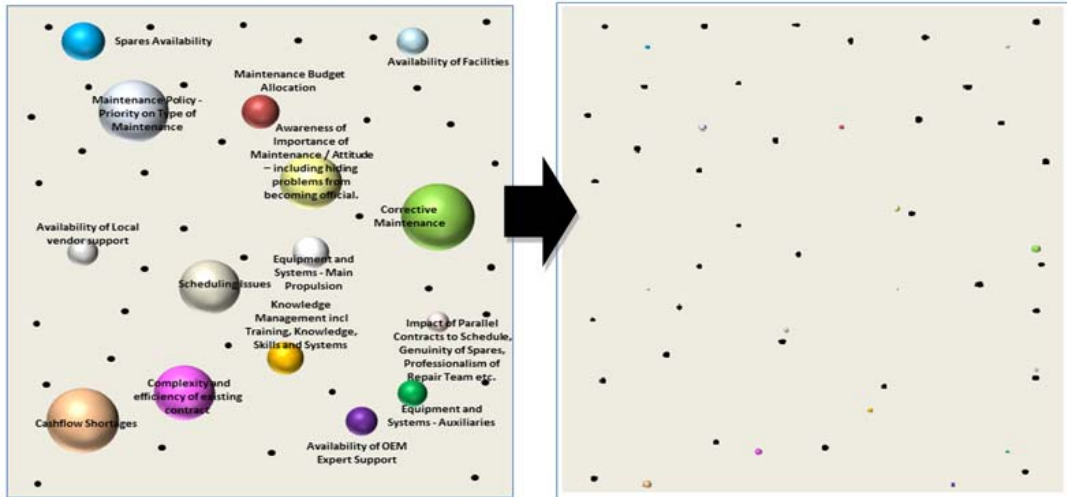


Figure 3: Example of reduction of severe DIFs.

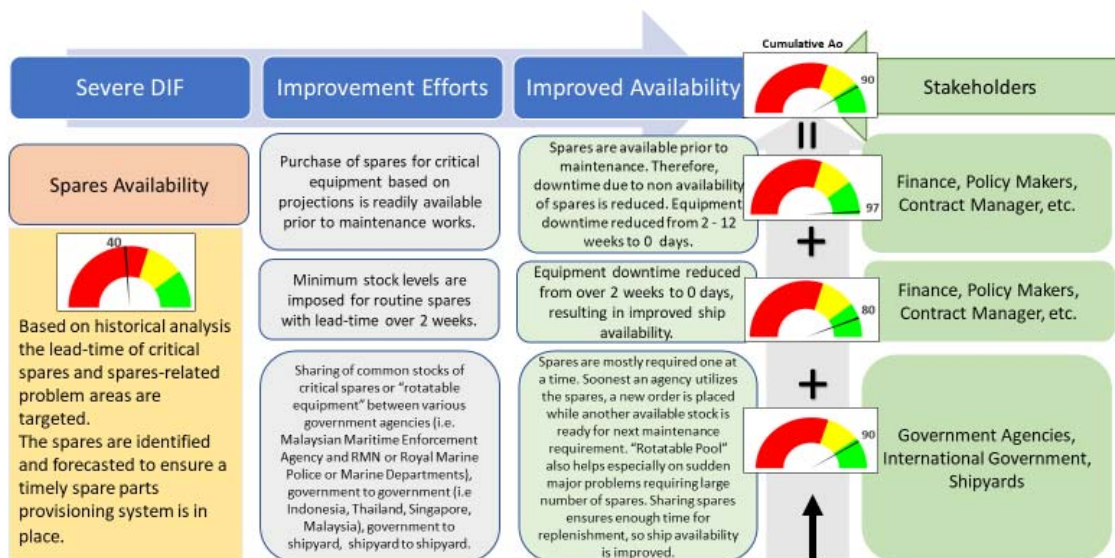


Figure 4: Illustration of Severe DIF "Spares Availability" Improvement Efforts by Stakeholders



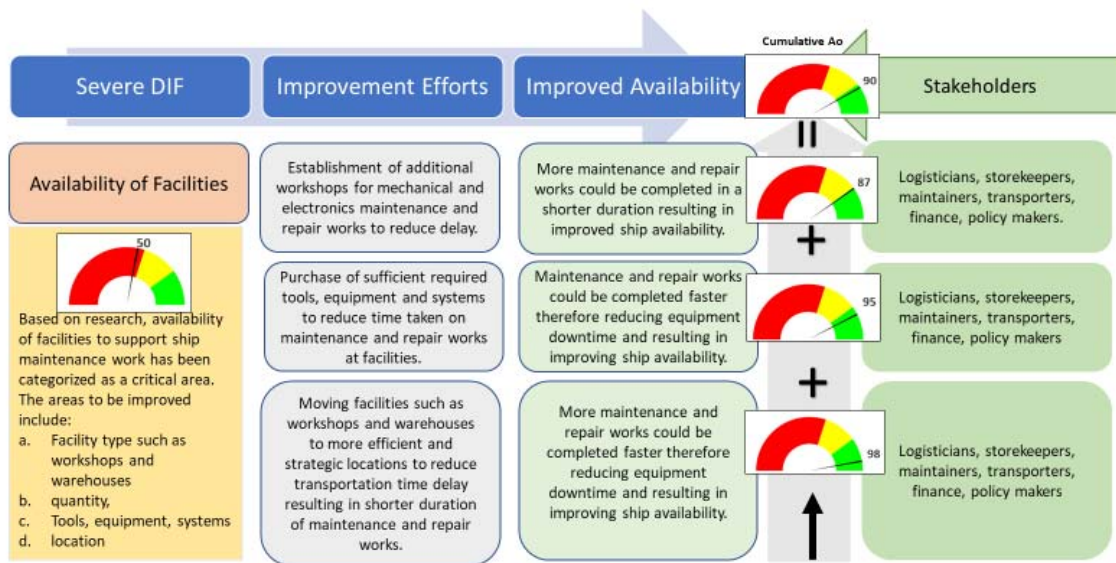


Figure 5: Illustration of Severe DIF “Availability of Facilities” Improvement Efforts by Stakeholders

### 3. RECOMMENDED 4-STEP AVAILABILITY IMPROVEMENT

Following the various graphical illustrations and introduction of a new simple perspective of the relationship between DIFs and Availability described above, the authors hereby summarize the simplified approach through the introduction of the “4-Steps to Availability Improvement” as described in Figure 6.

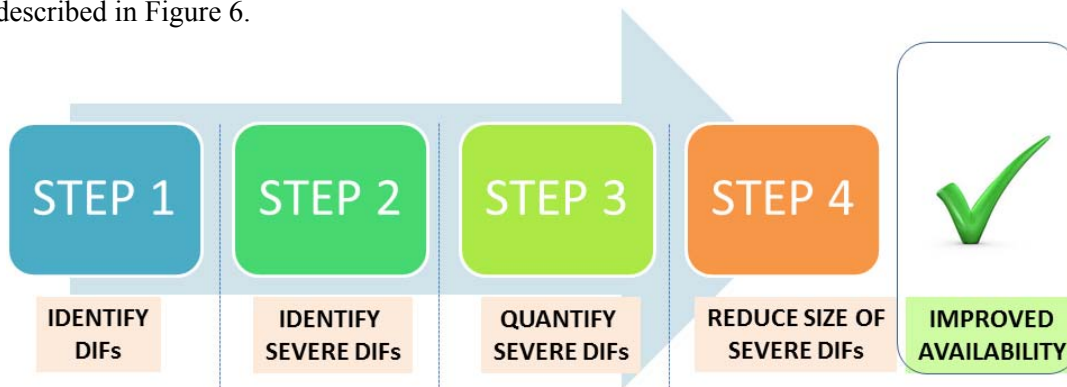


Figure 6: Four steps towards Availability Improvement.

### 4. CONCLUSION AND RECOMMENDATION FOR FUTURE STUDIES

Complex Systems could reasonably be replicated or simulated in a controlled environment i.e. in laboratory with an ascertained INPUT, a pre-determined PROCESS and a precisely measurable OUTPUT. But in open systems environment it becomes extremely complicated to manage. This is especially true for dynamic systems like naval ships whereby many systems operate simultaneously with interdependencies in series and in parallel as well as redundancies, on a floating and moving platform. The obvious answer is that there has not been any model successfully developed and proven to resolve the issues involving complex assets such as the

naval vessels, simply because if there has been any breakthrough, it would have been published and shared globally to be implemented. To date, models and simulations remain on small equipment and systems with many presumed conditions and assumptions which have not reached a stage to be implemented on complex systems.

The proposed 4-Step Availability Improvement philosophy focuses on the systematic reduction of DIFs based on severe or priority DIFs. The authors embarked on a journey to broaden the horizon on available knowledge by progressively evolving from the exhaustive screening of more than 700 literatures to identify the DIFs, until the introduction of a simplified “bite-size” approach for practitioners and stakeholders in general. From the extensive research, the authors have not found any previously-discovered “one-size fits all solution” towards this complex naval ship availability issue.

Nevertheless, it is evident on the valuable contribution of the authors in guiding stakeholders to place the appropriate efforts on tackling the identified DIFs with the aim of improving Naval Ship Availability. However, due to the time, resources and financial constraint involved in this exploratory but highly specialized research in naval ship maintenance which has spanned over 5 years, and in order for the results to remain current for the partial fulfillment of the Doctorate in Mechanical Engineering, the authors have concluded this exploratory research by evidently paving the way for more focused future research in all of the areas covered by the 50 DIFs individually and combined, including the 15 identified Severe DIFs.

## 5. ACKNOWLEDGEMENTS

The authors would like to acknowledge the support of this work by Ministry of Higher Education Malaysia on MyPhd scholarship on tuition fees, University Technology Malaysia and University Pertahanan Nasional Malaysia (UPNM) on academic guidance, Science and Technology Research Institute for Defence (STRIDE) for technical guidance, Boustead Heavy Industries Corporation Bhd (BHIC) and the Royal Malaysian Navy (RMN) for access to data and relevant personnel in enabling this study in partial fulfillment of a Doctorate in Mechanical Engineering.

## REFERENCES

- Abowitz, D. & Toole, M. (2010). Mixed method research: Fundamental issues of design, validity and reliability in construction research. *J. Construction Eng. Manage.*, **136**: 108-116.
- Adriaansen, L. (2004). *Subsea Control and Data Acquisition: Experience and Challenges*. John Wiley & Sons, New Jersey.
- Alabdulkarim, A.A., Ball, P. & Tiwari, A.(2004). Assessing asset monitoring levels for maintenance operations: A simulation approach. *J.Manuf. Tech. Manage.*, **26**: 632-659.
- Allman, K. & Nogales, X.E.D. (2015). *Impact Investment: A Practical Guide to Investment Process and Social Impact Analysis*. John Wiley & Sons, New Jersey.
- Allred, A.G. (1995). Quantitative evaluation of human-rating - The impact of solid propulsion on the reliability and safety of space launch vehicles. *AIAA Space Prog. Tech. Conf.*, 26-28 September 1995, Huntsville, Alabama.
- Al-Najjar, B. (1998). Improved effectiveness of vibration monitoring of rolling bearings in paper mills. Proceedings of the Institution of Mechanical Engineers, Part J. *J Eng. Tribology*, **212**: 111-120.
- AlShafiq, B.A, Mohd Zamani, A., Sunarsih, Mohd Najib, A.G., Ubaidah, M.A., Abdullah, A.B. & Nurhanani, A.A (2017a). Measuring severity of downtime influence factors to naval ship operational availability – A Delphi study, *Asia Int. Multidisciplinary Conf. 2017 (AIMC 2017)*, Universiti Teknologi Malaysia (UTM), Malaysia.

- Al-Shafiq, B.A, Mohd Zamani, A., Sunarsih, Mohd Najib, A.G., Ubaidah, M.A., Abdullah, A.B. & Nurhanani, A.A (2017b). Impact of severe downtime influence factors on operational availability of naval ships – From the contract and project management perspectives. *5<sup>th</sup> Int. Conf. Exhib. Energy Adv. Mater. (ICE-SEAM 2017)*, 16-19 October 2018, Melaka.
- Al-Shafiq, B.A, Mohd Zamani, A., Sunarsih, Mohd Najib, A.G., Ubaidah, M.A., Abdullah, A.B. & Nurhanani, A.A (2017c). Development of a downtime influence factor severity index for improvement of naval ship availability: A simple approach for the Malaysian patrol vessel in-service support contract. *7<sup>th</sup> IEEE Int. Conf. Contr. Syst. Comput. Eng (ICCSCE 2017)*, 24-26 November 2017, Penang.
- Al-Shafiq, B.A., Mohd Zamani, A., Ahmad, K.A. & Abdullah, A.B. (2018). Availability Oriented Contract Management Approach – A simplified view to a complex naval issue. *Defence S&T Tech. Bull.*, **11**: 132-153.
- Al-Shammari, M. (2009). *Customer Knowledge Management: People, Processes, and Technology*. IGI Global, Hershey, Pennsylvania.
- Apte, A.U., Apte, U.M & Rendon, R.G. (2008). Managing the services supply chain in the department of defense: an empirical study of current management practices. *5<sup>th</sup> Annual Acquisition Res. Symp. Nav. Postgrad. School, Acquisition Res., Creating Syner. Informed Change*, 14-15 May 2008, California.
- Atkinson, R. (1999). Project management: cost, time and quality, two best guesses and a phenomenon, its time to accept other success criteria. *Int. J. Project Manage.*, **17**: 337-342.
- Attwater, A. et al. (2014). Measuring the performance of asset management systems, *IET/IAM Asset Management Conference*. Institution of Engineering and Technology (IET), UK.
- Australian National Adit Office (2001). *Contract Management: Better Practice Guide*. Australian National Adit Office, Canberra.
- Aven, T. & Kørte, J. (2003). On the use of risk and decision analysis to support decision-making. *Reliab. Eng. Syst. Safety*, **79**: 289-299.
- Ayyub, B.M. (2000). *Methods for Expert-Opinion Elicitation of Probabilities and Consequences for Corps Facilities*. Institute for Water Resources, U.S. Army Corps of Engineers, US.
- Badiru, D. (2009). *Getting Things Done Through Project Management*. iUniverse, Indiana.
- Balafas, A., Krimizas, S. & Stage, J. (2010). *Impact of Logistics on Readiness and Life Cycle Cost: A Life Cycle Management Approach*. Naval Postgraduate School, California.
- Banaitiene, N. & Banaitis, A. (2012). *Risk Management in Construction Projects, in Risk Management – Current Issues and Challenges*. IntechOpen, London.
- Bartels, B. et al. (2012). *Strategies to the Prediction, Mitigation and Management of Product Obsolescence*. John Wiley & Sons, New Jersey.
- Bateson, J.T. (1985). *In-circuit Testing*. Springer, Netherlands.
- Bawa, H.S. (2009). *Workshop Practice, 2 Ed*. McGraw Hill Education, New York.
- Belkhamza, Z. & Wafa, S.A. (2012). *Measuring Organizational Information Systems Success: New Technologies and Practices*. IGI Global, Pennsylvania.
- Benedetto, G.L.D. (2014). *Additive Manufacturing and Obsolescence Management in the Defence Context*. Research US Department of Defense and US Army, pp. 9-11.
- Bianchetti, R.O. (2012). *How to Reduce the Depot Level Maintenance Delay in the Chilean Navy*. Master Thesis. International Masters School (IMS), pp. 62-73.
- Bil, C. & Mo, J. (2013). Obsolescence management of commercial-off-the-shelf (COTS), *Defence Syst., Concurrent Eng. Approaches Sustainable Product Dev Multi-Discipl. Environ*. Springer, Berlin, pp. 621-632.
- Blaikie, N.W.H. (1993) *Approaches to Social Enquiry*. Polity Press in association with Blackwell, Cambridge.
- Bloch, H.P. & Geitner, F.K (2012). *Machinery Failure Analysis and Troubleshooting*. Butterworth-Heinemann, Oxford.
- Boonstra, A., Boddy, D. & Bell, S. (2008). Stakeholder management in IOS projects: Analysis of an attempt to implement an electronic patient file. *European J. Inf. Syst.*, **17**: 100-111.

- Boyle, G., Little, J., Manning, J. & van der Krogt, R. (2011). A constraint-based approach to ship maintenance for the Irish Navy. *Irish Transport Research Network Conf. 2011*. University College Cork, Cork.
- Burford, L.D. (2012). *Project Management for Flat Organizations: Cost Effective Steps to Achieving Successful Results*. J. Ross Publishing, Florida.
- Carter, J. (2013). *The Construction of Commercial Contracts*. Bloomsbury Publishing, London.
- Carter, R.A. (2015). *Managing Mobile Assets*. Available online at: <https://www.highbeam.com/doc/1P3-3669108641.html> (Last access date: 1 August 2017).
- Chang, M.J. (1999). *Technologies for Improving Current and Future Light Water Reactor Operation and Maintenance: Development on the Basis of O and M Experiences — The Wano Perspective*. International Atomic Energy Agency, Kashiwazaki.
- Chermack, T.J. & Nimon, K. (2008). The effects of scenario planning on participant decision-making style. *Hum. Resour. Dev. Q.*, **19**: 351-372.
- Chitram, L. (2008). *Leadership impact on turnover among power engineers in the Oil Sands of Alberta*. ProQuest, Michigan.
- Ceric, A. (2011). Minimizing communication risk in construction: a delphi study of the key role of project managers. *J. Civil Eng. Manageme.*, **20**: 829-838.
- Clavareau, J. & Labeau, P.E. (2009). Maintenance and replacement policies under technological obsolescence. *Reliab. Eng. Syst. Safety*, **94**: 370-381.
- Coles, R., McDowell, D. & Kirwan, M.J. (2003). *Food Packaging Technology*. CRC Press, Florida.
- Colosi, L., Rothrock, L., Barton, R., Banks, J. & Reichard, K.. (2010). Effects of personnel availability and competency on fleet readiness. *IEEE Annual Conf. Prog. Health Manageme. Soc.*, China, pp. 1-9.
- Commission on Wartime Contracting, Afghanistan (2011). *Transforming Wartime: Contracting Controlling costs, reducing risks* in Commission on wartime contracting in Iraq and Afghanistan. Available online at: [www.wartimecontracting.gov](http://www.wartimecontracting.gov) (Last access date: 15 February 2015).
- Cooke, R. & Paulsen, J. (1997). Concepts for measuring maintenance performance and methods for analysing competing failure modes. *Reliab. Eng. Syst. Safety*, **55**: 135-141.
- Crane, A. & Livesey, S.M. (2003). Are you talking to me? Stakeholder communication and the risks and rewards of dialogue, in *Unfolding Stakeholder Thinking 2: Relationships, Communication, Reporting and Performance*, Greenleaf Publishing, Texas, pp.39-52.
- Darabaris, J. (2006). *Macroengineering: An Environmental Restoration Management Process*. CRC Press, Florida.
- Darnall, R.W. & Preston, J. M. (2010). *Project Management from Simple to Complex*. The Open University of Hong Kong, Hong Kong.
- Davis, K. (2014). Different stakeholder groups and their perceptions of project success. *Intern. J. Proj. Manag.*, **32**: 189-201.
- Dekker, R. (1996). Applications of maintenance optimization models: a review and analysis. *Reliab. Eng. Syst. Safety*, **51**: 229-240.
- Dekker, R. & Scarf, P.A. (1998). On the impact of optimisation models in maintenance decision making: the state of the art. *Reliab. Eng. Syst. Safety*, **60**: 111-119.
- Dell'Isola, A. & Vendittelli, A. (2015). Operational availability (Ao) of warships: A complex problem from concept to in service phase. *IEEE Metrology for Aerospace (MetroAeroSpace)*, 4-5 June 2015, Benevento.
- Dhillon, B.S. (2002). *Engineering Maintenance: A Modern Approach*. CRC Press, Florida.
- Dean, A.W. (2003). *A Statistical Evaluation of Risk Priority Numbers in Failure Modes and Effects Analysis Applied to the Prediction of Complex Systems*. PhD Thesis, Old Dominion University, Norfolk.
- Dearden, J.A., Lilien, G.L. & Yoon, E. 1999. Marketing and production capacity strategy for non-differentiated products: Winning and losing at the capacity cycle game. *Int. J. Res.*

- Marketing*, **16**: 57-74.
- Denman, J. (1999). *Air Force Depot Maintenance: Management Changes Would Improve Implementation of Reform Initiatives*. Diane Pub Co, Collingdale.
- Deodatis, G., Ellingwood, B.R. & Frangopol, M. (2014). *Safety, Reliability, Risk and Life-Cycle Performance of Structures and Infrastructures*. CRC Press, Florida.
- Deris, S., Omatu, S., Ohta, H., Kutar, S. & Samat, P.A. (1999). Ship maintenance scheduling by genetic algorithm and constraint-based reasoning. *Eur. J. Oper. Res.*, **112**: 489-502.
- Doig, A. (2012). *Fraud: The Counter Fraud Practitioner's Handbook*. Gower Publishing Ltd, Aldershot.
- Dollschnieder, S. (2010). *Contact, Care, Communicate : How Interpersonal Skills are the Foundation of Genuine Customer Service*. Xlibris Corporation, Bloomington.
- Driessen, M.A., Arts, J.J, van Houtum, G.J.J.A.N., Rustenburg, W.D. & Huisman, B. (2010). *Maintenance Spare Parts Planning and Control: A Framework for Control and Agenda for Future Research*. Beta Research School for Operations Management and Logistics, Beta working papers series 325, Eindhoven University of Technology, Netherlands.
- Eckstein, M. (2016). *New NAVSEA Commander's Intent: Complete Ship Maintenance on Time*. Available online at: <https://news.usni.org/2016/09/14/new-navsea-commanders-intent-complete-ship-maintenance-availabilities-on-time> (last access date: 1 January 2017).
- Edwards, D.J., Holt, G.D & Harris, F.C. (1998). Predictive maintenance techniques and their relevance to construction plant. *J. Quality Maintenance Eng.*, **4**: 25-37.
- Erkoyuncu, J., Roy, R., Williams, S., Colegrove, P., Martina, F. & Busachi, A. (2015). Opportunities for additive manufacturing to address component obsolescence challenges. In Freeman, J. & Paoli, G.P. (Eds.), *Perspective*. RAND Corporation, California.
- Erwin, S.I. (2014). *Navy's Holy Grail: Low-Maintenance Ships, Highly Skilled Sailors*. Available online at: [www.nationaldefensemagazine.org/blog/lists/posts/post.aspx?ID=1379](http://www.nationaldefensemagazine.org/blog/lists/posts/post.aspx?ID=1379) (Last access date: 1 June 2014).
- Eti, M.C., Ogaji, S.O.T & Probert, S.D. (2004). Implementing total productive maintenance in Nigerian manufacturing industries. *Appl. Energy*, **79**: 385-401.
- Farajiparvar, N. (2012). Increasing profitability supported by innovative methods and designing monitoring software in condition-based maintenance: A case study. *Int. J. Mech., Aerospace Ind. Mechatronic Manuf. Eng.*, **6** : 2530-2538.
- Finch, E. (2012). *Facilities Change Management*. Wiley-Blackwell, Oxford.
- Foerst, A.E. (2010). *Employee Theft in the Retail Industry: A Review of Current Research*, University of Florida, Florida.
- Ford, G., McMahon, C. & Rowley, C. (2013). Naval Surface Ship In-service Information Exploitation. *2nd Int. Through-life Eng. Services Conf*. Elsevier, Amsterdam.
- Forsthoffer, W.E. (2005). Auxiliary Systems. In *volume 4 of Forsthoffer's Rotating Equipment Handbooks*. Elsevier, Amsterdam, p.387.
- Freeman, J. et al. (2015). *Additive Manufacturing and Obsolescence Management in the Defence Context Perspective*. RAND Corporation, California.
- GAO (1981). *Navy Air Launched Missiles-Increased Availability Through Improved Inspection and Maintenance Scheduling Practices*. US Government Accountability Office (GAO), Washington D.C.
- GAO (1982). *Factors Limiting The Availability of F-15 Aircraft at the 1st Tactical Fighter Wing*. US General Accounting Office (GAO), Washington D.C.
- GAO (2002). *Information Management Challenges in Managing and Preserving Electronic Records: Congressional Requesters*, US General Accounting Office (GAO), Washington D.C.
- GAO (2005). *Defense Infrastructure Management Issues Requiring Attention in Utility Privatization*. US General Accounting Office (GAO), Washington D.C..
- GAO (2009). *High-Risk Series: An Update*, US General Accounting Office (GAO), Washington D.C..

- GAO (2014a). *Defense Inventory: Actions Needed to Improve the Defense Logistics Agency's Inventory Management*. U.S Government Accountability Office (GAO), Washington D.C..
- GAO (2014b). *Surface Ships : Navy Needs to Revise Its Decommissioning Policy to Improve Future Decision Making*. U.S Government Accountability Office (GAO), Washington D.C..
- GAO (2014c). *Aviation Workforce: Current and Future Availability of Aviation Engineering and Maintenance Professionals*. U.S. Government Accountability Office (GAO), Washington D.C..
- GAO (2015). *Navy Force Structure: Sustainable Plan and Comprehensive Assessment Needed to Mitigate Long-Term Risks to Ships Assigned to Overseas Homeports*. U.S. Government Accountability Office (GAO), Washington D.C..
- GAO (2015b). *Defense Facilities Consolidation and Disposal: Additional Opportunities to Reduce Fragmentation, Overlap, and Duplication and Achieve Other Financial Benefits*. U.S. Government Accountability Office (GAO), Washington D.C..
- GAO (2015c). *Ford Class Aircraft Carrier: Poor Outcomes are the Predictable Consequences of the Prevalent Acquisition Culture*. U.S. Government Accountability Office (GAO), Washington D.C..
- Garel, G. (2013). A history of project management models: From pre-models to the standard models. *Int. J. Proj. Manag.*, **31** : 663-669.
- Gibson, P. (2013). *The World of Customer Service, 3<sup>rd</sup> Ed.* South-Western CENGAGE Learning, Boston, Massachusetts.
- Gits, C.W. (1994). Structuring maintenance control systems. *Int. J. Oper. & Prod. Manag.*, **14** : 5-17.
- Glorian, D. & Spiegelberg, P.R. (1998). *Thermal Generating Plant (100 MW+) Availability and Unavailability Factors (Data 1994-1996)*. Joint UNIPED/WECC Committee on Availability of Thermal Generating Plant, UNIPED, Paris.
- Goh, L.B. & Yip, T. L. (2014). A way forward for ship classification and technical services. *Asian J. Shipping Logist.*, **30** : 51-74.
- Golding, H.L.W. & Griffis, H.S. (2003). *Increased PERSTEMPO, Retention and Navy Policy*, CNA Corporation, Chicago.
- Goossens, A. (2015) *Maintenance Policy Selection for Ships: An Investigation Using the Analytic Hierarchy Process*. PhD Thesis, University of Twente, Enschede.
- Gracht, H.A.v.d. (2012). Consensus measurement in delphi studies: Review and implications for future quality assurance. *Technol. Forecast. Soc.*, **79**: 1525-1536.
- Hamilton, T. (2016). *Optimisation of Preventive Maintenance in the Royal Australian Navy*. Master Thesis, University of South Australia, Adelaide.
- Harz, C.R. (1981). *Problems in Army Vehicle Maintenance: Results of a Questionnaire Survey*. Defense Advanced Research Projects Agency, RAND Corporation, California
- Hayes, R. (2014). *Retail Security and Loss Prevention*. Butterworth-Heinemann, Oxford..
- Henry, R. & Bil, C. (2015). Sustainment Management in the Royal Australian Navy. *Transdisciplinary Lifecycle Analysis of Systems – Proc. of the 22nd ISPE Inc. Int. Conf. on Concurrent Eng.*, IOS Press, Netherlands.
- House of Commons Defence Committee (2006). *The Defence Industrial Strategy*. Seventh Report of Session 2005-06, The Stationary Office Limited, London
- Na, H., Yi, L., Wang, Y.G., Liu, J.J., Bo, Z. & Lv, X.Z. (2012). Research on the mean logistic delay time of the development phrass. *Physcs. Proc.*, **33**: 375-379
- Houtum, G.-J.v. & Kranenburg, B. (2015). *Spare Parts Inventory Control under System Availability Constraints*. Springer, Berlin..
- Humbert, X.P. & Mastice, R.C. (2014). *Managing Risk by Cradle to Grave Contract Management*. Available online at: <http://www.europeanfinancialreview.com/?p=3245> (last access date: 1 December 2017).
- IAEA (2005). *The Power Reactor Information System (PRIS) and its extension to non-electrical Applications, Decommissioning and delayed Projects Information*. International Atomic

- Energy Agency (IAEA), Vienna.
- Jardine, A.K.S., Zhang, F. & Yan, H. (1996). Enhancing system reliability through maintenance decision making, *IEEE Int. Conf. Syst. Man, Cybernet.*, China.
- Jazouli, T. & Sandborn, P. (2011). Using PHM to meet availability-based contracting requirements, *IEEE Conf. Prognost. Health Manage.*, pp 1-12.
- Jonsson, P. (1997). The status of maintenance management in Swedish manufacturing firms. *Qual. Maint. Eng.*, **3**: 233-258.
- Kadry, S. (2013). *Diagnostics and Prognostics of Engineering Systems: Methods and Techniques*. IGI Global, Pennsylvania.
- Karampelas, P. (2013). *Techniques and Tools for Designing an online Social Network Platform*. 1 ed. Lecture Notes in Social Networks. Springer-Verlag, Vienna..
- Katsikas, S., Dimas, D., Defigos, A., Routzomanis, A. & Mermikli, K.. (2014). Wireless modular system for vessel engines monitoring, condition based maintenance and vessel's performance analysis, *2nd Europ. Conf. Prognost. Health Manage. Society*, France, pp. 1-10.
- Kazi, A.S. (2005). *Knowledge Management in the Construction Industry: A Socio-technical Perspective*. Idea Group Inc (IGI), Pennsylvania.
- Keller, A., Kar, G., Ludwig, H., Dan, A. & Hellerstein, J.L. (2002). Managing dynamic services: a contract based approach to a conceptual architecture, *IEEE Netw. Oper. Manag.. Symp.: Manag.. Solut. New Commun.s World*, 19 April 2002, Florence, Italy.
- Kerzner, H. (2013). *Project Management: A Systems Approach to Planning, Scheduling, and Controlling*, 11 Ed. John Wiley & Sons, New Jersey.
- Kobbacy, K.A.H. & Murthy, D.N.P. (2008). *Complex System Maintenance Handbook*. Springer Series in Reliability Engineering, Springer Science & Business Media, Berlin.
- Kowalski, T.J. (2002). *Planning and Managing School Facilities*. Greenwood Publishing Group, California.
- Kwak, Y.H. & Smith, B.M. (2009). Managing risks in mega defense acquisition projects: Performance, policy, and opportunities. *Int. J. Proj. Manag.*, **27**: 812-820.
- Ladetto, Q. (2015). *The Swiss Perspective on Emerging Technologies of Importance for the Swiss Military*. Available online at: <http://www.rand.org/pubs/perpective/.peni.html> (Last access date: 31 January 2017)
- Lawson, G., Wearne, S.H. & Iles-Smith, P. (1999). *Project Management for the Process Industries*. IChemE, London.
- Lazakis, I., Turan, O. & Aksu, S. (2010). Increasing ship operational reliability through the implementation of a holistic maintenance management strategy. *Ships Offshore Struc.*, **5**: 337-357.
- Lee, L. & Dobler, D. W. (1971). *Purchasing and Materials Management: Text and Cases*. McGraw-Hill, New York.
- Leva, M.C & McDonald, N. (2013). Action research and change management system in aviation. *Advances in Human Aspects of Aviation*, CRC Press, Florida.
- Lim, S., Berry, F. S & Lee, K.H. (2013). Stakeholders in the same bed with different dreams: Semantic network analysis of issue interpretation in risk policy related to mad cow disease. *J. Public Admin. Res. Theory*, **26** : 79-93.
- Lock, D. (2014). *The Essentials of Project Management, 4 Ed*. Routledge, Abingdon.
- Lowry, G., Turner, R.L & Fisher, J. (2006). The contribution of employment satisfaction factors to recruiting, retaining and career development of information systems and technology professionals. *Rev. Bus. Inform. Syst.*, **10**: 137-147.
- Ljungberg, J. & Grundén, K. (2009). Business values of electronic records management in SMEs. *Proc. 3rd Europ. Conf. Inform. Manag.. Eval., Acad. Conf. Ltd.* pp. 51-58.
- Lin, J.C., Leu, F.Y. & Chen, Y.P. (2015). *ReHRS: A Hybrid Redundant System for Improving Mapreduce Reliability and Availability. Modeling and Optimization in Science and Technologies, Vol. 4*. Springer International Publishing, New York.
- Lu, Y., Gao, Y., Cao, Z., Cui, J., Dong, Z. & Tian, Y. (2010). A study of health effects of long-

- distance ocean voyages on seamen using a data classification approach. *BMC Med. Inform. Decis. Mak.*, **10**: 10-13.
- Mafini, C. & Dubihlela, J. (2013). Determinants of military turnover of technical air-force specialists: An empirical case analysis. *Mediterranean J. Soc. Sci.*, **4**: 1-12.
- Mahaffey, J. (2014). *Atomic Accidents: A History of Nuclear Meltdowns and Disasters: From the Ozark mountains to Fukushima*. Open Road Media, New York.
- Marais, K.B. et al. (2013). Modeling the impact of maintenance on naval fleet total ownership cost. *7<sup>th</sup> Annual IEEE Syst. Conf. (SysCon)*, USA, pp. 801-808.
- Marquez, A.C. & Gupta, J.N.D. (2006). Contemporary maintenance management: process, framework and supporting pillars. *Int. J. Manag. Sci. (Omega)*, **34**: 313-326.
- Mathew, J. et al. (2006). Engineering asset management in the *First World Congress on Engineering Asset Management (WCEAM)*. Australia: Springer-Verlag, London.
- Mavris, D.N. (2007). *Design Methodology and Strategies Investigation for Complex Integrated Naval Systems*. Aeospace Systems Design Laboratory (ASDL): Atlanta, Georgia.
- McAfee, R.B. & Champagne, P.J. (1994). *Effectively Managing Troublesome Employees*. Greenwood Publishing Group, Connecticut.
- McIntosh, J. (2003). *Ernst & Young Study Estimates Retailers Lose \$46 Billion Annually to Inventory Shrinkage; Employee Theft is Biggest Problem*. Available online at <https://www.businesswire.com/news/home/20030513005050/en/Ernst-Young-Study-Estimates-Retailers-Lose-46> (last access date: 1 May 2015).
- McNamara, D., McNamara, D., Cunningham, A., Riahi, R. & Jenkinson, I. & Wang, J. (2015). *Modelling of Maintenance and Inspection Policies for Marine Systems using Monte Carlo Simulation and Delay-Time Analysis*. CRC Press, Florida.
- Mequignon, M. & Haddou, H.A. (2014). *Lifetime Environmental Impact of Buildings*. Springer Briefs in Applied Sciences and Technology, Springer International Publishing, New York.
- Miau, J.J. & Holdaway, R. (2013). *Reducing the Cost of Spacecraft Ground Systems and Operations*. Space Technology Proceedings, Springer Science & Business Media, - Technology & Engineering, Berlin.
- Moe, T.M. (1984). The new economics of organization. *American J. Polit. Sci.*, **28** : 739-777.
- Moir, I. & Seabridge. A. (2012). *Design and Development of Aircraft Systems, 2 Ed*. John Wiley & Sons, New Jersey.
- MOF (2011). *Policy and Guideline on Offset Programmes in Government Procurement*. Government of Malaysia, Ministry of Finance.
- Mokaya, S.O. & Kittony, L.K. (2008). Factors that influence labour turnover of aircraft maintenance engineers in Kenya: A case of Kenya airways. *Makerere University Bus. School Int. Manag. Conf.*, Kampala, Uganda, pp. 1-10.
- More, J. (2013). *Assessing Vendors: A Hands-On Guide to Assessing Infosec and IT Vendors*. Syngress, Massachusetts.
- Morris, R.A. & Sember, B.M. (2008). *Project Management That Works*. AMACOM, Toronto, Ontario.
- Nannapaneni, S., Dubey, A., Abdelwahed, S., Mahadevan, S. & Neema, S. (2014). A model-based approach for reliability assessment in component based systems. *Annual Conf. Progn. Health Manag. Soc.*, Fort Worth, Texas.
- Nasab, S.S., Selamat, H. & Masrom, M. (2015). A Delphi study of the important factors for bi system implementation in the public sector organizations. *Jurnal Teknologi*, **77** : 113-120.
- National Research Council (1993). *Fourth Dimension in Building: Strategies for avoiding Obsolescence*. The National Academies Press, Washington D.C.
- National Research Council (2003). *Sharing publication-related Data and Materials: Responsibilities of Authorship in the Life Sciences*. The National Academies Press, Washington D.C.
- Nepal, M.P. & Park, M. (2004). Downtime model development for construction equipment



- management. *Eng., Construct. Architect. Manag.*, **11** : 199-210.
- Odeh, A.M. & Battaineh, H.T. (2002). Causes of construction delay: traditional contracts. *Int. J. Proj. Manage.*, **20** : 67-73.
- Obeng-Odoom, F., Amedzro, L. (2011). Inadequate Housing in Ghana. *Urbani Izziv*, **22** : 127-137.
- Odeyinde, O. (2008). *Optimizing Rotating Equipment Maintenance Management in Nigerian Refineries*. Master of Engineering, North-West University, South Africa.
- Offenbeek, M.A.G.v. & Vos, J.F.J. (2016). An integrative framework for managing project issues across stakeholder groups. *Int. J. Proj. Manag.*, **34** : 44-57.
- OPNAVINST 3000.12A (2003). *Operational Availability of Equipments and Weapons Systems, Operation Naval Instruction*. Department of the Navy, U.S.A.
- Palvia, P.C, Palvia, P.E & Roche E.M (1996). *Global Information Technology and Systems Management: Key Issues and Trends*. Ivy League Publishing, Georgia.
- Pan, E., Liao, W. & Xi, L. (2012). A single machine-based scheduling optimisation model integrated with preventive maintenance policy for maximizing the availability. *Int. J. Ind. Syst. Eng.*, **10**.
- Park, M., Kim, W. & Yoon, Y. (2010). Scheduling decisions and their dynamic consequences on construction performance. *KSCE J. Civil Eng.*, **14**: 251-259.
- Parida, A. & Kumar, U. (2009). Maintenance productivity and performance measurement, in *Handbook of Maintenance Management and Engineering*. Springer, Berlin.
- Parliament, UK. (2008). *Recruiting and Retaining Armed Forces Personnel*. Fourteenth Report of Session 2007-08, D. Committee, House of Commons Parliamentary Publications United Kingdom.
- Pascual, R., Meruanea, V. & Rey P.A. (2008). On the effect of downtime costs and budget constraint on preventive and replacement policies. *Rel. Eng. Syst. Safety*, **93** : 144-151.
- Papavinasam, S. (2013). *Corrosion Control in the Oil and Gas industry*. Elsevier, Amsterdam.
- Pecht, M. (2009). *Product Reliability, Maintainability, and Supportability Handbook, 2<sup>nd</sup> d Ed.* CRC Press, Florida.
- Persson, A., J. & Stirna, J. (2015). Advanced information systems engineering workshops. *Workshop on Enterprise and Organizational Modeling and Simulation*. Springer, Sweden.
- Peters, R. (2014). *Reliable Maintenance Planning, Estimating, and Scheduling*. Gulf Professional Publishing, Oxford.
- Pizam, A. (2010). *International Encyclopedia of Hospitality Management*. Butterworth-Heinemann, Oxford.
- Pogačnik, B., Tavčar, J. & Duhovnik, J. (2015). Application of lean methods into aircraft maintenance processes. *Advances in Transdisciplinary Engineering*, pp. 259- 268.
- Popovic, V.M. et al. (2012). Optimisation of maintenance concept choice using risk-decision factor – a case study. *Int. J Syst. Sci.*, **43** : 1913-1926.
- Prasertrungruang, T. & Hadikusumo, B.H. (2009). Study of factors influencing the efficient management and downtime consequences of highway construction equipment in Thailand. *J. Constr. Eng.Manag.*, **135** : 2-11.
- Price, H. (2013). *Manage Change throughout the Contract Lifecycle*. OpenText™ Contract Management, Ontario.
- Psenka, C.E. (2008). *A Monumental Task: Translating Complex Knowledge in NASA's Human Space Flight Network* . Available online at: ProQuest; <http://gradworks.umi.com/33/41/3341579.html> (Last access date: 10 July 2014).
- RAND (1996). *Contracting for Weapon System Repair: An Examination of Alternative Approaches*. RAND Corporation, California.
- Reliability Analysis Centre (2004). *Operational Availability Handbook: Introduction to Operational Availability*. Vol. RAC-HDBK-3180, New York.
- Rendon, R.G. (2009). *Contract Management Process Maturity: Empirical Analysis of*

- Organizational Assessments*. Naval Postgraduate School, Monterey, California.
- Romzek, B.S. & Johnston, J.M. (2002). Effective contract implementation and management: A preliminary model. *J. Public Admin. Res Theory*, **12** : 423-453.
- Rusi Defence System (2012). *Transforming Warship Support: Class Output Management*. Defence Capability Programmes-Sea, The Royal United Institute for Defence and Security, London.
- Rendon, R.G. & Snider, K.F.(2008). *Management of Defense Acquisition Projects*. American Institute of Aeronautics and Astronautics (AIAA), Washington, D.C..
- Rendon, R.G. (2009). Contract changes management in *Contract Administration: Tools, Techniques and Best Practices*. Riverwood, Ontario.
- Rendon, R.G. (2009b). *Contract Management Process Maturity: Empirical Analysis of Organizational Assessments*. Technical Report NPS-CM-09-124, Acquisition Research Program, Naval Postgraduate School, Monterey, California.
- Reuvid, J. (2012). *Managing Business Risk: A Practical Guide to Protecting Your Business, 9 Ed.* Kogan Page Publishers, London.
- Ridgway, M., Atles, L.R. & Subhan A. (2009). Reducing equipment downtime: A new line of attack. *J. Clinical Eng.*, **34** : 200-204.
- Rojo, F.J.R., Roy, R. & Shehab, E. (2009). Obsolescence management for long-life contracts: State of the art and future trends. *Int. J. Adv. Manuf. Technol.*, **49** : 1235-1250.
- Rosenberger, M. & Pointner, F. (2015). High availability: definition, influencing factors and solutions. *Signal + Draht. Frauscher Sensortechnik GmbH (107) 6/2015*, pp. 32-37.
- Ross, J.M. (2009). Human factors for naval marine vehicle design and operation in *Human Factors in Defence*. Ashgate Publishing Ltd., Farnham.
- Royal Malaysian Navy (2011). *RMN Patrol Vessel - In-Service Support Contract*. RMN, Malaysia.
- Royal Malaysian Navy (2017). *RMN Vision and Mission*. Available online at: <http://www.navy.mil.my/index.php/misi- visi>. (Last access date: 31 Dec 2017).
- Zahedi-Seresht, M. et al. (2014). Construction project success ranking through the data envelopment analysis. *J. Data Envelopm. Analys.Decision Sci.*, pp. 1-13.
- Sahoo, T. (2013). *Process Plants: Shutdown and Turnaround Management*. CRC Press, Florida.
- Sandborn, P. (2013). *Cost Analysis of Electronic Systems.Vol.1*. World Scientific Publishing, Singapore.
- Sawyer, D. (1997). *Do It by Design: An Introduction to Human Factors in Medical Devices*. Centre for Devices and Radiological Health (CDRH), Silver Spring.
- Schreiber, F. (2007). *Maintenance Briefing Notes, Human Performance, Error Management*. Airbus, Leiden.
- Skoko, I., Jurčević, M. & Božić, D. (2013). Logistics aspects of offshore support vessels on the west africa market. *Scientif. J. Traf. Transport. Res.*, **25** : 586-593.
- Smith, R.M. (2005). *Chemical Process: Design and Integration*. John Wiley & Sons Ltd, New Jersey.
- Sinnasamy, Y., Mat Yassin, M.R., Sa'at, N.A., Faiz, H.N., Sutarji, A., Sulaiman, A., Tahir, I., Yaakob, R., Mohd Wazir, A.S., Salehuddin, K.A., Mohd Rashid, M.R., Zubir, A., Kasmoni, H., Louisnaden, E. & Ahmad, K.A. (2017). Recognition of most common diesel engine condition monitoring methods. *Defence S&T Tech. Bull*, **10** : 297-310.
- Soares, C.G. (2014). *Renewable Energies Offshore*. CRC Press, Florida.
- Stackley, S.J. (2009). *Memorandum for Distribution: Comprehensive Contracting and Depot Work Integration Policy for Non-nuclear Shipboard Maintenance and Modernization*. The Assistant Secretary of the Navy, United States of America, Washington DC.
- Stambaugh, K. & Barry, C. (2014). Naval ship structure service life considerations. *Nav. Eng. J.*, **126** : 103-117.
- Staub-French, S. & Nepal, M.P. (2007). Reasoning about component similarity in building product models from the construction perspective. *Automat. Constr.*, **17**: 11-21.
- Sullivan, P.E. (2011). *The Future for Naval Engineering Topics for the Research and*

- Development Community*. Special Report 306: Naval Engineering in the 21st Century the Science and Technology Foundation For Future Naval Fleets Committee, , Transportation Research Board of the National Academies, Washington, D.C..
- Swanson, L. (2001). Linking maintenance strategies to performance. *Int. J. Prod. Econ.*, **70** : 237-244.
- Sword, L.D. (2010). *Conflicts from Confused Roles and Responsibilities*. Available online at: <http://conflictcompetence.com>. (Last access date: 26 July 2010)
- Tan, W.G., Chan, T. & Gable, G.G. (2002). A structural model of software maintainer Effectiveness. *10th Australasian Conf. Inf. Syst.*, Wellington.
- Taska, L. & Barnes, A. (2012). *Rethinking Misbehavior and Resistance in Organizations*. Emerald Group Publishing, West Yorkshire.
- TDA (2010-2017), *Economic Enhancement Programme*. Technology Depository Agency (TDA) under Ministry of Finance Malaysia, Putrajaya.
- Thai, K.V (2004). Introduction to public procurement. *J.Public Procur.*, **4** : 312-318.
- Telsang, M.T. (2007). *Production Management*. Chand Limited, New Delhi.
- Temple, D. & Collette, M. (2013). Optimization of structural design to minimize lifetime maintenance cost of a naval vessel. *Analysis and Design of Marine Structures*. Taylor & Francis Group, London,
- Thomas, J. (2013). Study on causes and effects of employee turnover in construction industry. *Int. J. Sci. Res.*, **4** : 3041-3044.
- Tomkins, C. (2012). *Transforming Warship Support: Class Output Management*. RUSI Defence Systems, London
- Twigge-Molecey, C. & Price, T. (2013). *Materials Handling in Pyrometallurgy*. Elsevier, Amsterdam.
- U. S. Bureau of Mines (1988). *Information Circular*. University of Michigan, Michigan.
- U.S. Congress, (2004). *Tribute to Admiral Frank "Skip" Bowman*. U.S. Office of Technology Assessment, U.S.
- U.S. Navy (2012). *NAVSEA Instruction 4790.28, Risk Management for U.S. Naval Ship Maintenance Availabilities*. Naval Sea System Command (NAVSEA), Washington, D.C..
- U.S. Navy (2014). *NAVSEA Schedules FY15 Surface Ship Availabilities*. Naval Sea System Command (NAVSEA), Washington, D.C.
- U.S. Navy Research, Development and Acquisition (2006), *Naval "System of Systems" Systems Engineering Guidebook, Vol. I*. Office of the ASN (RDA), Washington, D.C..
- Walker, J.C. (2005). *Multi-Attribute Tradespace Exploration for US Navy Surface Ship Survivability: A Framework for Balancing Capability, Survivability, and Affordability*. Masters of Science in Mechanical Engineering, Massachusetts Institute of Technology, Massachusetts.
- Walsh, A. (2014). *Design, Integration & Project Management of Complex Engineering Programs - ASC*. The Institution of Engineers Australia, Barton ACT.
- Wang, J., Pillay, A. & Mokashi, A. (2010). Application of reliability centred maintenance in ship operations. *Safety and Reliability of Industrial Products, Systems and Structures*, Taylor & Francis Group, London.
- WEC/UNIPEDE (1991). Availability and unavailability factors of thermal generating plants. *Definitions and Methods of Calculation*. UNIPEDE, Paris.
- Wearne, S.H. (1993). *Principles of Engineering Organization, 2 Ed*. Telford, T. Insitute of Civil Engineers, London.
- Weibull, 2017. *Reliability Importance Measure of Components in a Complex System - Identifying the 20% in the 80/20 Rule*. Available online at: <http://www.weibull.com/hotwire/issue66/realbasics66.htm> (Last access date: 05 February 2018).
- Wiggins, J. (1985). *ESA Safety optimization study*. Hernandez Engineering, HEI-685/1026, Houston.
- Wilkinson, A. (2009). Scenarios practices: In search of theory. *J. Futures St.*, **13** : 107-114.

- Wilson, R. (2014). *A Comprehensive Guide to Project Management Schedule and Cost Control: Methods and Models for Managing the Project Lifecycle*. Pearson FT Press, London.
- Wilson, R. (2015). *Mastering Project Time Management, Cost Control, and Quality Management: Proven Methods for Controlling the Three Elements that Define Project Deliverables*. FT Press, New Jersey.
- Xia, B. & Chan, A.P.C. 2012. Measuring complexity for building projects: a delphi study. *Eng., Constr. Archit.Manag*, **19** : 7-24.
- Yuan, Z. (2016). *A Brief Literature Review on Ship Management in Maritime Transportation*. Technical Report No. TR/IRIDIA/2016-001, Institut de Recherches Interdisciplinaires et de Developments en Intelligence Artificielle (IRIDIA), Brussels.